Title
Thalamic circuit modulation by astrocytes

Author
Cho, Frances Sungsil

Publication Date
2022

Thalamic circuit modulation by astrocytes

by
Frances Sungsil Cho

DISSERTATION
Submitted in partial satisfaction of the requirements for degree of
DOCTOR OF PHILOSOPHY

in

Neuroscience

in the

GRADUATE DIVISION
of the
UNIVERSITY OF CALIFORNIA, SAN FRANCISCO

Approved:

DocuSigned by:
Vikaas Sohal
70A483C8DEB04E6...

Vikaas Sohal
Chair

DocuSigned by:
Anatol Kreitzer
D2...440...

Anatol Kreitzer

DocuSigned by:
Jeanne Paz
B...

Jeanne Paz

DocuSigned by:
Kira Poskanzer
64ED3BCFD209496...

Kira Poskanzer

Committee Members

Acknowledgements

The scientific work described in this dissertation represents a significant portion of my PhD journey, which has been challenging, humbling, and fulfilling beyond my expectations. This journey could not have happened without the profound support I have received from countless mentors, colleagues, friends, and family.

First and foremost, I would like to thank my advisor Dr. Jeanne Paz. It has been an immense privilege to be trained by Dr. Paz, and I will attempt to explain how she has shaped me as a scientist without dedicating an entire chapter of my dissertation. During my rotation, Dr. Paz's unreserved passion for the thalamus, electrophysiology, and curing neurological diseases encouraged me to dive head-first into the project which would become my dissertation work. Having introduced me to the beautiful landscape of neural circuits in the thalamus, she spent countless hours "in the field" with me, equipping me with the experimental tools, conceptual frameworks, and resources to embark upon my own expeditions. I knew I could rely on her to help me recalibrate every misstep as well as to celebrate every success. Dr. Paz exemplifies a fantastic balance of scientific depth and breadth, which I aspire to achieve. Anchored by her deep expertise and optimism, she explores widely and has encouraged me to follow suit; this spirit has launched multiple fruitful scientific collaborations and opportunities which have ultimately shaped my dissertation research and have been invaluable experiences for me. Dr. Paz showed me how scientific thought and discovery can happen anywhere, anytime—some of our most memorable discussions have taken place on a commuter train or a snow-covered hiking trail. She taught me to find joy even during the most mundane experiments and challenging peer-review processes. The exceptional scientific mentorship I received was accompanied by an equally exceptional professional and training environment. At the bench and beyond, Dr. Paz is deeply committed to empowering her trainees.

She has been my most vocal advocate over the years, and I have also witnessed her commitment to mentorship in the daily decisions and actions which go unspoken. She has nominated her trainees for awards and presentations, supported our attendance at numerous conferences, taught us valuable lessons in grantsmanship, encouraged us to mentor students, serve on committees, and find our own voice in promoting causes we are passionate about, and supported our well-being. As a result of Dr. Paz's leadership and encouragement, I have developed a broad network of scientific peers and mentors, found my own voice in efforts to promote justice, diversity, equity and inclusion-centered practices, and confidently embark upon my next scientific endeavor. To say that I am thankful for Dr. Paz's guidance is a vast understatement.

It has been a privilege to have been a part of the UCSF neuroscience community, and there are countless people who have made it an exceptional training environment. First, I would like to thank members of my qualifying exam committee for their guidance during an early critical period of my graduate work: Dr. Felice Dunn, Dr. Li Gan, Dr. Anna Molofsky, and Dr. Vikaas Sohal. I am grateful to members of my thesis committee: Dr. Anatol Kreitzer, Dr. Jeanne Paz, Dr. Kira Poskanzer, and Dr. Vikaas Sohal. They generously shared their expertise to help me see beyond the everyday experiments to think creatively, provided constructive guidance which helped me think critically, and encouraged me in numerous ways as I navigated the peer-review process.

I am grateful for the mentorship and support I received from numerous UCSF neuroscience community members throughout the years. Thank you to the neuroscience program directors from 2015–2022, Dr. Roger Nicoll, Dr. Anatol Kreitzer, and Dr. Sam Pleasure, and to the program administrators Pat Veitch and Lucita Nacionales, who welcomed and supported me from day one. I would like to thank Dr. Loren Frank, who inspired and enabled me to seek rigor in data analysis and supported me in gaining hands-on experience building computational models. I am thankful

for the privilege to have served on the neuroscience program's committee for Diversity, Equity, and Inclusion, and I continue to be inspired by the passion, humility, and impact of peers and faculty. I am particularly grateful to committee members Dr. Kira Poskanzer, Dr. Evan Feinberg, Dr. Lisa Gunaydin, and Dr. Aimee Kao, for their leadership, dedication, and allyship. I am grateful for Dr. D'Anne Duncan, a visionary and compassionate leader who has already transformed many aspects of justice, diversity, equity and inclusion at UCSF in a short time. Her mentorship has fundamentally changed my outlook on what it takes to be an effective advocate of justice in academic and research spaces.

Thank you to my graduate school cohort, Leah Dorman, Ben Mansky, Match McGregor, Michael Reitman, Selin Schamiloglu, Trisha Vaidyanathan, and Hannah Joo. I am inspired and uplifted by each of you, and am thankful for all the delicious food and libations, warm memories, cold bonfires, karaoke, dancing, and science we've shared.

My graduate work, partially described in this dissertation, was made possible by an incredible team of collaborators. It has been an immense pleasure and privilege to work with, and learn from, the labs of Dr. Anna Molofsky, Dr. Bal Khakh, Dr. Eleonora Aronica, Dr. John Rubenstein, Dr. Bruno Delord, and Dr. Jeanne Paz. I am especially grateful to have worked closely with Dr. Anna Molofsky and Dr. Ilia Vainchtein, who taught me much of what I know about glial biology, immunology, and transcriptomics. Their expertise and guidance helped shaped many of the interdisciplinary questions addressed in this dissertation.

I am privileged to call the Gladstone Institutes my scientific home. An organization which goes above and beyond to support its scientists in every manner, Gladstone has been a pillar of my graduate career. I am thankful for all the scientists who have become colleagues, mentors, and friends over the years. I am thankful to Dr. Françoise Chanut and Dr. Kathryn Claiborn, Senior

Scientific Editors at Gladstone, who taught an excellent course on the “nuts and bolts” of scientific writing and have provided me with indispensable feedback. I am thankful to Dr. Sudha Krishnamurthy for her advocacy and support in my professional development. I am thankful to all the administrative staff, animal facility staff, and core facility staff at Gladstone, without whom our research would not be possible. I am thankful for the leadership and support of current Gladstone President Dr. Deepak Srivastava, and the Director of the Gladstone Institutes of Neurological Disease, Dr. Lennart Mucke. I am grateful for the mentorship of Dr. Robert Mahley, founder of Gladstone Institutes, who has generously aided in my scientific and professional development, and inspires me with his lifelong commitment to basic research overcoming disease.

I would like to especially thank past and present members of the Paz Lab. I will never forget the mentorship of Dr. Alexandra Clemente, Dr. Stephanie Holden, and Dr. Stefanie Makinson during my first several years. Equal parts talented experimentalists and supportive colleagues, they were generous with their time and taught me the intricacies of slice physiology and troubleshooting electrical noise, coached me through my first chalk talk, showed me to unabashedly ask questions during seminars, and taught me how to enjoy graduate school. I am grateful for the support of my fellow lab mate, Morgane Leroux, who inspires me with her laser-focus, experimental rigor, and compassion. I am thankful to my exceptional colleagues in the Paz Lab throughout the years, with whom it’s been a pleasure to work: Dr. Bryan Higashikubo, Dr. Andrew Chang, Dr. Agnieszka Ciesielska, Dr. Yuliya Voskobiynyk, Dr. Jeremy Ford, Deanna Necula, Irene Lew, Sean Dailey; and to my newer colleagues in the Paz Lab, who have helped sustain a fun, creative, and constructive scientific atmosphere: Audrey Magsig, Vivianna Dennitis, Isaac Chang, Drew Willoughby, Clare Timbie, Britta Lindquist, Jeannie Giacchino, and Alexis Lupien-Meilleur.

I am grateful to all mentors I've had the privilege of crossing paths with as a young scientist, including Dr. Jeff Bronstein, Dr. Arthur Fitzmaurice, Dr. Chet Moritz, Dr. Barclay Morrison III, Dr. John Finan, and Dr. Christopher Hue. Thank you for your formative support and encouragement.

Finally, I owe my utmost gratitude to my loving family, without whom I would not be the scientist or person I am today. I am grateful for my extended family throughout California, Korea, and Switzerland who nurture and rejuvenate me. For my mother, who inspires me with her fierce and compassionate dedication to empowering neurodiverse individuals and families. For my father, who inspires me with his scientific curiosity, integrity, and knowledge. Together they sustain me with their unconditional love and support. And for my husband, who enriches me with endless passion, creativity, and love.

The work described in this dissertation was supported by the National Institutes of Health/National Institute of Neurological Disorders and Stroke, the National Science Foundation, the UCSF Discovery Fellows Program, and the Kavli Institute for Fundamental Neuroscience.

Contributions

Chapter 1 of this dissertation was written by Frances S. Cho, with parts adapted from the following book chapter with permission from Elsevier:

> Cho, F.S., Clemente, A., Holden, S., Paz, J.T. Chapter 19 - Thalamic models of seizures *in vitro*, in: Pitkänen, A., Buckmaster, P.S., Galanopoulou, A.S., Moshé, S.L. (editors), *Models of Seizures and Epilepsy* (Second Edition). Academic Press, pp. 273–284 (2017).

F.S.C., A.C., S.H., and J.T.P. wrote this book chapter collaboratively.

Chapter 1 also includes sections adapted from the qualifying exam proposal of the author, submitted towards the advancement of doctoral candidacy (2017).

Chapter 2 is reproduced in its entirety from a draft of a chapter that has been accepted for publication by Oxford University Press (OUP) in the forthcoming book *Jasper's Basic Mechanisms of the Epilepsies (5th Edition),* due for publication in December 2022, with permission from OUP:

> Cho, F.S. and Paz, J.T. Convergence of thalamic mechanisms in genetic epilepsies. Chapter in: Noebels, J.L., Avoli, M., Rogawski, M.A., Vezzani, A. & Delgado-Escueta, A.V. (editors), *Jasper's Basic Mechanisms of the Epilepsies* (5th edition). Oxford University Press, In Press (2022).

F.S.C. wrote this manuscript. F.S.C. and J.T.P. edited the manuscript.

Chapter 3 is reproduced in its entirety from the accepted version of this manuscript, with permission from the American Association for the Advancement of Science:

Vainchtein, I.D., Chin, G., Cho, F.S., Kelley, K.W., Miller, J.G., Chien, E., Liddelow, S.A., Nguyen, P., Inoue, H., Dorman, L., Akil, O., Joshita, S., Barres, B.A., Paz, J.T., Molofsky, A.B., Molofsky, A.V. Astrocyte-derived Interleukin-33 promotes microglial synapse engulfment and neural circuit development. *Science,* 359(6381) (2018). https://www.science.org/doi/10.1126/science.aal3589

I.D.V., G.C., A.V.M, and J.G.M. designed, performed, and analyzed most experiments. E.C.C., H.N-I, P.T.N., and L.C.D. contributed to experiments and data analysis. F.S.C and J.T.P. designed, performed, and analyzed the electrophysiology experiments. K.W.K and I.D.V designed and performed bioinformatics analyses. S.A.L. performed and analyzed culture experiments under supervision of B.A.B. O.A. performed and analyzed auditory testing. S.J. generated *Il33*$^{H2B\text{-}mCherry}$ mice. A.V.M and A.B.M designed experiments and wrote the manuscript together with I.D.V., G.C. and other authors.

Chapter 4 is reproduced in its entirety from the accepted version of this manuscript, with permission from the American Association for the Advancement of Science:

Cho, F.S., Vainchtein, I.D., Voskobiynkyk, Y., Morningstar, A.R., Aparicio, F., Ciesielska, A., Broekaart, D.W.M., Anink, J.J., van Vliet, E.A., Yu, X., Khakh, B.S., Aronica, E., Molofsky, A.V., Paz, J.T. Enhancing GAT-3 in thalamic astrocytes promotes resilience to brain injury in rodents. *Science Translational Medicine,* 14:652 (2022). https://www.science.org/doi/10.1126/scitranslmed.abj4310

F.S.C. and J.T.P. conceived the project. F.S.C. performed stereotaxic viral injections, electrocorticography implants, *in vivo* recordings and analysis, *ex vivo* electrophysiological studies and analysis, immunohistochemistry, and all related data analysis and visualization. I.D.V.

performed, analyzed, and interpreted fluorescence-activated cell sorting, bulk transcriptomics, and quantitative polymerase chain reaction studies. I.D.V. and F.S.C. performed, analyzed, and interpreted astrocyte morphology study. D.W.M.B., J.J.A., E.A.V., and E.A. performed, analyzed, and interpreted immunolabeling of post-mortem human tissue. B.S.K. and X.Y. generated the AAV2/5-*GfaABC1D*-GAT3-HA-mCherry construct. B.H., J.T.P., and F.S.C. developed custom MATLAB scripts for analysis of electrophysiology studies. F.A. performed, analyzed, and interpreted kainic acid seizure challenge in mice. F.S.C., A.R.M., and A.C. performed immunohistochemistry of mouse tissue. Y.V., A.C., and F.S.C. performed, analyzed, and interpreted spatial transcriptomic study. J.T.P., A.V.M., E.A., and B.S.K. acquired funding. F.S.C. and J.T.P. discussed and interpreted all data with respective authors. F.S.C. and J.T.P. wrote the original draft of the manuscript, and all authors participated in manuscript revisions.

Chapter 5 was written by Frances S. Cho.

Thalamic circuit modulation by astrocytes

Frances Sungsil Cho

Abstract

The thalamus, a subcortical brain structure involved in key aspects of sensation, perception, cognition, and consciousness, is endowed with intrinsic rhythmogenic properties and extensive reciprocal connections with the cerebral cortex. These reciprocal connections form thalamo-cortico-thalamic circuits which generate, synchronize, and propagate physiological brain rhythms such as sleep spindles. Disruptions in these circuits can cause sleep deficits, and generation of pathological rhythms like seizures. While the canonical thalamo-cortico-thalamic circuit diagram consists entirely of neurons and their synaptic connections, mounting evidence points to the profound impact of astrocytes in dynamically modulating circuit components. Astrocytes are non-neuronal glial cells that play diverse, complex roles in mediating normal neuronal function in the developing and mature brain, at the synaptic and circuit levels, in both health and disease (**Chapter 1**). Astrocytes are well-positioned to govern crucial aspects of thalamic circuit function, such as excitability and rhythmogenesis, which can be disrupted in neurological disorders such as epilepsy **(Chapter 2)**, but the precise mechanisms by which astrocytes modulate thalamic synapse and circuit function in development and disease are poorly understood. In **Chapter 3**, we demonstrate the critical role astrocytes play in shaping the developing thalamus of rodents by providing a key immune signal—IL-33 (interleukin-1 family cytokine interleukin-33)—to control the number of excitatory synapses. Its absence can lead to runaway excitation in the thalamus, paving the path for epileptic activity in mice. In **Chapter 4,** we demonstrate that reactive astrocytes can trigger aberrant synaptic and circuit function in the thalamus, providing strong evidence that they can be

drivers, rather than mere bystanders, of injury-related pathological sequelae such as post-traumatic epilepsy and sleep disruption. Furthermore, we identify an aspect of reactive astrocytes—GABA transporter GAT-3 loss of function—sufficient to confer pathological excitability in an otherwise normal thalamic circuit, and one which may underlie thalamic dysfunction observed in cases of brain injuries. In **Chapter 5**, we discuss our findings which highlight distinct forms of thalamic synapse modulation by astrocytes, as well as common pathways of astrocytic function in brain development and degeneration; we also speculate on the potential role of astrocytes in mediating the distinctive computational properties of the reticular thalamic nucleus. Altogether, our findings add to the growing evidence supporting the critical role of astrocytes in the modulation of thalamic circuits in physiological and pathological settings.

Table of Contents

List of Figures

Chapter 1

Chapter 2

Chapter 3

Chapter 4

List of Tables

Chapter 3

Chapter 4

Chapter 1 : Introduction

1.1. Overview of dissertation

In this dissertation, we aim to understand neuron-astrocyte interactions in the thalamus in health and disease **(Fig. 1.1)**. The thalamus is a subcortical rhythmogenic brain structure involved in key aspects of sensation, perception, cognition, and consciousness. Astrocytes are glial cells that play diverse, complex roles in mediating normal neuronal function in the developing and mature brain, at the synaptic and circuit levels (discussed below). Although astrocytes are well-positioned to govern two crucial aspects of thalamic microcircuits—rhythmogenesis and excitability (discussed in **Chapter 2**)—they have not yet been integrated into the canonical diagram of the thalamo-cortico-thalamic circuit. In **Chapters 3 and 4**, we use the rodent thalamus—composed of neural circuits relatively well-understood in terms of their observable inputs and outputs—to investigate the emerging role of astrocytes with special consideration of the following questions:

Cause vs. Consequence: are astrocytes capable of triggering functional consequences in thalamic circuits, or are they merely bystanders?

In **Chapter 3,** we report that astrocytes enable microglial phagocytosis of excitatory synapses in the developing somatosensory thalamus. In **Chapter 4**, we reveal that reactive astrocytes in the thalamus can drive robust aberrations in synaptic and circuit function. While there is mounting evidence that neuroinflammation is a consistent hallmark of the secondarily damaged thalamus after cortical injuries, the role of thalamic astrogliosis—remote from the initial site of injury—remained unknown. By selectively modeling one aspect of secondary damage observed in brain injuries, we found that reactive astrocytes in the thalamus could recapitulate several key pathological features that develop after cortical injuries, such as increased seizure risk, providing

evidence that reactive astrocytes in the thalamus can be drivers, rather than mere bystanders, of increased seizure risk after brain injury.

Health vs. Disease: how do thalamic astrocytes shape local synapses and circuits during development and in disease contexts?

In **Chapter 3**, we uncover the role of astrocytic innate immune signals in neural circuit development. We identify the interleukin-1 family cytokine interleukin-33 (IL-33) as a critical player in shaping healthy thalamic circuits. We later discuss the consequences of astrocytic IL33 deletion *in vivo,* which includes spontaneous epileptiform activity. In **Chapter 4**, we dissect the role of reactive astrocytes in the thalamus in pathological synaptic and circuit function. Reactive astrocytes play both adaptive and maladaptive roles in the aftermath of an insult to the nervous system, hence explaining why therapeutic strategies focused on broadly reducing neuroinflammation have not been successful. We identify an aspect of thalamic reactive astrocytes—GABA transporter GAT-3 loss of function—as sufficient to confer pathological excitability in an otherwise normal thalamic circuit. Furthermore, we demonstrate that enhancing GAT-3 in thalamic astrocytes boosts resilience after brain injuries in mice, suggesting that GAT-3 loss of function may underlie thalamic dysfunction observed in cases of brain injuries.

Finally, in **Chapter 5**, we discuss our findings which highlight distinct forms of astrocytic modulation of thalamic synapses, as well as common pathways of astrocytic function in brain development and degeneration; we also speculate on the potential role of astrocytes in mediating the distinctive computational properties of the reticular thalamic nucleus.

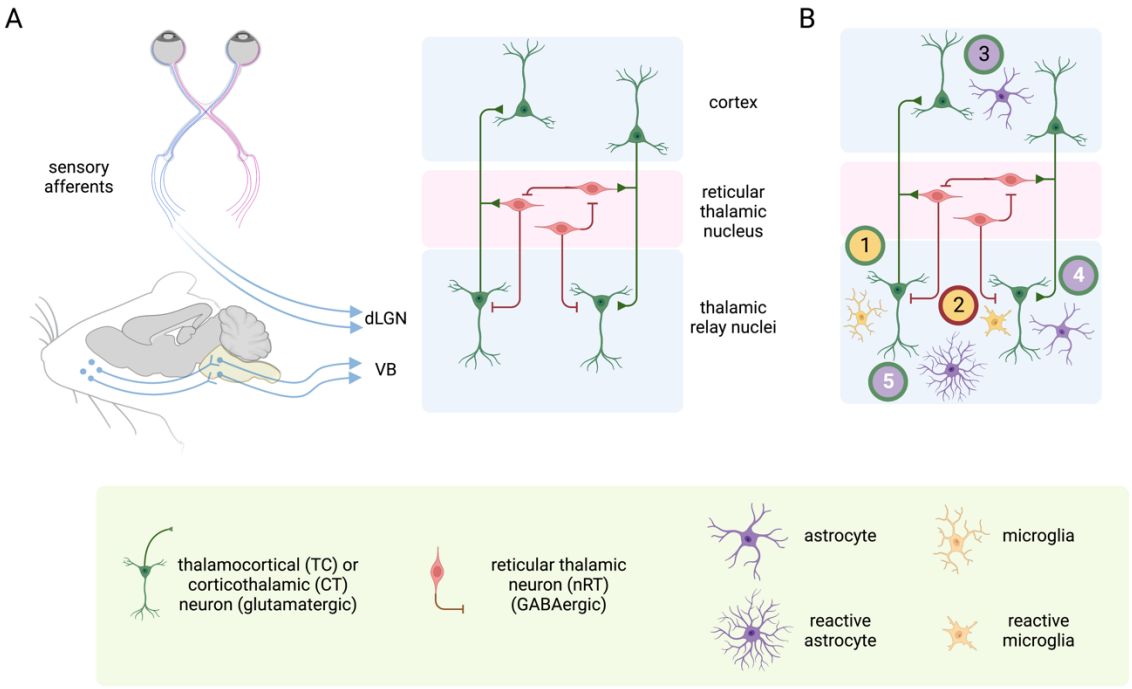

Figure 1.1. Integrating astrocytes into the canonical thalamo-cortico-thalamic circuit diagram.

(A) Simplified schematic of two well-established thalamo-cortico-thalamic circuits composed of neuronal components. Visual sensory information from the retina arrives in the dorsal lateral geniculate nucleus (dLGN), a thalamic relay nucleus composed of excitatory thalamocortical (TC) neurons which form reciprocal and topographical connections with excitatory corticothalamic (CT) neurons in primary visual cortex. Similarly, whisker somatosensory information from the brainstem arrives in the ventral basal (VB) nucleus of the thalamus, which in turn forms reciprocal and topographical connections with the primary somatosensory cortex. TC neurons in dLGN and VB form reciprocal connections with GABAergic neurons of the nRT, which also receive corticothalamic input from the topographically connected cortical regions. Additional details can be found in **Chapter 2**. **(B)** Modified thalamo-cortico-thalamic circuit schematic incorporating previous findings from others (①②③, black numerals) and new findings described in this dissertation (❹❺, white numerals) which elucidate the role of non-neuronal glial cells in rodent thalamic relay nuclei, in development and disease. Neuronal and glial components are defined in the green box. Neuronal and glial colors are used for the border and center of the enclosed numerals, respectively. The role of astrocytes in the nRT is relatively less understood and is omitted from this schematic. ① Thalamic microglia mediate activity-dependent pruning of excitatory retinogeniculate synapses in the postnatal developing dLGN via the classical complement pathway (Schafer et al., 2012). ② Thalamic reactive microglia prune inhibitory reticulothalamic synapses in the aging VB via the classical complement pathway in the absence of progranulin, a gene implicated in frontotemporal lobar degeneration (Lui et al., 2016). ③ Cortical astrocytes enable thalamocortical formation in the developing mouse visual cortex by secreting

the glycoprotein hevin (Singh et al., 2016). Cortical astrocytes also control the maturation of thalamocortical synapses in the developing mouse visual cortex by secreting the protein chordin-like 1 to regulate synaptic levels of GluA2-containing calcium impermeable AMPA glutamate receptors (Blanco-Suarez et al., 2018). ❹ Thalamic astrocytes mediate microglial phagocytosis of excess excitatory corticothalamic synapses in the developing VB via interleukin-33, as discussed in **Chapters 3 and 5** (Vainchtein et al., 2018; Han et al., 2021). ❺ Thalamic reactive astrocytes tune excitability of thalamocortical neurons in VB via loss of the GABA transporter GAT-3, as discussed in **Chapters 4 and 5** (Cho et al., 2022). Created with BioRender.com.

1.2. Astrocytes

This section is modified from the author's research proposal submitted for consideration of advancement to doctoral candidacy (2017).

Astrocytes are glial cells that play diverse, complex roles in mediating normal neuronal function in the developing and mature brain, at the synaptic and circuit levels. Astrocytes respond and signal to neurons and other astrocytes (Araque et al., 2014). In addition to providing metabolic support and enabling neurovascular coupling (Haydon and Carmignoto, 2006), astrocytes mediate various aspects of synaptic transmission by (1) regulating extracellular ionic milieu, (2) regulating neuronal supply of neurotransmitters such as glutamate and GABA through the astrocytic glutamate-glutamine cycle, and (3) expressing diverse repertoires of neurotransmitter reuptake transporters (Khakh and Sofroniew, 2015). Inter- and intracellular calcium signaling are thought to be critical components enabling astrocyte-neuronal interactions, although the functional significance of calcium activity is still an emerging field of research (Khakh and Sofroniew, 2015).

In addition to complex, reciprocal astrocyte-neuron signaling, astrocytes partake in intercellular communication via astroglial networks (Giaume et al., 2010). Astrocytes are organized into networks and are connected through gap junction channels that are regulated by extra- and intracellular signals. Gap junctions allow the exchange of ions and secondary messengers between astrocytes (Griemsmann et al., 2015). One method of intercellular

communication mediated by gap junctions is the propagation of calcium transients to neighboring astrocytes. These networks can cover large functional neuronal territories, thus astrocytes are equipped to simultaneously modulate the activity of groups of neurons. Indeed, astrocyte networks have been shown to coordinate neuronal synchronization in the hippocampus (Chever et al., 2016), olfactory bulb (Roux et al., 2015) and cortex (Poskanzer and Yuste, 2016), to modulate neuronal rhythmogenesis (Morquette et al., 2015), sculpt the suprachiasmatic nucleus to regulate circadian timekeeping (Brancaccio et al., 2017), and close the critical period for visual plasticity in the cortex (Ribot et al., 2021). Astrocytes in nearly every brain region have also been found to play key roles in a range of behavioral contexts (reviewed by Nagai et Khakh, Neuron, 2021). Cortical astrocytes regulate distinct features of sleep-wake transitions (sleep depth and duration) through distinct G-protein-coupled receptor signaling pathways *in vivo* (Vaidyanathan et al., 2021). Thalamic astrocytes control sensory acuity and shape sensory discrimination behavior through tonic GABA (Kwok et al., 2020). Thus, astrocyte networks are emerging as critical players in the modulation of neural circuits in various physiological settings.

To what extent astrocyte function and astrocyte-neuron interactions are similar or different across brain regions remains an open investigation (Boisvert et al., 2018; Kastanenka et al., 2019; Khakh and Sofroniew, 2015). Furthermore, while astrocytes also interact with microglia—another class of glial cells in the brain with emerging roles in neuronal synaptic function—microglia will not be a major focus of this dissertation.

1.3.Thalamic astrocytes tune GABAergic synaptic transmission

This section is adapted from part of the book chapter written by Cho et al., 2017.

Astrocytes tune the balance between excitation and inhibition by modulating GABAergic and glutamatergic synaptic function (reviewed by Mederos and Perea, 2019). This balance is jeopardized in epileptic disorders (reviewed by Paz and Huguenard, 2015a and 2015b). Notably, astrocytes are a source and regulator of GABA, and they can affect different modes of GABAergic transmission. While astrocytes are involved in diverse aspects of GABAergic inhibitory signaling across the brain, here we will focus on the influence of astrocytes in shaping thalamic circuit rhythmogenesis and excitability.

Astrocytes mediate the glutamate-glutamine cycle, which regulates the neuronal supply of glutamate and GABA, as well as thalamic network oscillations (reviewed by Halassa et al., 2010). The astrocytic glutamine-glutamate cycle is critical for normal neuronal function. Neurons cannot synthesize glutamate or GABA from glucose, but they can convert glutamine (released by astrocytes) to either glutamate or GABA using phosphate-activated glutaminase or glutamate decarboxylase, respectively (Bak et al., 2006). *Ex vivo* studies using horizontal thalamic slice preparations demonstrated the critical role of the astrocytic glutamate-glutamine cycle in sustaining thalamic rhythms seen during epileptiform activity (Bryant et al., 2009; Yang et al., 2011). Furthermore, in the thalamus, plasmalemmal glutamate and GABA transporters are located exclusively on astrocytes (De Biasi et al., 1998). Altogether, astrocytes are equipped to influence neurotransmitter reuptake and consequently, levels of glutamate and GABA.

Thalamic neurons produce several types of GABAergic currents, depending on the location and subunit composition of GABA receptors, the ionic milieu, the cell type, and the brain region. These currents can be further modulated by neighboring astrocytes. For example, GAT-1 and

GAT-3 are the primary GABA-transporter (GAT) subtypes expressed in the rodent brain including the thalamus, where GAT-3 is predominantly expressed in astrocytes (De Biasi et al., 1998). GAT-1 and GAT-3 differentially modulate the amplitude and duration of inhibitory post-synaptic currents mediated by $GABA_B$ receptors. In thalamic slices, GAT-3 is localized far from synapses and is well-positioned to regulate GABA diffusion and activation of extrasynaptic $GABA_B$ receptors (Beenhakker and Huguenard, 2010). In similar thalamic slice preparations, thalamic astrocytes were shown to release GABA and contribute to slow outward currents mediated by δ subunit–containing $GABA_A$ receptors in TC neurons (Jimenez-Gonzalez et al., 2011). Astrocytic regulation of thalamic GABA can have profound effects on behavior *in vivo*. For example, dysfunctional GAT-1 is a culprit of thalamocortical absence seizures in genetic absence epilepsy rats from Strasbourg (Cope et al., 2009), and thalamic astrocytes control tactile acuity via tonic GABA, enabling astrocytic control of sensory discrimination behavior in mice (Kwak et al., 2020).

In addition to modulating GABAergic transmission, thalamic astrocytes are involved in other forms of synaptic transmission, such as NMDAR-mediated slow-inward currents in neighboring neurons within horizontal thalamic slices (Pirttimaki and Parri, 2012). They also mediate the switch from tonic- to burst-firing mode by regulating extracellular Ca^{2+} concentrations in neurons within transverse slices of the trigeminal main sensory nucleus (Morquette et al., 2015). Thus, astrocytes can clearly play meaningful and diverse roles in regulating synaptic transmission in the thalamus.

Recent studies have uncovered the role of cortical astrocytes in thalamocortical synapse development (reviewed by Allen and Eroglu, 2017). Cortical astrocytes secrete Hevin to enable thalamocortical synapse formation in the developing mouse visual cortex (Singh et al., 2016), and secrete Chordin-like 1 to control synapse maturation (and thereby to inhibit plasticity) by

regulating synaptic levels of GluA2 AMPA receptors (Blanco-Suarez et al., 2018). However, the role of thalamic astrocytes in specifying the other components of the circuit—corticothalamic, intra-thalamic synapses—remains less understood.

1.4. Astrocytes in thalamic pathology

In response to neurological insults, astrocytes become reactive and undergo morphological, molecular and functional changes, a process called astrogliosis (Anderson et al., 2016; Burda and Sofroniew, 2014; Escartin et al., 2021; Liddelow et al., 2017; Sun and Jakobs, 2012; Zamanian et al., 2012). This neuroinflammatory response occurs in many neurological disorders (Jo et al., 2014; Patel et al., 2019; Robel and Sontheimer, 2016; Vezzani et al., 2019), and can be both adaptive and maladaptive (Anderson et al., 2016; Burda and Sofroniew, 2014; Escartin et al., 2021; Liddelow et al., 2017; Zamanian et al., 2012). Although animal models have provided important insights into the various functions of astrocytes, in many settings it has been challenging to determine whether reactive astrocytes are a cause and/or consequence of changes in neuronal network activity (Ortinski et al., 2010; Patel et al., 2019; Robel et al., 2015; Robel and Sontheimer, 2016; Vezzani et al., 2019). An additional challenge is the molecular and functional heterogeneity of astrocytes across brain regions in healthy and diseased brain states (Boisvert et al., 2018; Clarke et al., 2018; Kelley et al., 2018; Khakh and Sofroniew, 2015; Liddelow et al., 2017; Soreq et al., 2017; Zamanian et al., 2012). Previous studies relied on transgenic mice with brain-wide astrogliosis, thus, region-specific consequences of reactive astrocytes remained under-investigated (Robel et al., 2015). Recent studies have elucidated how astrocytes can mediate local changes, such as neurotoxicity and diminished synaptogenesis (Liddelow et al., 2017). If and how reactive astrocytes in one brain region can affect neuronal activity in distal brain areas is unknown, but this

question is of particular interest in understanding the function of the thalamus, a brain region with extensive long-range connections with the cortex.

Thalamic astrogliosis is observed after cortical injuries such as traumatic brain injury (TBI) in humans (reviewed by Grossman and Inglese, 2016) and rodent models (Hazra et al., 2014; Holden et al., 2021; Necula et al., 2021), and cortical stroke in humans (Pappata et al., 2000) and rodent models (Cao et al., 2020; Paz et al., 2010), and has been implicated in chronic neurological and cognitive deficits that develop after such injuries (Cao et al., 2020; Grossman and Inglese, 2016; Paz et al., 2013). Given the central role of the thalamus as a rhythmogenic structure that is implicated in sensation, perception, and consciousness and has a central role in regulating cortical rhythms in humans and rodents (Crunelli and Hughes, 2010; Fogerson and Huguenard, 2016; Jeanmonod et al., 1996; Steriade et al., 1996, 1993), understanding if and how reactive astrocytes in the thalamus can initiate the development of pathological circuits and control cortical rhythms is of broad fundamental and translational interest.

References

Anderson MA, Burda JE, Ren Y, Ao Y, Shea TMO, Kawaguchi R, Coppola G, Khakh BS, Deming TJ, Michael V. 2016. Astrocyte scar formation aids central nervous system axon regeneration. *Nature* **532**:195–200. doi:10.1038/nature17623

Araque A, Carmignoto G, Haydon PG, Oliet SHR, Robitaille R, Volterra A. 2014. Gliotransmitters travel in time and space. *Neuron* **81**:728–739. doi:10.1016/j.neuron.2014.02.007

Blanco-Suarez E, Liu TF, Kopelevich A, Allen NJ. 2018. Astrocyte-Secreted Chordin-like 1 Drives Synapse Maturation and Limits Plasticity by Increasing Synaptic GluA2 AMPA Receptors. *Neuron* **100**:1116-1132.e13. doi:10.1016/j.neuron.2018.09.043

Boisvert MM, Erikson GA, Shokhirev MN, Allen NJ. 2018. The Aging Astrocyte Transcriptome from Multiple Regions of the Mouse Brain. *Cell Rep* **22**:269–285. doi:10.1016/j.celrep.2017.12.039

Brancaccio M, Patton AP, Chesham JE, Maywood ES, Hastings MH. 2017. Astrocytes Control Circadian Timekeeping in the Suprachiasmatic Nucleus via Glutamatergic Signaling. *Neuron* **93**:1420-1435.e5. doi:10.1016/j.neuron.2017.02.030

Burda JE, Sofroniew M V. 2014. Review Reactive Gliosis and the Multicellular Response to CNS Damage and Disease. *Neuron* **81**:229–248. doi:10.1016/j.neuron.2013.12.034

Cao Z, Harvey SS, Bliss TM, Cheng MY, Steinberg GK. 2020. Inflammatory Responses in the Secondary Thalamic Injury After Cortical Ischemic Stroke. *Front Neurol* **11**:1–12. doi:10.3389/fneur.2020.00236

Chever O, Dossi E, Pannasch U, Derangeon M, Rouach N. 2016. Astroglial networks promote neuronal coordination. *Sci Signal* **9**:1–9. doi:10.1126/scisignal.aad3066

Cho FS, Vainchtein ID, Voskobiynkyk Y, Morningstar A., Aparicio F, Ciesielska A, Broekaart

DWM, Anink JJ, van Vliet EA, Yu X, Khakh BS, Aronica E, Molofsky AV, Paz JT. 2022. Enhancing GAT-3 in thalamic astrocytes promotes resilience to brain injury in rodents. *Sci Transl Med* **14**. doi:10.1126/scitranslmed.abj4310

Clarke LE, Liddelow SA, Chakraborty C, Münch AE, Heiman M, Barres BA. 2018. Normal aging induces A1-like astrocyte reactivity. *Proc Natl Acad Sci U S A* **115**:E1896–E1905. doi:10.1073/pnas.1800165115

Cope DW, Di Giovanni G, Fyson SJ, Orbán G, Errington AC, Lőrincz ML, Gould TM, Carter DA, Crunelli V. 2009. Enhanced tonic GABAA inhibition in typical absence epilepsy. *Nat Med* **15**:1392–1398. doi:10.1038/nm.2058.Enhanced

Crunelli V, Hughes SW. 2010. The slow (1 Hz) rhythm of non-REM sleep: A dialogue between three cardinal oscillators. *Nat Neurosci* **13**:9–17. doi:10.1038/nn.2445

Escartin C, Galea E, Lakatos A, O'Callaghan JP, Petzold GC, Serrano-Pozo A, Steinhäuser C, Volterra A, Carmignoto G, Agarwal A, Allen NJ, Araque A, Barbeito L, Barzilai A, Bergles DE, Bonvento G, Butt AM, Chen W-T, Cohen-Salmon M, Cunningham C, Deneen B, De Strooper B, Díaz-Castro B, Farina C, Freeman M, Gallo V, Goldman JE, Goldman SA, Götz M, Gutiérrez A, Haydon PG, Heiland DH, Hol EM, Holt MG, Iino M, Kastanenka K V, Kettenmann H, Khakh BS, Koizumi S, Lee CJ, Liddelow SA, MacVicar BA, Magistretti P, Messing A, Mishra A, Molofsky A V, Murai KK, Norris CM, Okada S, Oliet SHR, Oliveira JF, Panatier A, Parpura V, Pekna M, Pekny M, Pellerin L, Perea G, Pérez-Nievas BG, Pfrieger FW, Poskanzer KE, Quintana FJ, Ransohoff RM, Riquelme-Perez M, Robel S, Rose CR, Rothstein JD, Rouach N, Rowitch DH, Semyanov A, Sirko S, Sontheimer H, Swanson RA, Vitorica J, Wanner I-B, Wood LB, Wu J, Zheng B, Zimmer ER, Zorec R, Sofroniew M V, Verkhratsky A. 2021. Reactive astrocyte nomenclature, definitions, and future directions. *Nat*

Neurosci. doi:10.1038/s41593-020-00783-4

Fogerson PM, Huguenard JR. 2016. Tapping the Brakes: Cellular and Synaptic Mechanisms that Regulate Thalamic Oscillations. *Neuron* **92**:687–704. doi:10.1016/j.neuron.2016.10.024

Giaume C, Koulakoff A, Roux L, Holcman D, Rouach N. 2010. Astroglial networks: a step further in neuroglial and gliovascular interactions. *Nat Rev Neurosci* **11**:87–99. doi:10.1038/nrn2757

Griemsmann S, Höft SP, Bedner P, Zhang J, Von Staden E, Beinhauer A, Degen J, Dublin P, Cope DW, Richter N, Crunelli V, Jabs R, Willecke K, Theis M, Seifert G, Kettenmann H, Steinhäuser C. 2015. Characterization of panglial gap junction networks in the thalamus, neocortex, and hippocampus reveals a unique population of glial cells. *Cereb Cortex* **25**:3420–3433. doi:10.1093/cercor/bhu157

Grossman EJ, Inglese M. 2016. The role of thalamic damage in mild traumatic brain injury. *J Neurotrauma* **33**:163–167. doi:10.1089/neu.2015.3965

Han RT, Vainchtein ID, Schlachetzki JCM, Cho FS, Dorman LC, Johung T, Ahn E, Barron JT, Nakao-Inoue H, Joshi A, Molofsky AB, Glass CK, Paz JT, Molofsky A V. 2021. Interleukin-33 coordinates a microglial phagocytic response and limits corticothalamic excitability and seizure susceptibility. *bioRxiv* 1–52.

Haydon PG, Carmignoto G. 2006. Astrocyte Control of Synaptic Transmission and Neurovascular Coupling. *Physiol Rev* **86**:1009–1031. doi:10.1152/physrev.00049.2005

Hazra A, Macolino C, Elliott MB, Chin J. 2014. Delayed thalamic astrocytosis and disrupted sleep-wake patterns in a preclinical model of traumatic brain injury. *J Neurosci Res* **92**:1434–1445. doi:10.1002/jnr.23430

Holden SS, Grandi FC, Aboubakr O, Higashikubo B, Cho FS, Chang AH, Forero AO, Morningstar AR, Mathur V, Kuhn LJ, Suri P, Sankaranarayanan S, Andrews-Zwilling Y, Tenner AJ, Luthi

A, Aronica E, Corces MR, Yednock T, Paz JT. 2021. Complement factor C1q mediates sleep spindle loss and epileptic spikes after mild brain injury. *Science* **373**. doi:10.1126/science.abj2685

Jeanmonod D, Magnin M, Morel A. 1996. Low-threshold calcium spike bursts in the human thalamus: Common physiopathology for sensory, motor and limbic positive symptoms. *Brain* **119**:363–375. doi:10.1093/brain/119.2.363

Jo S, Yarishkin O, Hwang YJ, Chun YE, Park M, Woo DH, Bae JY, Kim T, Lee J, Chun H, Park HJ, Lee DY, Hong J, Kim HY, Oh SJ, Park SJ, Lee H, Yoon BE, Kim Y, Jeong Y, Shim I, Bae YC, Cho J, Kowall NW, Ryu H, Hwang E, Kim D, Lee CJ. 2014. GABA from reactive astrocytes impairs memory in mouse models of Alzheimer's disease. *Nat Med* **20**:886–896. doi:10.1038/nm.3639

Kastanenka K V., Moreno-Bote R, De Pittà M, Perea G, Eraso-Pichot A, Masgrau R, Poskanzer KE, Galea E. 2019. A roadmap to integrate astrocytes into Systems Neuroscience. *Glia* 1–22. doi:10.1002/glia.23632

Kelley KW, Nakao-Inoue H, Molofsky A V., Oldham MC. 2018. Variation among intact tissue samples reveals the core transcriptional features of human CNS cell classes. *Nat Neurosci* **21**:1171–1184. doi:10.1038/s41593-018-0216-z

Khakh BS, Sofroniew M V. 2015. Diversity of astrocyte functions and phenotypes in neural circuits. *Nat Neurosci* **18**:942–952. doi:10.1038/nn.4043

Kwak H, Koh W, Kim Sangwoo, Song K, Shin JI, Lee JM, Lee EH, Bae JY, Ha GE, Oh JE, Park YM, Kim Sunpil, Feng J, Lee SE, Choi JW, Kim KH, Kim YS, Woo J, Lee D, Son T, Kwon SW, Park KD, Yoon BE, Lee J, Li Y, Lee H, Bae YC, Lee CJ, Cheong E. 2020. Astrocytes Control Sensory Acuity via Tonic Inhibition in the Thalamus. *Neuron* **108**:691-706.e10.

doi:10.1016/j.neuron.2020.08.013

Liddelow SA, Guttenplan KA, Clarke LE, Bennett FC, Bohlen CJ, Schirmer L, Bennett ML, Münch AE, Chung W-S, Peterson TC, Wilton DK, Frouin A, Napier BA, Panicker N, Kumar M, Buckwalter MS, Rowitch DH, Dawson VL, Dawson TM, Stevens B, Barres BA. 2017. Neurotoxic reactive astrocytes are induced by activated microglia. *Nature* **541**:481–487. doi:10.1038/nature21029

Lui H, Zhang J, Makinson SR, Cahill MK, Kelley KW, Huang HY, Shang Y, Oldham MC, Martens LH, Gao F, Coppola G, Sloan SA, Hsieh CL, Kim CC, Bigio EH, Weintraub S, Mesulam MM, Rademakers R, MacKenzie IR, Seeley WW, Karydas A, Miller BL, Borroni B, Ghidoni R, Farese R V., Paz JT, Barres BA, Huang EJ. 2016. Progranulin Deficiency Promotes Circuit-Specific Synaptic Pruning by Microglia via Complement Activation. *Cell* **165**:921–935. doi:10.1016/j.cell.2016.04.001

Mederos S, Perea G. 2019. GABAergic-astrocyte signaling: A refinement of inhibitory brain networks. *Glia* 1842–1851. doi:10.1002/glia.23644

Morquette P, Verdier D, Kadala A, Féthière J, Philippe AG, Robitaille R, Kolta A. 2015. An astrocyte-dependent mechanism for neuronal rhythmogenesis. *Nat Neurosci* **18**:844–854. doi:10.1038/nn.4013

Necula D, Cho FS, He A, Paz JT. 2021. Secondary thalamic neuroinflammation after focal cortical stroke and traumatic injury mirrors corticothalamic functional connectivity. *J Comp Neurol*. doi:10.1002/cne.25259

Ortinski PI, Dong J, Mungenast A, Yue C, Takano H, Watson DJ, Haydon PG, Coulter DA. 2010. Selective induction of astrocytic gliosis generates deficits in neuronal inhibition. *Nat Neurosci* **13**:584–91. doi:10.1038/nn.2535

Pappata S, Levasseur M, Gunn RN, Myers R, Crouzel C, Syrota A, Jones T, Kreutzberg GW, Banati RB. 2000. Thalamic microglial activation in ischemic stroke detected in vivo by PET and [(11)C]PK11195. *Neurology* **55**:1052–1054. doi:10.1212/WNL.55.7.1052

Patel DC, Tewari BP, Chaunsali L, Sontheimer H. 2019. Neuron–glia interactions in the pathophysiology of epilepsy. *Nat Rev Neurosci* **20**:282–297. doi:10.1038/s41583-019-0126-4

Paz JT, Christian CA, Parada I, Prince DA, Huguenard JR. 2010. Focal Cortical Infarcts Alter Intrinsic Excitability and Synaptic Excitation in the Reticular Thalamic Nucleus. *J Neurosci* **30**:5465–5479. doi:10.1523/JNEUROSCI.5083-09.2010

Paz JT, Davidson TJ, Frechette ES, Delord B, Parada I, Peng K, Deisseroth K, Huguenard JR. 2013. Closed-loop optogenetic control of thalamus as a tool for interrupting seizures after cortical injury. *Nat Neurosci* **16**:64–70. doi:10.1038/nn.3269

Poskanzer KE, Yuste R. 2016. Astrocytes regulate cortical state switching in vivo. *Proc Natl Acad Sci U S A* **2016**:1–10. doi:10.1073/pnas.1520759113

Ribot J, Breton R, Calvo CF, Moulard J, Ezan P, Zapata J, Samama K, Moreau M, Bemelmans AP, Sabatet V, Dingli F, Loew D, Milleret C, Billuart P, Dallérac G, Rouach N. 2021. Astrocytes close the mouse critical period for visual plasticity. *Science* **373**:77–81. doi:10.1126/science.abf5273

Robel S, Buckingham SC, Boni JL, Campbell SL, Danbolt NC, Riedemann T, Sutor B, Sontheimer H. 2015. Reactive Astrogliosis Causes the Development of Spontaneous Seizures. *J Neurosci* **35**:3330–3345. doi:10.1523/JNEUROSCI.1574-14.2015

Robel S, Sontheimer H. 2016. Glia as drivers of abnormal neuronal activity. *Nat Neurosci* **19**:28–33. doi:10.1038/nn.4184

Roux L, Madar A, Lacroix MM, Yi C, Benchenane K, Giaume C. 2015. Astroglial Connexin 43 Hemichannels Modulate Olfactory Bulb Slow Oscillations. *J Neurosci* **35**:15339–52. doi:10.1523/JNEUROSCI.0861-15.2015

Schafer DP, Lehrman EK, Kautzman AG, Koyama R, Mardinly AR, Yamasaki R, Ransohoff RM, Greenberg ME, Barres BA, Stevens B. 2012. Microglia Sculpt Postnatal Neural Circuits in an Activity and Complement-Dependent Manner. *Neuron* **74**. doi:10.1016/j.neuron.2012.03.026

Singh SK, Stogsdill JA, Pulimood NS, Dingsdale H, Kim YH, Pilaz LJ, Kim IH, Manhaes AC, Rodrigues WS, Pamukcu A, Enustun E, Ertuz Z, Scheiffele P, Soderling SH, Silver DL, Ji RR, Medina AE, Eroglu C. 2016. Astrocytes Assemble Thalamocortical Synapses by Bridging NRX1α and NL1 via Hevin. *Cell* **164**:183–196. doi:10.1016/j.cell.2015.11.034

Soreq L, Rose J, Soreq E, Hardy J, Trabzuni D, Cookson MR, Smith C, Ryten M, Patani R, Ule J. 2017. Major Shifts in Glial Regional Identity Are a Transcriptional Hallmark of Human Brain Aging. *Cell Rep* **18**:557–570. doi:10.1016/j.celrep.2016.12.011

Steriade M, Contreras D, Amzica F, Timofeev I. 1996. Synchronization of fast (30-40 Hz) spontaneous oscillations in intrathalamic and thalamocortical networks. *J Neurosci* **16**:2788–2808. doi:10.1523/jneurosci.16-08-02788.1996

Steriade M, McCormick DA, Sejnowski TJ. 1993. Thalamocortical oscillations in the sleeping and aroused brain. *Science* **262**:679–85. doi:10.1126/science.8235588

Sun D, Jakobs TC. 2012. Structural remodeling of astrocytes in the injured CNS. *Neuroscientist* **18**:567–588. doi:10.1177/1073858411423441

Vainchtein ID, Chin G, Cho FS, Kelley KW, Miller JG, Chien EC, Liddelow SA, Nguyen PT, Nakao-inoue H, Dorman LC, Akil O, Joshita S, Barres BA, Paz JT, Molofsky AB, Molofsky

A V. 2018. Astrocyte-derived interleukin-33 promotes microglial synapse engulfment and neural circuit development. *Science* **359**:1269–1273.

Vezzani A, Balosso S, Ravizza T. 2019. Neuroinflammatory pathways as treatment targets and biomarkers in epilepsy. *Nat Rev Neurol* **15**:459–472. doi:10.1038/s41582-019-0217-x

Zamanian J, Xu L, Foo L, Nouri N, Zhou L, Giffard R, Barres B. 2012. Genomic Analysis of Reactive Astrogliosis. *J Neurosci* **32**:6391–6410. doi:10.1523/JNEUROSCI.6221-11.2012.Genomic

Chapter 2 : Convergence of thalamic mechanisms in genetic epilepsies

Abstract:

The thalamus, a deep brain structure with broad connectivity, is endowed with intrinsic and synaptic properties enabling its ability to generate rhythmic activity. Thalamic rhythmogenesis is critical in regulating brain states related to sleep and consciousness. One of the most common pathologies associated with disrupted thalamic rhythmogenesis is epileptic seizures associated with altered consciousness. In this chapter, we first describe key structural, synaptic, cellular, and biophysical elements underlying the rhythmogenic properties of the thalamus, and then describe how diverse perturbations of these properties in rodent genetic models ultimately generate or facilitate seizures. We briefly highlight recent studies which have identified mechanisms of thalamic involvement in the development or modulation of epilepsies acquired following incidents such as traumatic brain injury and ischemic stroke. Understanding how diverse etiologies converge upon thalamic hyperexcitability can pinpoint elements of vulnerability, resilience, redundancy, necessity, and sufficiency in the thalamo-cortico-thalamic circuit. Understanding how the thalamus generates and modulates aberrant activity—even when it is not the primary or sole site of genetic perturbation—will be key to identifying therapeutic targets and paradigms to treat epilepsies. Such efforts will benefit from continued advancements in our knowledge of cell-type heterogeneity, meso- and macro-scale connectivity, and interspecies differences in the thalamus.

2.1. Introduction

The thalamus, a subcortical diencephalic structure involved in sleep, arousal, consciousness, and cognition, has been a site of investigation in seizures since the 1940s, starting with experimental studies in cats and monkeys by Dempsey, Morison, Jasper, and Droogleever-Fortuyn. These studies showed that intralaminar stimulation evoked bilateral 3-Hz spike-and-wave discharges and behavioral arrest (reviewed by Jasper, 1948, 1991). In 1950, the first depth recordings in the thalamus during *petit mal* seizures (now known as "absence seizures") were obtained from patients with absence type epilepsy (Spiegel and Wycis, 1950), and subsequent studies of thalamic activity during seizures supported the hypothesis that *"the clinical case of petit mal epilepsy is due to a disturbance in the thalamus which causes a rhythmic discharge throughout the cortex"* (Williams, 1953). While there has been a debate on whether the seizures initiate in cortex or thalamus, thalamic firing has indeed been found necessary to maintain absence seizures in rodents (Sorokin et al., 2017). The study of epileptic discharges, in both patients and animal models, has yielded basic insights about thalamic organization and function. Reciprocally, advances in our understanding of thalamic structure and function have elucidated mechanisms of the generation and propagation of epileptic activity such as spike-wave discharges underlying absence seizures, and has opened avenues for the therapeutic modulation of seizures.

Endowed with extensive, reciprocal connections with the entire cerebral cortex and other subcortical structures (Jones, 1985), and possessing rhythmogenic properties (reviewed by Fogerson and Huguenard, 2016), the thalamus plays a critical role in the generation of normal and pathological synchronized oscillatory activity (Steriade et al., 1993). Decades of research have revealed disruptions in thalamocortical excitability and synchrony as a convergence point for epileptic activity related to multiple genetic etiologies and pharmacological manipulations. More

recently, cell-type specific optogenetic tools have enabled causal manipulations of rodent thalamocortical synapses and circuits, demonstrating a role for the thalamus as a "choke-point" in certain forms of seizures and epilepsies (Paz et al., 2013; reviewed by Paz and Huguenard, 2015). Indeed, deep brain stimulation of the anterior thalamus is an FDA-approved treatment for refractory focal epilepsy (reviewed by Fisher and Velasco, 2014).

By understanding exactly which aspects of thalamic function are vulnerable—or resilient—to disruptions, we can clarify strategies to effectively interfere with seizure expression while minimizing side effects. In this chapter, we describe the key anatomical, structural, cellular, and biophysical elements of the thalamus which confer its rhythmogenic properties. We then provide a brief overview of the extensive literature on genetic rodent models of seizures, with particular emphasis on the diverse role of calcium channels in absence seizures and compensatory changes in the thalamocortical network. Finally, we briefly discuss recent work highlighting thalamic involvement in the development or modulation of epilepsies acquired after brain injuries.

2.2. Thalamic organization and rhythmogenesis

The thalamus is composed of various nuclei embedded in diverse, multi-regional neural circuits, whose complexity and detailed connectivity are not yet fully understood (reviewed by Halassa and Sherman, 2019; Shepherd and Yamawaki, 2021). Given the widespread connectivity between thalamus and the entire cerebral cortex, the thalamus is well-positioned to control the generation and maintenance of cortical rhythms. Furthermore, the thalamus is notable for its generation and maintenance of synchronous oscillatory activity (reviewed by Steriade, McCormick and Sejnowski, 1993; Huguenard and McCormick, 2007; Beenhakker and Huguenard, 2009; Crunelli and Hughes, 2010; Fogerson and Huguenard, 2016). Such network oscillations are considered

critical substrates of states of arousal, sleep, and consciousness (reviewed by Steriade and Llinas, 1988; Steriade, McCormick and Sejnowski, 1993; McCormick and Bal, 1997; Crunelli et al., 2018).

Three cardinal rhythms of the thalamus include delta, spindles, and slow-wave oscillations, all of which occur during non-rapid eye movement (NREM) sleep (reviewed by Crunelli and Hughes, 2010; Fogerson and Huguenard, 2016; Fernandez and Lüthi, 2020). We will describe them in Section 2.6. Key features of the thalamus which enable the generation of these synchronous rhythms include cell-intrinsic firing properties, microcircuit connectivity (i.e. local connectivity between neighboring neurons), long-range connections with distal brain regions like the cerebral cortex and basal ganglia (reviewed by Deschênes, Veinante and Zhang, 1998; Jones, 2007; Paz et al., 2007; Charpier, Beurrier and Paz, 2010), and the precise timing of synaptic inputs (reviewed by Huguenard and McCormick, 2007). The cellular and circuit properties underlying the generation and regulation of these oscillations can subserve aberrant oscillations underlying epileptic seizures, and will therefore be reviewed in the following sections. Thalamic connectivity with basal ganglia will not be reviewed in this chapter (for review, see Charpier et al., 2010; Paz et al., 2005)

2.3. Structural elements of thalamic and thalamo-cortico-thalamic circuits: from gross anatomy to cell types

The multiple nuclei of the thalamus are each embedded in reciprocal microcircuits (i.e. between thalamic relay nuclei and the reticular thalamic nucleus) or long-range thalamo-cortico-thalamic circuits (i.e. between thalamic relay nuclei and cortex) (**Fig. 2.1**).

The reticular thalamic nucleus (abbreviated nRT for *nucleus reticularis thalami*) is a thin shell of GABAergic neurons which surrounds the lateral boundary of dorsal thalamocortical (TC) relay nuclei (Houser et al., 1980; Pinault, 2004). nRT neurons form reciprocal connections with glutamatergic neurons in thalamic relay nuclei (Guillery and Sherman, 2002; Jones, 1975; Sherman and Guillery, 1996) and receive corticothalamic (CT) collateral afferents; thus, the nRT provides both feedback and feedforward inhibition in the thalamus, and critically shapes net thalamic output (reviewed by Pinault, 2004; Paz and Huguenard, 2015; Halassa and Acsády, 2016; Crabtree, 2018) (**Fig. 1.1**). Approximately 10-25% of synapses in the nRT are GABAergic (Liu and Jones, 1999; Williamson et al., 1993). There is histological and ultrastructural evidence that the nRT receives GABAergic input from the external segment of the globus pallidus in squirrel monkeys (Asanuma, 1994), the substantia nigra pars reticulata in cats (Paré et al., 1990), the basal forebrain and mesopontine tegmentum in rats (Jourdain et al., 1989), and notably, from the nRT itself in cats, rats and mice (Clemente-Perez et al., 2017; Houser et al., 1980; Liu and Jones, 1999; Pinault et al., 1995). However, the existence of functional, GABAergic synapses between nRT neurons is debated (discussed below).

The majority of thalamic territory is occupied by various thalamic relay nuclei, which earned the term "relay" due to their well-studied role in transmitting afferent sensory information to other brain regions. Other than the nRT, sources of GABAergic inhibition in thalamic relay nuclei include the zona incerta, anterior pretectal nucleus, basal ganglia (including substantia nigra pars reticulata, internal globus pallidus, ventral pallidum), and the pontine reticular formation, which are well described elsewhere (reviewed by Halassa and Acsády, 2016). Based on their primary afferent source, thalamic relay nuclei are broadly organized into first-order and higher-order nuclei. First-order nuclei receive sensor-specific driving input from subcortical sources,

while higher-order nuclei receive driving input from the cortex (reviewed by Halassa and Sherman, 2019). Based on their input-output connectivity, thalamic relay nuclei can also be broadly organized into sensory, limbic, motor, and executive/cognitive domains, which are preserved along the thalamo-cortico-reticular pathway (Sherman and Guillery, 1996; Jones, 2007; also see recent studies, e.g. Harris *et al.*, 2019; Phillips *et al.*, 2019). The vast majority of neurons in thalamic relay nuclei are glutamatergic and are called "thalamocortical" (TC) neurons because they form reciprocal, long-range, excitatory and topographic connections with cortical neurons. For example, key aspects of visual information processing involve TC neurons in the dorsal lateral geniculate nucleus (dLGN), which receive retinal input, project to primary visual cortex (V1), and receive corticothalamic input from V1; in addition, dLGN neurons form reciprocal connections with the GABAergic neurons of the nRT, which also receive corticothalamic input from V1 (Sherman and Guillery, 1996). Similarly, key aspects of somatosensory information processing involve TC neurons from the ventrobasal nucleus (VB), which receive input from the spinothalamic tract and medial lemniscus (Mo et al., 2017), project to primary somatosensory cortex (S1), and receive corticothalamic input from S1; in addition, VB neurons form reciprocal connections with the GABAergic neurons of the nRT, which also receive corticothalamic input from S1 (Deschênes et al., 1998; Jones, 2009) (**Fig. 1.1**). The somatosensory VB-S1-nRT circuit is one of the most well-characterized circuits in the context of basic intrinsic and synaptic properties, and in rodent models of seizures and epilepsy (discussed below).

To understand the cellular basis of thalamocortical rhythmic activity, it is important to understand the relevant cell types and their connectivity (i.e. microcircuit motifs). Thalamo-cortico-thalamic circuits consist of multiple key cell types, including glutamatergic TC relay neurons in thalamic relay nuclei, glutamatergic corticothalamic (CT) neurons, primarily in cortical

layers 5 and 6, and GABAergic neurons in the nRT (**Fig. 2.1B**) (Deschênes et al., 1998; Shepherd and Yamawaki, 2021). Although there is increasing appreciation of cell-type heterogeneity among these populations (Clemente-Perez et al., 2017; Li et al., 2020; Martinez-Garcia et al., 2020; Phillips et al., 2019), the basic organization of the following microcircuit motifs in the thalamus is generally accepted (reviewed by Paz and Huguenard, 2015):

Thalamo-cortico-thalamic motifs:

- ***Recurrent excitation****: formed by reciprocal glutamatergic projections; prominent in cortical networks*
- ***Feed-forward inhibition****: disynaptic component, whereby excitatory inputs recruit local inhibition en route to its recipient; can effectively modulate strength of the efferent signal*

Intra-thalamic motifs:

- ***Feed-back inhibition****: reciprocally connected glutamatergic and GABAergic neurons; an inhibitory mechanism to control local excitatory activity*
- ***Counter-inhibition****: reciprocally connected GABAergic neurons*

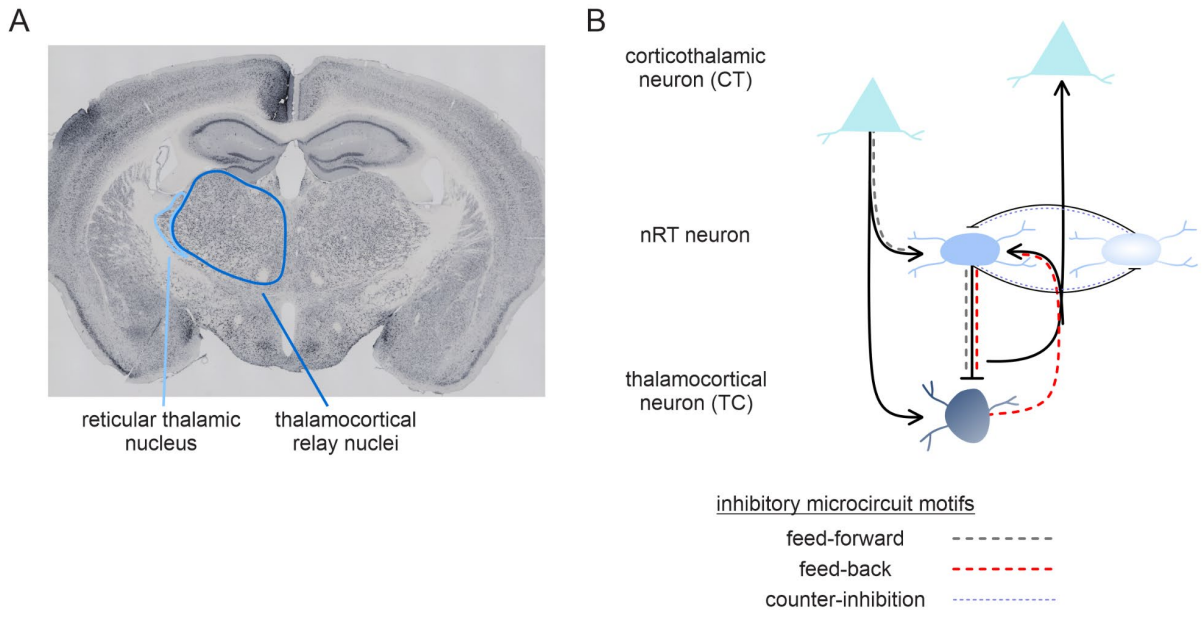

Figure 2.1. Basic structural elements of thalamic and thalamo-cortico-thalamic circuits.

(A) Coronal section of mouse brain labeled with the neuronal nuclear protein NeuN. Colored regions highlight the reticular thalamic nucleus (known as nRT, for *nucleus reticularis thalami*) and thalamocortical relay nuclei. **(B)** Schematic of thalamo-cortico-thalamic circuit highlighting microcircuit motifs, especially intra-nRT and feed-forward inhibition.

In addition to distinct cell-type specific connectivity patterns, these microcircuits also have distinct layer-specific connectivity patterns (Halassa and Sherman, 2019; Shepherd and Yamawaki, 2021). For example, in first-order thalamic relay nuclei such as the dLGN and VB, TC neurons send long-range glutamatergic projections to related cortical regions in a topographic manner, primarily in layer 4 (Deschênes et al., 1998; Jones, 2007). Layer 6 CT neurons send long-range glutamatergic projections to TC neurons, and also form glutamatergic collaterals onto nRT which enable feedforward inhibition of TC neurons (Jones, 2007; Sherman, 2007).

Functional connections between nRT neurons, which form a reciprocal counter-inhibition microcircuit, introduce a distinct set of principles into the framework of thalamic function in health

and disease (Crabtree, 2018; Huntsman et al., 1999; Makinson et al., 2017; Paz and Huguenard, 2015; Sohal and Huguenard, 2003). Gap junction-coupled intra-nRT electrical synapses have been consistently demonstrated by multiple groups (Deleuze and Huguenard, 2006; Landisman et al., 2002; Long et al., 2004). However, the existence of intra-nRT chemical GABAergic synapses has been a subject of controversy (reviewed by Paz and Huguenard, 2015; Crabtree, 2018), with multiple electrophysiological studies suggesting their existence and functionality in rats, mice, and ferrets (Deleuze and Huguenard, 2006; Makinson et al., 2017; Shu and McCormick, 2002), and others failing to find them (Cruikshank et al., 2010; Hou et al., 2016; Parker et al., 2009). Nevertheless, in this chapter we refer to several studies which highlight the relevance of intra-nRT connections for thalamic circuit synchrony.

Disruptions in these microcircuit motifs may lead to thalamic hyperexcitability and seizures. For example, the *Gria4*$^{-/-}$ mouse model of absence epilepsy exhibits a specific and selective deficit of the excitatory cortico-nRT pathway (Paz et al., 2011). With the resulting loss of feed-forward inhibition of TC cells via the excitatory cortico-nRT pathway (which normally balances direct cortico-TC excitation), TC cells activated by corticothalamic excitation become hyperexcitable, paving the way for the generation of pathological oscillations (Paz et al., 2011). As another example, in mice lacking the $GABA_A$ receptor β3 subunit, a selective loss of $GABA_AR$-mediated inhibition in reciprocally connected nRT neurons leads to dramatic thalamic hypersynchrony in slices, highlighting the de-synchronizing role of counter-inhibition within the nRT (Huntsman et al., 1999; Sohal et al., 2000; Sohal and Huguenard, 2003). This role is further supported by the observation that selective loss of the voltage-gated sodium channel *Scn8a* in nRT neurons, which leads to loss of intra-nRT, but not nRT-TC, inhibition, causes mice to develop spontaneous absence seizures (Makinson et al., 2017).

2.4. Thalamic firing

TC and nRT neurons are generally thought to exhibit two distinct firing modes: tonic firing in response to depolarization (Jahnsen and Llinás, 1984), and burst firing (in response to hyperpolarization, or depolarization in nRT) (Steriade and Llinas, 1988; Huguenard, 1996; Sherman, 2001; however, see Wolfart *et al.*, 2005). During states of arousal (e.g. wake), thalamic neurons are relatively depolarized and exhibit "tonic" firing of action potentials at low frequencies; such tonic firing is proposed to be involved in sensory information processing (Sherman, 2007; Swadlow et al., 2002). During states of low arousal (e.g. sleep), thalamic neurons are relatively hyperpolarized and exhibit high-frequency bursts of action potentials. Burst firing can occur periodically through both cell-intrinsic and circuit mechanisms (as described in Section 2.6), it is a critical building block of thalamic oscillations (Beenhakker and Huguenard, 2009; Fogerson and Huguenard, 2016; Llinás and Steriade, 2006). T-type voltage-gated calcium channels (subtypes Cav3.1, Cav3.2, and Cav3.3) are crucial elements of burst firing in thalamic neurons and are described in detail in Section 2.5.

Oscillatory burst firing is a critical substrate of sleep. It is abolished in the nRT neurons of Cav3.3$^{-/-}$ mice, whereas tonic firing is not, according to *ex vivo* whole-cell patch clamp recordings (Astori et al., 2011). Lack of Cav3.3-mediated oscillatory bursting results in a selective reduction of the sleep-associated sigma frequency band power during NREM where sleep spindles occur. Thus, Cav3.3-mediated burst firing has been proposed to be the predominant pacemaker underlying sleep spindles in the thalamus (Astori et al., 2011).

Burst firing is also a critical substrate of thalamic seizures, because of its involvement in spike-and-wave discharges (SWD). Generalized SWDs are hallmarks of absence seizures (reviewed by Crunelli and Leresche, 2002; Blumenfeld, 2005; Tenney and Glauser, 2013;

Fogerson and Huguenard, 2016). The electroencephalographic (EEG) features of SWDs are bilateral, high-amplitude events composed of stereotyped spike-and-wave signatures which typically occur at 3-4.5 Hz in humans and 6-10 Hz in rodents (reviewed by Crunelli and Leresche, 2002; Tenney and Glauser, 2013; Fogerson and Huguenard, 2016). Multi-unit recordings have shown that TC, CT, and cortical neurons exhibit synchronous burst-firing, time-locked to the "spike" component of the SWD *in vivo* in rats and mice (Inoue et al., 1993; Sorokin et al., 2017); at the intracellular level, TC and nRT neurons exhibit burst firing correlated with the "spike" component of the SWD in *vivo* in rats (Paz et al., 2007; Slaght et al., 2002).

Recent studies have provided further compelling evidence for the role of thalamic burst firing in seizures (reviewed by Huguenard, 2019). Sorokin and colleagues expressed a stable step-function opsin (Yizhar et al., 2011) in VB TC neurons of Wistar Albino Glaxo from Rijswijk (WAG/Rij) rats and stargazer mice—rodent models of absence epilepsy (Sorokin et al., 2017)—which enabled them to switch the firing mode of TC cells between tonic and burst mode. They found that toggling the firing from bursting to tonic mode stopped ongoing absence seizures. Stable step-function opsins have also been used to demonstrate the role of TC bursting in atypical, non-convulsive seizures observed in a mouse model of Dravet Syndrome—seizures that have been found in human patients (Ritter-Makinson et al., 2019). Thus, there is strong evidence for the role of thalamic neuronal population bursting in the maintenance of non-convulsive seizures (Sorokin et al., 2017). Consistent with these findings, in a different rodent model of absence epilepsy—the Genetic Absence Epilepsy Rat from Strasbourg (GAERS), McCafferty and colleagues have found that the output of TC neurons during absence seizures is strong and rhythmic even though burst firing in each TC cell is infrequent, suggesting that bursting in each TC cell is not required for maintaining the seizure (McCafferty et al., 2018). In contrast, burst firing in nRT neurons is very

robust during absence seizures and likely serves to synchronize the TC output to the cortex (McCafferty et al., 2018; Slaght et al., 2002).

Ultimately, the thalamocortical network dynamics underlying seizures is likely an emergent property of both cell-intrinsic mechanisms (e.g. T-type mediated burst firing) and circuit properties (e.g. cortical feed-forward inhibition of the thalamus). Nevertheless, given that disruptions to firing mode can alter thalamic synchrony in ways that can lead to seizures, and that thalamic synchrony depends in part on T-type calcium channels, we next provide an overview of the key enabler of thalamic switching in firing mode: the low-threshold T-type calcium channel.

2.5. Calcium channels and thalamic firing

2.5.1. Calcium channels

Voltage-gated calcium channels (VGCCs) are widely expressed throughout the mammalian body and brain (reviewed by Catterall, 2000), and support numerous critical functions including cellular excitability, synaptic transmission, and synaptic plasticity (reviewed by Catterall and Few, 2008) (**Fig. 2.2**). VGCCs are organized into two main classes, distinguished by their biophysical properties: high-voltage activated (HVA) VGCCs, which include L-type, N-type, and P/Q-type channels (Nowycky et al., 1985; Rajakulendran et al., 2012), and low-voltage activated (LVA) VGCCs, which include T-type calcium channels (Perez-Reyes, 2003); R-type channels are considered to have intermediate properties (Randall and Tsien, 1997; Soong et al., 1993) and are discussed further in Section 2.7. VGCCs are composed of four or five distinct subunits, including a pore-forming α1 subunit (of which there are three families, Cav1, Cav2, Cav3), a transmembrane complex of α2 and δ subunits, an intracellular β subunit, and in some cases a transmembrane γ subunit (Catterall, 2000). Because the α1 subunit contains the conduction pore, voltage sensors,

gating mechanisms, and most of the known sites of channel regulation, its family and subtype typically correlate with whether the calcium channel is of the HVA or LVA type (Catterall and Few, 2008). Here we provide an overview of LVA T-type calcium channels, given their prominent role in thalamic bursting rhythmogenesis (which we will describe in Section 2.6). The role of HVA R and P/Q-type calcium channels in seizures will be discussed in Section 2.7.

2.5.2. Spotlight on T-type calcium channels and burst firing

T-type calcium channels are critical determinants of thalamic neuron electrophysiology (Huguenard, 1996). In addition to their activation at low voltages, T-type calcium channels have unique inactivation properties (time-dependent inactivation, steady-state inactivation, and recovery from inactivation), as well as lower conductance (thus resulting in transient and "tiny" currents), compared to HVA VGCCs. Thus, currents generated by T-type calcium channels (referred to as I_T, or T-type current) are uniquely positioned to regulate cellular excitability and firing pattern, particularly near the resting membrane potential in neurons with robust burst firing behaviors (discussed further in Section 2.6).

In TC neurons at resting membrane potential (between -60 to -65 mV), the majority of T-type calcium channels are in an inactivated state. Hyperpolarization (to at least -70mV) enables de-inactivation, and subsequent depolarization leads to activation which allows a transient influx of Ca^{2+} and generates the low-threshold spike (LTS), also known as the rebound plateau potential. The LTS further depolarizes the membrane potential such that voltage-gated sodium channels generate action potentials, culminating in a barrage of rebound high-frequency burst firing. At this point, T-type calcium channels are inactivated (reviewed by Cheong and Shin, 2013; Fogerson and

Huguenard, 2016). The sequence of events that underlies oscillatory activity is summarized in **Figure 2.3** and discussed further in section 2.6.2 in various pathophysiological contexts.

2.5.3. Spatial distribution of T-type calcium channel subunits

The α1 subunit of T-type calcium channels are encoded by the Ca_V3 family, which consists of 3 subtypes which are differentially expressed in the brain. Within the rodent thalamus, channels containing $Ca_V3.1$ (encoded by *Cacna1g*) are the primary source of T-type calcium channels in TC neurons. nRT neurons primarily express the $Ca_V3.3$-containing T-type calcium channel (encoded by *Cacna1i)* and to a lesser extent, $Ca_V3.2$-containing T-type channel calcium (encoded by *Cacna1h*) (Joksovic et al., 2006; Talley et al., 1999) (**Fig. 2.2**). Differences among the 3 subtypes of T-type calcium channels include inactivation kinetics and recovery from steady-state inactivation. Because inactivation influences the ability of T-type calcium channels to trigger a LTS, the expression pattern and subcellular localization of subtypes are important considerations for thalamic electrophysiological properties. T-type channels are prominently expressed in the soma and dendrites. In rodent TC neurons, electrophysiological, immunohistochemical, and computational models have found that $Ca_V3.1$ is prominently expressed in the soma and dendrites as well. While the distribution along the dendritic axis remains debated (e.g. Destexhe *et al.*, 1998; Parajuli *et al.*, 2010), it is a particularly interesting question given that the spatial distribution should shape the interaction of synaptic inputs, burst generation, and downstream calcium-mediated signaling pathways (e.g. Cueni *et al.*, 2008; Crandall, Govindaiah and Cox, 2010).

TC neurons mainly express $Ca_V3.1$-containing channels, which recover from inactivation the fastest out of the three subtypes (reviewed by Cheong and Shin, 2013). nRT neurons mainly express $Ca_V3.3$-containing channels, which display relatively slow inactivation and are nearly

voltage-independent (Huguenard and Prince, 1992). This results in longer calcium-dependent spike bursts generated in nRT, which translates into longer bouts of GABA release onto TC neurons. Thus, the difference in inactivation kinetics critically determines the precise timing and rhythmicity of the intra-thalamic oscillations.

The rich literature in this field is well-described in other reviews (reviewed by Crunelli, Cope and Hughes, 2006; Cheong and Shin, 2013; Fogerson and Huguenard, 2016). In the future, increased specificity of genetic manipulations and increased sampling capacity of recording techniques may lead to a more definitive understanding of the combinations of calcium channel subtypes in distinct cell types that are necessary and sufficient for the expression of various rhythmic oscillations.

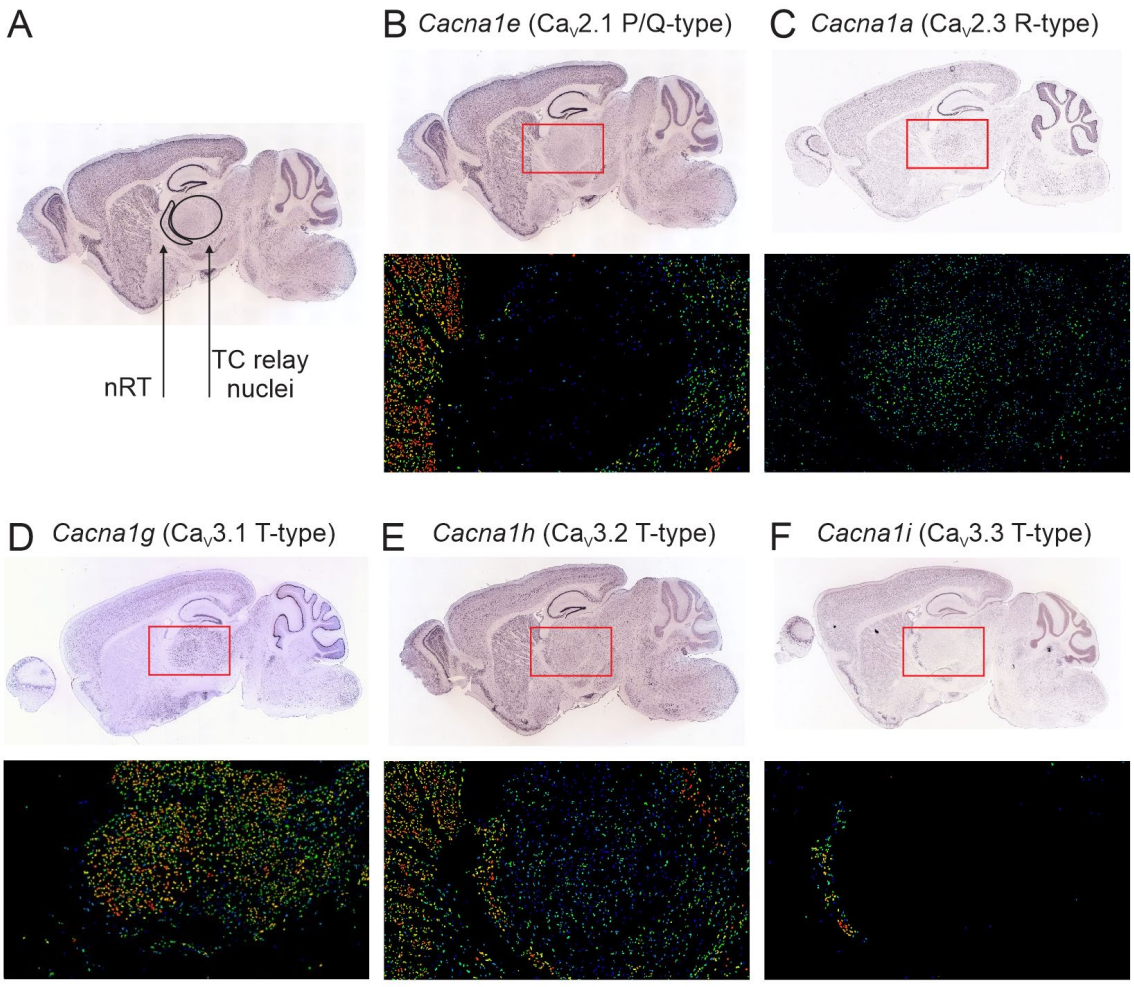

Figure 2.2. $Ca_V3.1$ and $Ca_V3.3$ are the dominant T-type calcium channel subunits expressed in TC relay nuclei and in the nRT.

(A) Sagittal section of mouse brain indicating location of the nRT and TC relay nuclei (labels are not drawn to scale). All images obtained from the Allen Brain Atlas (https://mouse.brain-map.org/search/index). **(B-C)** Top: in-situ hybridization of mRNA probes against the α1 subunit of high-voltage activated P/Q and R-type calcium channels. Bottom: fluorescent expression in magnified region (red box) to highlight the relative expression in nRT and TC relay nuclei. Staining intensity should not be compared across subunits, which were performed as different experiments; however, regional heterogeneity of subunit expression can be appreciated in each section. **(D-F)** Same as in B-C, but for three α1 subunits types of low-voltage activated T-type calcium channels. Note the selective expression of *Cacna1i* (encoding the $Ca_V3.3$ T-type subunit) in the nRT, and lack of expression of *Cacna1g* (encoding the $Ca_V3.1$ T-type subunit) in the nRT. All images (A-F) obtained from the Allen Brain Atlas, as described in (Lein et al., 2007).

2.6. Rhythmogenesis in the thalamus: adaptive and maladaptive mechanisms

Thalamic circuits play key roles in local and global oscillations (reviewed by Huguenard and McCormick, 2007; Fogerson and Huguenard, 2016; Crunelli *et al.*, 2018). Three cardinal rhythms of the thalamus during NREM sleep include delta (1-4 Hz), spindles (7-15 Hz), and slow-wave oscillations (<1 Hz). Recent work has also unveiled the thalamic involvement in alpha waves (8-13 Hz) (Hughes et al., 2011) and gamma oscillations (30-90 Hz) (Hoseini et al., 2021), which will not be addressed in this chapter. We have already highlighted how burst firing is mediated by T-type calcium channels (Section 2.5). Below we discuss how these channels, along with cellular and circuit properties of the thalamus, enable the generation of delta, spindles, and slow-wave rhythms, and what disruptions in these circuits can hijack these rhythms and contribute to seizures.

2.6.1. Delta oscillations

TC relay neurons display intrinsic pacemaker activity in the 1-4 Hz frequency range; this frequency band, referred to as delta, is associated with deep sleep (i.e. stage 3 NREM) and anesthesia (Brown et al., 2010).

Cell-intrinsic mechanisms: This pacemaker activity arises from an intrinsic interplay between two currents generated by the low-threshold T-type calcium channel (I_T) and the hyperpolarization-activated cyclic nucleotide-gated (HCN) (I_h) (Destexhe et al., 1996; McCormick and Pape, 1990; Nuñez et al., 1992; Soltesz et al., 1991) (**Fig. 2.3**). Upon sufficient membrane hyperpolarization, I_T is de-inactivated and I_h is activated. I_h is a slowly-developing, non-inactivating inward current which has a depolarizing effect. I_h depolarization of the membrane activates I_T and triggers an LTS, which further depolarizes the membrane and triggers Na^+-dependent action potentials. The

depolarization associated with the LTS deactivates I_h; in the absence of I_h activation, the membrane hyperpolarizes, which then re-activates I_h and de-inactivates I_T, and the cycle continues.

Synaptic mechanisms: Synchronization of this autonomously generated delta-frequency membrane oscillation is thought to be mediated by cortico-TC and cortico-nRT-TC feedforward inhibition during cortical UP states (Neske, 2016; Steriade et al., 1991). The extent to which (and the mechanisms whereby) this local thalamic delta-frequency oscillation contributes to global delta waves observed in the EEG during NREM sleep has been an active area of research. Global $Ca_V3.1^{-/-}$ mice lack delta waves at the EEG level (Lee et al., 2004), at least in part due to the loss of burst firing in TC neurons (Kim et al., 2001). Recent studies employing optogenetic and chemogenetic techniques have suggested that the nRT is capable of modulating delta waves in spatially restricted regions of the rodent cortex (Fernandez et al., 2018; Lewis et al., 2015).

Pro-epileptic mechanisms: Disruption of calcium channels appears to be a common node of dysfunction across various genetic models of absence seizures. T-type calcium channels have been the most widely studied calcium channels in absence epilepsy, and the diverse ways in which I_T has been linked to absence seizures are discussed further in Section 2.7.2. The disruption of I_h in the thalamus can also promote thalamic hyperexcitability and seizures. For instance, deletion of HCN2, an I_h subunit prominently expressed in both the thalamic relay nuclei and the nRT (Notomi and Shigemoto, 2004), leads to spontaneous absence seizures in mice. Although I_h plays a key role in pacemaker bursting activity, the loss of I_h in TC neurons in these models can still lead to seizures because it can lead to hyperpolarization of TC neurons, which in turn facilitates the de-inactivation of T-type calcium channels and burst firing (Chung et al., 2009; Ludwig et al., 2003). Interestingly,

deletion of the tetratricopeptide-repeat-containing Rab8b-interaction protein (TRIP8b), an auxiliary subunit of HCN channels expressed in TC and CT neurons but not in nRT neurons, results in a milder absence seizure phenotype (Heuermann et al., 2016). Thus, preservation of I_h in the nRT of TRIP8b$^{-/-}$ mice appears to partially constrain the heightened excitability of the thalamocortical circuit due to the loss of I_h in TC neurons. This property is reminiscent of the apparent ability of nRT I_h to constrain cortico-nRT synaptic integration in normal contexts (Ying et al., 2007), and suggests that I_h in the nRT confers partial resilience to hyperexcitability in the circuit.

Thalamic I_h can also be disrupted in the context of epileptogenesis. In a rodent model of post-stroke epilepsy, whereby stroke in the S1 cortex leads to secondary injury in the VB thalamus, TC neurons exhibited alterations in the biophysical properties of I_h, such as depolarized half-activation voltage (Paz et al., 2013). Biophysical modeling demonstrated that these changes in I_h were sufficient to enhance thalamic network oscillations, and optogenetic inhibition of these hyperexcitable TC neurons was sufficient to abort epileptic seizures (Paz et al., 2013).

Finally, I_h in TC neurons has also been reported to be increased, rather than decreased, in two different rat models of absence epilepsy (Cain et al., 2015; Kanyshkova et al., 2012). Perhaps a noteworthy commonality across several of these models featuring I_h disruption (in which I_h is abolished in both TC and nRT, I_h is abolished in TC, or I_h exhibits depolarized half-activation) is that they result in seizures which appear to have slower internal frequencies than typical absence seizures observed in rodents. While typical rodent SWDs are 6-10 Hz (Fogerson and Huguenard, 2016) and generally faster than typical human SWDs which are 3-4.5 Hz (Tenney and Glauser, 2013), the mice described above exhibited SWDs in the range of 5 Hz (HCN2$^{-/-}$ mice), 5.3$\pm$1.7 Hz

(Trip8b$^{-/-}$ mice), and 4-5 Hz (post-stroke epilepsy rats) (Chung et al., 2009; Heuermann et al., 2016; Ludwig et al., 2003; Paz et al., 2013).

2.6.2. Spindle oscillations

Spindle oscillations (7-15 Hz), a global rhythmic signature of stage 2 NREM sleep, emerge in the intrathalamic circuit as a result of recurrently connected TC and nRT neurons, which exhibit alternating bouts of rebound burst firing (Fernandez and Lüthi, 2020; Llinás and Steriade, 2006).

Cell-intrinsic mechanisms: nRT neurons exhibit intrinsic rhythmicity in the spindle frequency range (7-15 Hz), which can be maintained for up to 1 second following release from hyperpolarization (von Krosigk et al., 1993). This intrinsic oscillation in nRT arises from the interplay of I_T and Ca^{2+}-dependent small-conductance-type 2 potassium channels (SK2 channels) (Cueni et al., 2008; Köhler et al., 1996; Wimmer et al., 2012), similar to the interplay of I_T and I_h which gives rise to the intrinsic delta oscillation in TC neurons described above. Ca^{2+} influx through the $Ca_v3.3$ subtype (the main T-type calcium channel in nRT) activates the SK2 channel-mediated K^+ current (I_{SK}), which generates a slow afterhyperpolarization (AHP) following the LTS burst. The slow AHP allows the de-inactivation of I_T, and thus the cycle of repetitive burst firing continues (Cueni et al., 2008) (**Fig. 2.3**). Another key contributor is the $Ca_v3.2$ R-type calcium channel, which has been proposed to enable prolonged elevation of Ca^{2+} required for induction of the slow AHP, which in turn is critical for allowing the continued oscillatory bursting in nRT (Paz and Huguenard, 2012; Zaman et al., 2011).

Synaptic mechanisms: During a spindle oscillation, rhythmic firing of nRT neurons triggers a transient burst of IPSPs in reciprocally connected TC neurons. The barrage of IPSPs, mediated by both $GABA_A$ and $GABA_B$ receptors, transiently hyperpolarizes TC neurons such that I_T is de-inactivated. Upon release of inhibition from nRT, TC neurons fire LTS-mediated rebound bursts, which in turn re-excite nRT neurons and initiate another nRT burst (Fogerson and Huguenard, 2016; Huguenard and Prince, 1994a) (**Fig. 2.3**). The precise timing of this interplay is influenced by the duration of the IPSPs (governed by the relative expression of $GABA_A$ vs. $GABA_B$ receptors in the recipient TC neurons), as well as the kinetics of the LTS (governed by the T-type calcium channel subtype expressed in each cell type). Optogenetic activation of nRT neurons can drive spindles and spindle-like oscillations (Halassa et al., 2011; Barthó et al., 2014; Fernandez et al., 2018); however, a causal role of the nRT in naturally occurring spindles has yet to be established.

Pro-epileptic mechanisms: The relationship between spindle oscillations and SWDs is an unresolved debate (reviewed by Beenhakker and Huguenard, 2009; Leresche et al., 2012). Recent studies have provided support for the hypothesis that spindles can be hijacked into epileptiform activity. Children with childhood epilepsy with centrotemporal spikes (the most common focal epilepsy syndrome) exhibit transient, sleep-activated focal deficits in spindles (Kramer et al., 2021). Using high-density EEGs during sleep and cognitive testing, the authors found an inverse relationship between spike and spindle rate during NREM sleep. In addition, they found that spindle rate predicted performance on cognitive tasks. These findings provide compelling support for the hypothesis that the same underlying thalamocortical circuit can give rise to spindles and epileptic activity (Beenhakker and Huguenard, 2009), as well as underlie seizures and cognitive dysfunction (Kramer et al., 2021).

Further support for the shared circuit hypothesis comes from a recent study of a rodent model of thalamocortical dysfunction following mild traumatic brain injury (TBI) (Holden et al., 2021). Unilateral injury in the primary somatosensory cortex led to chronic secondary damage of the thalamus, including loss of nRT neurons and a selective deficit in nRT synaptic function, but not in CT and TC neuronal functions. These mice develop epileptic spikes and exhibit a loss in sleep spindles; both changes were focal to the S1 cortex ipsilateral to injury (Holden et al., 2021).

2.6.3. Slow oscillations

Finally, thalamic circuits can also generate a slow oscillation (<1 Hz) (reviewed by Crunelli and Hughes, 2010; Neske, 2016; Crunelli et al., 2018), although it was traditionally considered to be exclusively generated in cortical networks (Steriade et al., 1993). The slow rhythm, present in almost all NREM stages, has been proposed to organize periods of sleep spindles and delta waves (Crunelli and Hughes, 2010). Both TC and nRT neurons have been shown to play an active role in shaping the slow rhythm during sleep. In TC neurons, the slow oscillation arises from the interplay of I_T and the leak K^+ current, and is influenced by Ca^{2+}-activated nonselective cation (CAN) current and mGluR1a activation (Hughes et al., 2002). In nRT neurons, the slow oscillation arises from I_T and I_h, as well as being influenced by the CAN current, a Ca^{2+}-activated K^+ current, and a Na^+-activated K^+ current (Blethyn et al., 2006).

Pro-epileptic mechanisms: Pathological slow oscillations such as the slow spike-and-wave discharges (1.5-2.5 Hz) are observed in certain epilepsies such as Lennox-Gastaut Syndrome (Steriade and Amzica, 2003), but the mechanisms that lead to these remain largely unknown.

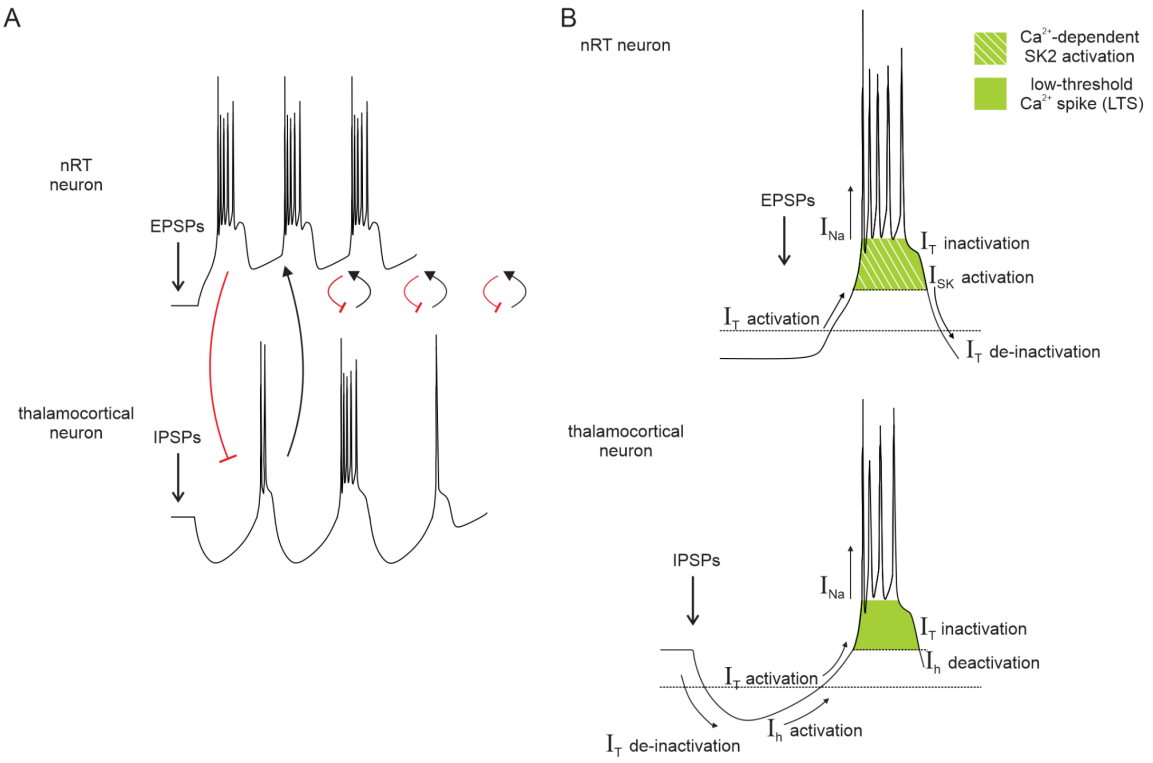

Figure 2.3. Cell-intrinsic and synaptic properties enabling thalamic burst firing and rhythmogenesis.

(A) Schematic of the interplay between nRT and TC neurons, which gives rise to rhythmic activity in the intra-thalamic circuit such as spindle oscillations (described further in Section 2.6.2). Cortical EPSPs arrive at an nRT neuron (top), resulting in a high-frequency burst of action potentials. Rhythmic firing of nRT neurons triggers a transient burst of IPSPs in reciprocally connected TC neurons. The barrage of IPSPs, mediated by both $GABA_A$ and $GABA_B$ receptors, transiently hyperpolarizes TC neurons such that I_T is de-inactivated. Upon release of inhibition from nRT, TC neurons fire LTS-mediated rebound bursts, which in turn re-excite nRT neurons and initiate another nRT burst (reviewed by Fogerson and Huguenard, 2016). **(B)** Mechanisms of burst firing in nRT (Top) and TC (Bottom) neurons. Top: nRT neurons exhibit intrinsic rhythmicity in the spindle frequency range which arises from the interplay of I_T and I_{SK} (described further in Section 2.6.2). In this schematic, the resting membrane potential of nRT neurons is hyperpolarized below the activation threshold of I_T (dotted horizontal line); thus, upon receiving excitatory synaptic input, sufficient levels of $Ca_v3.3$ are available to be activated, and I_T mediates an LTS. Ca^{2+} influx through $Ca_v3.3$ activates I_{SK}, which leads to a slow AHP which allows the de-inactivation of I_T. Thus, the cycle of repetitive burst firing continues (not shown). Bottom: TC neurons exhibit pacemaker activity in the delta frequency range which arises from an intrinsic interplay between I_T and I_h (described further in Section 2.6.1). Abbreviations: E/IPSPs (excitatory/inhibitory postsynaptic potentials); TC (thalamocortical neuron); nRT (reticular thalamic neuron); I_T (current mediated by T-type Ca^{2+} channels); I_{SK} (current mediated by Ca^{2+}-dependent small-conductance-type 2 potassium (SK2) channels); I_h (current mediated by

hyperpolarization-activated cyclic nucleotide-gated (HCN) channels); LTS (low-threshold calcium spike); AHP (afterhyperpolarization).

2.7. The thalamus in absence epilepsy and beyond

There is a growing appreciation of the genetic determinants underlying a number of epilepsies linked to thalamic dysfunction. For instance, Childhood Absence Epilepsy (CAE) has been linked with multiple susceptibility loci and polymorphisms in genes encoding voltage-gated calcium channels and GABA receptors, which will be discussed below.

Another epileptic condition also associated with aberrant thalamocortical network activity is Lennox-Gastaut Syndrome (LGS), a severe childhood epileptic encephalopathy characterized by multiple seizure types (Scheffer et al., 2017). Although LGS was not traditionally recognized as having a genetic etiology, recent advances in whole-exome sequencing have identified genetic variations in LGS patients, including loci encoding voltage-gated calcium channels (Yang et al., 2021). In LGS, epileptic activity is detected both in the cortex and in the centromedian thalamic nucleus, during generalized paroxysmal fast activity and slow spike-and-wave (1-2 Hz) epileptic discharges (Dalic et al., 2020; Velasco et al., 1991; Warren et al., 2020). Notably, high-frequency deep brain stimulation of the centromedian thalamus has been shown to alleviate seizure frequency in some LGS patients (Fisher and Velasco, 2014; Velasco et al., 2006; Warren et al., 2020), confirming the importance of the thalamus in this disorder.

In the case of Dravet Syndrome, a severe myoclonic epilepsy of infancy and epileptic encephalopathy with a known monogenic mutation in *SCN1A* (Claes et al., 2001; Dravet, 2011) (further described in Section 2.7.4), a small but notable clinical study has implicated the potential modulatory role of the thalamus: deep brain stimulation of the centromedian thalamus resulted in seizure reduction in one of two patients with Dravet Syndrome (Andrade et al., 2010).

In this section, we will discuss findings from rodent models of genetic epilepsies and highlight the diversity of etiologies which feature some extent of disruption to thalamic firing and connectivity (reviewed by Beenhakker and Huguenard, 2009; Cheong and Shin, 2013; Maheshwari and Noebels, 2014; Paz and Huguenard, 2015; Fogerson and Huguenard, 2016; Gobbo, Scheller and Kirchhoff, 2021). In particular, we will highlight disruptions of the rhythmogenic machinery in thalamic neurons in two epilepsies: CAE, for which there is an abundance of evidence for thalamic involvement, and Dravet Syndrome, for which there exists limited but convincing evidence for thalamic involvement. Understanding how various genetic etiologies converge upon a similar phenotype can pinpoint elements of vulnerability, resilience, redundancy, necessity, and sufficiency in the thalamocortical circuit, and help enumerate strategies to intervene, prevent, or compensate for epileptic activity.

2.7.1. Insights from human genetic studies of absence epilepsy

The role of the thalamus in epilepsy has been best-characterized in the context of typical absence seizures (formerly known as *petit mal* seizures), which occur in several idiopathic generalized epilepsies such as CAE and juvenile epilepsies (Scheffer et al., 2017). Absence seizures are characterized by generalized SWDs which occur alongside abrupt behavioral arrest and partial or complete loss of consciousness. SWDs consist of stereotyped spike-and-wave signatures which occur at 3-10 Hz, depending on the species (generally, 6-10 Hz in rodents, and 3-4.5 Hz in humans; (reviewed by Crunelli and Leresche, 2002; Blumenfeld, 2005; Tenney and Glauser, 2013; Fogerson and Huguenard, 2016), typically lasts 2-30 seconds, and occur frequently (few to several hundreds of times a day (Panayiotopoulos, 2008). SWDs are bilateral, high-amplitude waveforms,

easily detected by cortical EEG, and are well-understood to reflect an aberrant, hypersynchronous thalamocortical network.

CAE includes a group of genetically determined epilepsies—some of which show strong familial inheritance and incomplete penetrance—with SWDs being inherited as an autosomal-dominant feature (Crunelli and Leresche, 2002). Numerous susceptibility loci and polymorphisms with various extents of linkage to CAE have been identified (reviewed by Crunelli and Leresche, 2002; Maheshwari and Noebels, 2014), and the evidence indicates that absence epilepsies are complex polygenic disorders. CAE-associated mutations have been identified in genes encoding for voltage-gated calcium channel subunits such as *CACNA1A, CACNA1G, CACNA1H, and CACNG3,* some of which are described further in Section 2.7.3 (Chen et al., 2003; Everett et al., 2007; Jouvenceau et al., 2001; Liang et al., 2006). Human genetic studies of CAE identified mutations in genes that encode GABA receptor subunits, including *GABRG2* (Baulac et al., 2001; Wallace et al., 2001), *GABRA1, and GABRB3* (reviewed by Cheong and Shin, 2013).

While genetic mutations identified in human patients typically inform the design of preclinical disease models, in some cases, the identification of genetic mutations in humans has provided powerful support for mechanisms of seizure generation previously identified from genetic and pharmacological models in rodents *in vivo* and *ex vivo.* For example, the pro-epileptic effects of the mutation in the *GABRB2* gene identified in human patients, which abolished benzodiazepine-induced potentiation of GABA currents when expressed in a heterologous cell system (Wallace et al., 2001) was consistent with the previously identified anti-oscillatory mechanism of clonazepam—a benzodiazepine anti-epileptic drug used to treat absence seizures (Farrello, 1986)—in rodent *ex vivo* thalamic slices wherein inadequate endogenous $GABA_AR$-

mediated inhibition of nRT neurons leads to strengthening of the synchronizing nRT-TC output (Huguenard, 1999; Huguenard and Prince, 1994b).

Absence epilepsies are rarely monogenic disorders, and variants in a given gene may not all lead to aberrant function. Thus, it is critical to understand how single-nucleotide polymorphisms (SNP) identified within the same locus give rise to epileptic cells and circuits. For example, Vitko and colleagues carried out a functional characterization of 12 SNPs found in the *CACANA1* ($Ca_V3.2$) locus of CAE patients in a heterologous cell system, then used computational modeling to understand the impact of various SNPs on T-type calcium channel function; interestingly, some, but not all, SNPs were predicted to increase burst firing propensity (Vitko et al., 2005). Such efforts will only be facilitated by the increased access to whole-exome sequencing and patient-derived induced pluripotent stem cell platforms, and will aid in the development of precision therapies for patients with epilepsy (Klassen et al., 2011; Noebels, 2017).

2.7.2. T-type calcium channels in genetic models of absence epilepsy

Basic science and epilepsy research alike have been advanced by rodent models carrying monogenic mutations in genes encoding voltage-gated calcium channels, GABA receptors, and glutamate receptors subunits associated with absence epilepsy (reviewed by Maheshwari and Noebels, 2014). Such rodent models have provided a fertile foundation for the investigation of the thalamus's contribution to aberrant oscillations, in some cases at the level of specific synapses (e.g. Paz et al., 2011).

For thalamic neurons, I_T critically determines the coordinated rhythmic bursting between TC and nRT neurons (described in Section 2.2.6). Unsurprisingly, aberrant calcium channel function—and subsequent changes to cellular and circuit excitability and/or firing—often leads to

thalamic hyperexcitability and seizures. Aberrant T-type calcium channel function can arise from a mutation in a channel subunit, a compensatory reaction, and/or the interaction of multiple susceptibility variants. Here, we **review diverse ways in which T-type calcium channels have been linked to absence seizures.**

Two of the three T-type calcium channel subtypes have been linked to absence epilepsy in human genetic studies: gain-of-function polymorphisms in the *CACNA1H* gene (encoding $Ca_V3.2$) to sporadic CAE, and functional polymorphisms in the *CACNA1G* gene (encoding CaV3.1) to juvenile absence syndromes (reviewed by Maheshwari and Noebels, 2014). Similarly, enhanced T-type calcium channel function—and subsequently, enhanced burst firing—in thalamic neurons seems to be a common feature across multiple rodent models of absence epilepsies. For instance, nRT neurons in GAERS rats display elevated amplitude of I_T (Tsakiridou et al., 1995) and increased $Ca_V3.2$ mRNA (Talley et al., 2000), owing to a gain-of-function point mutation in *Cacna1h* (Powell et al., 2009). And $Ca_V3.1^{-/-}$ mice—in which burst firing, but not tonic firing, is abolished in TC neurons—are resistant to SWDs induced by baclofen ($GABA_BR$ agonist) and gamma-hydroxybutyrate (Kim et al., 2001). Accordingly, overexpression of $Ca_V3.1$ results in increased T-type calcium currents in TC neurons (although rebound burst firing was not measured) and spontaneous, ethosuximide-sensitive absence seizures (Ernst et al., 2009). The latter two did not investigate the nRT, because it expressed very low levels of endogenous and exogenous $Ca_V3.1$. Nevertheless, we cannot rule out the possibility that nRT neurons made post-translational compensatory changes in T-type calcium channels in these conditions.

Even when T-type calcium channels are not directly affected by mutations, they appear to be critical components of spontaneous absence seizures in genetically determined rodent models. Across several inbred mouse strains exhibiting absence epilepsy and ataxia, spontaneous mutations

have been identified in various subunits of P/Q-type calcium channels (e.g. $Ca_V2.1/\alpha1A$ subunit in *tottering* mice; β4 subunit in *lethargic* mice; and γ2 subunit in *stargazer* mice; (reviewed by Maheshwari and Noebels, 2014); notably, the mutation in *Cacna1a* was identified in *tottering* mice prior to the first discovery of a mutation in the human *CACNA1A* gene in cases of CAE (Fletcher et al., 1996; Jouvenceau et al., 2001). Interestingly, in *tottering, lethargic,* and *stargazer* mice with mutations in P/Q-type calcium channels, T-type calcium channels exhibit compensatory changes in their electrophysiological properties despite no changes in mRNA expression of their α1 subunits (Zhang et al., 2002). In particular, whole-cell recordings of TC neurons in thalamic slice preparations demonstrated increased peak current density and depolarized shifts in the steady-state inactivation curve (i.e. increased availability of T-type calcium channel availability upon activation threshold) (Zhang et al., 2002). Although I_T properties of nRT neurons were not assessed, the changes observed in TC neurons were hypothesized to favor the enhanced cellular excitability, rhythmic bursting, and overall propensity to generate SWDs observed in these mice. Indeed, a later study cross-bed these P/Q-channel-deficient mice with T-channel-deficient mice and provided compelling evidence that T-type $Ca_V3.1/\alpha1G$ is a crucial component of the absence seizure phenotype in these mice: when harboring double null mutations in both $Ca_V2.1/\alpha1A$ and $Ca_V3.1/\alpha1G$ subunits, TC neurons are depleted of I_T and these mice displayed no SWDs (Song et al., 2004). Yet another example are the HCN2-deficient mice which exhibit spontaneous absence seizures (Ludwig et al., 2003). TC neurons in $HCN2^{-/-}$ mice exhibit a complete loss of I_h, which leads to TC neuron hyperpolarization, which facilitates T-type calcium channel de-inactivation and therefore facilitates burst firing; *ex vivo* thalamic slices exhibited hypersynchronous oscillatory activity which was blocked by a T-type calcium channel inhibitor (Ludwig et al., 2003). Finally, ethosuximide, a T-type calcium channel antagonist, reduces absence seizures in GAERS rats

(Polack and Charpier, 2009). Altogether, these studies provide strong support for the critical role of T-type calcium channels in absence seizures.

Nonetheless, several studies have called into question the extent to which I_T-mediated burst firing in various components of single TC versus nRT cells is necessary for the generation of absence seizures (reviewed by Crunelli and Leresche, 2002; Cheong and Shin, 2013; Maheshwari and Noebels, 2014). For example, in GAERS rats and in a pharmacological model of absence seizures, McCafferty and colleagues have reported infrequent burst firing in TC neurons during absence seizures but an increased burst firing in nRT neurons (McCafferty et al., 2018). They suggested that despite the rare burst firing of TC neurons, overall thalamic output (i.e. shaped by both TC and nRT) remained strong and rhythmic during seizures (McCafferty et al., 2018). An alternative interpretation is that it is I_T-mediated burst firing in the nRT neurons, and not the TC neurons, that is critical to the expression of absence seizures in these rat models. On the other hand, Lee and colleagues have reported that burst firing in nRT neurons is not essential for pharmacologically-induced absence seizures in mice (Lee et al., 2014). Mice harboring double mutations of $Ca_V3.2$ and $Ca_V3.3$ displayed enhanced pharmacologically-induced SWDs despite the complete abolishment of nRT burst firing; the authors attributed the SWD susceptibility to an increase in nRT tonic firing (Lee et al., 2014). In spite of these controversies, there is abundant evidence for the powerful role of T-type calcium channels—and their disruptions—in mediating thalamic hyperexcitability and SWDs, as discussed above.

2.7.3. R-type and P/Q-type channels in genetic models of absence epilepsy

Although T-type calcium channels have sustained the most attention in the study of thalamic rhythms and seizures in the past decades, the role of R-type and P/Q-type calcium channels in

thalamic hypersynchrony and hyperexcitability cannot be discounted. Loss-of-function mutations in *CACNA1A* (encoding the Cav2.1 subunit of P/Q-type channels) have been identified in CAE (Jouvenceau et al., 2001). In addition, de novo pathogenic variants in *CACNA1E* (encoding the Cav2.3 subunit of R-type channels) have recently been identified in patients with developmental and epileptic encephalopathies (Helbig et al., 2018). Although these patients were not reported to exhibit absence seizures, the Cav2.3 subunit is highly expressed in nRT neurons (Soong et al., 1993; Weiergräber et al., 2006), and has recently been shown to play an important role in oscillatory burst firing of the nRT and in pharmacologically-induced SWDs (Paz and Huguenard, 2012; Zaman et al., 2011). R-type calcium channels are structurally similar to HVA calcium channels, yet exhibit electrophysiological properties closer to T-type calcium channels; a critical difference however, is that R-type channels are activated at higher thresholds than T-type channels (Randall and Tsien, 1997; Soong et al., 1993). In nRT neurons of Cav2.3$^{-/-}$ mice, or nRT neurons of WT mice in the presence of SNX-482 (a specific blocker of R-type channels), reduced AHP rendered them unable to generate oscillatory bursts. Notably, genetic deletion or pharmacological blockade of R-type channels promoted resilience to gamma-hydroxybutyrate-induced SWDs in mice, suggesting that nRT oscillatory bursts, enabled by R-type mediated-AHP, are critical for generation of SWDs (Zaman et al., 2011).

P/Q-type channels are widely expressed throughout the central nervous system but especially abundant in presynaptic terminals in Purkinje and granule cells of the cerebellum. Unlike post-synaptic T-type calcium channels which play a major role in shaping firing properties, HVA P/Q-type channels are primarily involved in coupling calcium influx to neurotransmitter release in presynaptic terminals (reviewed by Rajakulendran, Kaski and Hanna, 2012). Loss-of-function mutations in various subunits of P/Q-type channels lead to absence epilepsy, in some

cases accompanied by ataxia (Noebels, 2012); the enhancement of T-type channel function in mice harboring these mutations was described earlier (Section 2.7.2). Investigations of rodent absence models harboring P/Q-type loss-of-function mutations have highlighted another source of vulnerability at the synaptic level: an incomplete overlap of P/Q-type subunit family members across the brain (Noebels, 2012). Different brain regions have distinct patterns of β1-4 subunit expression; thus, P/Q-type calcium channel composition, and thus function, is differentially affected. One of the earliest demonstrations of "subunit reshuffling" (a compensatory process) was in lethargic mice, which exhibit SWDs and ataxia (Burgess et al., 1999). In the cerebellum of lethargic mice, in the absence of the β4 subunit, there is increased steady-state association of the α1A subunit with β2 and β3 subunits instead; these complexes generate functional P/Q-type channel, with normal amplitude and voltage-dependence of the P-type current in dissociated cerebellar Purkinje neurons (Burgess et al., 1999). Interestingly, thalamic nuclei appear to lack significant expression of β1 and β3 subunits, thus decreasing the chance that the α1A subunit can form a functional heteromer in the absence of a functional β4 subunit (Noebels, 2012).

Thus, selective deficits or compensations at specific synapses may arise from regulatory subunit "reshuffling." In addition, cell-type specific alternative splicing of various subunits may also explain resilience and vulnerability (Noebels, 2012).

2.7.4. SK channels and thalamic bursting in Dravet Syndrome

Dravet Syndrome is a childhood epileptic encephalopathy associated with severe non-convulsive seizures and sudden unexplained death in epilepsy. It is caused by loss of function mutations in the *SCN1A* gene encoding the type I voltage-gated sodium channel (Claes et al., 2001; Dravet, 2011; Han et al., 2020). In mouse models of Dravet Syndrome, cortical inhibitory neurons exhibit

reduced excitability, consistent with a loss of function in a channel critical for action potential generation and propagation (Rubinstein et al., 2015). Specific inactivation of *Scn1a* in parvalbumin-positive interneurons in the hippocampus and cortex increases seizure susceptibility (Dutton et al., 2013). Hypoexcitability of parvalbumin-positive cortical interneurons has been reported to normalize in adulthood in mouse models, suggesting there may be other mechanisms which explain the ongoing, chronic epilepsy in Dravet Syndrome (Favero et al., 2018). Recent work by our group has uncovered a surprising role for thalamic bursting in Dravet Syndrome.

Given that *Scn1a* is highly expressed in parvalbumin-positive nRT cells, our group investigated thalamic firing in the *Scn1a*-deficient mouse model of Dravet Syndrome (Ritter-Makinson et al., 2019). We found that GABAergic nRT neurons—but not glutamatergic TC neurons—exhibited heightened intrinsic excitability, most notably in the form of augmented rebound burst firing. Interestingly, enhanced nRT rebound burst firing was due to a compensatory reduction in the calcium-activated small potassium current (I_{SK}) density rather than an enhancement of the low-threshold T-type calcium current. While nRT neurons also exhibited changes expected from *Scn1a* loss-of-function such as depolarized action potential threshold and increased action potential width, nRT neurons fired more action potentials in response to depolarization. This finding was in contrast to the decreased excitability of cortical inhibitory neurons described in previous studies. Moreover, reducing SK conductance, but not the sodium conductance, in a biophysical model was sufficient to generate enhanced rebound bursts as observed in nRT neurons. As a consequence of SK-deficit mediated augmentation of nRT burst firing, mice exhibited thalamic microcircuit hyperexcitability, an *ex vivo* hallmark of seizures involving the thalamus (reviewed by Cho et al., 2017). Finally, treatment with an SK channel agonist (1-ethyl-2-benzimidazolinone, or EBIO) was sufficient to reduce the frequency of non-

convulsive seizures in Dravet Syndrome mice. Altogether, we propose that *Scn1a* loss-of-function results in a compensatory reduction of I_{SK} in nRT neurons, which contributes to enhanced input resistance and intrinsic excitability, and increased rebound burst firing. Augmented burst firing in nRT neurons recruits stronger oscillatory bursting in the intra-thalamic circuit, which maintains non-convulsive seizures (Ritter-Makinson et al., 2019).

This study demonstrated a novel role for the thalamus in a type of non-convulsive seizures observed in human patients. It also points to a novel role for SK2 channels (a normal component of nRT rhythmicity; (Cueni et al., 2008)), and raises questions about how this compensatory mechanism arises from a *Scn1a* loss of function mutation. Importantly, by tapping into the rhythmogenic machinery of thalamic neurons, this study identified the nRT as a potential novel therapeutic target to treat non-convulsive seizures in Dravet Syndrome.

2.8. The emerging role of the thalamus in acquired epilepsies

While the thalamus has been well-studied in the context of genetic epilepsies, there is also an increasing appreciation of thalamic involvement in acquired epilepsies such as those that develop after acute insults and in mesial temporal lobe epilepsies. Following cortical injuries such as traumatic brain injury and stroke, the thalamus sustains robust and chronic secondary damage including neurodegeneration and neuroinflammation in humans (Grossman and Inglese, 2016; Pappata et al., 2000; Scott et al., 2015) and in rodent models (Cao et al., 2020; Hazra et al., 2014; Holden et al., 2021; Necula et al., 2021; Paz et al., 2010). Thalamic damage has gained increasing recognition as a prognostic biomarker of post-traumatic epileptogenesis (PTE) in rodent models (Immonen et al., 2013; Manninen et al., 2021; Paz et al., 2010; Pitkänen et al., 2021), and has also been suggested as a biomarker of cognitive impairment after TBI in patients (Grossman et al.,

2012; Ramlackhansingh et al., 2011). Despite being remote from the initial epileptogenic insult, the thalamus can modulate seizure activity in rodent models of PTE (Paz et al., 2013; Paz and Huguenard, 2015), and is the only FDA-approved brain region for deep brain stimulation in patients with refractory temporal lobe epilepsy (Fisher and Velasco, 2014).

Neuroinflammation, commonly implicated in epileptogenesis, has been notoriously challenging to dissect and target effectively (reviewed by Aronica *et al.*, 2017; Klein *et al.*, 2018; Patel *et al.*, 2019; Vezzani, Balosso and Ravizza, 2019). The extent to which neuroinflammation—specifically in the thalamus—can drive epileptogenic changes following injuries, and whether it can be a disease-modifying target in the context of PTE, is an active field of investigation.

Our group recently conducted a systematic study of secondary thalamic inflammation across four distinct thalamocortical circuits in two rodent models of cortical lesions and found that secondary thalamic neuroinflammation mirrors functional connectivity of thalamocortical circuits (Necula et al., 2021). Such investigations, coupled with open access to large-scale anatomical and functional connectivity atlases—e.g. the Allen Mouse Brain Connectivity Atlas (Harris et al., 2019), the Janelia MouseLight project (Winnubst et al., 2019), and the Allen Brain Observatory (Siegle et al., 2021)—may help start to elucidate potential "rules" by which secondary neuroinflammation evolves after cortical injuries.

Neuroinflammation following stroke or TBI colocalizes with robust changes in cellular and circuit properties of the thalamus. In rodents, cortical stroke and TBI both lead to thalamic circuit hyperexcitability and thalamocortical epileptic discharges (Holden et al., 2021; Paz et al., 2013, 2010). Our group recently identified the C1q complement pathway as a mediator of the chronic emergence of epileptic activity and sleep disruption after mild TBI in mice (Holden et al., 2021), highlighting the feasibility and promise of targeting thalamic neuroinflammation to prevent circuit

dysfunction after injuries. Altogether, thalamic neuroinflammation appears to be a meaningful hallmark of chronic changes implicated in epileptogenesis. Whether neuronal-glial interactions in the secondarily damaged thalamus can drive such pathology is investigated in **Chapter 4**.

2.9. Conclusions

In summary, we have reviewed evidence of pro-epileptic disruptions in thalamic and thalamocortical circuits, and propose that the thalamus as a key convergence point of dysfunction in genetic epilepsies. Understanding how the thalamus generates and modulates aberrant activity will aid in the identification of therapeutic targets and paradigms to treat epilepsies.

What aspects of thalamic organization and function predisposes the thalamus to vulnerability? The thalamus generates **vigorous rhythmic burst firing at the cellular and microcircuit levels,** and the mechanics underlying such firing appears to be **vulnerable to genetic perturbations**. However, whether that means they can just as easily be "corrected", without equally debilitating off-target effects, remains to be seen.

Cell-intrinsic vulnerabilities: We reviewed diverse ways in which T-type calcium channels, as well as R-type and P/Q-type channels, have been linked to absence seizures, including mutations which lead to direct or compensatory increases in the magnitude of I_T, or to changes in channel subunit expression and composition. We particularly highlighted the abundant evidence that **burst firing properties of thalamic neurons appear to be a common node of dysfunction** across genetic models of epilepsies. One novel and notable example is the identification of a compensatory reduction of the SK current and subsequent increase of nRT burst firing in a *Scn1a* loss-of-function mouse model of Dravet Syndrome (Ritter-Makinson et al., 2019). The finding that

pharmacological augmentation of the SK current reduced the severity of non-convulsive seizures suggests that restoring burst firing, even when it may not be the sole or primary electrophysiological disruption, can be potentially beneficial in modulating seizures.

Micro-circuit vulnerabilities: We also reviewed the diverse ways in which disruptions to feed-forward inhibition and counter-inhibition increase the propensity of thalamic circuits to become hypersynchronous and hyperexcitable. Further investigations of what mediates selective vulnerability of specific synapses, and whether restoration of unperturbed microcircuit functions can compensate for pro-epileptic changes, will undoubtedly be fruitful in identifying therapeutic strategies to prevent and treat seizures.

Are there similar vulnerabilities in the thalamocortical circuit across genetic and acquired epilepsies and what are they? Thalamic damage after cortical injuries has recently emerged as a biomarker of PTE. Due to its broad connectivity, focal and even remote damage to the thalamus is well-positioned to mediate disruptions in "bystander" circuits which are not immediately involved in seizure dynamics. Thus, recent advances in our understanding of thalamic organization and function in various psychiatric and cognitive conditions (e.g. Krol et al., 2018)—which can often be comorbidities of seizures—may be harnessed to understand and modulate the potentially far-reaching role (beyond seizure activity) of the thalamus in acquired epilepsies. Ultimately, if the thalamus is indeed an "Achilles' heel"—a critical node of dysfunction—in the context of epilepsy, then understanding how diverse genetic and acquired etiologies converge upon thalamic hyperexcitability will pinpoint elements that contribute to its vulnerability as well as those that contribute to its resilience.

Acknowledgments: J.T.P. is supported by NIH/NINDS grant R01NS096369, the Department of Defense (EP150038), and the Gladstone Institutes. F.S.C. is supported by NINDS F31 NS111819-01A1. The authors would like to thank Drs. Francoise Chanut and Kathryn Claiborn for editorial assistance. F.S.C. would also like to thank Dr. Tilo Gschwind for constructive feedback and insightful discussions.

References

Andrade DM, Hamani C, Lozano AM, Wennberg RA. 2010. Dravet syndrome and deep brain stimulation: Seizure control after 10 years of treatment. *Epilepsia* **51**:1314–1316. doi:10.1111/j.1528-1167.2009.02408.x

Aronica E, Bauer S, Bozzi Y, Caleo M, Dingledine R, Gorter JA, Henshall DC, Kaufer D, Koh S, Löscher W, Louboutin JP, Mishto M, Norwood BA, Palma E, Poulter MO, Terrone G, Vezzani A, Kaminski RM. 2017. Neuroinflammatory targets and treatments for epilepsy validated in experimental models. *Epilepsia* **58**:27–38. doi:10.1111/epi.13783

Asanuma C. 1994. GABAergic and pallidal terminals in the thalamic reticular nucleus of squirrel monkeys. *Exp Brain Res* **101**:439–451. doi:10.1007/BF00227337

Astori S, Wimmer RD, Prosser HM, Corti C, Corsi M, Liaudet N, Volterra A, Franken P, Adelman JP, Lüthi A. 2011. The Ca v3.3 calcium channel is the major sleep spindle pacemaker in thalamus. *Proc Natl Acad Sci U S A* **108**:13823–13828. doi:10.1073/pnas.1105115108

Barthó P, Slézia A, Mátyás F, Faradzs-Zade L, Ulbert I, Harris KD, Acsády L. 2014. Ongoing network state controls the length of sleep spindles via inhibitory activity [SUPP]. *Neuron* **82**:1367–1379. doi:10.1016/j.neuron.2014.04.046

Baulac S, Huberfeld G, Gourfinkel-An I, Mitropoulou G, Beranger A, Prud'homme JF, Baulac M, Brice A, Bruzzone R, LeGuern E. 2001. First genetic evidence of GABAA receptor dysfunction in epilepsy: A mutation in the γ2-subunit gene. *Nat Genet* **28**:46–48. doi:10.1038/ng0501-46

Beenhakker MP, Huguenard JR. 2009. Neurons that Fire Together Also Conspire Together: Is Normal Sleep Circuitry Hijacked to Generate Epilepsy? *Neuron* **62**:612–632. doi:10.1016/j.neuron.2009.05.015

Blethyn KL, Hughes SW, Tóth TI, Cope DW, Crunelli V. 2006. Neuronal basis of the slow (<1 Hz) oscillation in neurons of the nucleus reticularis thalami in vitro. *J Neurosci* **26**:2474–2486. doi:10.1523/JNEUROSCI.3607-05.2006

Blumenfeld H. 2005. Cellular and Network Mechanisms of Spike-Wave Seizures. *Epilepsia* **46**:21–33. doi:10.1017/S1472928807000209

Brown EN, Lydic R, Schiff ND. 2010. General Anesthesia, Sleep, and Coma. *N Engl J Med* **363**:2638–2650. doi:10.1056/NEJMra0808281

Burgess DL, Biddlecome GH, McDonough SI, Diaz ME, Zilinski CA, Bean BP, Campbell KP, Noebels JL. 1999. β subunit reshuffling modifies N- and P/Q-type Ca2+ channel subunit compositions in lethargic mouse brain. *Mol Cell Neurosci* **13**:293–311. doi:10.1006/mcne.1999.0748

Cain SM, Tyson JR, Jones KL, Snutch TP. 2015. Thalamocortical neurons display suppressed burst-firing due to an enhanced Ih current in a genetic model of absence epilepsy. *Pflugers Arch Eur J Physiol* **467**:1367–1382. doi:10.1007/s00424-014-1549-4

Cao Z, Harvey SS, Bliss TM, Cheng MY, Steinberg GK. 2020. Inflammatory Responses in the Secondary Thalamic Injury After Cortical Ischemic Stroke. *Front Neurol* **11**:1–12. doi:10.3389/fneur.2020.00236

Catterall WA. 2000. Structure and Regulation of Voltage-Gated Ca2+ Channels. *Annu Rev Cell Dev Biol* **16**:555. doi:10.1146/annurev.cellbio.16.1.521

Catterall WA, Few AP. 2008. Calcium Channel Regulation and Presynaptic Plasticity. *Neuron* **59**:882–901. doi:10.1016/j.neuron.2008.09.005

Charpier S, Beurrier C, Paz JT. 2010. The Subthalamic Nucleus: From In Vitro to In Vivo Mechanisms, Handbook of Behavioral Neuroscience. Elsevier Inc. doi:10.1016/B978-0-12-

374767-9.00015-9

Chen Y, Lu J, Pan H, Zhang Y, Wu H, Xu K, Liu X, Jiang Y, Bao X, Yao Z, Ding K, Lo WHY, Qiang B, Chan P, Shen Y, Wu X. 2003. Association between genetic variation of CACNA1H and childhood absence epilepsy. *Ann Neurol* **54**:239–243. doi:10.1002/ana.10607

Cheong E, Shin HS. 2013. T-type Ca2+ channels in normal and abnormal brain functions. *Physiol Rev* **93**:961–992. doi:10.1152/physrev.00010.2012

Cho FS, Clemente A, Holden S, Paz JT. 2017. Thalamic Models of Seizures In VitroPitkänen, Buckmaster, Galanopoulou, Moshé (Editors): Models of Seizures and Epilepsy, Second Edition. Academic Press. pp. 273–284. doi:10.1016/B978-0-12-804066-9.00019-5

Chung WK, Shin M, Jaramillo TC, Leibel RL, LeDuc CA, Fischer SG, Tzilianos E, Gheith AA, Lewis AS, Chetkovich DM. 2009. Absence epilepsy in apathetic, a spontaneous mutant mouse lacking the h channel subunit, HCN2. *Neurobiol Dis* **33**:499–508. doi:10.1016/j.nbd.2008.12.004

Claes L, Del-Favero J, Ceulemans B, Lagae L, Van Broeckhoven C, De Jonghe P. 2001. De novo mutations in the sodium-channel gene SCN1A cause severe myoclonic epilepsy of infancy. *Am J Hum Genet* **68**:1327–1332. doi:10.1086/320609

Clemente-Perez A, Makinson SR, Higashikubo B, Brovarney S, Cho FS, Urry A, Holden SS, Wimer M, Dávid C, Fenno LE, Acsády L, Deisseroth K, Paz JT. 2017. Distinct thalamic reticular cell types differentially modulate normal and pathological cortical rhythms. *Cell Rep* **19**:2130–2142. doi:10.1016/j.celrep.2017.05.044

Crabtree JW. 2018. Functional diversity of thalamic reticular subnetworks. *Front Syst Neurosci* **12**:1–18. doi:10.3389/fnsys.2018.00041

Crandall SR, Govindaiah G, Cox CL. 2010. Low-threshold Ca2+ current amplifies distal dendritic

signaling in thalamic reticular neurons. *J Neurosci* **30**:15419–15429. doi:10.1523/JNEUROSCI.3636-10.2010

Cruikshank SJ, Urabe H, Nurmikko A V., Connors BW. 2010. Pathway-Specific Feedforward Circuits between Thalamus and Neocortex Revealed by Selective Optical Stimulation of Axons. *Neuron* **65**:230–245. doi:10.1016/j.neuron.2009.12.025

Crunelli V, Cope D, Hughes SW. 2006. Thalamic T-type Ca2+ channels and NREM sleep. *Cell Calcium* **40**:175–190. doi:10.1016/j.ceca.2006.04.022

Crunelli V, Hughes SW. 2010. The slow (1 Hz) rhythm of non-REM sleep: A dialogue between three cardinal oscillators. *Nat Neurosci* **13**:9–17. doi:10.1038/nn.2445

Crunelli V, Larincz ML, Connelly WM, David F, Hughes SW, Lambert RC, Leresche N, Errington AC. 2018. Dual function of thalamic low-vigilance state oscillations: Rhythm-regulation and plasticity. *Nat Rev Neurosci* **19**:107–118. doi:10.1038/nrn.2017.151

Crunelli V, Leresche N. 2002. Childhood absence epilepsy: Genes, channels, neurons and networks. *Nat Rev Neurosci* **3**:371–382. doi:10.1038/nrn811

Cueni L, Canepari M, Luján R, Emmenegger Y, Watanabe M, Bond CT, Franken P, Adelman JP, Lüthi A. 2008. T-type Ca 2+ channels, SK2 channels and SERCAs gate sleep-related oscillations in thalamic dendrites. *Nat Neurosci* **11**:683–692. doi:10.1038/nn.2124

Dalic LJ, Warren AEL, Young JC, Thevathasan W, Roten A, Bulluss KJ, Archer JS. 2020. Cortex leads the thalamic centromedian nucleus in generalized epileptic discharges in Lennox-Gastaut syndrome. *Epilepsia* **61**:2214–2223. doi:10.1111/epi.16657

Deleuze C, Huguenard JR. 2006. Distinct electrical and chemical connectivity maps in the thalamic reticular nucleus: Potential roles in synchronization and sensation. *J Neurosci* **26**:8633–8645. doi:10.1523/JNEUROSCI.2333-06.2006

Deschênes M, Veinante P, Zhang ZW. 1998. The organization of corticothalamic projections: Reciprocity versus parity. *Brain Res Rev* **28**:286–308. doi:10.1016/S0165-0173(98)00017-4

Destexhe A, Bal T, Mccormick DA, Sejnowski TJ. 1996. Ionic mechanisms underlying synchronized oscillations and propagating waves in a model of ferret thalamic slices. *J Neurophysiol* **76**:2049–2070. doi:10.1152/jn.1996.76.3.2049

Destexhe A, Neubig M, Ulrich D, Huguenard J. 1998. Dendritic Low-Threshold Calcium Currents in Thalamic Relay Cells. *J Neurosci* **18**:3574–3588. doi:10.1523/jneurosci.18-10-03574.1998

Dravet C. 2011. The core Dravet syndrome phenotype. *Epilepsia* **52**:3–9. doi:10.1111/j.1528-1167.2011.02994.x

Dutton SB, Makinson CD, Papale LA, Shankar A, Balakrishnan B, Nakazawa K, Escayg A. 2013. Preferential inactivation of SCN1A in parvalbumin interneurons increases seizure susceptibility. *Neurobiol Dis* **49**:211–220. doi:10.1016/j.nbd.2012.08.012

Ernst WL, Zhang Y, Yoo JW, Ernst SJ, Noebels JL. 2009. Genetic enhancement of thalamocortical network activity by elevating α1G-mediated low-voltage-activated calcium current induces pure absence epilepsy. *J Neurosci* **29**:1615–1625. doi:10.1523/JNEUROSCI.2081-08.2009

Everett K V., Chioza B, Aicardi J, Aschauer H, Brouwer O, Callenbach P, Covanis A, Dulac O, Eeg-Olofsson O, Feucht M, Friis M, Goutieres F, Guerrini R, Heils A, Kjeldsen M, Lehesjoki AE, Makoff A, Nabbout R, Olsson I, Sander T, Sirén A, McKeigue P, Robinson R, Taske N, Rees M, Gardiner M. 2007. Linkage and association analysis of CACNG3 in childhood absence epilepsy. *Eur J Hum Genet* **15**:463–472. doi:10.1038/sj.ejhg.5201783

Farrello K. 1986. Benzodiazepines in the Treatment of Children with Epilepsy. *Epilepsia* **27**:S45–S52. doi:10.1111/j.1528-1157.1986.tb05733.x

Favero M, Sotuyo NP, Lopez E, Kearney JA, Goldberg EM. 2018. A transient developmental window of fast-spiking interneuron dysfunction in a mouse model of dravet syndrome. *J Neurosci* **38**:7912–7927. doi:10.1523/JNEUROSCI.0193-18.2018

Fernandez LMJ, Lüthi A. 2020. Sleep spindles: Mechanisms and functions. *Physiol Rev* **100**:805–868. doi:10.1152/physrev.00042.2018

Fernandez LMJ, Vantomme G, Osorio-Forero A, Cardis R, Béard E, Lüthi A. 2018. Thalamic reticular control of local sleep in mouse sensory cortex. *Elife* **7**:1–25. doi:10.7554/eLife.39111

Fisher RS, Velasco AL. 2014. Electrical brain stimulation for epilepsy. *Nat Rev Neurol* **10**:261–270. doi:10.1038/nrneurol.2014.59

Fletcher CF, Lutz CM, O'Sullivan TN, Shaughnessy JD, Hawkes R, Frankel WN, Copeland NG, Jenkins NA. 1996. Absence epilepsy in tottering mutant mice is associated with calcium channel defects. *Cell* **87**:607–617. doi:10.1016/S0092-8674(00)81381-1

Fogerson PM, Huguenard JR. 2016. Tapping the Brakes: Cellular and Synaptic Mechanisms that Regulate Thalamic Oscillations. *Neuron* **92**:687–704. doi:10.1016/j.neuron.2016.10.024

Gobbo D, Scheller A, Kirchhoff F. 2021. From Physiology to Pathology of Cortico-Thalamo-Cortical Oscillations: Astroglia as a Target for Further Research. *Front Neurol* **12**:1–26. doi:10.3389/fneur.2021.661408

Grossman EJ, Ge Y, Jensen JH, Babb JS, Miles L, Reaume J, Silver JM, Grossman RI, Inglese M. 2012. Thalamus and cognitive impairment in mild traumatic brain injury: A diffusional kurtosis imaging study. *J Neurotrauma* **29**:2318–2327. doi:10.1089/neu.2011.1763

Grossman EJ, Inglese M. 2016. The role of thalamic damage in mild traumatic brain injury. *J Neurotrauma* **33**:163–167. doi:10.1089/neu.2015.3965

Guillery RW, Sherman SM. 2002. Thalamic relay functions and their role in corticocortical communication: Generalizations from the visual system. *Neuron* **33**:163–175. doi:10.1016/S0896-6273(01)00582-7

Halassa MM, Acsády L. 2016. Thalamic Inhibition: Diverse Sources, Diverse Scales. *Trends Neurosci* **39**:680–693. doi:10.1016/j.tins.2016.08.001

Halassa MM, Sherman SM. 2019. Thalamocortical Circuit Motifs: A General Framework. *Neuron* **103**:762–770. doi:10.1016/j.neuron.2019.06.005

Halassa MM, Siegle JH, Ritt JT, Ting JT, Feng G, Moore CI. 2011. Selective optical drive of thalamic reticular nucleus generates thalamic bursts and cortical spindles. *Nat Neurosci* **14**:1118–1120. doi:10.1038/nn.2880

Han Z, Chen C, Christiansen A, Ji S, Lin Q, Anumonwo C, Liu C, Leiser SC, Meena, Aznarez I, Liau G, Isom LL. 2020. Antisense oligonucleotides increase Scn1a expression and reduce seizures and SUDEP incidence in a mouse model of Dravet syndrome. *Sci Transl Med* **12**. doi:10.1126/SCITRANSLMED.AAZ6100

Harris JA, Mihalas S, Hirokawa KE, Whitesell JD, Choi H, Bernard A, Bohn P, Caldejon S, Casal L, Cho A, Feiner A, Feng D, Gaudreault N, Gerfen CR, Graddis N, Groblewski PA, Henry AM, Ho A, Howard R, Knox JE, Kuan L, Kuang X, Lecoq J, Lesnar P, Li Y, Luviano J, McConoughey S, Mortrud MT, Naeemi M, Ng L, Oh SW, Ouellette B, Shen E, Sorensen SA, Wakeman W, Wang Q, Wang Y, Williford A, Phillips JW, Jones AR, Koch C, Zeng H. 2019. Hierarchical organization of cortical and thalamic connectivity. *Nature* **575**:195–202. doi:10.1038/s41586-019-1716-z

Hazra A, Macolino C, Elliott MB, Chin J. 2014. Delayed thalamic astrocytosis and disrupted sleep-wake patterns in a preclinical model of traumatic brain injury. *J Neurosci Res* **92**:1434–1445.

doi:10.1002/jnr.23430

Helbig KL, Lauerer RJ, Bahr JC, Souza IA, Myers CT, Uysal B, Schwarz N, Gandini MA, Huang S, Keren B, Mignot C, Afenjar A, Billette de Villemeur T, Héron D, Nava C, Valence S, Buratti J, Fagerberg CR, Soerensen KP, Kibaek M, Kamsteeg EJ, Koolen DA, Gunning B, Schelhaas HJ, Kruer MC, Fox J, Bakhtiari S, Jarrar R, Padilla-Lopez S, Lindstrom K, Jin SC, Zeng X, Bilguvar K, Papavasileiou A, Xin Q, Zhu C, Boysen K, Vairo F, Lanpher BC, Klee EW, Tillema JM, Payne ET, Cousin MA, Kruisselbrink TM, Wick MJ, Baker J, Haan E, Smith N, Corbett MA, MacLennan AH, Gecz J, Biskup S, Goldmann E, Rodan LH, Kichula E, Segal E, Jackson KE, Asamoah A, Dimmock D, McCarrier J, Botto LD, Filloux F, Tvrdik T, Cascino GD, Klingerman S, Neumann C, Wang R, Jacobsen JC, Nolan MA, Snell RG, Lehnert K, Sadleir LG, Anderlid BM, Kvarnung M, Guerrini R, Friez MJ, Lyons MJ, Leonhard J, Kringlen G, Casas K, El Achkar CM, Smith LA, Rotenberg A, Poduri A, Sanchis-Juan A, Carss KJ, Rankin J, Zeman A, Raymond FL, Blyth M, Kerr B, Ruiz K, Urquhart J, Hughes I, Banka S, Hedrich UBS, Scheffer IE, Helbig I, Zamponi GW, Lerche H, Mefford HC. 2018. De Novo Pathogenic Variants in CACNA1E Cause Developmental and Epileptic Encephalopathy with Contractures, Macrocephaly, and Dyskinesias. *Am J Hum Genet* **103**:666–678. doi:10.1016/j.ajhg.2018.09.006

Heuermann RJ, Jaramillo TC, Ying SW, Suter BA, Lyman KA, Han Y, Lewis AS, Hampton TG, Shepherd GMG, Goldstein PA, Chetkovich DM. 2016. Reduction of thalamic and cortical Ih by deletion of TRIP8b produces a mouse model of human absence epilepsy. *Neurobiol Dis* **85**:81–92. doi:10.1016/j.nbd.2015.10.005

Holden SS, Grandi FC, Aboubakr O, Higashikubo B, Cho FS, Chang AH, Forero AO, Morningstar AR, Mathur V, Kuhn LJ, Suri P, Sankaranarayanan S, Andrews-Zwilling Y, Tenner AJ, Luthi

A, Aronica E, Corces MR, Yednock T, Paz JT. 2021. Complement factor C1q mediates sleep spindle loss and epileptic spikes after mild brain injury. *Science* **373**. doi:10.1126/science.abj2685

Hoseini MS, Higashikubo B, Cho FS, Chang AH, Clemente-Perez A, Lew I, Ciesielska A, Stryker MP, Paz JT. 2021. Gamma rhythms and visual information in mouse V1 specifically modulated by somatostatin+ neurons in reticular thalamus. *Elife* **10**:1–24. doi:10.7554/elife.61437

Hou G, Smith AG, Zhang ZW. 2016. Lack of intrinsic GABAergic connections in the thalamic reticular nucleus of the mouse. *J Neurosci* **36**:7246–7252. doi:10.1523/JNEUROSCI.0607-16.2016

Houser CR, Vaughn JE, Barber RP, Roberts E. 1980. GABA Neurons are the Major Cell Type of the Nucleus Reticularis Thalami. *Brain Res* **200**:341–354. doi:10.1017/CBO9781107415324.004

Hughes SW, Cope DW, Blethyn KL, Crunelli V. 2002. Cellular Mechanisms of the Slow (<1 Hz) Oscillation in Thalamocortical Neurons In Vitro. *Neuron* **33**:947–958. doi:10.1016/s0896-6273(02)00623-2

Hughes SW, Lorincz ML, Blethyn K, Kékesi KA, Juhász G, Turmaine M, Parnavelas JG, Crunelli V. 2011. Thalamic gap junctions control local neuronal synchrony and influence macroscopic oscillation amplitude during EEG alpha rhythms. *Front Psychol* **2**:1–11. doi:10.3389/fpsyg.2011.00193

Huguenard J. 2019. Current Controversy: Spikes, Bursts, and Synchrony in Generalized Absence Epilepsy: Unresolved Questions Regarding Thalamocortical Synchrony in Absence Epilepsy. *Epilepsy Curr* **19**:105–111. doi:10.1177/1535759719835355

Huguenard JR. 1999. Neuronal circuitry of thalamocortical epilepsy and mechanisms of antiabsence drug action. In: Delgado-Escueta AV, Wilson WA, Olsen RW, Porter RJ, editors. Jasper's Basic Mechanisms of the Epilepsies. Philadelphia: Lippincott Williams & Wilkins. pp. 991–999.

Huguenard JR. 1996. Low-Threshold Calcium Currents in Central Nervous System Neurons. *Annu Rev Physiol* **58**:329–348. doi:10.1146/annurev.physiol.58.1.329

Huguenard JR, McCormick DA. 2007. Thalamic synchrony and dynamic regulation of global forebrain oscillations. *Trends Neurosci* **30**:350–356. doi:10.1016/j.tins.2007.05.007

Huguenard JR, Prince D a. 1994a. Intrathalamic rhythmicity studied in vitro: nominal T-current modulation causes robust antioscillatory effects. *J Neurosci* **14**:5485–502.

Huguenard JR, Prince D a. 1994b. Clonazepam suppresses GABAB-mediated inhibition in thalamic relay neurons through effects in nucleus reticularis. *J Neurophysiol* **71**:2576–2581.

Huguenard JR, Prince DA. 1992. A novel T-type current underlies prolonged Ca2+-dependent burst firing in GABAergic neurons of rat thalamic reticular nucleus. *J Neurosci* **12**:3804–3817. doi:10.1523/jneurosci.12-10-03804.1992

Huntsman MM, Porcello DM, Homanics GE, DeLorey TM, Huguenard JR. 1999. Reciprocal Inhibitory Connections and Network Synchrony in the Mammalian Thalamus. *Science* **283**:541–543. doi:10.1126/science.283.5401.541

Immonen R, Kharatishvili I, Gröhn O, Pitkänen A. 2013. MRI biomarkers for post-traumatic epileptogenesis. *J Neurotrauma* **30**:1305–1309. doi:10.1089/neu.2012.2815

Inoue M, Duysens J, Vossen JMH, Coenen AML. 1993. Thalamic multiple-unit activity underlying spike-wave discharges in anesthetized rats. *Brain Res* **612**:35–40. doi:10.1016/0006-8993(93)91641-5

Jahnsen H, Llinás R. 1984. Ionic basis for the electro-responsiveness and oscillatory properties of guinea-pig thalamic neurones in vitro. *J Physiol* **349**:227–247. doi:10.1113/jphysiol.1984.sp015154

Jasper HH. 1991. Current evaluation of the concepts of centrecephalic and cortico-reticular seizures. *Electroencephalogr Clin Neurophysiol* **78**:2–11. doi:10.1016/0013-4694(91)90012-S

Jasper HH. 1948. Charting the Sea of Brain Waves. *Science* **108**:343–347. doi:10.1126/science.108.2805.343

Joksovic PM, Nelson MT, Jevtovic-Todorovic V, Patel MK, Perez-Reyes E, Campbell KP, Chen CC, Todorovic SM. 2006. CaV3.2 is the major molecular substrate for redox regulation of T-type Ca2+ channels in the rat and mouse thalamus. *J Physiol* **574**:415–430. doi:10.1113/jphysiol.2006.110395

Jones EG. 2009. Synchrony in the interconnected circuitry of the thalamus and cerebral cortex. *Ann N Y Acad Sci* **1157**:10–23. doi:10.1111/j.1749-6632.2009.04534.x

Jones EG. 2007. The Thalamus. Cambridge, UK: Cambridge University Press.

Jones EG. 1985. The Thalamus. Plenum Press. doi:10.1007/978-1-4615-1749-8

Jones EG. 1975. Some aspects of the organization of the thalamic reticular complex. *J Comp Neurol* **162**:285–308. doi:10.1002/cne.901620302

Jourdain A, Semba K, Fibiger HC. 1989. Basal forebrain and mesopontine tegmental projections to the reticular thalamic nucleus: an axonal collateralization and immunohistochemical study in the rat. *Brain Res* **505**:55–65. doi:10.1016/0006-8993(89)90115-7

Jouvenceau A, Eunson LH, Spauschus A, Ramesh V, Zuberi SM, Kullmann DM, Hanna MG. 2001. Human epilepsy associated with dysfunction of the brain P/Q-type calcium channel. *Lancet* **358**:801–807. doi:10.1016/S0140-6736(01)05971-2

Kanyshkova T, Meuth P, Bista P, Liu Z, Ehling P, Caputi L, Doengi M, Chetkovich DM, Pape HC, Budde T. 2012. Differential regulation of HCN channel isoform expression in thalamic neurons of epileptic and non-epileptic rat strains. *Neurobiol Dis* **45**:450–461. doi:10.1016/j.nbd.2011.08.032

Kim D, Song I, Keum S, Lee T, Jeong MJ, Kim SS, McEnery MW, Shin HS. 2001. Lack of the burst firing of thalamocortical relay neurons and resistance to absence seizures in mice lacking α1G T-type Ca2+ channels. *Neuron* **31**:35–45. doi:10.1016/S0896-6273(01)00343-9

Klassen T, Davis C, Goldman A, Burgess D, Chen T, Wheeler D, McPherson J, Bourquin T, Lewis L, Villasana D, Morgan M, Muzny D, Gibbs R, Noebels J. 2011. Exome sequencing of ion channel genes reveals complex profiles confounding personal risk assessment in epilepsy. *Cell* **145**:1036–1048. doi:10.1016/j.cell.2011.05.025

Klein P, Dingledine R, Aronica E, Bernard C, Blümcke I, Boison D, Brodie MJ, Brooks-Kayal AR, Engel J, Forcelli PA, Hirsch LJ, Kaminski RM, Klitgaard H, Kobow K, Lowenstein DH, Pearl PL, Pitkänen A, Puhakka N, Rogawski MA, Schmidt D, Sillanpää M, Sloviter RS, Steinhäuser C, Vezzani A, Walker MC, Löscher W. 2018. Commonalities in epileptogenic processes from different acute brain insults: Do they translate? *Epilepsia* **59**:37–66. doi:10.1111/epi.13965

Köhler M, Hirschberg B, Bond CT, Kinzie JM, Marrion N V., Maylie J, Adelman JP. 1996. Small-conductance, calcium-activated potassium channels from mammalian brain. *Science* **273**:1709–1714. doi:10.1126/science.273.5282.1709

Kramer MA, Stoyell SM, Chinappen D, Ostrowski LM, Spencer ER, Morgan AK, Emerton BC, Jing J, Westover MB, Eden UT, Stickgold R, Manoach DS, Chu CJ. 2021. Focal sleep spindle deficits reveal focal thalamocortical dysfunction and predict cognitive deficits in sleep

activated developmental epilepsy. *J Neurosci* **41**:1816–1829. doi:10.1523/JNEUROSCI.2009-20.2020

Krol A, Wimmer RD, Halassa MM, Feng G. 2018. Thalamic Reticular Dysfunction as a Circuit Endophenotype in Neurodevelopmental Disorders. *Neuron* **98**:282–295. doi:10.1016/j.neuron.2018.03.021

Landisman CE, Long MA, Beierlein M, Deans MR, Paul DL, Connors BW. 2002. Electrical synapses in the thalamic reticular nucleus. *J Neurosci* **22**:1002–1009. doi:10.1523/jneurosci.22-03-01002.2002

Lee J, Kim D, Shin HS. 2004. Lack of delta waves and sleep disturbances during non-rapid eye movement sleep in mice lacking α1G-subunit of T-type calcium channels. *Proc Natl Acad Sci U S A* **101**:18195–18199. doi:10.1073/pnas.0408089101

Lee SE, Lee J, Latchoumane C, Lee B, Oh SJ, Saud ZA, Park C, Sun N, Cheong E, Chen CC, Choi EJ, Lee CJ, Shin HS. 2014. Rebound burst firing in the reticular thalamus is not essential for pharmacological absence seizures in mice. *Proc Natl Acad Sci U S A* **111**:11828–11833. doi:10.1073/pnas.1408609111

Lein ES, Hawrylycz MJ, Ao N, Ayres M, Bensinger A, Bernard A, Boe AF, Boguski MS, Brockway KS, Byrnes EJ, Chen Lin, Chen Li, Chen TM, Chin MC, Chong J, Crook BE, Czaplinska A, Dang CN, Datta S, Dee NR, Desaki AL, Desta T, Diep E, Dolbeare TA, Donelan MJ, Dong HW, Dougherty JG, Duncan BJ, Ebbert AJ, Eichele G, Estin LK, Faber C, Facer BA, Fields R, Fischer SR, Fliss TP, Frensley C, Gates SN, Glattfelder KJ, Halverson KR, Hart MR, Hohmann JG, Howell MP, Jeung DP, Johnson RA, Karr PT, Kawal R, Kidney JM, Knapik RH, Kuan CL, Lake JH, Laramee AR, Larsen KD, Lau C, Lemon TA, Liang AJ, Liu Y, Luong LT, Michaels J, Morgan JJ, Morgan RJ, Mortrud MT, Mosqueda NF, Ng LL,

Ng R, Orta GJ, Overly CC, Pak TH, Parry SE, Pathak SD, Pearson OC, Puchalski RB, Riley ZL, Rockett HR, Rowland SA, Royall JJ, Ruiz MJ, Sarno NR, Schaffnit K, Shapovalova N V., Sivisay T, Slaughterbeck CR, Smith SC, Smith KA, Smith BI, Sodt AJ, Stewart NN, Stumpf KR, Sunkin SM, Sutram M, Tam A, Teemer CD, Thaller C, Thompson CL, Varnam LR, Visel A, Whitlock RM, Wohnoutka PE, Wolkey CK, Wong VY, Wood M, Yaylaoglu MB, Young RC, Youngstrom BL, Yuan XF, Zhang B, Zwingman TA, Jones AR. 2007. Genome-wide atlas of gene expression in the adult mouse brain. *Nature* **445**:168–176. doi:10.1038/nature05453

Leresche N, Lambert RC, Errington AC, Crunelli V. 2012. From sleep spindles of natural sleep to spike and wave discharges of typical absence seizures: Is the hypothesis still valid? *Pflugers Arch Eur J Physiol* **463**:201–212. doi:10.1007/s00424-011-1009-3

Lewis LD, Voigts J, Flores FJ, Ian Schmitt L, Wilson MA, Halassa MM, Brown EN. 2015. Thalamic reticular nucleus induces fast and local modulation of arousal state. *Elife* **4**:1–23. doi:10.7554/eLife.08760

Li Y, Lopez-Huerta VG, Adiconis X, Levandowski K, Choi S, Simmons SK, Arias-Garcia MA, Guo B, Yao AY, Blosser TR, Wimmer RD, Aida T, Atamian A, Naik T, Sun X, Bi D, Malhotra D, Hession CC, Shema R, Gomes M, Li T, Hwang E, Krol A, Kowalczyk M, Peça J, Pan G, Halassa MM, Levin JZ, Fu Z, Feng G. 2020. Distinct subnetworks of the thalamic reticular nucleus. *Nature* **583**:819–824. doi:10.1038/s41586-020-2504-5

Liang J, Zhang Y, Wang J, Pan H, Wu H, Xu K, Liu X, Jiang Y, Shen Y, Wu X. 2006. New variants in the CACNA1H gene identified in childhood absence epilepsy. *Neurosci Lett* **406**:27–32. doi:10.1016/j.neulet.2006.06.073

Liu XB, Jones EG. 1999. Predominance of corticothalamic synaptic inputs to thalamic reticular

nucleus neurons in the rat. *J Comp Neurol* **414**:67–79. doi:10.1002/(SICI)1096-9861(19991108)414:1<67::AID-CNE6>3.0.CO;2-Z

Llinás RR, Steriade M. 2006. Bursting of thalamic neurons and states of vigilance. *J Neurophysiol* **95**:3297–308. doi:10.1152/jn.00166.2006

Long MA, Landisman CE, Connors BW. 2004. Small Clusters of Electrically Coupled Neurons Generate Synchronous Rhythms in the Thalamic Reticular Nucleus. *J Neurosci* **24**:341–349. doi:10.1523/JNEUROSCI.3358-03.2004

Ludwig A, Budde T, Stieber J, Moosmang S, Wahl C, Holthoff K, Langebartels A, Wotjak C, Munsch T, Zong X, Feil S, Feil R, Lancel M, Chien KR, Konnerth A, Pape HC, Biel M, Hofmann F. 2003. Absence epilepsy and sinus dysrhythmia in mice lacking the pacemaker channel HCN2. *EMBO J* **22**:216–224. doi:10.1093/emboj/cdg032

Maheshwari A, Noebels JL. 2014. Monogenic models of absence epilepsy. windows into the complex balance between inhibition and excitation in thalamocortical microcircuits, 1st ed, Progress in Brain Research. Elsevier B.V. doi:10.1016/B978-0-444-63326-2.00012-0

Makinson CD, Tanaka BS, Sorokin JM, Wong JC, Christian CA, Goldin AL, Escayg A, Huguenard JR. 2017. Regulation of Thalamic and Cortical Network Synchrony by Scn8a. *Neuron* **93**:1165-1179.e6. doi:10.1016/j.neuron.2017.01.031

Manninen E, Chary K, Lapinlampi N, Andrade P, Paananen T, Sierra A, Tohka J, Gröhn O, Pitkänen A. 2021. Acute thalamic damage as a prognostic biomarker for post-traumatic epileptogenesis. *Epilepsia* 1–13. doi:10.1111/epi.16986

Martinez-Garcia RI, Voelcker B, Zaltsman JB, Patrick SL, Stevens TR, Connors BW, Cruikshank SJ. 2020. Two dynamically distinct circuits drive inhibition in the sensory thalamus, Nature. Springer US. doi:10.1038/s41586-020-2512-5

McCafferty C, David F, Venzi M, Lorincz ML, Delicata F, Atherton Z, Recchia G, Orban G, Lambert RC, Di Giovanni G, Leresche N, Crunelli V. 2018. Cortical drive and thalamic feed-forward inhibition control thalamic output synchrony during absence seizures. *Nat Neurosci* **21**:744–756. doi:10.1038/s41593-018-0130-4

McCormick DA, Bal T. 1997. Sleep and arousal: Thalamocortical mechanisms. *Annu Rev Neurosci* **20**:185–215. doi:10.1146/annurev.neuro.20.1.185

McCormick DA, Pape H-C. 1990. Properties of a Hyperpolarization-Activated Cation Current and Its Role in Rhythmic Oscillation in Thalamic Relay Neurones. *J Physiol* 291–318. doi:10.1113/jphysiol.1990.sp018331

Mo C, Petrof I, Viaene AN, Sherman SM. 2017. Synaptic properties of the lemniscal and paralemniscal pathways to the mouse somatosensory thalamus. *Proc Natl Acad Sci U S A* **114**:E6212–E6221. doi:10.1073/pnas.1703222114

Necula D, Cho FS, He A, Paz JT. 2021. Secondary thalamic neuroinflammation after focal cortical stroke and traumatic injury mirrors corticothalamic functional connectivity. *J Comp Neurol*. doi:10.1002/cne.25259

Neske GT. 2016. The slow oscillation in cortical and thalamic networks: Mechanisms and functions. *Front Neural Circuits* **9**:1–25. doi:10.3389/fncir.2015.00088

Noebels J. 2017. Precision physiology and rescue of brain ion channel disorders. *J Gen Physiol* **149**:533–546. doi:10.1085/jgp.201711759

Noebels JL. 2012. The Voltage-Gated Calcium Channel and Absence Epilepsy In: Noebels JL, Avoli M, Rogawski MA, Olsen RW, Delgado-Escueta A V, editors. Jasper's Basic Mechanisms of the Epilepsies. Bethesda: National Center for Biotechnology Information (US). pp. 702–713. doi:10.1093/med/9780199746545.003.0054

Notomi T, Shigemoto R. 2004. Immunohistochemical Localization of Ih Channel Subunits, HCN1-4, in the Rat Brain. *J Comp Neurol* **471**:241–276. doi:10.1002/cne.11039

Nowycky MC, Fox AP, Tsien RW. 1985. Three types of neuronal calcium channel with different calcium agonist sensitivity. *Nature* **316**. doi:10.1038/316440a0

Nuñez A, Amzica F, Steriade M. 1992. Intrinsic and synaptically generated delta (1-4 Hz) rhythms in dorsal lateral geniculate neurons and their modulation by light-induced fast (30-70 Hz) events. *Neuroscience* **51**:269–284. doi:10.1016/0306-4522(92)90314-R

Panayiotopoulos CP. 2008. Typical absence seizures and related epileptic syndromes: Assessment of current state and directions for future research. *Epilepsia* **49**:2131–2147. doi:10.1371/journal.pntd.0000461.2325

Pappata S, Levasseur M, Gunn RN, Myers R, Crouzel C, Syrota A, Jones T, Kreutzberg GW, Banati RB. 2000. Thalamic microglial activation in ischemic stroke detected in vivo by PET and [(11)C]PK11195. *Neurology* **55**:1052–1054. doi:10.1212/WNL.55.7.1052

Parajuli LK, Fukazawa Y, Watanabe M, Shigemoto R. 2010. Subcellular distribution of α1G subunit of T-type calcium channel in the mouse dorsal lateral geniculate nucleus. *J Comp Neurol* **518**:4362–4374. doi:10.1002/cne.22461

Paré D, Hazrati LN, Parent A, Steriade M. 1990. Substantia nigra pars reticulata projects to the reticular thalamic nucleus of the cat: a morphological and electrophysiological study. *Brain Res* **535**:139–146. doi:10.1016/0006-8993(90)91832-2

Parker PRL, Cruikshank SJ, Connors BW. 2009. Stability of electrical coupling despite massive developmental changes of intrinsic neuronal physiology. *J Neurosci* **29**:9761–9770. doi:10.1523/JNEUROSCI.4568-08.2009

Patel DC, Tewari BP, Chaunsali L, Sontheimer H. 2019. Neuron–glia interactions in the

pathophysiology of epilepsy. *Nat Rev Neurosci* **20**:282–297. doi:10.1038/s41583-019-0126-4

Paz JT, Bryant AS, Peng K, Fenno L, Yizhar O, Frankel WN, Deisseroth K, Huguenard JR. 2011. A new mode of corticothalamic transmission revealed in the Gria4(-/-) model of absence epilepsy. *Nat Neurosci* **14**:1167–73. doi:10.1038/nn.2896

Paz JT, Chavez M, Saillet S, Deniau J, Charpier S. 2007. Activity of Ventral Medial Thalamic Neurons during Absence Seizures and Modulation of Cortical Paroxysms by the Nigrothalamic Pathway. *J Neurosci* **27**:929–941. doi:10.1523/JNEUROSCI.4677-06.2007

Paz JT, Christian CA, Parada I, Prince DA, Huguenard JR. 2010. Focal Cortical Infarcts Alter Intrinsic Excitability and Synaptic Excitation in the Reticular Thalamic Nucleus. *J Neurosci* **30**:5465–5479. doi:10.1523/JNEUROSCI.5083-09.2010

Paz JT, Davidson TJ, Frechette ES, Delord B, Parada I, Peng K, Deisseroth K, Huguenard JR. 2013. Closed-loop optogenetic control of thalamus as a tool for interrupting seizures after cortical injury. *Nat Neurosci* **16**:64–70. doi:10.1038/nn.3269

Paz JT, Huguenard JR. 2015. Microcircuits and their interactions in epilepsy: is the focus out of focus? *Nat Neurosci* **18**:351–9. doi:10.1038/nn.3950

Paz JT, Huguenard JR. 2012. R U OK? The novel therapeutic potential of R channels in epilepsy. *Epilepsy Curr* **12**:75–76. doi:10.5698/1535-7511-12.2.75

Paz JT, Polack P-O, Slaght SJ, Deniau J-M, Charpier S. 2005. Propagation of Cortical Paroxysms in Basal Ganglia Circuits During Absence Seizures In: Bolam JP, Ingham CA, Magill PJ, editors. The Basal Ganglia VIII. Advances in Behavioral Biology, Vol 56. Boston, MA: Springer. pp. 55–63. doi:10.1007/0-387-28066-9_5

Perez-Reyes E. 2003. Molecular physiology of low-voltage-activated T-type calcium channels.

Physiol Rev **83**:117–161. doi:10.1152/physrev.00018.2002

Phillips JW, Schulmann A, Hara E, Winnubst J, Liu C, Valakh V, Wang L, Shields BC, Korff W, Chandrashekar J, Lemire AL, Mensh B, Dudman JT, Nelson SB, Hantman AW. 2019. A repeated molecular architecture across thalamic pathways. *Nat Neurosci* **22**:1925–1935. doi:10.1038/s41593-019-0483-3

Pinault D. 2004. The thalamic reticular nucleus: Structure, function and concept. *Brain Res Rev* **46**:1–31. doi:10.1016/j.brainresrev.2004.04.008

Pinault D, Bourassa J, Deschênes M. 1995. The Axonal Arborization of Single Thalamic Reticular Neurons in the Somatosensory Thalamus of the Rat. *Eur J Neurosci* **7**:31–40. doi:10.1111/j.1460-9568.1995.tb01017.x

Pitkänen A, Paananen T, Kyyriäinen J, Das Gupta S, Heiskanen M, Vuokila N, Bañuelos-Cabrera I, Lapinlampi N, Kajevu N, Andrade P, Ciszek R, Lara-Valderrábano L, Ekolle Ndode-Ekane X, Puhakka N. 2021. Biomarkers for posttraumatic epilepsy. *Epilepsy Behav* **121**:107080. doi:10.1016/j.yebeh.2020.107080

Polack P, Charpier S. 2009. Ethosuximide converts ictogenic neurons initiating absence seizures into normal neurons in a genetic model. *Epilepsia* **50**:1816–1820. doi:10.1111/j.1528-1167.2009.02047.x

Powell KL, Cain SM, Ng C, Sirdesai S, David LS, Kyi M, Garcia E, Tyson JR, Reid CA, Bahlo M, Foote SJ, Snutch TP, O'Brien TJ. 2009. A Cav3.2 T-type calcium channel point mutation has splice-variant-specific effects on function and segregates with seizure expression in a polygenic rat model of absence epilepsy. *J Neurosci* **29**:371–380. doi:10.1523/JNEUROSCI.5295-08.2009

Rajakulendran S, Kaski D, Hanna MG. 2012. Neuronal P/Q-type calcium channel dysfunction in

inherited disorders of the CNS. *Nat Rev Neurol* **8**:86–96. doi:10.1038/nrneurol.2011.228

Ramlackhansingh AF, Brooks DJ, Greenwood RJ, Bose SK, Turkheimer FE, Kinnunen KM, Gentleman S, Heckemann RA, Gunanayagam K, Gelosa G, Sharp DJ. 2011. Inflammation after trauma: Microglial activation and traumatic brain injury. *Ann Neurol* **70**:374–383. doi:10.1002/ana.22455

Randall AD, Tsien RW. 1997. Contrasting biophysical and pharmacological properties of T-type and R-type calcium channels. *Neuropharmacology* **36**:879–893. doi:10.1016/S0028-3908(97)00086-5

Ritter-Makinson S, Clemente-Perez A, Higashikubo B, Cho FS, Holden SS, Bennett E, Chkaidze A, Rooda OHJE, Cornet MC, Hoebeek FE, Yamakawa K, Cilio MR, Delord B, Paz JT. 2019. Augmented Reticular Thalamic Bursting and Seizures in Scn1a-Dravet Syndrome. *Cell Rep* **26**:54–64. doi:10.1016/j.celrep.2018.12.018

Rubinstein M, Han S, Tai C, Westenbroek RE, Hunker A, Scheuer T, Catterall WA. 2015. Dissecting the phenotypes of Dravet syndrome by gene deletion. *Brain* **138**:2219–2233. doi:10.1093/brain/awv142

Scheffer IE, Berkovic S, Capovilla G, Connolly MB, French J, Guilhoto L, Hirsch E, Jain S, Mathern GW, Moshé SL, Nordli DR, Perucca E, Tomson T, Wiebe S, Zhang YH, Zuberi SM. 2017. ILAE classification of the epilepsies: Position paper of the ILAE Commission for Classification and Terminology. *Epilepsia* **58**:512–521. doi:10.1111/epi.13709

Scott G, Hellyer PJ, Ramlackhansingh AF, Brooks DJ, Matthews PM, Sharp DJ. 2015. Thalamic inflammation after brain trauma is associated with thalamo-cortical white matter damage. *J Neuroinflammation* **12**:1–5. doi:10.1186/s12974-015-0445-y

Shepherd GMG, Yamawaki N. 2021. Untangling the cortico-thalamo-cortical loop: cellular pieces

of a knotty circuit puzzle. *Nat Rev Neurosci* **22**:389–406. doi:10.1038/s41583-021-00459-3

Sherman SM. 2007. The thalamus is more than just a relay. *Curr Opin Neurobiol* **17**:417–422. doi:10.1016/j.conb.2007.07.003

Sherman SM. 2001. A wake-up call from the thalamus. *Nat Neurosci* **4**. doi:10.1038/85973

Sherman SM, Guillery RW. 1996. Functional organization of thalamocortical relays. *J Neurophysiol* **76**:1367–1395. doi:10.1152/jn.1996.76.3.1367

Shu Y, McCormick DA. 2002. Inhibitory interactions between ferret thalamic reticular neurons. *J Neurophysiol* **87**:2571–2576. doi:10.1152/jn.00850.2001

Siegle JH, Jia X, Durand S, Gale S, Bennett C, Graddis N, Heller G, Ramirez TK, Choi H, Luviano JA, Groblewski PA, Ahmed R, Arkhipov A, Bernard A, Billeh YN, Brown D, Buice MA, Cain N, Caldejon S, Casal L, Cho A, Chvilicek M, Cox TC, Dai K, Denman DJ, de Vries SEJ, Dietzman R, Esposito L, Farrell C, Feng D, Galbraith J, Garrett M, Gelfand EC, Hancock N, Harris JA, Howard R, Hu B, Hytnen R, Iyer R, Jessett E, Johnson K, Kato I, Kiggins J, Lambert S, Lecoq J, Ledochowitsch P, Lee JH, Leon A, Li Y, Liang E, Long F, Mace K, Melchior J, Millman D, Mollenkopf T, Nayan C, Ng L, Ngo K, Nguyen T, Nicovich PR, North K, Ocker GK, Ollerenshaw D, Oliver M, Pachitariu M, Perkins J, Reding M, Reid D, Robertson M, Ronellenfitch K, Seid S, Slaughterbeck C, Stoecklin M, Sullivan D, Sutton B, Swapp J, Thompson C, Turner K, Wakeman W, Whitesell JD, Williams D, Williford A, Young R, Zeng H, Naylor S, Phillips JW, Reid RC, Mihalas S, Olsen SR, Koch C. 2021. Survey of spiking in the mouse visual system reveals functional hierarchy. *Nature* **592**:86–92. doi:10.1038/s41586-020-03171-x

Slaght SJ, Leresche N, Deniau J-M, Crunelli V, Charpier S. 2002. Activity of thalamic reticular neurons during spontaneous genetically determined spike and wave discharges. *J Neurosci*

22:2323–2334. doi:22/6/2323 [pii]

Sohal VS, Huguenard JR. 2003. Inhibitory interconnections control burst pattern and emergent network synchrony in reticular thalamus. *J Neurosci* **23**:8978–8988. doi:23/26/8978 [pii]

Sohal VS, Huntsman MM, Huguenard JR. 2000. Reciprocal Inhibitory Connections Regulate the Spatiotemporal Properties of Intrathalamic Oscillations. *J Neurosci* **20**:1735–1745. doi:10.1523/JNEUROSCI.20-05-01735.2000

Soltesz I, Lightowler S, Leresche N, Jassik-Gerschenfeld D, Pollard CE, Crunelli V. 1991. Two inward currents and the transformation of low-frequency oscillations of rat and cat thalamocortical cells. *J Physiol* **441**:175–197. doi:10.1113/jphysiol.1991.sp018745

Song I, Kim D, Choi S, Sun M, Kim Y, Shin HS. 2004. Role of the α1G T-type calcium channel in spontaneous absence seizures in mutant mice. *J Neurosci* **24**:5249–5257. doi:10.1523/JNEUROSCI.5546-03.2004

Soong TW, Stea A, Hodson CD, Dubel SJ, Vincent SR, Snutch TP. 1993. Structure and functional expression of a member of the low voltage - Activated calcium channel family. *Science* **260**:1133–1136. doi:10.1126/science.8388125

Sorokin JM, Davidson TJ, Frechette E, Abramian AM, Deisseroth K, Huguenard JR, Paz JT. 2017. Bidirectional Control of Generalized Epilepsy Networks via Rapid Real-Time Switching of Firing Mode. *Neuron* **93**:194–210. doi:10.1016/j.neuron.2016.11.026

Spiegel EA, Wycis HT. 1950. Thalamic recordings in man with special reference to seizure discharges. *Electroencephalogr Clin Neurophysiol* **2**:23–27. doi:https://doi.org/10.1016/0013-4694(50)90003-4

Steriade M, Amzica F. 2003. Sleep Oscillations Developing into Seizures in Corticothalamic Systems. *Epilepsia* **44**:9–20. doi:10.1111/j.0013-9580.2003.12006.x

Steriade M, Dossi RC, Nunez A. 1991. Network modulation of a slow intrinsic oscillation of cat thalamocortical neurons implicated in sleep delta waves: Cortically induced synchronization and brainstem cholinergic suppression. *J Neurosci* **11**:3200–3217. doi:10.1523/jneurosci.11-10-03200.1991

Steriade M, Llinas R. 1988. The functional states of the thalamus and the associated neuronal interplay. *Physiol Rev* **68**. doi:10.1152/physrev.1988.68.3.649

Steriade M, McCormick DA, Sejnowski TJ. 1993. Thalamocortical oscillations in the sleeping and aroused brain. *Science* **262**:679–85. doi:10.1126/science.8235588

Swadlow HA, Gusev AG, Bezdudnaya T. 2002. Activation of a cortical column by a thalamocortical impulse. *J Neurosci* **22**:7766–7773. doi:10.1523/jneurosci.22-17-07766.2002

Talley EM, Cribbs LL, Lee JH, Daud A, Perez-Reyes E, Bayliss DA. 1999. Differential distribution of three members of a gene family encoding low voltage-activated (T-type) calcium channels. *J Neurosci* **19**:1895–1911. doi:10.1523/jneurosci.19-06-01895.1999

Talley EM, Solórzano G, Depaulis A, Perez-Reyes E, Bayliss DA. 2000. Low-voltage-activated calcium channel subunit expression in a genetic model of absence epilepsy in the rat. *Mol Brain Res* **75**:159–165. doi:10.1016/S0169-328X(99)00307-1

Tenney JR, Glauser TA. 2013. The current state of absence epilepsy: Can we have your attention? *Epilepsy Curr* **13**:135–140. doi:10.5698/1535-7511-13.3.135

Tsakiridou E, Bertollini L, De Curtis M, Avanzini G, Pape HC. 1995. Selective increase in T-type calcium conductance of reticular thalamic neurons in a rat model of absence epilepsy. *J Neurosci* **15**:3110–3117. doi:10.1523/jneurosci.15-04-03110.1995

Velasco AL, Velasco F, Jiménez F, Velasco M, Castro G, Carrillo-Ruiz JD, Fanghänel G, Boleaga

B. 2006. Neuromodulation of the centromedian thalamic nuclei in the treatment of generalized seizures and the improvement of the quality of life in patients with Lennox-Gastaut syndrome. *Epilepsia* **47**:1203–1212. doi:10.1111/j.1528-1167.2006.00593.x

Velasco M, Velasco F, Alcalá H, Dávila G, Díaz-de-León AE. 1991. Epileptiform EEG Activity of the Centromedian Thalamic Nuclei in Children with Intractable Generalized Seizures of the Lennox-Gastaut Syndrome. *Epilepsia* **32**:310–321. doi:10.1111/j.1528-1157.1991.tb04657.x

Vezzani A, Balosso S, Ravizza T. 2019. Neuroinflammatory pathways as treatment targets and biomarkers in epilepsy. *Nat Rev Neurol* **15**:459–472. doi:10.1038/s41582-019-0217-x

Vitko I, Chen Y, Arias JM, Shen Y, Wu XR, Perez-Reyes E. 2005. Functional characterization and neuronal modeling of the effects of childhood absence epilepsy variants of CACNA1H, a T-type calcium channel. *J Neurosci* **25**:4844–4855. doi:10.1523/JNEUROSCI.0847-05.2005

von Krosigk M, Bal T, Mccormick DA. 1993. Cellular Mechanisms of a Synchronized Oscillation in the Thalamus. *Science* **261**:361–364. doi:10.1126/science.8392750

Wallace RH, Marini C, Petrou S, Harkin LA, Bowser DN, Panchal RG, Williams DA, Sutherland GR, Mulley JC, Scheffer IE, Berkovic SF. 2001. Mutant GABA A receptor γ2-subunit in childhood absence epilepsy and febrile seizures. *Nat Genet* **28**:49–52. doi:10.1038/88259

Warren AEL, Dalic LJ, Thevathasan W, Roten A, Bulluss KJ, Archer J. 2020. Targeting the centromedian thalamic nucleus for deep brain stimulation. *J Neurol Neurosurg Psychiatry* **91**:339–349. doi:10.1136/jnnp-2019-322030

Weiergräber M, Henry M, Krieger A, Kamp M, Radhakrishnan K, Hescheler J, Schneider T. 2006. Altered seizure susceptibility in mice lacking the Cav2.3 E-type Ca2+ channel. *Epilepsia*

47:839–850. doi:10.1111/j.1528-1167.2006.00541.x

Williams D. 1953. A Study of Thalamic and Cortical Rhythms in Petit Mal. *Brain* **76**:50–69. doi:10.1093/brain/76.1.50

Williamson AM, Ohara PT, Ralston HJ. 1993. Electron microscopic evidence that cortical terminals make direct contact onto cells of the thalamic reticular nucleus in the monkey. *Brain Res* **631**:175–179. doi:10.1016/0006-8993(93)91207-9

Wimmer RD, Astori S, Bond CT, Rovó Z, Chatton JY, Adelman JP, Franken P, Lüthi A. 2012. Sustaining sleep spindles through enhanced SK2-channel activity consolidates sleep and elevates arousal threshold. *J Neurosci* **32**:13917–13928. doi:10.1523/JNEUROSCI.2313-12.2012

Winnubst J, Bas E, Ferreira TA, Wu Z, Economo MN, Edson P, Arthur BJ, Bruns C, Rokicki K, Schauder D, Olbris DJ, Murphy SD, Ackerman DG, Arshadi C, Baldwin P, Blake R, Elsayed A, Hasan M, Ramirez D, Dos Santos B, Weldon M, Zafar A, Dudman JT, Gerfen CR, Hantman AW, Korff W, Sternson SM, Spruston N, Svoboda K, Chandrashekar J. 2019. Reconstruction of 1,000 Projection Neurons Reveals New Cell Types and Organization of Long-Range Connectivity in the Mouse Brain. *Cell* **179**:268-281.e13. doi:10.1016/j.cell.2019.07.042

Wolfart J, Debay D, Le Masson G, Destexhe A, Bal T. 2005. Synaptic background activity controls spike transfer from thalamus to cortex. *Nat Neurosci* **8**:1760–1767. doi:10.1038/nn1591

Yang JO, Choi MH, Yoon JY, Lee JJ, Nam SO, Jun SY, Kwon HH, Yun S, Jeon SJ, Byeon I, Halder D, Kong J, Lee B, Lee J, Kang JW, Kim NS. 2021. Characteristics of Genetic Variations Associated With Lennox-Gastaut Syndrome in Korean Families. *Front Genet* **11**:1–11. doi:10.3389/fgene.2020.590924

Ying SW, Jia F, Abbas SY, Hofmann F, Ludwig A, Goldstein PA. 2007. Dendritic HCN2 channels constrain glutamate-driven excitability in reticular thalamic neurons. *J Neurosci* **27**:8719–8732. doi:10.1523/JNEUROSCI.1630-07.2007

Yizhar O, Fenno LE, Prigge M, Schneider F, Davidson TJ, O'Shea DJ, Sohal VS, Goshen I, Finkelstein J, Paz JT, Stehfest K, Fudim R, Ramakrishnan C, Huguenard JR, Hegemann P, Deisseroth K. 2011. Neocortical excitation/inhibition balance in information processing and social dysfunction. *Nature* **477**:171–178. doi:10.1038/nature10360

Zaman T, Lee K, Park C, Paydar A, Choi JH, Cheong E, Lee CJ, Shin HS. 2011. CaV2.3 Channels Are Critical for Oscillatory Burst Discharges in the Reticular Thalamus and Absence Epilepsy. *Neuron* **70**:95–108. doi:10.1016/j.neuron.2011.02.042

Zhang Y, Mori M, Burgess DL, Noebels JL. 2002. Mutations in high-voltage-activated calcium channel genes stimulate low-voltage-activated currents in mouse thalamic relay neurons. *J Neurosci* **22**:6362–6371. doi:10.1523/jneurosci.22-15-06362.2002

Chapter 3 : Astrocyte-derived Interleukin-33 promotes microglial synapse engulfment and neural circuit development

---

Abstract

Neuronal synapse formation and remodeling is essential to central nervous system (CNS) development and is dysfunctional in neurodevelopmental diseases. Innate immune signals regulate tissue remodeling in the periphery, but how this impacts CNS synapses is largely unknown. Here we show that the IL-1 family cytokine Interleukin-33 (IL-33) is produced by developing astrocytes and is developmentally required for normal synapse numbers and neural circuit function in the spinal cord and thalamus. We find that IL-33 signals primarily to microglia under physiologic conditions, that it promotes microglial synapse engulfment, and that it can drive microglial-dependent synapse depletion *in vivo*. These data reveal a cytokine-mediated mechanism required to maintain synapse homeostasis during CNS development.

Introduction

Neuronal synapse formation depends on a complex interplay between neurons and their glial support cells (Clarke and Barres, 2013; Molofsky et al., 2012). Astrocytes provide structural, metabolic, and trophic support for neurons. Gray matter astrocytes are in intimate contact with neuronal synapses and are poised to sense local neuronal cues. In contrast, microglia are the primary immune cells of the CNS parenchyma. Microglia regulate multiple phases of developmental circuit refinement (Ransohoff and Cardona, 2010; Salter and Beggs, 2014), both inducing synapse formation (Miyamoto et al., 2016; Parkhurst et al., 2013) and promoting synapse engulfment (Paolicelli et al., 2011; Schafer et al., 2012), in part via complement, an effector arm

of the innate immune system (Stevens et al., 2007). Excess complement activity has been implicated in schizophrenia, a neurodevelopmental disorder that includes cortical gray matter thinning and synapse loss (Sekar et al., 2016), suggesting that microglial synapse engulfment may have broad implications for neuropsychiatric disease.

Despite the emerging roles of astrocytes and microglia in neuronal synapse formation and remodeling, how they coordinate synaptic homeostasis *in vivo* remains obscure. Interleukin-33 (IL-33) is an IL-1 family member with well described roles as a cellular alarmin released from nuclear stores following tissue damage, including in spinal cord injury (Gadani et al., 2015; Pomeshchik et al., 2015), stroke (Luo et al., 2015) and Alzheimer's disease (Fu et al., 2016). Whereas many cytokines are primarily defined by their roles in inflammation and disease (*e.g.* IL-1, TNF-α or IL-6), IL-33 also promotes homeostatic tissue development and remodeling (Molofsky et al., 2015). The CNS undergoes extensive synapse remodeling during postnatal brain development, but a role for IL-33 or other stromal-derived cytokines is unknown. Here we report that IL-33 is produced postnatally by synapse-associated astrocytes, is required for synaptic development in the thalamus and spinal cord, and signals to microglia to promote increased synaptic engulfment. These findings reveal a physiologic requirement for cytokine-mediated immune signaling in brain development.

Results

We previously developed methods to identify functionally heterogeneous astrocytes by expression profiling of distinct CNS regions (Molofsky et al., 2014). In a RNA sequencing screen of developing forebrain astrocytes (P9; flow sorted using an *Aldh1l1-eGFP* reporter) we identified the cytokine Interleukin-33 (IL-33) as a candidate that is both astrocyte-enriched and heterogeneously expressed by astrocytes throughout the CNS (**Fig. S1A-C**). We confirmed

astrocyte-specific developmental expression of IL-33 in spinal cord and thalamus using a nuclear localized *Il33* reporter (*Il33*$^{mCherry/+}$ **Fig. 3.1A**) and validated these findings with flow cytometry and protein immunostaining (**Fig. S3.2)**. By adulthood, a subset of oligodendrocytes also co-labeled with IL-33 (**Fig. S3.2C-E**), consistent with prior reports (Gadani et al., 2015). Thus, astrocytes are the primary source of IL-33 during postnatal synapse maturation.

Although most IL-33 positive cells were astrocytes, not all developing astrocytes expressed IL-33, and this number increased in the early postnatal period (**Fig. S3.3;** (Wicher et al., 2013)**).** In fact, IL-33 was detected only in gray matter, where most synapses are located (**Fig. 3.1B, Fig. S3.2H, Fig. S3.3D**). In the thalamus, which receives regionally distinct sensory synaptic inputs, IL-33 expression in the visual nucleus (dLGN) increased sharply coincident with eye opening (P12-P14, **Fig. 3.1C, D**). Removal of afferent sensory synapses by enucleation at birth prevented this developmental increase in IL-33 expression (**Fig. 3.1E, F**), whereas dark rearing, in which synapse maturation is largely preserved (Hooks and Chen, 2006) had no effect. Molecular profiling of IL-33 positive astrocytes in both thalamus and spinal cord (**Fig. 3.1G, H**), revealed a negative correlation with white matter astrocyte markers (*GFAP, Vimentin*), enrichment for genes involved in astrocyte synaptic functions (connexin-30/*Gjb6* (Pannasch et al., 2014)), and enrichment in G-protein coupled and neurotransmitter receptors (e.g. *Adora2b*, *Adra2a;* **Table 3.1 to 3.3**). Together, these data demonstrate that IL-33 expression is correlated with synaptic maturation and marks a subset of astrocytes potentially sensitive to synaptic cues, raising the question of whether IL-33 plays a role in synapse development.

To test whether IL-33 regulates neural circuit development and function, we examined the effect of IL-33 deletion on synapse numbers and circuit activity. In the thalamus, a region with high IL-33 expression, an intrathalamic circuit between the ventrobasal nucleus (VB) and the

reticular nucleus of the thalamus (RT) displays spontaneous oscillatory activity that can also be evoked by stimulating the internal capsule that contains cortical afferents (Lui et al., 2016; Paz et al., 2010). We quantified this oscillatory activity in slices from young adult mice (P30-P40) which revealed enhanced evoked activity in response to stimulation (**Fig. 3.2A, B; Fig. S3.4A-B)** as well as elevated spontaneous firing in the absence of IL-33 (**Fig. 3.2C; Fig. S3.4C**). This increase could result at least in part from enhanced numbers of glutamatergic synapses. To investigate this hypothesis, we performed whole-cell patch-clamp recordings of VB neurons to quantify miniature excitatory postsynaptic currents (mEPSCs; **Fig. 3.2D**). We found that the frequency of mEPSCs was enhanced in VB neurons from IL-33-deficient mice, whereas the amplitude and the kinetics were unchanged (**Fig. S3.4D**). Together, these results suggest that IL-33 deficiency leads to excess excitatory synapses and a hyperexcitable intrathalamic circuit.

In the spinal cord, α-motor neurons (α-MN) are the primary outputs of the sensorimotor circuit and receive inputs from excitatory (vGlut2+) and inhibitory (VGAT+) interneurons (**Fig. 3.2E,** (Arber, 2012)). We conditionally deleted IL-33 from astrocytes (*hGFAPcre* (Molofsky et al., 2014), **Fig. S3.5A**), and found increased numbers of excitatory and inhibitory inputs onto α-MN at P30; global deletion of *Il1rl1 (ST2)* (**Fig. 3.2F-I**) *or Il33* (**Fig. S3.5B, C**) phenocopied this finding. Neuronal soma size, interneuron numbers, and oligodendrocyte numbers were unchanged (**Fig. S3.5D-F)**. However, by adulthood, IL-33 deficiency led to increased gray matter expression of glial fibrillary acidic protein (GFAP; **Fig. S3.5G-H**), a marker of tissue stress. We also found that *Il33*$^{-/-}$ animals had deficits in acoustic startle response, a sensorimotor reflex mediated by motor neurons in the brainstem and spinal cord (**Fig. 3.2J, K**; (Koch, 1999). Auditory acuity and gross motor performance were normal (**Fig. S3.5 I-J**). Taken together, these data demonstrate that IL-33 is required for normal synapse numbers and circuit function in the thalamus and spinal cord.

To determine the cellular targets of IL-33 signaling we first quantified expression of its obligate co-receptor IL1RL1 (ST2) (Molofsky et al., 2015). We detected *Il1rl1* in microglia by RNA sequencing (7.1± 2.1 FPKM), and by quantitative PCR, in contrast to astrocytes, neurons, or the lineage negative fraction (**Fig. 3.3A).** The transcriptome of acutely isolated microglia from *Il33*$^{-/-}$ animals revealed 483 significantly altered transcripts, including reduced expression of NF-κB targets (e.g. *Tnf, Nfkbia*, *Nfkbiz*, *Tnfaip3*; **Fig. 3.3B-C; Fig. S3.6A, additional data table S2**), consistent with diminshed NF-κB signaling (Ruland, 2011). The transcriptome of *Il33*$^{-/-}$ astrocytes was unchanged (**Fig. S3.6B**), strongly arguing against cell autonomous roles of IL-33 in this context. These data demonstrate physiologic signaling by IL-33 to microglia during brain development, raising the question of whether it promotes physiologic microglial functions.

Given the increased synapse numbers in IL-33 deficient animals, we tested whether IL-33 is required for microglial synapse engulfment. We detected engulfed PSD-95+ synaptic puncta within spinal cord microglia throughout development, as in other CNS regions (Paolicelli et al., 2011; Schafer et al., 2012), and found decreased engulfment in microglia from *Il33*$^{-/-}$ animals (P15; **Fig. 3.3D**). This was further validated by dye labeling of spinal cord motor neurons, which revealed fewer dye filled microglia in *Il33*$^{-/-}$ (**Fig. S3.7**). Conversely, local injection of IL-33 increased PSD-95 within microglia in both spinal cord (**Fig. 3.3E**) and thalamus (**Fig. S3.8A-B**), and altered markers consistent with microglial activation, including IL1RL1-dependent downregulation of P2Y12 (**Fig. S3.9A-C,** (Haynes et al., 2006)). In vitro, IL-33 promoted synaptosome engulfment by purified microglia, whereas the canonical IL-1 family member IL-1β had no effect (**Fig. S3.9D-E**). *In vivo*, injection of IL-33 into the developing spinal cord led to two-fold depletion of excitatory synapses (colocalized vGlut2/PSD-95) whereas conditional deletion of IL1RL1 from microglia partly reversed this effect (*Cx3cr1cre: Il1rl1*$^{fl/fl}$, **Fig. 3.3F, G)**. In

comparison, global loss of *Il1rl1* completely reversed IL-33 dependent synapse depletion in spinal cord (**Fig. S3.10**) and thalamus (**Fig. S3.8C-D)**, suggesting that non-microglial sources of ST2 could also contribute. These data indicate that IL-33 regulates synapse numbers *in vivo* at least in part via IL1RL1 receptor-mediated signaling in microglia.

Our data reveal a mechanism of astrocyte-microglial communication that is required for synapse homeostasis during CNS development. We propose that astrocyte-derived IL-33 serves as a rheostat, helping to tune microglial synapse engulfment during neural circuit maturation and remodeling (**Fig. S3.11**). Key unanswered questions include the nature of the cues that induce astrocyte *Il33* expression, the mechanism of IL-33 release, and the signals downstream of IL-33 that promote microglial function. These data also raise the broader question of how this process impacts neural circuit function. Synapses are the most tightly regulated variable in the developing CNS (Chovatiya and Medzhitov, 2014) and are a primary locus of dysfunction in neurodevelopmental diseases. *Il33* is one of five genes that molecularly distinguishes astrocytes from neural progenitors in developing human forebrain (Pollen et al., 2015), suggesting possibly conserved roles in the human CNS. Defining whether signals like IL-33 are permissive or instructive, promiscuous or synapse specific, is a first step towards understanding how neural circuits remodel during development and under stress.

Acknowledgements

We are grateful to the Molofsky labs, Poskanzer lab, R.M. Locksley, and J.R. Chan for helpful comments on the manuscript. Thanks to the J. Huguenard lab for the thalamic network analysis code, to J.P Girard for $Il33^{lacZ}$ mice, R.T. Lee for $Il33^{fl/fl}$ and $Il1rl1^{fl/fl}$, M. Colonna and the Mucosal

Immunology Studies Team (MIST) for *Il33*$^{H2B\text{-}mCherry}$, D. Julius for the P2Y12 antibody, and the Gladstone Genomics and Behavioral Cores (P30NS065780) for technical contributions.

Funding

A.V.M is supported by a Pew Scholars Award, NIMH (K08MH104417), the Brain and Behavior Research Foundation, and the Burroughs Wellcome Fund. A.B.M is supported by the NIDDK (K08DK101604) and the Larry L. Hillblom Foundation. J.T.P is supported by NINDS (R01NS096369). S.A.L. is supported by the Australian National Health and Medical Research Council (GNT1052961), and the Glenn Foundation Glenn Award. F.S.C (NSF #1144247) and P.T.N. were supported by Graduate Student Fellowships from the National Science Foundation.

Authors contributions

I.D.V., G.C., A.V.M, and J.G.M. designed, performed and analyzed most experiments. E.C.C., H.N-I, P.T.N., and L.C.D. contributed to experiments and data analysis. F.S.C and J.T.P. designed, performed and analyzed the electrophysiology experiments. K.W.K and I.D.V designed and performed bioinformatics analyses. S.A.L. performed and analyzed culture experiments under supervision of B.A.B. O.A. performed and analyzed auditory testing. S.J. generated Il33-H2B-mCherry mice. A.V.M and A.B.M designed experiments and wrote the manuscript together with I.D.V., G.C. and other authors.

Materials & Methods

***Mice*:** All mouse strains were maintained in the University of California San Francisco specific pathogen–free animal facility, and all animal protocols were approved by and in accordance with

the guidelines established by the Institutional Animal Care and Use Committee and Laboratory Animal Resource Center. Littermate controls were used for all experiments when feasible, and all mice were backcrossed >10 generations on a C57Bl/6 background unless otherwise indicated. The following mouse strains were used as referenced in the text: For global deletion of IL-33, *Il33*$^{lacZ/lacZ}$ knockins were used (Pichery et al., 2012); lacZ reporter assays utilized heterozygote animals from the same line, and global deletion of *Il1rl1* (ST2) used a knockout line (Hoshino et al., 1999). Astrocyte specific deletion of IL-33 in spinal cord utilized transgenic line *hGFAPcre* (Zhuo et al., 2001) as previously validated in spinal cord (Molofsky et al., 2014). Microglial/monocyte specific deletion utilized *Cx3cr1cre* (Yona et al., 2013). *Il33*$^{fl/fl}$ and *Il1rl1*$^{fl/fl}$ were obtained from the Richard Lee lab (Chen et al., 2015) and were on a mixed genetic background. Astrocyte reporter line Aldh111^{eGFP} is a BAC transgenic generated by the GENSAT project (Gong et al., 2003); regional expression profiling in Fig. S1 was done on a Swiss-Webster background, all other experiments were on a N>5 C57Bl/6 background. Cx3cr1^{eGFP} is a knockin allele (Jung et al., 2000). For fluorescent IL-33 reporter assays, a novel *Il33*^{mCherry} line developed in the Colonna Lab (Washington University, USA) was used. Mice were derived from an insertional mutation of a gene trap cassette into the intron upstream of exon 5 of the *Il33* gene. The cassette consists of a mouse En2 splicing acceptor (SA) and an H2B nuclear localization tag fused to the mCherry reporter and followed by a viral 2A peptide sequence and a puromycin resistance cassette.

CNS injections: All brain injections were performed with a Kopf stereotaxic apparatus with a microdispensing pump (World Precision Instruments) holding a beveled glass needle with 50 μM outer diameter, to inject IL-33 at 1mg/ml concentration or vehicle control. For perinatal injections

and synapsin-1 quantifications, mice were anesthetized by hypothermia, headfixed with a custom clay mold, and 1 µl of Il33 or vehicle was injected into the right lateral ventricle. Mice were allowed to recover in their home cage, and euthanized by perfusion 18 hours later. For PSD-95 quantifications in the spinal cord, P14 mice were anesthetized by isoflurane and headfixed with earbars. A laminectomy at the T12 vertebrae was performed to expose the dorsal spinal cord. Z-depth was established at the surface of the spinal cord and the needle was lowered to a depth of DV=0.3 mm. 100 nl of solution was slowly infused at a rate of 3 nl/sec, and left in place for 5 minutes following injection to allow for local diffusion. Mice were euthanized by perfusion 18 hours following injection and processed for immunohistochemistry.

Flow cytometry*:* P9-P15 animals were perfused with ice-cold HBSS-Ca/Mg free until clear and CNS regions were microdissected under a dissecting microscope and meninges were removed. When for RNA sequencing, the tissue was dissociated with papain 20 U/ml (Worthington) for 80 minutes at 33°C as previously described. For P2ry12 qPCR tissues were dissociated using a tissue homogenizer as previously described (Galatro et al., 2017). For Il1rl1/ST2 qPCR accutase was used to dissociate and protocol for sorting neurons, astrocytes, and microglia was followed as described by Srinivasan et al. 2016 (Srinivasan et al., 2016). At ages P13 and above, a 22% percoll gradient was added to deplete myelin (Galatro et al., 2017). Cells were sorted on a BD Facs Aria III and gated on forward/side scatter, live/dead by DAPI exclusion, Aldh1l1-GFP to isolate astrocytes, CD11b/CD45/Ly6C (eBioscience/Biolegend) to identify microglia and exclude peripheral macrophages, and Neun-GFP (EMD Millipore) for neurons. In some cases where a single population was defined, CD11b was used in subsequent experiments. Aldh1l1-eGFP/IL33-mCherry experiments were gated as indicated, following side-scatter, live-dead, and microglia exclusion by CD11b.

RNA isolation: RNA was isolated using TRIZOL reagent (Invitrogen), DNAse digested to remove genomic DNA contamination, and further purified using the RNAeasy Kit (Qiagen). For mCherry and all qPCR analyses, cells were placed directly into Qiagen RNAeasy RLT+ buffer and kept overnight at -80°C prior to isolation with the RNeasy plus Micro Kit (Qiagen). For qPCR analysis, RNA was reverse transcribed using a high capacity cDNA reverse transcription kit and random primers (Applied Biosystems). cDNA was diluted 1:100 in the final qPCR reaction. qPCR was performed on an ABI qPCR machine using Sybr green.

RNA sequencing: cDNA was generated from full length RNA using the NuGEN RNA- Seq V2 kit which uses the single primer isothermal amplification method to deplete ribosomal RNA, and sheared by Covaris to yield uniform size fragments. The NuGen Ultralow kit was used to add adapters, barcoding and amplification. Library was purified using Agencourt XP magnetic beads, QC'd with an agilent bioanalyzer, and quantified by qPCR. For data in Fig. S3.1, RNA sequencing was performed in two separate batches (regional astrocyte data not including spinal cord and *Il33* data from spinal cord). 3 or 4 libraries were pooled per lane for single end (SE50) sequencing. For the regional astrocyte data, over 44 M reads were sequenced per sample (range 44 – 60 M reads) using an Illumina HiSeq 2000. For data in Fig. 3.1H and Fig. 3.3B, C, over 79 M reads were sequenced per sample (range 79 – 133 M reads) on an Illumina HiSeq 4000.

Bioinformatics Read quality was assessed using fastqc (Andrews, 2010) and the first 5 bases of each read from the regional astrocyte data and the first 11 bases of each read from the Il33 data were trimmed and aligned to the Mus Musculus genome (Ensembl GRCm38) (Aken et al., 2016) using TopHat2 (version 2.0.11) with bowtie2 (version 2.2.3) (Kim et al., 2013). TopHat2 was run with the following arguments "--no-coverage-search --segment-length 20 --segment-mismatches

1" with the genes.gtf file from Ensembl GRCm38. Gene counts were created from the alignment files using htseq-count (version 0.6.1p1) with default parameters (Anders et al., 2015). From raw count files, DESeq2 (Love et al., 2014) was used to detect differentially expressed genes with cooksCutoff=False. FPKM values were generated using cuffquant and cuffnorm from the cufflinks suite of software tools (Trapnell et al., 2010). Quantile normalized FPKM values are reported. For analysis of astrocytes differentially expressing IL33-mCherry, the consensus list of 444 candidates was obtained with the following filters: 1) Significant in the combined differential expression analysis (pAdj<0.01). 2) Moderately expressed (mean FPKM > 20 in at least one condition/region of the IL33-mCherry+ or IL33-mCherry- samples), 3) astrocyte-enriched (2-fold in Aldh1l1+/Aldh1l1- in at least one brain region from the astrocyte heterogeneity screen in Fig. S3.1).

LacZ staining: Slides were incubated at 37°C in a solution of 1% 0.1M Potassium Ferricyanide, 1% 0.1M Potassium Ferrocyanide 0.5% Xgal, 0.2% 1M Magnesium Chloride in PBS. 37°C until color was clearly discernible under light microscope (~3.5 hours). All slides used in quantitations were stained together to avoid batch effects. Images were acquired on a Leica M80 stereomicroscope and quantified in ImageJ using the mean pixel intensity in a specified area.

Antibodies: For immunohistochemistry, primary antibody staining was done either overnight at 4°C or 1hr at room temperature (20°C) in 5% serum and 0.4% Triton, following antigen retrieval for 2min at 95°C in 0.01M citrate buffer, pH 6.0. Antibodies used for IHC included goat ChAT 1:100 (Millipore), mouse NeuN 1:500 (Millipore), guinea pig vGluT2 1:5000 (Millipore), Rabbit VGAT 1:4000 (Synaptic Systems), rat GFAP 1:1000 (Invitrogen), chick anti-GFP 1:500 (Abcam), Rabbit anti- RFP (In living colors, Clontech), anti B-galactosidase (abcam ab9361), synapsin 1,

rabbit p2y12 (gift of D. Julius), rabbit PSD-95 (invitrogen 51-6900), rabbit IBA-1 (Wako), mouse CC1 (Millipore OP80), Rabbit anti Olig2 (gift of C. Stiles), Alexa Fluor 555 rabbit anti-fluorescein IgG (Molecular Probes), and DAPI Fluoromount-G (SouthernBiotech). Antibodies used for both IHC and western blotting were Goat anti-IL- 33 (1:500, R&D Systems AF 3626); Rabbit anti-Aldh1l1 (1:2000, Abcam ab87117), Rabbit anti-Goat HRP-linked secondary (1:1000, BioRad 1721034); and Goat anti-Rabbit HRP-linked secondary (1:5000; CST 7074S).

Western blotting: Tissues were flash frozen on dry ice, then sonicated for 20 seconds in lysis buffer (50 mM tris-HCl, 1 mM EDTA, 1% Tx-100, 150 mM NaCl). The sample was centrifuged for 10 minutes at 15,000 rpm at four degrees Celsius and the pellet was discarded. Samples were run on a denaturing gel and transferred to PVDF membrane, blocked with 5% milk in TBST for 1 hour at room temperature, incubated in primary antibody overnight at 4°C and secondary at room temperature for one hour, and developed with ECL plus.

Synaptosome/myelin purification: Synaptosomes were purified as described previously (Dunkley et al., 2008), and conjugated with pHrodoTM Red, succinimidyl ester (Thermo Fisher Scientific, P36600) in 0.1 M sodium carbonate (pH 9.0) at room temperature with gentle agitation. After two-hour incubation, unbound pHrodo was washed-out by multiple rounds of centrifugation and pHrodo-conjugated synaptosomes/myelin were re- suspended with isotonic buffer containing 5% DMSO for subsequent freezing.

Microglial in vitro engulfment assay: Microglia were purified by immunopanning from postnatal day 6 rat cortices and cultured as previously described (Liddelow et al., 2017). Briefly, cortices were digested enzymatically with papain (100U, Worthington) then mechanically dissociated to generate a single cell suspension that was incubated on successive

negative panning plates to remove endothelial cells and oligodendrocyte lineage cells before positive selecting for microglia with a CD45-coated panning plate. Isolated microglia were cultured in PDL-coated 96-well plates at a density of 1000 cells/well in a defined culture media containing DMEM/F-12 (Thermo Fisher Scientific, 11320033), 100U/ml penicillin, 100ug/ml streptomycin, 100 nM Na-selenite, 10 ng/ml transferrin, and 5 ug/ml N-acetyl cysteine, with 1% heat inactivated FCS (Sigma). Engulfment assays were conducted at 7DIV: microglia were incubated with IL-33 and either 5 µl pHrodo-conjugated purified synaptosomes or 800 µg/ml media pHrodo- conjugated myelin debris, and plates were imaged at 1 h intervals for 24 h with an epifluorescence time lapse microscope (IncuCyte Zoom® System) to reveal engulfed pHrodo-conjugated particles. For image processing analysis, we took 9 images/well using 20x objective lens from random areas of the 96-well plates and calculated the phagocytic index (PI) by measuring the area of engulfed synaptosomes/myelin (fluorescent signal) normalized to the area of microglia using ImageJ. Engulfment ability was calculated by normalizing PI of control and IL-33 treated microglia.

Synapse quantifications*:* Sensorimotor synapses onto motor neuron soma were quantified as previously described (Molofsky et al., 2014). Images were collected using a Leica SP5 confocal microscope using an objective with a numerical aperture of 1.4. Counts of synaptic puncta per MN soma represent pooled data from ChAT+ NeuN+ **α**-MNs at both cervical and lumbar levels versus littermate controls. Experimenter was blinded to genotype for all quantifications. Other images were collected on a Zeiss LSM confocal. Synapse co-localization for pre-and postsynaptic markers (Fig. 3F, G, Fig. S10) was quantified by determining co-localization of PSD-95 and vGlut2 in optical sections of ventrobasal thalamus. Briefly, images were collected on a Zeiss LSM 780 laser scanning confocal using standardized imaging parameters throughout, and colocalization was

analyzed using an ImageJ script developed by the Eroglu lab (v1.29 PunctaAnalyzer plugin (Risher et al., 2014; Singh et al., 2016)). Image quality was checked by repeating analyses after 90° rotation of one channel to verify that co-localization was not due to random chance.

Microglial in vivo engulfment assay: For IL-33 injection experiments, microglia were analyzed from a region clearly outside the injection tract, but within the zone of IL-33 dependent microglial morphologic changes (~200 μm). Z-stacks encompassing entire microglia were collected on a Zeiss laser scanning confocal microscope with a 63x objective (NA1.4); laser power and gain were consistent across all experiments. Images were analyzed using Imaris software (Bitplane) by creating a 3D surface rendering of microglia, thresholded to ensure microglia processes were accurately reconstructed, and maintained consistent thereafter. This rendering was used to mask the PSD-95 channel, and the "Spots" function was used to define the number of PSD-95+ puncta entirely within the surface. For PSD-95 engulfment assays in $Il33^{+/+}$ and $Il33^{-/-}$ mice, similar analysis parameters were used, focusing on the spinal cord ventral horn.

For quantification of microglial dye engulfment, P10 mice were placed under anesthesia and a hindlimb incision was made to expose the gastrocnemius muscle. Using a bevelled glass pipette, 1-2 ul of fluoroscein labeled dextran dye (Invitrogen, lysine fixable, MW 3000) at 100 mg/ml in 1% lysolethecin/PBS was slowly bulk loaded into the muscle over 15 minutes. The animal was allowed to recover and anesthetized by perfusion 3 days later. Lumbar spinal cord sections were stained with rabbit anti- fluorescein and chick anti-GFP and all sections containing dye filled neurons were imaged using similar parameters as above. For quantification, only microglia in which at least one process was in contact with a motor neuron were considered.

Sensorimotor startle testing: Behavioral testing was performed with adult female mice (6-14 weeks; mean 9.6) including littermate controls; experimenters were blinded to genotype throughout. Mice were placed in an isolated chamber and habituated for 5 minutes to 64 dB background, then exposed to a series of 40 ms acoustic pulses at varying intensities for approximately 15 minutes at random intervals, for a total of 70 trials. Average and maximum amplitudes (N) of pulses were measured for each mouse.

Rotarod testing: Mice were placed on an accelerating rotarod from 2-80 RPM over 120 seconds. Time-to-fall was averaged over 10 trials per animal.

Auditory brainstem reflex (ABR) testing*:* Hearing tests were performed as previously described (Akil et al., 2012). with female mice (7-15 weeks; mean 10.8); experimenter was blinded to genotype throughout. Briefly, mice were anesthetized with Ketamine/xylazine, placed in a sound-proof chamber, and evoked acoustic brainstem response thresholds were recorded using subdermal needle electrodes at the vertex, below the pinna of the left ear (reference), and below the contralateral ear (ground). Stimuli were clicks (5ms duration; 31Hz, mixed tones) and tone pips at 8, 16, and 32 kHz (10ms duration; cos2 shaping; 21Hz). Measurements recorded using the TDT BioSig III system (Tucker Davis Technologies). For each stimulus, electroencephalographic (EEG) activity was recorded for 20 ms at a sampling rate of 25kHz, filtered (0.3-3kHz), and waveforms from 512 stimuli were averaged for click responses, and 1000 stimuli for frequency specific stimuli (8, 16 and 32 kHz). ABR waveforms were recorded in 5 dB sound pressure level (SPL) intervals down from the maximum amplitude. The threshold was defined as the lowest stimulus level at which response peaks for waves I-V were clearly and repetitively present upon inspection. These threshold judgments were confirmed by analysis of stored waveforms. The

comparison of each group of animals was performed using 1 way ANOVA with Bonferroni post-hoc testing.

Thalamic slice electrophysiology slice preparation: Mice were euthanized with 4% isoflurane, then perfused with ice-cold cutting solution containing 234 mM sucrose, 2.5 mM KCl, 1.25 mM NaH2PO4, 10 mM MgSO4, 0.5 mM CaCl2, 26 mM NaHCo3, and 11 mM glucose equilibrated with 95% O2 and 5% CO2. Following decapitation and removal of the brain, we prepared 400 uM or 250 uM thick horizontal thalamic slices (for circuit recordings and for whole cell patch clamp recordings, respectively) containing the ventrobasal thalamus and the nucleus reticular thalamus with a Leica VT1200 microtome (Leica Microsystems). Slices were initially incubated at 34°C for 1 hour, and then at room temperature in artificial cerebrospinal fluid (ACSF) containing 126 mM NaCl, 2.5 mM KCl, 1.25 mM NaH2PO4, 2 mM MgCl2, 2 mM CaCl2, 26 mM NaHCO3, and 10 mM glucose, equilibrated with 95% O2 and 5% CO2, pH 7.4.

Thalamic slice electrophysiology extracellular circuit recordings: Recordings were performed as described (Paz et al., 2013, 2010). Briefly, horizontal sections (400-um thick) were placed in a humidified, oxygenated interface chamber perfused with oxygenated ACSF, supplemented with 300 uM glutamine for metabolic support, at a rate of 2 mL/min at 34°C. Extracellular multi-unit recordings were obtained from VB thalamus using a 16-channel multi-electrode array (Neuronexus). Signals were acquired then amplified by 10,000 and band-pass filtered between 100 Hz and 6 kHz (RZ5 system, Tucker-Davis Technologies). A bipolar tungsten electrode was placed in the internal capsule, and was used to deliver electrical stimulation of 50 V for 100 us, every 30 seconds for 20 sweeps. Spike detection was performed using MATLAB code adapted from John Huguenard's Lab (Sorokin et al., 2017). The most active channel of each slice was included for

analysis, and statistical analyses were performed with OriginPro. For analysis of evoked oscillations, a region from 250-750 ms was selected for analysis to exclude the direct stimulus response, and significance was calculated from a firing rate frequency histogram of this time region. For spontaneous oscillations, data was collected from similar preparations but without stimulation.

Thalamic slice electrophysiology intracellular whole-cell patch clamp recordings: Recordings were performed as previously described (Paz et al., 2010). Briefly, horizontal sections (250-um thick) were placed in a chamber perfused with oxygenated ACSF supplemented with 1uM tetrodotoxin and 50 mM picrotoxin to isolate miniature excitatory post- synaptic currents (mEPSCs). Recording electrodes were made of borosilicate glass (resistance 2.5-4 MOhm) and filled with intracellular solution containing 120 mM potassium gluconate, 11 mM KCl, 1 mM MgCl2, 1 mM CaCl2, 10 mM HEPES, and 1 mM EGTA, adjusted to 290 mOsm and pH 7.4. VB cells, which were visualized by differential contrast optics with a Zeiss Axioskop microscope, were included in the analysis only if the access resistance was <25 MOhm. mEPSCs were recorded in voltage- clamp mode for 10 minutes for each neuron, and were analyzed using ClampFit, WDetecta, and MATLAB. Experimenter was blinded to genotype.

Figures

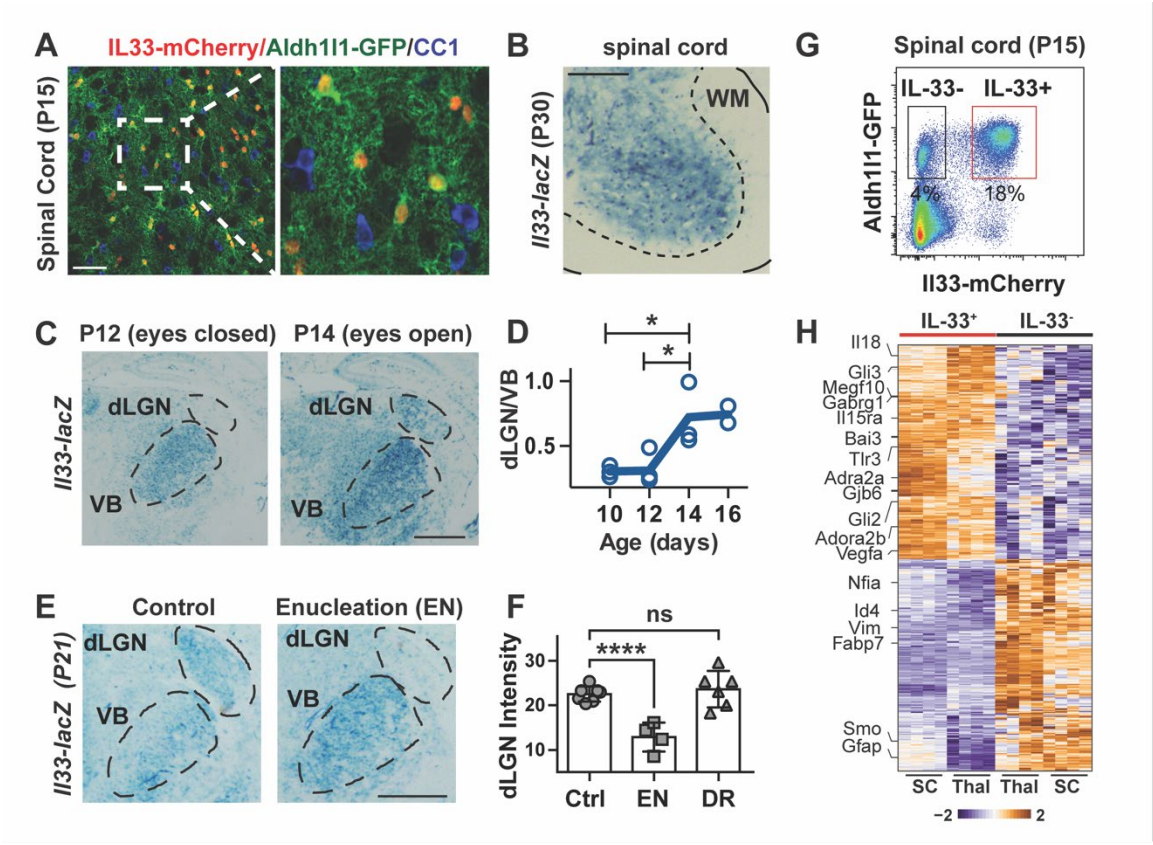

Figure 3.1. IL-33 is developmentally induced in synapse-associated astrocytes.
(**A)** Representative image of *Il33*^{mCherry} with *Aldh1l1-eGFP*+ astrocytes and oligodendrocyte marker CC1 in spinal cord ventral horn (scale = 50 μm). (**B)** Gray matter restricted expression of *Il33*^{lacZ} in the spinal cord at P30 (scale = 0.5 mm). **(C, D)** *Il33*^{lacZ} increases in the visual thalamus (dLGN) during eye opening, normalized to sensorimotor thalamus (VB) (scale = 0.5 mm). **(E)** Representative images of *Il33*^{lacZ} in P21 thalamus in littermate controls and after perinatal enucleation (scale = 0.5 mm). (**F)** *Il33*^{lacZ} mean pixel intensity in dLGN. **(G)** Representative flow plot of spinal cord from *Il33*^{mCherry}*/Aldh1l1-eGFP* mice at P15 with sorting gates indicated. (**H)** Heatmap of the top 444 differentially expressed genes in Il33-mCherry^{+} vs. mCherry^{-} astrocytes in spinal cord and thalamus (FC>2, pAdj<0.05), select candidates highlighted. **Statistics:** One-way ANOVA with Tukey's post hoc comparison or student's t-test. All points represent independent biological replicates. * p<0.05, **** p<0.0001.

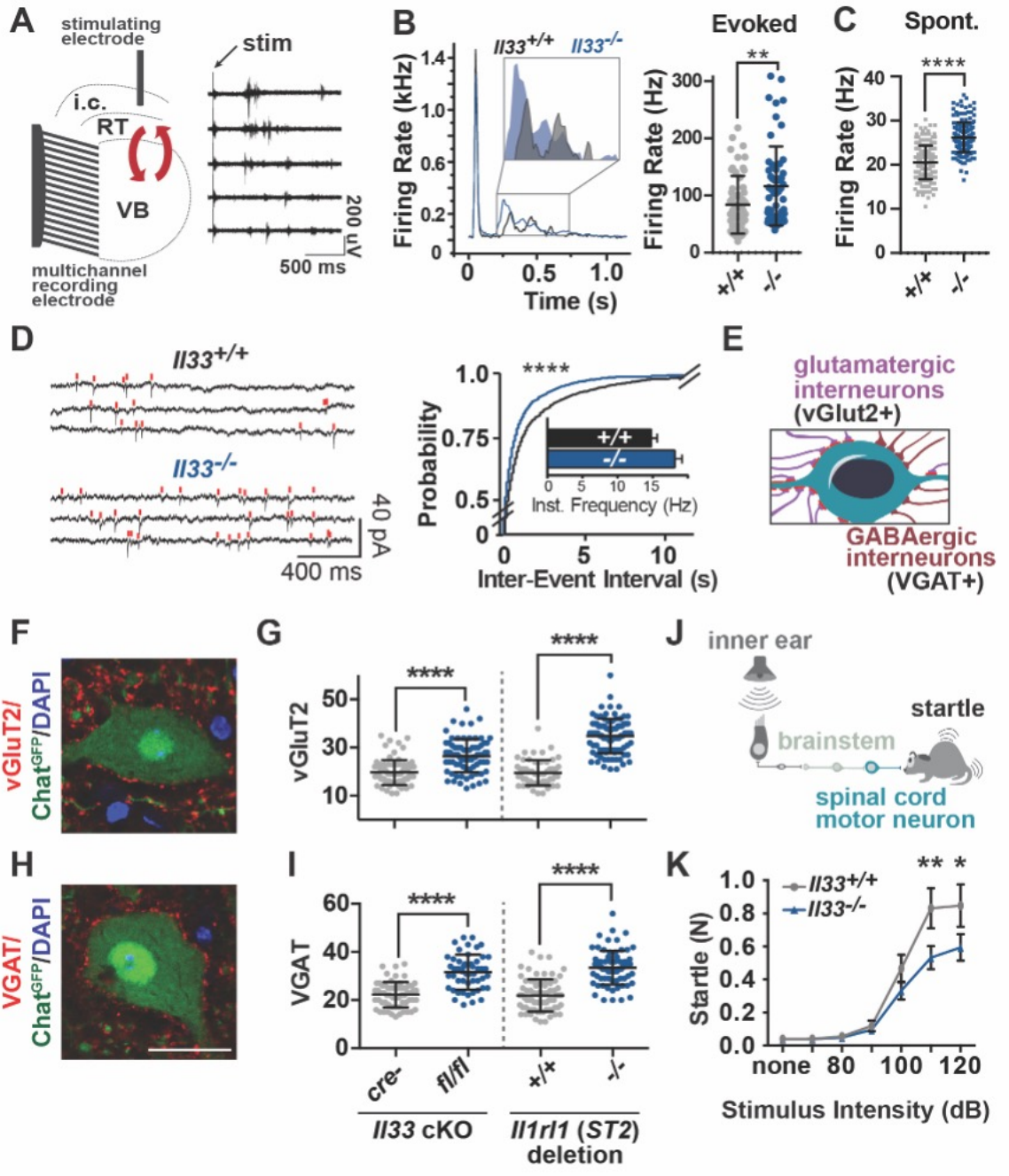

Figure 3.2. IL-33 deficiency leads to excess synapses and abnormal thalamic and sensorimotor circuit function.

(A) Schematic of extracellular recording setup to measure circuit activity between ventrobasal (VB) and reticular thalamic nuclei (RT) with representative recording showing activity in five channels after stimulation of the internal capsule (i.c.) that contains cortical afferents. Red arrows indicate reciprocal VB-RT connections. **(B)** Average traces and quantification of mean firing rates reveal higher evoked firing in *Il33*$^{-/-}$. **(C)** Quantification of mean firing rates in the absence of stimulation reveals increased spontaneous firing in *Il33*$^{-/-}$. **(D)** Representative traces and

quantification of intracellular patch-clamp recordings from neurons in the VB show increased miniature excitatory postsynaptic currents (mEPSCs) in *Il33*$^{-/-}$. **(E)** Schematic of motor neuron synaptic afferents. **(F, G)** Representative image and quantification of excitatory inputs per motor neuron after conditional deletion of *Il33* (hGFAPcre) or global deletion of *Il1rl1*. **(H, I)** Inhibitory (VGAT+) inputs in the same mice (scale = 25 μm). **(J)** Schematic of startle pathway. **(K)** Impaired sensorimotor startle in *Il33*$^{-/-}$ animals. **Statistics:** Data in **B-C** from WT: n=6-8 slices, 2 mice. KO: n=14-15 slices, 3 mice, points are individual recordings. Data in **B** analyzed by Mann-Whitney and **C** with student's t test. Data in **D** from n=23-25 cells and 3-4 mice/group analyzed by Kolmogorov-Smirnov test. Data in **F - I** from n=3 animals, >75 neurons per genotype, student's t-test; points are individual neurons. **K** is n=12/group, two-way ANOVA with Sidak's multiple comparisons. *p<0.05, **p<0.01, ****p<.0001. B-I are mean±SD, K is mean±SEM.

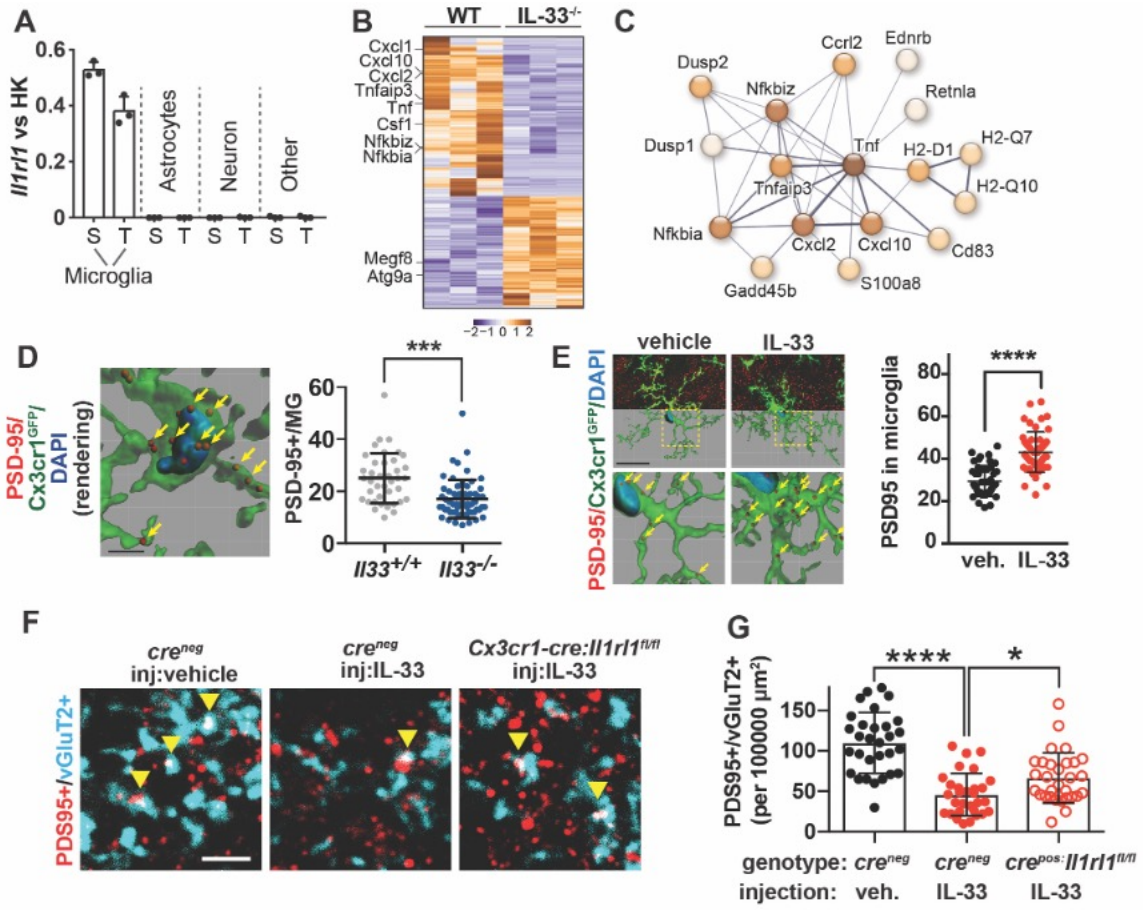

Figure 3.3. IL-33 drives microglial synapse engulfment during development.
(**A)** Expression of *Il1rl1* by qPCR of flow-sorted populations (S=spinal cord, T=thalamus.) **(B)** 484 differentially expressed genes in spinal cord microglia at pAdj<0.05. **(C)** Functionally associated gene clustering (STRING) identifies immune genes enriched in wild-type vs *Il33*$^{-/-}$ microglia. **(D)** PSD-95 puncta within microglia (yellow arrows) after IL-33 deletion (scale = 4 µM)**. (E)** Representative image and quantification of engulfed PSD-95 in vehicle or IL-33 injected spinal cord (Scale= 20 µm). **(F-G)** Colocalized pre-and postsynaptic puncta in spinal cord ventral horn at P14 (yellow arrows) after IL-33 injection into control mice or in littermates with conditional deletion of *Il1rl1* (*Cx3cr1*^{cre} ; scale = 3 µm). **Statistics:** Points in **A** represent mice, in **D-G** individual microglia from N=3-5 animals/group, in **G** images from N=5 mice/group. In **D, E** student's t-test and in **G** a one-way ANOVA with Tukey's post hoc comparison, *p<0.05, ***p<0.001, ****p<0.0001, all data are mean±SD.

Supplemental Figures

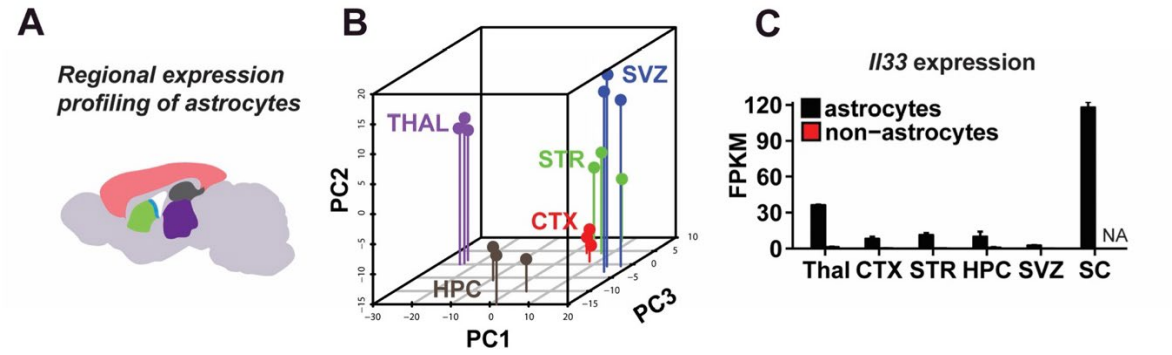

Supplemental Figure 3.1. Screening of regionally heterogeneous astrocytes identifies the candidate gene Il33.

(A) Schematic indicating regions used for expression profiling of astrocytes: cortex (red), striatum (green), subventricular zone (blue), hippocampus (brown) and thalamus (purple). **(B)** Principal component analysis of RNAseq data from Aldh1l1- eGFP+ astrocytes at P9 brain identifies regional gene expression differences. **(C)** Normalized reads of Il33 in Aldh1l1-eGFP+ astrocytes and Aldh1l1- (non-astrocytes) from the five brain regions at P9 and spinal cord at P12 ('NA'=not assessed; FPKM=Fragments per Kilobase of transcript per Million mapped reads). Mean±SEM from n=3/condition.

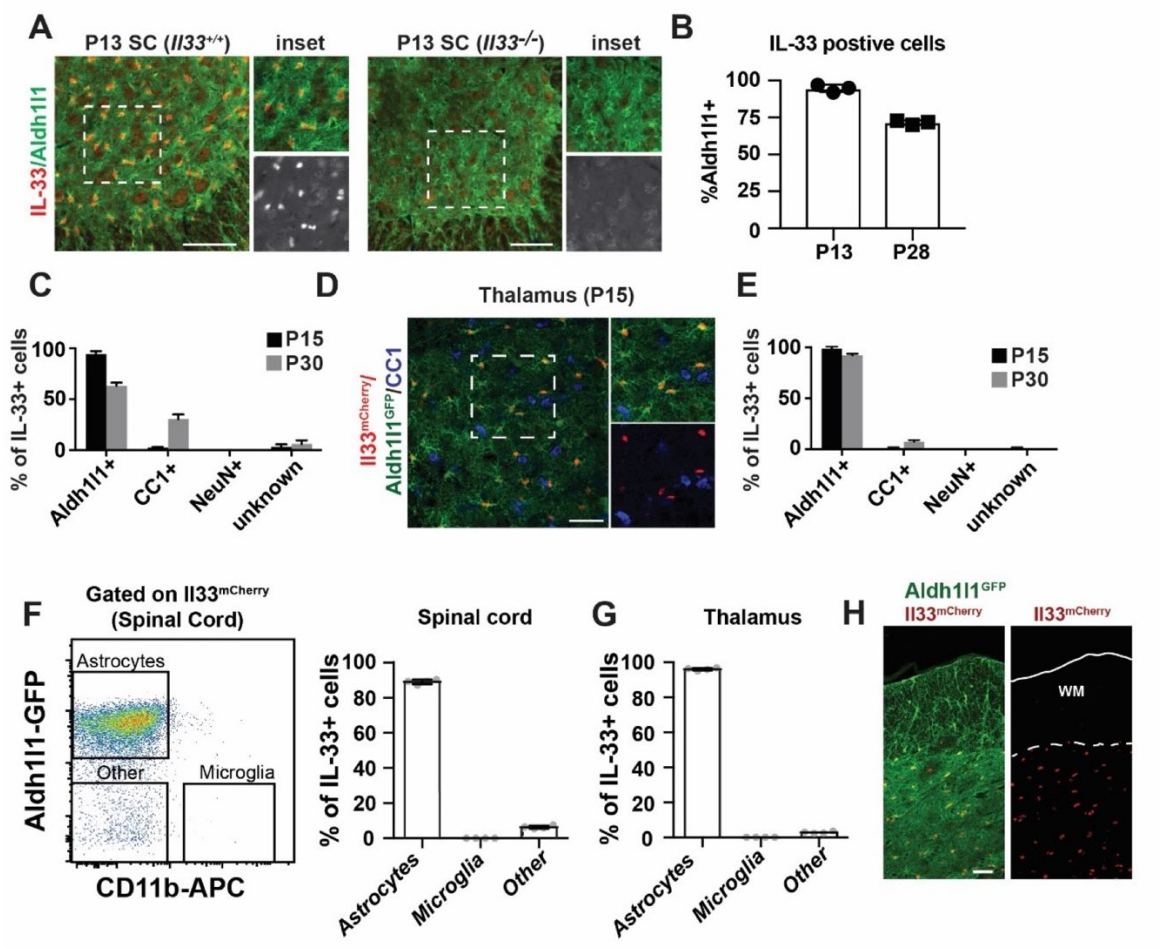

Supplemental Figure 3.2. IL-33 is expressed in protoplasmic astrocytes during postnatal development.

(A, B) Representative immunostaining and quantification of IL-33 protein with ALDH1L1 immunolabeling of astrocytes in WT and Il33-/- spinal cord gray matter (n = 3/condition; scale = 100 μm). **(C)** Quantification of Fig. 1A showing percent Il33mCherry co-localization with Aldh1l1-eGFP+ astrocytes and the oligodendrocyte marker CC1 in spinal cord at P15 and P30 (n = 3/condition). **(D, E)** Immunostaining and quantification of thalamic Il33mCherry with cell-type specific markers at P15 and P30 (n = 3/condition; scale = 50 μm). **(F-G)** IL-33 is not expressed in microglia in spinal cord or thalamus, flow cytometry of P15 spinal cord pre-gated on all Il33-mCherry+ cells (n=4). **(H)** IL-33 is gray matter restricted in spinal cord (WM=white matter; scale=50 μm).

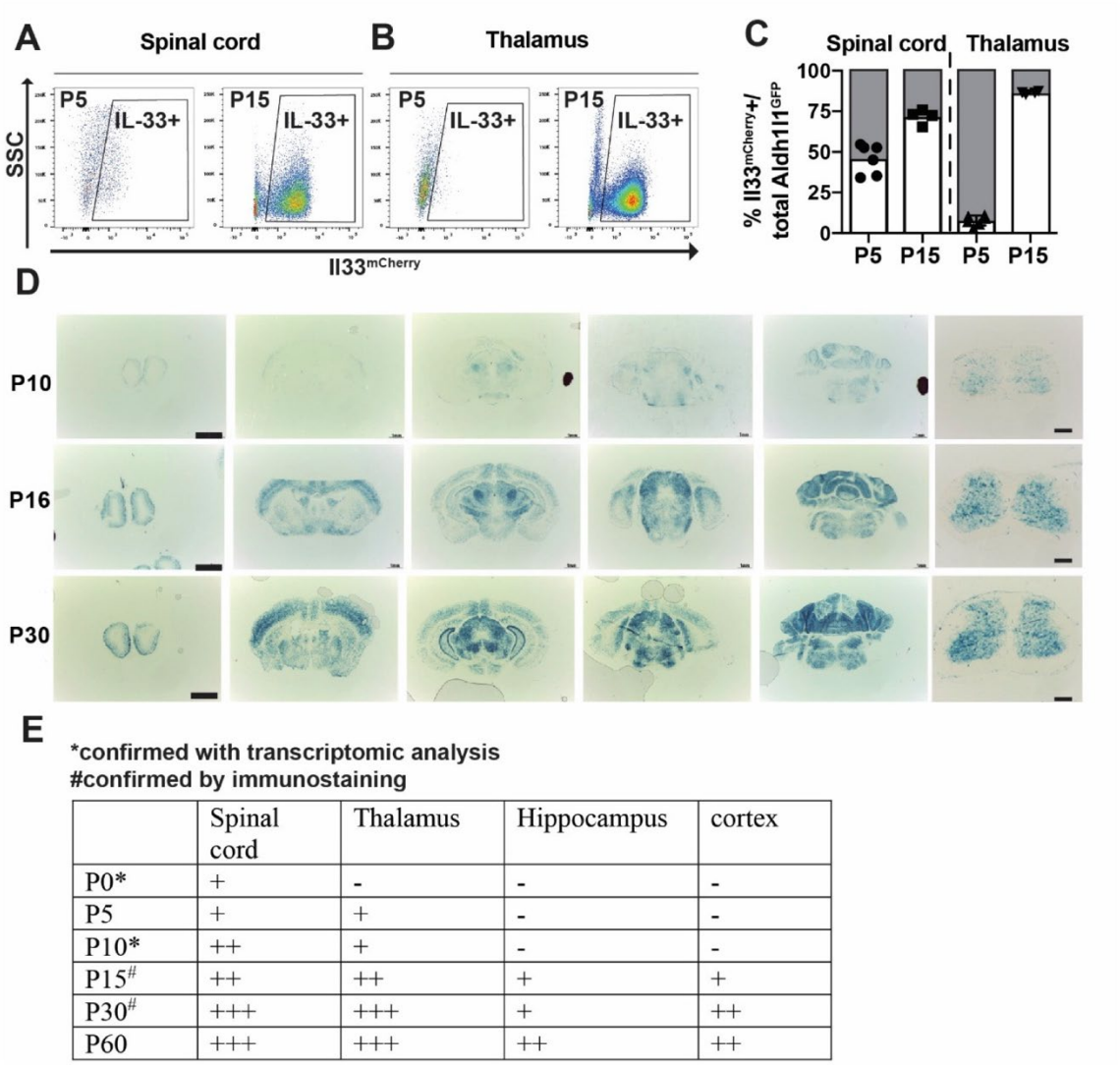

E

*confirmed with transcriptomic analysis
#confirmed by immunostaining

	Spinal cord	Thalamus	Hippocampus	cortex
P0*	+	-	-	-
P5	+	+	-	-
P10*	++	+	-	-
P15#	++	++	+	+
P30#	+++	+++	+	++
P60	+++	+++	++	++

Supplemental Figure 3.3. Il33 increases during postnatal development.

(A, B) Representative flow cytometry plots of thalamus and spinal cord from Il33mCherry/Aldh1l1-eGFP mice at P5 and P15 gated on pre-gated on Aldh1l1-GFP. **(C)** Quantification of percent IL33+ astrocytes (n=4-6/condition) shows an increase over development, but some astrocytes remain IL-33 negative. **(D)** Time course of Il33-lacZ expression in brain and spinal cord (Scale =2 mm in brain, 250 μm in spinal cord). **(E)** Summary table of IL-33 expression during development based on reporter assays, transcriptomic analyses, and immunostaining.

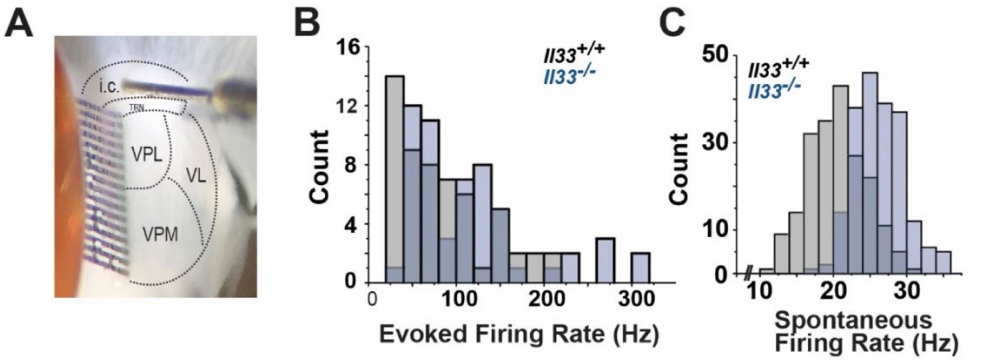

D

	Amp (pA)	Rise Time (ms)	Half-Width (ms)	Decay Tau (ms)	Charge (fC)
Il33$^{+/+}$	-10.76 ± 0.33	0.81 ± 0.06	3.0 ± 0.15	4.5 ± 0.29	-49.2 ± 2.5
Il33$^{-/-}$	-10.5 ± 0.4	0.88 ± 0.05	3.1 ± 0.12	4.2 ± 0.20	-42.9 ± 2.2
P-value	ns	ns	ns	ns	ns

Supplemental Figure 3.4. Additional controls for thalamic slice extracellular and intracellular recordings.

(A) Photograph of the extracellular circuit recording setup indicates a representative thalamic slice with 16-channel extracellular electrode (left) and stimulating electrode in the internal capsule (top). Anatomical overlay includes the subdivisions of the ventrobasal thalamus (VPL, VPM, and VL), the internal capsule which contains glutamatergic cortical afferents, and the TRN (thalamic reticular nucleus), which projects inhibitory feedback onto the ventrobasal thalamus. The initial stimulation retrogradely stimulates thalamus in a direct fashion (stimulus indicated in Fig. 3.2A), whereas the signal after 250 ms represents the oscillatory intrathalamic response to stimulation of the cortical afferents. **(B-C)** Histograms representing the same extracellular recording data as shown in Fig. 3.2B-C, analyzing the time 250ms-750ms post-stim. Evoked firing data in B is a non-normal distribution in response to the stimulus, whereas the spontaneous oscillations are appx 10-fold lower frequency and follow a normal distribution of values. **(D)** Intracellular patch clamp recordings: Additional measured parameters for recordings of VB thalamus shown in Fig. 3.2D-E show no differences in presynaptic strength, synapse proximal-distal distribution, and other parameters (mean±sem; student's t-test).

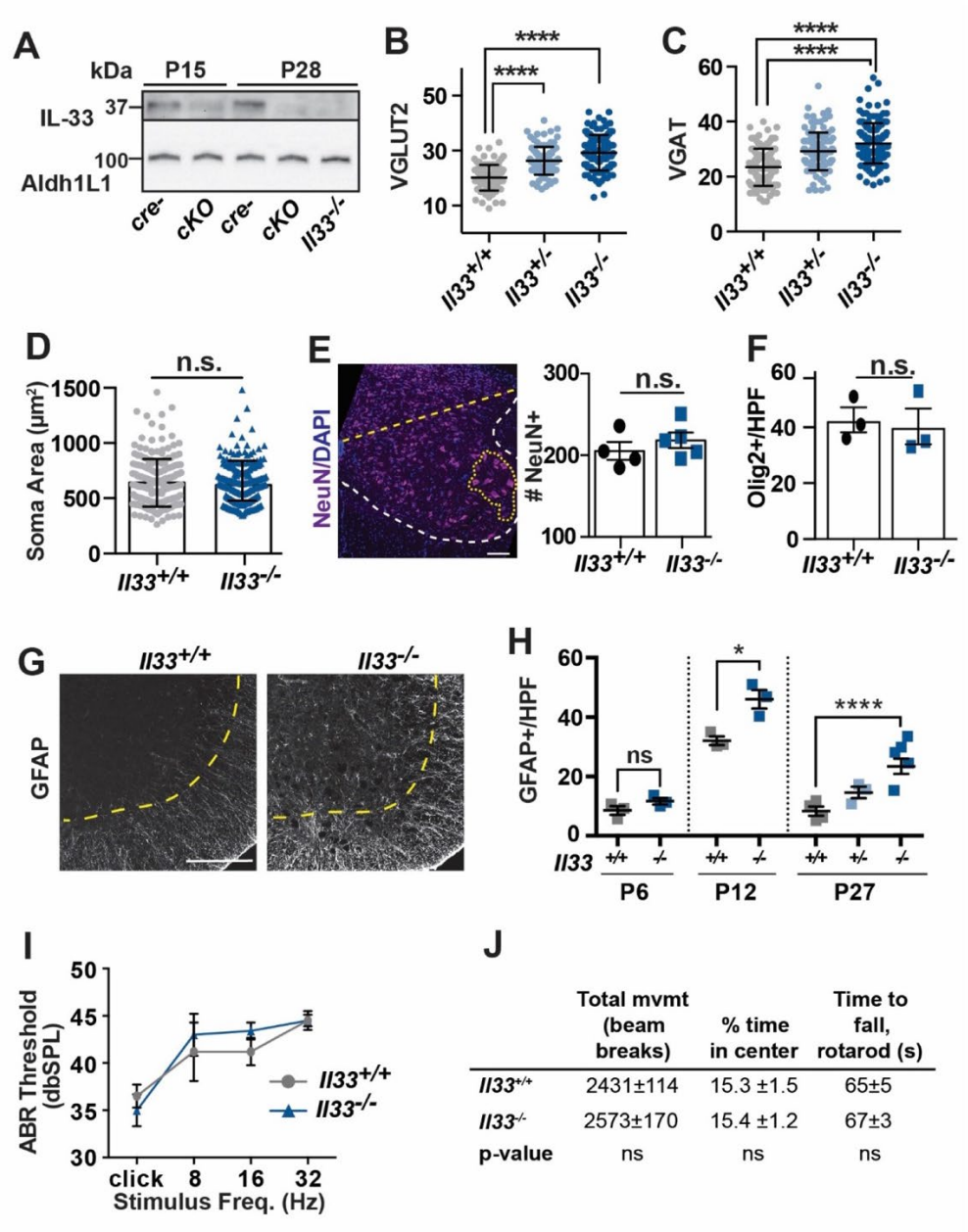

	Total mvmt (beam breaks)	% time in center	Time to fall, rotarod (s)
Il33$^{+/+}$	2431±114	15.3 ±1.5	65±5
Il33$^{-/-}$	2573±170	15.4 ±1.2	67±3
p-value	ns	ns	ns

Supplemental Figure 3.5. Additional experiments quantifying the effects of IL-33 deletion on spinal cord synaptic properties and sensorimotor behaviors.

(A) Western blot of IL-33 protein in cre- littermates and hGFAPcre+:Il33fl/fl(cKO) animals validates efficient deletion of IL-33 by P30. **(B, C)** Quantification of increased excitatory (vGlut2+) and inhibitory (VGAT+) inputs per motor neuron soma after global deletion of Il33. **(D)** No changes in soma size of motor neurons quantified for synaptic puncta analysis. **(E)** Representative image of ventral horn NeuN+ interneurons (dotted lines denote quantification area; scale = 100 µm). Quantification shows normal ventral horn interneuron numbers in Il33-/- animals (n=4-5/condition). **(F)** Olig2+ cells in lumbar ventral horn at P12 (n=3/condition). **(G)**

Representative images of GFAP expression in spinal cord at P27, dotted line indicates gray/white matter boundary (scale = 50 μm). **(H)** Increase in GFAP+ cells in the spinal cord gray matter during development in Il33-/- mice (n=3-5/condition). **(I)** Normal auditory acuity in Il33-/- mice as assessed by brainstem auditory evoked potentials (data from n=5/group). **(J)** Additional behavioral quantifications showing total movement and percent time in center vs. periphery of arena during open field testing and time-to fall on rotarod testing (n=12/group.) Statistics: Data in B-C from cervical and lumbar sections from 4 Il33+/+, 3 Il33+/-, and 5 Il33-/- mice, n > 95 total neurons per genotype, analyzed by one-way ANOVA with Tukey's post hoc comparison. All other data analyzed by student's t-test. For all panels *P<0.05, ****P<0.0001.

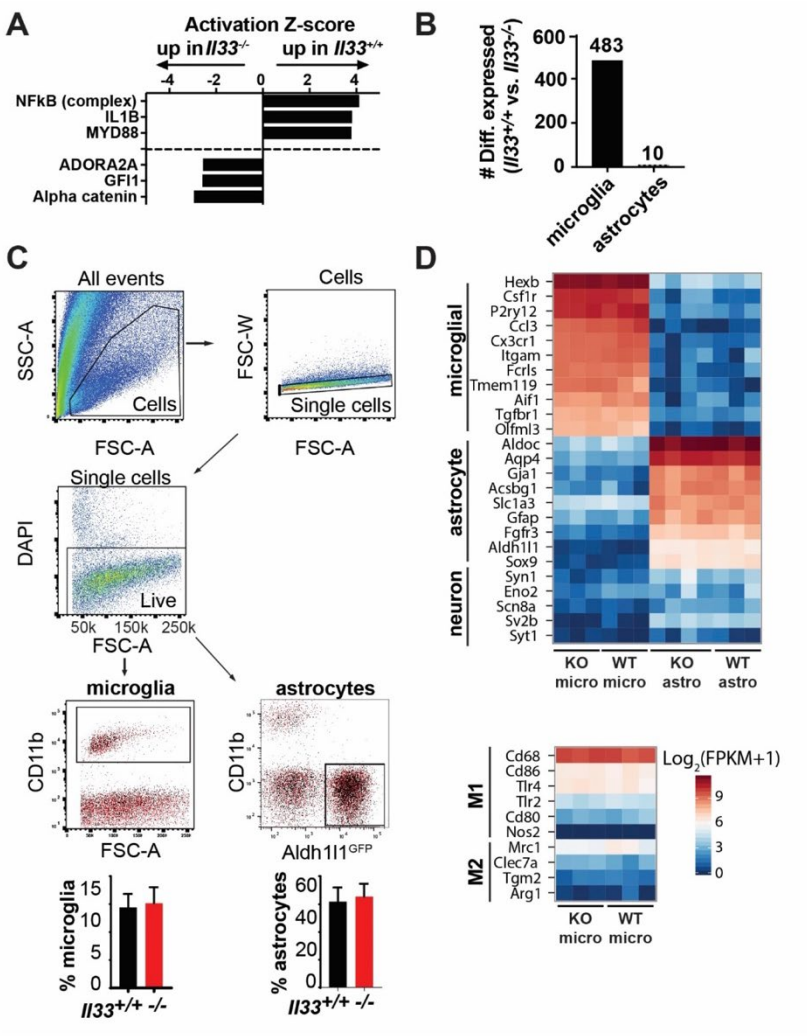

Supplemental Figure 3.6. Flow isolation and RNA sequencing of astrocytes and microglia from Il33-/- animals.

(A) Ingenuity Pathways Analysis of "upstream" pathways differentially expressed in microglia from Il33-/- vs. Il33+/+ spinal cord ranked by z-score. **(B)** Number of differentially expressed genes between Il33+/+ and Il33-/- astrocytes and microglia at FC>2, pAdj<0.05 (n=3/group for microglia and 4/group for astrocytes) indicates minimal gene expression changes in astrocytes. **(C)** FACS gating scheme for samples sorted for RNAseq analysis. (D) Heatmaps of cell-type specific genes to assess sort purity. No difference in markers of macrophage polarization.

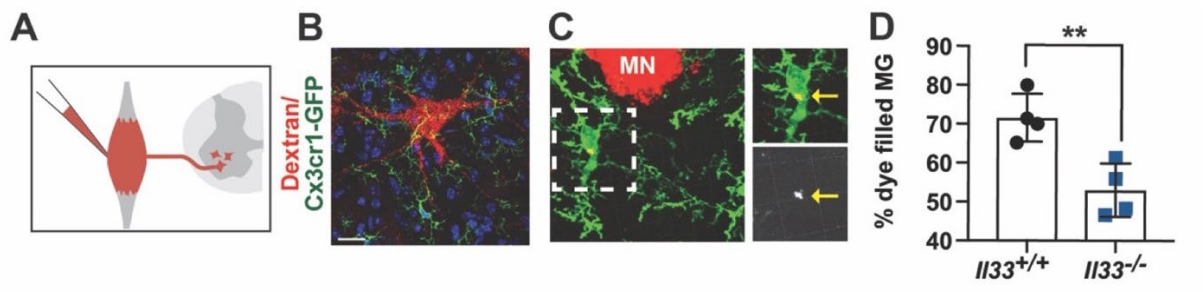

Supplemental Figure 3.7. Decrease in motor neuron-specific engulfment by microglia in Il33-deficient animals.

(A) Schematic of muscle dye fill. **(B)** Low-power view of sparsely labeled motor neuron in the ventral horn after dye fill (scale = 20 μm). **(C)** Representative image of dye engulfment by perineuronal microglia. **(D)** Percent microglia engulfing dye in control and Il33-/- mice. Statistics: Data in (D) from 180-220 microglia from 4 animals per condition. Significance calculated with student's t-test. ** $p<0.01$.

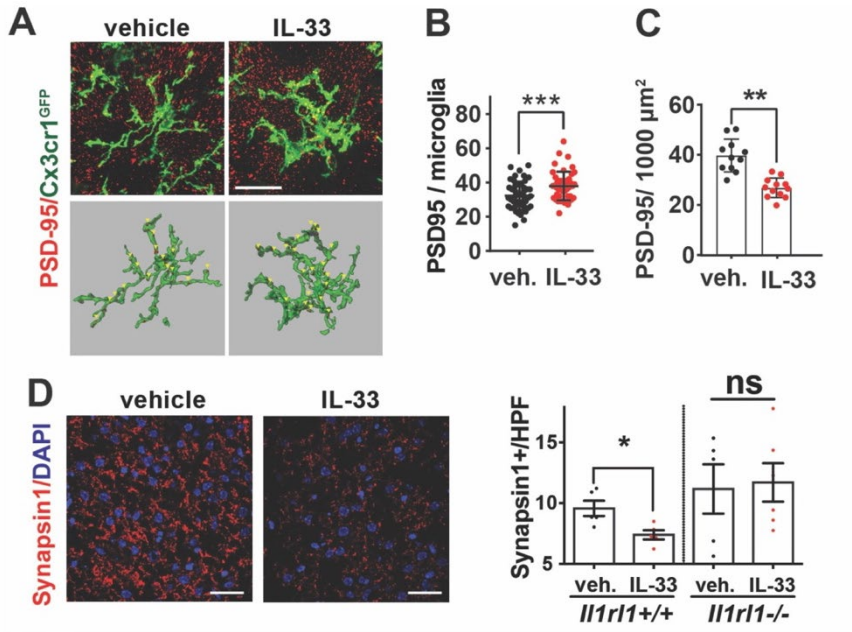

Supplemental Figure 3.8. IL-33 promotes synapse engulfment and leads to depletion of synaptic markers in the developing thalamus.

(A) Representative image and rendering of microglial/PSD-95 co-localization in the thalamus after vehicle or IL-33 injection (scale=20 µm). **(B)** Quantification of PSD-95 puncta within individual microglia (>45 total microglia from n=3/ condition.) **(C)** Quantification of PSD-95+ puncta in the surrounding neuropil after vehicle or IL-33 injection (n=3/ condition) at P15. **(D)** Representative images and quantification of synaptic puncta using pan-presynaptic marker synapsin-1 per 1000 µm2 optical slice in the thalamus at P4. All data quantified 18 hours after IL-33 injection (n=3 animals/condition; scale = 25 µm). Statistics: A, B are mean±SD, D is SEM. For all, student's t-test with *p<0.05, **p<0.01, ***p<0.001, ****p<0.0001.

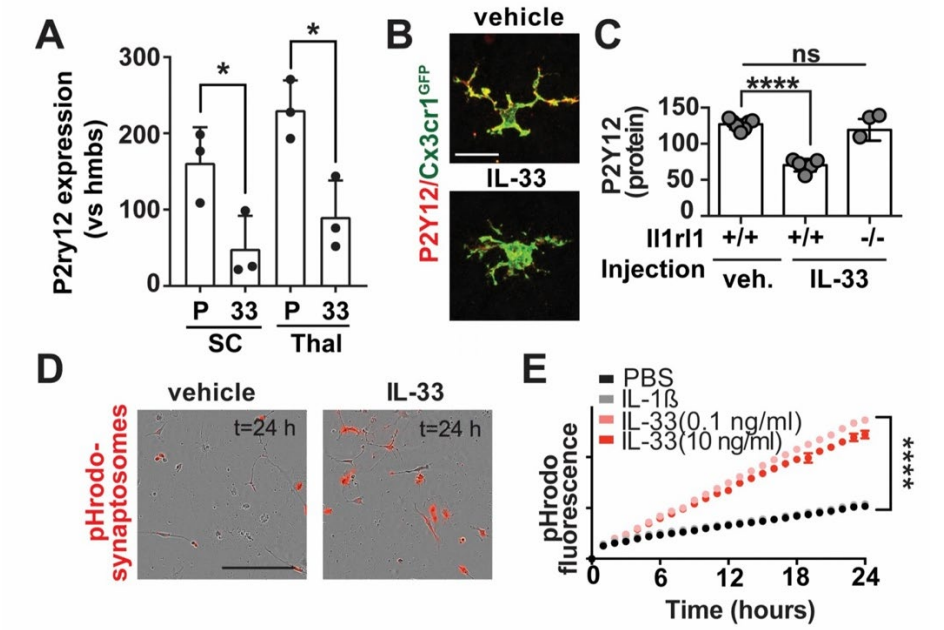

Supplemental Figure 3.9. Exogenous IL-33 promotes microglial phenotypic changes associated with immune activation and promotes microglial synaptosome engulfment in vitro.

(A) RT-qPCR for P2ry12 on spinal cord and thalamus microglia from PBS and IL-33 injected (4 hours post injection). **(B)** Decreased P2y12 protein and shortened process length 18 hours after IL-33 injection (scale =10 μm). **(C)** Quantification of P2y12 protein intensity after IL-33 injection into control or Il1rl1-/- animals. **(D)** Representative images of in vitro microglial synaptosome engulfment 24 hours after addition of IL-33. **(E)** Quantification of pHrodo-labeled synaptosome engulfment (n=4 independent experiments). Statistics: In A-C dots represent individual animals. A, C are mean±SD; E is mean±SEM. In A student's t-test, in C, E one-way ANOVA with Tukey's post hoc comparison. For all *p<0.05, ****p<0.0001.

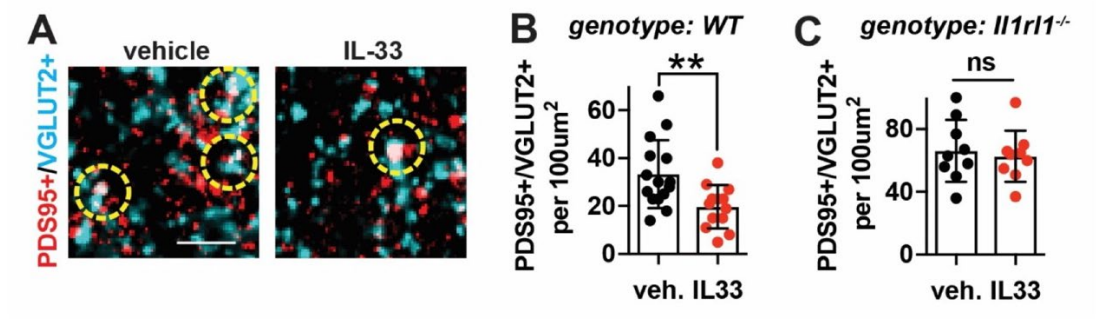

Supplemental Figure 3.10. IL-33 promotes synapse depletion in spinal cord in an IL1RL1-dependent manner.

(A) Representative images of co-localized excitatory synaptic puncta (scale = 12.5 μm). **(B, C)** quantification of co-localized synapse numbers after vehicle or IL-33 injection in wild type or IL1RL1-/- animals. Dots show technical replicates of total n=3 animals per group. Analyzed with student's t-test, **p<0.01.

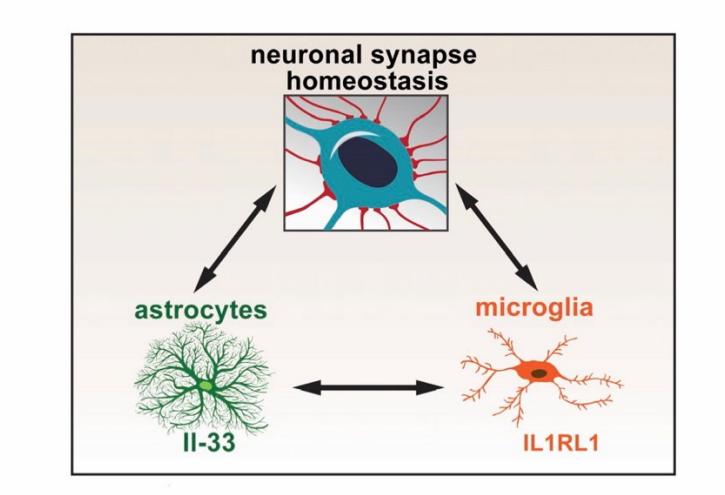

Supplemental Figure 3.11. IL-33 regulates developmental synapse homeostasis.

Table 3.1. Expression of known astrocyte markers in IL33-mCherry positive vs. negative astrocytes.

	FPKM (pos)	FPKM (neg)	Fold-change	p-value	
Synapse-associated astrocyte markers					
Mertk	71	30	**2.37**	0.002	***
Gjb6 (Cx30)	519	216	**2.41**	0.000	****
Gja1 (Cx43)	512	280	**1.83**	0.000	****
White matter astrocyte markers					
Gfap	26	104	**0.25**	0.002	***
Vim	11	171	**0.06**	0.000	****
Reported pan-astrocytic markers					
Acsbg1	193	155	**1.25**	0.069	**ns**
Aldh1l1	22	22	**0.97**	0.856	**ns**
Aldoc	891	1140	**0.78**	0.296	**ns**
Aqp4	1092	964	**1.13**	0.559	**ns**
Fabp7 (Blbp)	636	987	**0.64**	0.001	***
Fgfr3	252	99	**2.54**	0.000	****
Glul	559	554	**1.01**	0.927	**ns**
Id3	95	90	**1.06**	0.841	**ns**
Slc1a3 (Glast)	418	311	**1.34**	0.313	**ns**
Slc1a2 (GLT-1)	2236	1827	**1.22**	0.186	**ns**
Sox9	51	57	**0.90**	0.486	**ns**

Table 3.2. Top differentially expressed genes increased in IL33-mCherry positive astrocytes, sorted by Ingenuity category.

Symbol	Entrez Gene Name	FPKM (mean)	p-value	Log Ratio	Fold-change
Transcriptional regulators					
HIF3A	hypoxia inducible factor 3 alpha	4836	6.44E-12	1.77	**3.4**
PREB	prolactin regulatory element binding	657	0.00011	1.012	**2.0**
HDAC8	histone deacetylase 8	780	0.000447	0.989	**2.0**
IRX2	iroquois homeobox 2	319	0.0014	0.933	**1.9**
TEF	TEF, PAR bZIP transcription factor	1409	7.3E-09	0.858	**1.8**
TSC22D3	TSC22 domain family member 3	2152	0.000596	0.844	**1.8**
PAX6	paired box 6	621	3.9E-09	0.722	**1.6**
GLI2	GLI family zinc finger 2	1044	0.00219	0.704	**1.6**
GLI3	GLI family zinc finger 3	1988	0.000516	0.533	**1.4**
KMT2C	lysine methyltransferase 2C	12238	0.00000289	0.527	**1.4**
G protein coupled receptors					
ADORA2B	adenosine A2b receptor	560	1.87E-09	1.482	**2.8**
LGR6	leucine rich repeat containing GPCR6	1631	0.000111	1.335	**2.5**
ADRA2A	adrenoceptor alpha 2A	1241	0.0000263	1.108	**2.2**
GPR146	G protein-coupled receptor 146	1596	0.00000112	1.053	**2.1**
S1PR1	sphingosine-1-phosphate receptor 1	9074	0.00000431	0.987	**2.0**
ADGRG1	adhesion GPCR G1 (GPR56)	8054	0.0000367	0.936	**1.9**
FZD1	frizzled class receptor 1	5681	0.00565	0.912	**1.9**
GPR37L1	GPCR 37 like 1	5385	0.000747	0.912	**1.9**
ADGRB3	adhesion GPCR B3 (BAI3)	4244	2.42E-22	0.807	**1.7**
TAPT1	transmembrane anterior posterior transformation 1	1808	0.0000595	0.799	**1.7**
transmembrane receptor					
F3	coagulation factor III, tissue factor	5375	4.76E-19	1.776	**3.4**
IL15RA	interleukin 15 receptor alpha	569	2.6E-17	1.696	**3.2**
GHR	growth hormone receptor	1856	0.0000763	1.113	**2.2**
ITGA6	integrin subunit alpha 6	5364	0.0000123	0.996	**2.0**
LRP1B	LDL receptor related protein 1B	3290	0.000214	0.966	**2.0**
LGR4	leucine rich repeat containing G protein-coupled receptor 4	1226	8.05E-11	0.948	**1.9**
LIFR	leukemia inhibitory factor receptor alpha	5118	0.00000285	0.839	**1.8**
TLR3	toll like receptor 3	4453	0.000922	0.798	**1.7**
VCAM1	vascular cell adhesion molecule 1	9101	0.000134	0.725	**1.7**
MEGF10	multiple EGF like domains 10	3054	0.00406	0.578	**1.5**

Table 3.3. Top differentially expressed genes decreased in IL-33-mCherry positive astrocytes, sorted by Ingenuity category.

Symbol	Entrez Gene Name	FPKM (mean)	p-value	Log Ratio	Fold-change
Transcriptional regulators					
FOXJ1	forkhead box J1	297	1.51E-27	-4.004	**0.1**
PLAGL1	PLAG1 like zinc finger 1	742	4.08E-15	-3.999	**0.1**
ID4	inhibitor of DNA binding 4, HLH protein	916	4.46E-12	-1.923	**0.3**
GLIS3	GLIS family zinc finger 3	941	0.000000319	-1.597	**0.3**
NFIX	nuclear factor I X	4297	0.00000243	-1.208	**0.4**
EPAS1	endothelial PAS domain protein 1	12014	1.85E-09	-1.178	**0.4**
NEO1	neogenin 1	5760	6.03E-12	-0.875	**0.5**
NFIA	nuclear factor I A	16500	0.000000059	-0.837	**0.6**
CKAP5	cytoskeleton associated protein 5	4518	3.89E-08	-0.793	**0.6**
ZBTB20	zinc finger and BTB domain containing 20	25365	0.0000423	-0.783	**0.6**
MEN1	menin 1	252	0.00976	-0.725	**0.6**
WWTR1	WW domain containing transcription regulator 1	1867	0.000638	-0.695	**0.6**
NFIC	nuclear factor I C	1625	0.00324	-0.69	**0.6**
NACC2	NACC family member 2	2422	0.00774	-0.637	**0.6**
ZNF423	zinc finger protein 423	1180	0.00456	-0.61	**0.7**
HLF	HLF, PAR bZIP transcription factor	3503	0.0036	-0.583	**0.7**
RFX3	regulatory factor X3	3993	0.00105	-0.541	**0.7**
G protein coupled receptors					
SMO	smoothened, frizzled class receptor	2533	0.0000131	-0.705	**0.6**
Transmembrane receptor					
SFRP1	secreted frizzled related protein 1	289	3.62E-13	-2.728	**0.2**
SEMA6A	semaphorin 6A	6268	5.96E-22	-2.006	**0.2**
IL6ST	interleukin 6 signal transducer	5039	6.38E-08	-0.929	**0.5**

Other Supplementary Materials for Chapter 3 include the following:

Supplemental Table 3.1. Differentially expressed genes in Il33-positive and negative astrocytes. Full FPKM data for differentially expressed astrocyte-enriched genes in both spinal cord and thalamic Il33+ vs. negative astrocytes at postnatal day 15 (Thresholded at p-Adj<0.05, FC>1.5)

Supplemental Table 3.2. Differentially expressed genes in microglia and astrocytes from Il33-/- animals. Count data for the full list of genes differentially expressed in microglia (484 genes) and astrocytes (10 genes) from Il33-/- spinal cords at postnatal day 12 (Thresholded at p-Adj<0.05).

References

Aken BL, Ayling S, Barrell D, Clarke L, Curwen V, Fairley S, Fernandez Banet J, Billis K, García Girón C, Hourlier T, Howe K, Kähäri A, Kokocinski F, Martin FJ, Murphy DN, Nag R, Ruffier M, Schuster M, Tang YA, Vogel JH, White S, Zadissa A, Flicek P, Searle SMJ. 2016. The Ensembl gene annotation system. *Database (Oxford)* **2016**:1–19. doi:10.1093/database/baw093

Akil O, Seal RP, Burke K, Wang C, Alemi A, During M, Edwards RH, Lustig LR. 2012. Restoration of Hearing in the VGLUT3 Knockout Mouse Using Virally Mediated Gene Therapy. *Neuron* **75**. doi:10.1016/j.neuron.2012.05.019

Anders S, Pyl PT, Huber W. 2015. HTSeq-A Python framework to work with high-throughput sequencing data. *Bioinformatics* **31**. doi:10.1093/bioinformatics/btu638

Andrews S. 2010. FastQC: A Quality Control Tool for High Throughput Sequence Data [Online]. Available online at: http://www.bioinformatics.babraham.ac.uk/projects/fastqc/.

Arber S. 2012. Motor Circuits in Action: Specification, Connectivity, and Function. *Neuron*. doi:10.1016/j.neuron.2012.05.011

Chen WY, Hong J, Gannon J, Kakkar R, Lee RT. 2015. Myocardial pressure overload induces systemic inflammation through endothelial cell IL-33. *Proc Natl Acad Sci U S A* **112**. doi:10.1073/pnas.1424236112

Chovatiya R, Medzhitov R. 2014. Stress, inflammation, and defense of homeostasis. *Mol Cell*. doi:10.1016/j.molcel.2014.03.030

Clarke LE, Barres BA. 2013. Emerging roles of astrocytes in neural circuit development. *Nat Rev Neurosci* **14**:311–321. doi:10.1038/nrn3484

Dunkley PR, Jarvie PE, Robinson PJ. 2008. A rapid percoll gradient procedure for preparation of synaptosomes. *Nat Protoc* **3**. doi:10.1038/nprot.2008.171

Fu AKY, Hung KW, Yuen MYF, Zhou X, Mak DSY, Chan ICW, Cheung TH, Zhang B, Fu WY, Liew FY, Ip NY. 2016. IL-33 ameliorates Alzheimer's disease-like pathology and cognitive decline. *Proc Natl Acad Sci U S A* **113**. doi:10.1073/pnas.1604032113

Gadani SP, Walsh JT, Smirnov I, Zheng J, Kipnis J. 2015. The Glia-Derived Alarmin IL-33 Orchestrates the Immune Response and Promotes Recovery following CNS Injury. *Neuron* **85**. doi:10.1016/j.neuron.2015.01.013

Galatro TF, Vainchtein ID, Brouwer N, Boddeke EWGM, Eggen BJL. 2017. Isolation of Microglia and Immune Infiltrates from Mouse and Primate Central Nervous System In: Clausen BE, Laman JD, editors. Inflammation: Methods and Protocols, Methods in Molecular Biology. pp. 75–81. doi:10.1007/978-1-4939-6786-5

Gong S, Zheng C, Doughty ML, Losos K, Didkovsky N, Schambra UB, Nowak NJ, Joyner A, Leblanc G, Hatten ME, Heintz N. 2003. A gene expression atlas of the central nervous system based on bacterial artificial chromosomes. *Nature* **425**. doi:10.1038/nature02033

Haynes SE, Hollopeter G, Yang G, Kurpius D, Dailey ME, Gan WB, Julius D. 2006. The P2Y12 receptor regulates microglial activation by extracellular nucleotides. *Nat Neurosci* **9**. doi:10.1038/nn1805

Hooks BM, Chen C. 2006. Distinct Roles for Spontaneous and Visual Activity in Remodeling of the Retinogeniculate Synapse. *Neuron* **52**. doi:10.1016/j.neuron.2006.07.007

Hoshino K, Kashiwamura SI, Kuribayashi K, Kodama T, Tsujimura T, Nakanishi K, Matsuyama T, Takeda K, Akira S. 1999. The absence of interleukin I receptor-related T1/ST2 does not affect T helper cell type 2 development and its effector function. *J Exp Med* **190**. doi:10.1084/jem.190.10.1541

Jung S, Aliberti J, Graemmel P, Sunshine MJ, Kreutzberg GW, Sher A, Littman DR. 2000.

Analysis of Fractalkine Receptor CX 3 CR1 Function by Targeted Deletion and Green Fluorescent Protein Reporter Gene Insertion . *Mol Cell Biol* **20**. doi:10.1128/mcb.20.11.4106-4114.2000

Kim D, Pertea G, Trapnell C, Pimentel H, Kelley R, Salzberg SL. 2013. TopHat2: Accurate alignment of transcriptomes in the presence of insertions, deletions and gene fusions. *Genome Biol* **14**. doi:10.1186/gb-2013-14-4-r36

Koch M. 1999. The neurobiology of startle. *Prog Neurobiol* **59**:107–128. doi:10.1016/S0301-0082(98)00098-7

Liddelow SA, Guttenplan KA, Clarke LE, Bennett FC, Bohlen CJ, Schirmer L, Bennett ML, Münch AE, Chung W-S, Peterson TC, Wilton DK, Frouin A, Napier BA, Panicker N, Kumar M, Buckwalter MS, Rowitch DH, Dawson VL, Dawson TM, Stevens B, Barres BA. 2017. Neurotoxic reactive astrocytes are induced by activated microglia. *Nature* **541**:481–487. doi:10.1038/nature21029

Love MI, Huber W, Anders S. 2014. Moderated estimation of fold change and dispersion for RNA-seq data with DESeq2. *Genome Biol* **15**:1–21. doi:10.1186/s13059-014-0550-8

Lui H, Zhang J, Makinson SR, Cahill MK, Kelley KW, Huang HY, Shang Y, Oldham MC, Martens LH, Gao F, Coppola G, Sloan SA, Hsieh CL, Kim CC, Bigio EH, Weintraub S, Mesulam MM, Rademakers R, MacKenzie IR, Seeley WW, Karydas A, Miller BL, Borroni B, Ghidoni R, Farese R V., Paz JT, Barres BA, Huang EJ. 2016. Progranulin Deficiency Promotes Circuit-Specific Synaptic Pruning by Microglia via Complement Activation. *Cell* **165**:921–935. doi:10.1016/j.cell.2016.04.001

Luo Y, Zhou Y, Xiao W, Liang Z, Dai J, Weng X, Wu X. 2015. Interleukin-33 ameliorates ischemic brain injury in experimental stroke through promoting Th2 response and

suppressing Th17 response. *Brain Res* **1597**. doi:10.1016/j.brainres.2014.12.005

Miyamoto A, Wake H, Ishikawa AW, Eto K, Shibata K, Murakoshi H, Koizumi S, Moorhouse AJ, Yoshimura Y, Nabekura J. 2016. Microglia contact induces synapse formation in developing somatosensory cortex. *Nat Commun* **7**. doi:10.1038/ncomms12540

Molofsky AB, Savage AK, Locksley RM. 2015. Interleukin-33 in Tissue Homeostasis, Injury, and Inflammation. *Immunity*. doi:10.1016/j.immuni.2015.06.006

Molofsky A V., Kelley KW, Tsai HH, Redmond SA, Chang SM, Madireddy L, Chan JR, Baranzini SE, Ullian EM, Rowitch DH. 2014. Astrocyte-encoded positional cues maintain sensorimotor circuit integrity. *Nature* **509**. doi:10.1038/nature13161

Molofsky A V., Krenick R, Ullian E, Tsai HH, Deneen B, Richardson WD, Barres BA, Rowitch DH. 2012. Astrocytes and disease: A neurodevelopmental perspective. *Genes Dev*. doi:10.1101 /gad.188326.112

Pannasch U, Freche D, Dallérac G, Ghézali G, Escartin C, Ezan P, Cohen-Salmon M, Benchenane K, Abudara V, Dufour A, Lübke JHR, Déglon N, Knott G, Holcman D, Rouach N. 2014. Connexin 30 sets synaptic strength by controlling astroglial synapse invasion. *Nat Neurosci* **17**. doi:10.1038/nn.3662

Paolicelli RC, Bolasco G, Pagani F, Maggi L, Scianni M, Panzanelli P, Giustetto M, Ferreira TA, Guiducci E, Dumas L, Ragozzino D, Gross CT. 2011. Synaptic pruning by microglia is necessary for normal brain development. *Science* **333**:1456–8. doi:10.1126/science.1202529

Parkhurst CN, Yang G, Ninan I, Savas JN, Yates JR, Lafaille JJ, Hempstead BL, Littman DR, Gan WB. 2013. Microglia promote learning-dependent synapse formation through brain-derived neurotrophic factor. *Cell* **155**. doi:10.1016/j.cell.2013.11.030

Paz JT, Christian CA, Parada I, Prince DA, Huguenard JR. 2010. Focal Cortical Infarcts Alter

Intrinsic Excitability and Synaptic Excitation in the Reticular Thalamic Nucleus. *J Neurosci* **30**:5465–5479. doi:10.1523/JNEUROSCI.5083-09.2010

Paz JT, Davidson TJ, Frechette ES, Delord B, Parada I, Peng K, Deisseroth K, Huguenard JR. 2013. Closed-loop optogenetic control of thalamus as a tool for interrupting seizures after cortical injury. *Nat Neurosci* **16**:64–70. doi:10.1038/nn.3269

Pichery M, Mirey E, Mercier P, Lefrancais E, Dujardin A, Ortega N, Girard J-P. 2012. Endogenous IL-33 Is Highly Expressed in Mouse Epithelial Barrier Tissues, Lymphoid Organs, Brain, Embryos, and Inflamed Tissues: In Situ Analysis Using a Novel Il-33–LacZ Gene Trap Reporter Strain . *J Immunol* **188**. doi:10.4049/jimmunol.1101977

Pollen AA, Nowakowski TJ, Chen J, Retallack H, Sandoval-Espinosa C, Nicholas CR, Shuga J, Liu SJ, Oldham MC, Diaz A, Lim DA, Leyrat AA, West JA, Kriegstein AR. 2015. Molecular Identity of Human Outer Radial Glia during Cortical Development. *Cell* **163**. doi:10.1016/j.cell.2015.09.004

Pomeshchik Y, Kidin I, Korhonen P, Savchenko E, Jaronen M, Lehtonen S, Wojciechowski S, Kanninen K, Koistinaho J, Malm T. 2015. Interleukin-33 treatment reduces secondary injury and improves functional recovery after contusion spinal cord injury. *Brain Behav Immun* **44**. doi:10.1016/j.bbi.2014.08.002

Ransohoff RM, Cardona AE. 2010. The myeloid cells of the central nervous system parenchyma. *Nature*. doi:10.1038/nature09615

Risher WC, Patel S, Kim IH wa., Uezu A, Bhagat S, Wilton DK, Pilaz LJ, Singh Alvarado J, Calhan OY, Silver DL, Stevens B, Calakos N, Soderling SH, Eroglu C. 2014. Astrocytes refine cortical connectivity at dendritic spines. *Elife* **3**. doi:10.7554/eLife.04047

Ruland J. 2011. Return to homeostasis: Downregulation of NF-κB responses. *Nat Immunol*.

doi:10.1038/ni.2055

Salter MW, Beggs S. 2014. Sublime microglia: Expanding roles for the guardians of the CNS. *Cell*. doi:10.1016/j.cell.2014.06.008

Schafer DP, Lehrman EK, Kautzman AG, Koyama R, Mardinly AR, Yamasaki R, Ransohoff RM, Greenberg ME, Barres BA, Stevens B. 2012. Microglia Sculpt Postnatal Neural Circuits in an Activity and Complement-Dependent Manner. *Neuron* **74**. doi:10.1016/j.neuron.2012.03.026

Sekar A, Bialas AR, De Rivera H, Davis A, Hammond TR, Kamitaki N, Tooley K, Presumey J, Baum M, Van Doren V, Genovese G, Rose SA, Handsaker RE, Daly MJ, Carroll MC, Stevens B, McCarroll SA. 2016. Schizophrenia risk from complex variation of complement component 4. *Nature* **530**. doi:10.1038/nature16549

Singh SK, Stogsdill JA, Pulimood NS, Dingsdale H, Kim YH, Pilaz LJ, Kim IH, Manhaes AC, Rodrigues WS, Pamukcu A, Enustun E, Ertuz Z, Scheiffele P, Soderling SH, Silver DL, Ji RR, Medina AE, Eroglu C. 2016. Astrocytes Assemble Thalamocortical Synapses by Bridging NRX1α and NL1 via Hevin. *Cell* **164**:183–196. doi:10.1016/j.cell.2015.11.034

Sorokin JM, Davidson TJ, Frechette E, Abramian AM, Deisseroth K, Huguenard JR, Paz JT. 2017. Bidirectional Control of Generalized Epilepsy Networks via Rapid Real-Time Switching of Firing Mode. *Neuron* **93**:194–210. doi:10.1016/j.neuron.2016.11.026

Srinivasan K, Friedman BA, Larson JL, Lauffer BE, Goldstein LD, Appling LL, Borneo J, Poon C, Ho T, Cai F, Steiner P, Van Der Brug MP, Modrusan Z, Kaminker JS, Hansen D V. 2016. Untangling the brain's neuroinflammatory and neurodegenerative transcriptional responses. *Nat Commun* **7**. doi:10.1038/ncomms11295

Stevens B, Allen NJ, Vazquez LE, Howell GR, Christopherson KS, Nouri N, Micheva KD,

Mehalow AK, Huberman AD, Stafford B, Sher A, Litke AMM, Lambris JD, Smith SJ, John SWM, Barres BA. 2007. The Classical Complement Cascade Mediates CNS Synapse Elimination. *Cell* **131**:1164–1178. doi:10.1016/j.cell.2007.10.036

Trapnell C, Williams BA, Pertea G, Mortazavi A, Kwan G, Van Baren MJ, Salzberg SL, Wold BJ, Pachter L. 2010. Transcript assembly and quantification by RNA-Seq reveals unannotated transcripts and isoform switching during cell differentiation. *Nat Biotechnol* **28**. doi:10.1038/nbt.1621

Wicher G, Husic E, Nilsson G, Forsberg-Nilsson K. 2013. Developmental expression of IL-33 in the mouse brain. *Neurosci Lett* **555**. doi:10.1016/j.neulet.2013.09.046

Yona S, Kim KW, Wolf Y, Mildner A, Varol D, Breker M, Strauss-Ayali D, Viukov S, Guilliams M, Misharin A, Hume DA, Perlman H, Malissen B, Zelzer E, Jung S. 2013. Fate Mapping Reveals Origins and Dynamics of Monocytes and Tissue Macrophages under Homeostasis. *Immunity* **38**. doi:10.1016/j.immuni.2012.12.001

Zhuo L, Theis M, Alvarez-Maya I, Brenner M, Willecke K, Messing A. 2001. hGFAP-cre transgenic mice for manipulation of glial and neuronal function in vivo. *Genesis* **31**. doi:10.1002/gene.10008

Chapter 4 : Enhancing GAT-3 in thalamic astrocytes promotes resilience to brain injury in rodents

---

Abstract

Inflammatory processes induced by brain injury are important for recovery; however, when uncontrolled, inflammation can be deleterious, likely explaining why most anti-inflammatory treatments have failed to improve neurological outcomes after brain injury in clinical trials. In the thalamus, chronic activation of glial cells, a proxy of inflammation, has been suggested as indicator of increased seizure risk and cognitive deficits that develop after cortical injury. Furthermore, lesions in the thalamus, more than other brain regions, have been reported in patients with viral infections associated with neurological deficits, such as SARS-CoV-2. However, the extent to which thalamic inflammation is a driver or byproduct of neurological deficits remains unknown. Here, we found that thalamic inflammation in mice was sufficient to phenocopy the cellular and circuit hyperexcitability, enhanced seizure risk, and disruptions in cortical rhythms that develop after cortical injury. In our model, downregulation of the GABA transporter GAT-3 in thalamic astrocytes mediated this neurological dysfunction. In addition, GAT-3 was decreased in regions of thalamic reactive astrocytes in mouse models of cortical injury. Enhancing GAT-3 in thalamic astrocytes prevented seizure risk, restored cortical states, and was protective against severe chemoconvulsant-induced seizures and mortality in a mouse model of traumatic brain injury, emphasizing the potential of therapeutically targeting this pathway. Altogether, our results identified a potential therapeutic target for reducing negative outcomes after brain injury.

Introduction

Neuroinflammation that occurs after brain lesions such as traumatic brain injury (TBI) and stroke is a double-edged sword, contributing to both recovery and pathogenesis (Llorente et al., 2021; Russo and McGavern, 2016; Shi et al., 2021; Simon et al., 2017; Vezzani et al., 2019). Accordingly, most anti-inflammatory treatments have failed to prevent neurological deficits after brain injuries in clinical trials (Russo and McGavern, 2016; Simon et al., 2017). Untangling the adaptive and maladaptive aspects of neuroinflammation is a crucial step in developing targeted treatments that could promote brain recovery without jeopardizing the adaptive aspects of the neuroinflammatory process.

Accumulating evidence suggests that the thalamus is particularly vulnerable to secondary damage, even when the initial injury occurred at a remote location. In both humans and rodent models, chronic thalamic inflammation is observed after TBI (Grossman and Inglese, 2016; Hazra et al., 2014; Holden et al., 2021; Maxwell et al., 2006; Ramlackhansingh et al., 2011; Scott et al., 2015) and cortical stroke (Cao et al., 2020; Pappata et al., 2000; Paz et al., 2010). The development of secondary and persistent thalamic inflammation—particularly gliosis—has been suggested to be an indicator of neurological dysfunction after injury resulting in cognitive impairment (Ramlackhansingh et al., 2011) and seizure risk (Paz et al., 2010). In addition, thalamic lesions and/or thrombotic strokes have been reported among patients with viral infections caused by West Nile Virus (Beattie et al., 2013; Guth et al., 2014), and those with altered mental status following SARS coronavirus-2 (SARS-CoV-2) infection (Abel et al., 2020; Poyiadji et al., 2020). Mice intranasally infected with SARS-CoV-2 have high viral antigen presence in the thalamus compared to other brain regions (Zheng et al., 2020). Since the thalamus plays a central role in cognition, sleep and seizures in humans and rodents (Crunelli and Hughes, 2010; Fogerson and Huguenard,

2016; Jeanmonod et al., 1996; Jones, 2001; Steriade et al., 1996, 1993), it is well-positioned to be involved in diverse neurological deficits observed across insults, such as cognitive impairments, sleep disruption and epileptogenesis (Grossman et al., 2012; Grossman and Inglese, 2016; Paz and Huguenard, 2015). Thalamic astrogliosis—in which astrocytes become reactive and undergo changes that affect neuronal function (Burda and Sofroniew, 2014; Colombo and Farina, 2016; Escartin et al., 2021; Liddelow et al., 2017; Llorente et al., 2021; Sun and Jakobs, 2012; Zamanian et al., 2012)—has been observed in both humans and rodents after cortical injuries (Cao et al., 2020; Hazra et al., 2014; Holden et al., 2021; Maxwell et al., 2006; Paz et al., 2010).

Here, we sought to determine the extent to which thalamic astrogliosis is a driver or bystander of neurological dysfunction, and whether this process could be therapeutically targeted. To this end, we developed a mouse model of thalamic astrogliosis and investigated its effects on local neurons, micro-circuits, and on cortical states associated with cognition.

Results

Thalamic astrogliosis is observed in post-mortem human tissue with a history of cortical injury and in mouse models of cortical injury

Human imaging studies in patients with mild TBI have suggested that the chronic thalamic gliosis that develops secondarily after cortical lesions is an indicator of cognitive dysfunction (Grossman and Inglese, 2016). To investigate the role of astrogliosis in cortical stroke and TBI, we first performed immunostaining for the astrocytic marker glial fibrillary acidic protein (GFAP)—a molecular marker of many types of reactive astrocytes (Escartin et al., 2021)—in post-mortem thalamic and peri-lesional cortical tissue obtained from human brains with a history of ischemic stroke or TBI; a subset of subjects also had a history of epilepsy (2 of 7 subjects had epilepsy prior

to injury, and 3 of 7 subjects developed epilepsy after injury) (**Fig. 4.1**, and **Tables 4.1 and 4.2**). The thalamus and peri-lesional cortex of subjects with stroke or TBI exhibited discrete GFAP-positive cells with astrocyte-like morphology, compared to the dim, diffuse GFAP labeling in control subjects (**Fig. 4.1A**). Putative astrocyte morphology ranged from resting (Fig. 4.1A; cortex, control, inset) to reactive, featuring somatic hypertrophy and thick processes (Fig. 4.1A; thalamus and cortex, stroke, inset). These changes were evident both acutely and years after stroke or TBI, and were supported by a semi-quantitative analysis of GFAP immunoreactivity (**Table 4.2**).

Similarly, in two mouse models of injury—unilateral photothrombotic stroke or controlled cortical impact in the somatosensory cortex (a model of TBI)—GFAP was elevated in the thalamus, without gross hippocampal damage (**Fig. 4.1B**), in agreement with previous findings (Cao et al., 2020; Hazra et al., 2014; Holden et al., 2021; Necula et al., 2021; Paz et al., 2010).

Viral transduction of thalamic astrocytes induces persistent reactive astrocytes

To generate reactive astrocytes in the thalamus, we injected an AAV construct expressing enhanced green fluorescent protein (eGFP) from a truncated portion of the GFAP promoter (AAV2/5-Gfa104-eGFP) (Ortinski et al., 2010) unilaterally in the ventrobasal (VB) somatosensory thalamus (**Fig. 4.1C** and **Fig. S4.1, A and B**), This paradigm was originally developed to selectively transduce hippocampal astrocytes and render them reactive, as determined by hypertrophy and increased GFAP expression (Ortinski et al., 2010), although the molecular mechanisms of virus-induced reactive astrogliosis remain unknown.

To characterize the effects of the viral transduction on thalamic astrocytes, we assessed immunohistochemical, morphological and transcriptomic features of astrocytes three weeks following viral transduction. GFAP was increased in the thalamus ipsilateral to injection (**Fig.**

4.1D), consistent with the work in the hippocampus (Ortinski et al., 2010). The location of thalamic astrogliosis in our model was similar to that observed in rodent models of cortical injuries (**Fig. 4.1B**). The increase in GFAP in the viral transduction model persisted for at least nine months specifically in the ipsilateral thalamus, but not in other brain regions (**Fig. S4.1C**). Thus, the viral transduction model recapitulated two key features of astrogliosis following cortical injury—the specific location within the dorsal thalamus, and the chronic presence of reactive astrocytes in the thalamus (Holden et al., 2021).

To evaluate astrocyte morphology, we used an EAAT2-tdTomato transgenic reporter mouse line (Morel et al., 2014), which enabled sparse labeling and tracing of individual thalamic astrocytes (**Fig. 4.1E**). Using Sholl analysis to assess arborization of astrocytic processes (Ferreira et al., 2014), we observed somatic hypertrophy and a reduction in process branching in eGFP-positive astrocytes ipsilateral to viral injection (eGFP-positive/tdT-positive) relative to eGFP-negative/tdT-positive astrocytes (**Fig. 4.1F**). Thus, viral transduction of thalamic astrocytes recapitulates morphological features of reactive astrogliosis (Ortinski et al., 2010; Patel et al., 2019; Sun and Jakobs, 2012).

We next performed transcriptomic profiling of virally-transduced thalamic astrocytes acutely isolated by fluorescence-activated cell sorting (FACS; **Fig. 4.1, G and H**, and **Fig. S4.2**). Hierarchical clustering of FACS-isolated samples revealed that eGFP-positive astrocytes, which represented ~18% of astrocytes isolated from the thalamus, were distinct from their eGFP-negative counterparts (**Fig. S4.3, A to C**). We found robust upregulation of canonical reactivity genes *Gfap, Vim, CD44,* and *Serpina3n* (Liddelow et al., 2017; Zamanian et al., 2012) in eGFP-positive astrocytes (**Fig. 4.1H**). Comparing this transcriptomic profile with a published analysis of reactive astrocytes revealed upregulation of "pan-reactive" astrocyte genes (Liddelow et al., 2017),

although there was no bias towards the subsets of reactive astrocyte genes that were selectively induced by lipopolysaccharide injection or ischemic stroke (middle cerebral artery occlusion model) in that study (Liddelow et al., 2017) (**Fig. 4.3D**). Finally, we found alterations in multiple genes related to astrocytic modulation of glutamate and GABA (**Fig. 4.1H**), pinpointing molecular features of reactive astrocytes which might impact neural activity. Given that viral transduction of thalamic astrocytes reproducibly induces immunohistochemical, morphological and transcriptomic features of astrocyte reactivity observed across models (Escartin et al., 2021; Ortinski et al., 2010; Patel et al., 2019; Sun and Jakobs, 2012), hereon we refer to virally transduced astrocytes as reactive astrocytes.

Viral-induced thalamic astrogliosis did not lead to abnormalities in standard assays of spontaneous locomotion, anxiety, olfaction, nociception, context-dependent learning, and grooming three weeks post-injection (**Fig. S4.4**).

Reactive astrocytes enhance intra-thalamic microcircuit excitability

The effects of reactive astrocytes on local microcircuit excitability were assessed in acute brain slices that preserve the connectivity between VB thalamus and the reticular thalamic nucleus (nRT). We focused on the VB-nRT microcircuit because: 1) VB thalamus—the center of viral transduction—showed the strongest and most persistent astrogliosis overtime (**Fig. S4.1**); 2) the VB-nRT connections can be maintained in slices and reliably generate circuit oscillations, unlike connections between nRT and other thalamic nuclei; 3) Multi-unit activity in VB thalamus is a proxy for the strength of the oscillatory activity in the VB-nRT microcircuit (Cho et al., 2017; Cueni et al., 2008; Huntsman et al., 1999; Paz et al., 2013; Ritter-Makinson et al., 2019).

Electrical stimulation was delivered in the internal capsule, which contains corticothalamic and thalamocortical axons, and the resulting multi-unit activity was recorded three weeks following induction of reactive astrocytes (**Fig. 4.2**). Stimulation of the internal capsule produced robust multi-unit activity, characterized by an immediate "direct response," due to direct activation of corticothalamic axons and/or retrograde activation of thalamocortical neurons, followed by a "delayed response," characterized by repeated action potential bursts (**Fig. 4.2, A to C**), characteristic of the reciprocal VB-nRT oscillatory circuit activity (Cho et al., 2017; Cueni et al., 2008; Huntsman et al., 1999; Paz et al., 2013; Ritter-Makinson et al., 2019). Thalamic slices with astrogliosis exhibited an augmented delayed response characterized by more bursts and longer circuit oscillations **(Fig. 4.2D**). Beyond the site of maximal responsiveness in each slice, we also examined the spatial and temporal synchrony of neural activity across all recording sites. Evoked oscillatory activity in thalamic slices with astrogliosis had higher oscillation indices (Huntsman et al., 1999; Sorokin et al., 2017) (**Fig. 4.2, B and E**), although the spatial extent of the direct response was not altered, suggesting that astrogliosis enhanced the rhythmogenic properties of the intra-thalamic microcircuit across a larger region.

Reactive astrocytes facilitate low-threshold-calcium spikes in thalamocortical neurons by increasing extrasynaptic tonic inhibition

To determine how reactive astrocytes cause hyperexcitability in the VB-nRT microcircuit, we investigated cellular excitability and synaptic function in excitatory and inhibitory neurons in thalamic brain slices (Cope et al., 2009, 2005; Paz et al., 2010) (**Tables 4.3 to 4.8**).

Thalamocortical neurons in VB thalamus from mice with thalamic astrogliosis exhibited hyperpolarized action potential (AP) threshold (**Fig. 4.3**, **A and B**), and no difference in the resting

membrane potential (**Fig. 4.3C**). The difference in AP threshold was abolished when membrane potential was held at -75 mV in both groups (**Table 4.4**). Furthermore, the post-inhibitory rebound low-threshold calcium spike (LTS), mediated by T-type Ca^{2+} currents (Coulter et al., 1989), occurred at more hyperpolarized membrane potentials (**Fig. 4.3D**) and was accompanied by enhanced AP firing (**Fig. S4.5, A to C**). T-type Ca^{2+} current properties were similar in thalamocortical neurons from both groups (**Table 4.5**), as was the hyperpolarization-activated depolarizing sag potential (**Fig. S4.5, D to G**).

In mice with thalamic astrogliosis, thalamocortical neurons showed a three-fold increase in extrasynaptic $GABA_AR$-mediated current (hereon referred to as tonic GABA current or I_{TONIC}) (**Fig. 4.3E**), but no change in the frequency or biophysical properties of spontaneous inhibitory and excitatory synaptic currents (**Fig. 4.3F** and **Table S4.6**). $GABA_AR$ antagonist picrotoxin normalized the AP threshold, LTS threshold, and rebound burst AP firing (**Fig. 4.3, B to D**, and **Fig. S4.5C**).

In contrast with thalamocortical neurons, nRT neurons showed no change in intrinsic membrane excitability (**Table 4.7**) or in spontaneous synaptic currents (**Table 4.8**).

Thalamic reactive astrocytes enhance seizure risk in mice via tonic inhibition in thalamocortical neurons

Given that enhanced I_{TONIC} in the rodent thalamus has been implicated in hyperexcitability and seizures in genetic and pharmacological models of epilepsies (Cope et al., 2009; Lee and Maguire, 2014), we asked whether thalamic astrogliosis—which increased I_{TONIC} in adult wildtype mice (**Fig. 4.3E**)—led to heightened seizure susceptibility in mice.

Three weeks following induction of thalamic astrogliosis, a low dose of the pro-convulsive agent Pentylenetetrazol (PTZ; 5 mg/kg, intra-peritoneal, i.p.) was sufficient to induce epileptiform discharges associated with behavioral freezing in mice with thalamic astrogliosis but not in control mice (**Fig. 4.4, A to D**). Epileptiform discharges were prominent in the primary somatosensory cortex S1, a major recipient of inputs from VB thalamus (Agmon et al., 1993), and generalized to other cortical areas (**Fig. S4.6A**). These epileptiform discharges were similar to those reported in rodent models of epilepsies in terms of peak frequency and generalization (Cope et al., 2009; Ritter-Makinson et al., 2019; Wagnon et al., 2015). Increased seizure susceptibility persisted for at least seven months (**Fig. S4.6B**), consistent with the persistent thalamic astrogliosis (**Fig. S4.1**). Mice in which astrocytes were transduced with a low titer of the same viral construct (previously shown to not induce astrocyte reactivity (Ortinski et al., 2010)) did not exhibit enhanced seizure risk (**Fig. S4.6C**). Mice with thalamic astrogliosis also had a heightened response to Kainic Acid (10 mg/kg i.p.) (**Fig. 4.4, E to G,** and **Fig. S4.6D**). Altogether, these results show that unilateral induction of reactive astrocytes in the thalamus enhances susceptibility to both non-convulsive and generalized tonic-clonic seizures, as assessed by pro-convulsive agents that act through different mechanisms (GABA and glutamate).

In the thalamus, δ-subunit-containing extrasynaptic $GABA_A$ receptors generate I_{TONIC} (Cope et al., 2009, 2005; Lee and Maguire, 2014). Thus, to investigate whether preventing the increase in I_{TONIC} could prevent astrogliosis-induced seizure risk, we conditionally deleted the $GABA_A$ receptor δ-subunit (δ-$GABA_AR$) unilaterally in thalamocortical neurons of adult *Gabrd*$^{Fl/Fl}$ mice (Lee and Maguire, 2013) (**Fig. 4.4H**). Thalamic astrogliosis did not increase I_{TONIC} in thalamocortical neurons in these mice (**Fig. 4.4I**), and did not increase seizure risk (**Fig. 4.4J**),

indicating that astrogliosis-induced increase in I_{TONIC} in thalamocortical neurons is necessary for the development of hyperexcitability.

Enhancing GAT-3 in thalamic astrocytes prevents astrogliosis-induced seizure risk and cortical rhythm perturbations in mice

Astrocytes take up GABA from the extracellular space, mainly via the GABA transporters GAT-1 and GAT-3 (Beenhakker and Huguenard, 2010; Cope et al., 2009; Pirttimaki et al., 2013). Given the alterations in multiple genes linked to GAT regulation (Yu et al., 2018) in our transcriptomic study (**Fig. 4.1H**), we investigated whether the expression of these transporters was altered in reactive astrocytes. Three weeks following viral induction of astrogliosis, GAT-3 expression was reduced in the ipsilateral thalamus, and *Slc6a11* transcripts (encoding GAT-3) were reduced in reactive astrocytes (**Fig. 4.5, A to C**). The reduction of GAT-3 mRNA was specific to eGFP-transfected reactive astrocytes (**Fig. 4.5C**, and **Fig. S4.7A and B**), and there was no evidence of compensatory changes in GAT-1 mRNA (**Fig. S4.7C and D**).

Enhancing GAT-3 expression unilaterally in thalamic astrocytes by transducing mice with an astrocyte-specific viral construct (AAV2/5-GfaABC1D-GAT3) (Yu et al., 2018) at the same time as the induction of thalamic astrogliosis (**Fig. 4.5D**) counteracted the enhanced I_{TONIC} in thalamocortical neurons (**Fig. 4.5E**) and protected mice from increased seizure risk (**Fig. 4.5F**).

We next investigated whether induction of reactive astrocytes in the thalamus could initiate long-term changes in cortical rhythms. Seven weeks post-induction of thalamic astrogliosis, spectral analysis revealed a unilateral reduction in the sigma (12-15 Hz) and gamma (30-75 Hz) power, but not in total power (**Fig. 4.6, A to C** and **Table 4.9**). The reduction of sigma power was

specific to the 12-hr light cycle, whereas the reduction of gamma power was specific to the 12-hr dark cycle (**Table 4.9**).

Enhancement of GAT-3 expression in thalamic astrocytes protected from the loss of sigma and gamma power in the ipsilateral cortex (**Fig. 4.6D** and **Table 4.9**).

Enhancing GAT-3 in thalamic astrocytes reduces chemoconvulsant-induced seizure severity and mortality in a mouse model of cortical injury

We investigated whether similar reductions of thalamic GAT-3 transcripts occurred, and whether enhancing thalamic GAT-3 would confer resilience, in a mouse model of cortical injury. First, we performed 10x Visium Spatial Transcriptomics on tissue obtained from mice after TBI, stroke, or a sham procedure (**Fig. 4.7** and **Fig. S4.8**). Portions of the thalamus exhibited a higher number of *Gfap* transcripts and other markers of astrogliosis six weeks following stroke or TBI (**Fig. 4.7, A to C**, and **Fig. S4.9**). Elevated *Gfap* expression was associated with reduced *Slc6a11* expression in the thalamus (**Fig. 4.7, D and E**), whereas no correlation was found in the cortex (**Fig. S4.9**).

Enhancing GAT-3 in thalamic astrocytes ipsilateral to cortical TBI (**Fig. S4.10A**) increased survival following PTZ challenge; 5/12 TBI mice died following the PTZ challenge, whereas all 10 TBI mice that received astrocytic GAT-3 treatment survived (**Fig. S4.10B**). Furthermore, GAT-3 treatment resulted in reduced seizure severity following TBI (**Fig. S4.10C, D**).

We next investigated GAT-3 expression in human brain samples. Using a recently described method to deconvolute cell-type specific and brain-region specific transcriptional signatures from thousands of neurotypical adult human brain samples (Kelley et al., 2018), we found that *SLC6A11* (encoding GAT-3) was highly expressed in the thalamus-containing diencephalon relative to all genes detected in this region (**Fig. 4.8A**). Comparing the fidelity of

SLC6A11 expression to transcriptional signatures of the major brain cell types showed that *SLC6A11* expression was highly correlated to an astrocyte transcriptional signature and not to neurons, oligodendrocytes, or microglia (**Fig. 4.8B** and **Fig. S4.11**), consistent with ultrastructural studies suggesting that GAT-3 is predominantly expressed in astrocytes in the rodent thalamus (De Biasi et al., 1998; Vitellaro-Zuccarello et al., 2003). We next performed immunostaining for GAT-3 in post-mortem thalamic and peri-lesional cortical tissue obtained from human brains with a history of ischemic stroke or TBI (**Fig. 4.8**, **Fig. S4.11**, and **Tables 4.1 and 4.2**). The extent of co-localization between GAT-3 and GFAP-positive putative astrocytes varied, prominent in some cases (such as thalamus and cortex of control subject, **Fig. 4.8, C and D**) and less prominent in others (such as thalamus of stroke and TBI subject, **Fig. 4.8C**). In a blinded, semi-quantitative scoring of GAT-3 intensity, thalamic samples from control subjects displayed a median score of 3 (corresponding to dense GAT-3 immunoreactivity), whereas thalamic samples from subjects with stroke or TBI displayed, respectively, a median score of 2 (moderate GAT-3) and 2.5 (moderate to dense GAT-3) (**Table 4.2**). Cortical samples from control subjects, as well as peri-lesional cortical samples from subjects with stroke or TBI, displayed a median score of 2 (moderate GAT-3) (**Table 4.2**).

Discussion

Here we demonstrate that neuroinflammation in the mouse thalamus can drive enhanced cellular and microcircuit excitability, seizure risk, and aberrant changes in cortical states in mice. Our findings pinpoint astrocytic GAT-3 as a link between neuroinflammation and long-term network dysfunction, and as a potential therapeutic target for repairing circuit dynamics and promoting resilience following brain insults characterized by secondary and persistent thalamic neuroinflammation. Although astrocyte dysfunction has been widely documented in cellular and circuit hyperexcitability in the context of epilepsy (Maroso et al., 2010; Patel et al., 2019; Robel et al., 2015; Robel and Sontheimer, 2016; Senatorov et al., 2019; Steinhäuser and Seifert, 2012; Vezzani et al., 2019), untangling whether reactive astrocytes are a cause and/or consequence of changes in neuronal network activity remains challenging (Ortinski et al., 2010; Robel et al., 2015; Robel and Sontheimer, 2016; Vezzani et al., 2019). In the thalamus, astrogliosis has been suggested to be a predictor of long-term consequences of cortical lesions such as epilepsy and cognitive impairment (Grossman et al., 2012; Grossman and Inglese, 2016; Paz et al., 2010; Ramlackhansingh et al., 2011). Given the role of the thalamus as a regulator of thalamocortical rhythms and higher cognitive processes, understanding if and how reactive astrocytes in the thalamus can initiate development of pathological circuit dynamics is of broad fundamental and translational interest. To address this gap, we used a viral construct (Ortinski et al., 2010) to selectively transduce astrocytes in the mouse thalamus, recapitulating secondary thalamic astrogliosis, but in the absence of a cortical lesion. The long-term consequences of thalamic astrogliosis included increased seizure risk, and disruption of adaptive cortical rhythms in the sigma and gamma bands. These effects of thalamic astrogliosis are reminiscent of maladaptive outcomes of cortical injuries, such as increased seizure risk in mice and patients (Klein et al.,

2018), and reduced sigma-related sleep spindles in mice (Andrade et al., 2017; Holden et al., 2021) linked to sleep-wake disturbances in patients (Ouellet et al., 2015). Therefore, rather than being a mere bystander in the pathological sequelae of brain injuries, thalamic astrogliosis in mice can initiate robust, sustained aberrations in thalamocortical rhythms—gain-of-function in pathological rhythms and loss-of-function in adaptive rhythms—as had been suggested by previous studies (Holden et al., 2021) but not yet demonstrated directly.

How might thalamic reactive astrocytes drive maladaptive circuit function? In the mouse model of thalamic astrogliosis, reactive astrocytes downregulated the GAT-3 GABA transporter, leading to increased I_{TONIC} in thalamocortical neurons, resulting in increased neuronal excitability, and increased intra-thalamic micro-circuit excitability (**Fig. S4.12**). Enhancing GAT-3 in mouse thalamic astrocytes prevented astrogliosis-induced neuronal hyperexcitability and restored cortical sigma and gamma power, supporting the conclusion that the maladaptive outcomes were driven by reactive astrocytes. As in our mouse model of thalamic astrogliosis, GAT-3 was also decreased in regions of thalamic reactive astrocytes in mouse models of cortical stroke and TBI. The identification of *SLC6A11*—encoding GAT-3—as a risk gene for epilepsy in humans (Schijns et al., 2020), and the data showing that pharmacological blockade of GAT-3 strengthens epileptiform oscillations in rats *ex vivo* (Lu et al., 2020) suggest a link between GAT-3 and brain hyperexcitability. We found that enhancing astrocytic GAT-3 unilaterally in the thalamus prevented the increased seizure risk in the mouse model of thalamic astrogliosis, and reduced chemoconvulsant-induced seizure severity and mortality in a mouse model of cortical injury.

At the mechanistic level, our study suggests that enhancing GAT-3 could act through reducing excess I_{TONIC} in thalamocortical neurons. In these cells, I_{TONIC} is mediated by the δ-subunit-containing $GABA_AR$ (encoded by *Gabrd*). *GABRD* is a susceptibility locus for

generalized epilepsies, and increased I_{TONIC} has been implicated in epilepsy (Cope et al., 2009; Lee and Maguire, 2014). Astrocytic GAT-3 plays a key role in the regulation of extrasynaptic GABA in the thalamus (Beenhakker and Huguenard, 2010), which contributes to I_{TONIC} in thalamocortical neurons. In support of our hypothesis, preventing the increase in I_{TONIC} via conditional *Gabrd* deletion in thalamocortical neurons also prevented astrogliosis-driven hyperexcitability.

In the peri-lesional cortex of rodents, phasic and tonic GABA currents may play opposing roles in the aftermath of stroke (Clarkson et al., 2010; Hiu et al., 2016). I_{TONIC} has diverse region- and cell type-specific effects (Lee and Maguire, 2014). Thus, selectively counteracting the maladaptive components is critical in promoting repair. Although we did not examine changes in I_{TONIC} in thalamocortical neurons in TBI mice, our finding that enhancing thalamic GAT-3 prevented PTZ-induced mortality in TBI mice supports the idea that targeting thalamic astrocytic GAT-3 may be a viable strategy to decrease seizure risk following cortical injury.

Astrocytic GAT-3 activity and modulation of neuronal I_{TONIC} should be evaluated as possible therapeutic targets in the context of neuroinflammation associated with increased seizure risk. Indeed, dysfunction of GATs and I_{TONIC} have been implicated in various disorders associated with both chronic neuroinflammation and increased seizure risk, such as stroke (Clarkson et al., 2010) and Alzheimer's disease (Jo et al., 2014). Secondary and persistent astrogliosis of the thalamus is a predictor of long-term consequences of cortical lesions such as epilepsy and cognitive impairment (Grossman et al., 2012; Grossman and Inglese, 2016; Paz et al., 2010; Ramlackhansingh et al., 2011), and perturbations of cortical rhythms driven by thalamic astrogliosis (discussed above) phenocopy the changes observed in the aftermath of brain injuries. The secondarily damaged thalamus can be targeted to abort post-stroke epileptic seizures in rodents (Paz et al., 2013) and protect against chemoconvulsant-induced mortality in mice with TBI

(discussed above). Based on our findings showing that GAT-3 loss-of-function is a hallmark of thalamic astrogliosis, and that increasing GAT-3 specifically in thalamic astrocytes is beneficial in multiple mouse models, we propose that GAT-3 loss-of-function is a node of failed homeostatic plasticity and a key component of reactive astrocyte dysfunction which enables the far-reaching consequences of thalamic astrogliosis. In the sclerotic hippocampus, loss of GAT-1 is accompanied by an upregulation in GAT-3, suggesting a compensatory homeostatic mechanism (Lee et al., 2006; Wu et al., 2014). However, in the setting of thalamic inflammation, loss of GAT-3 was not associated with transcriptional upregulation of GAT-1. In the thalamus of humans and mice, *Slc6a11* (encoding GAT-3) is almost exclusively expressed in astrocytes (De Biasi et al., 1998; Vitellaro-Zuccarello et al., 2003), whereas *Slc6a1* (encoding GAT-1) is expressed similarly across astrocytes and neurons. Therefore, we speculate that loss of GAT-3 in thalamic astrocytes might be particularly detrimental because of a homeostatic failure to compensate for lost function. We propose that enhancing GAT-3 in reactive astrocytes might promote brain resilience to injuries.

The mouse model of thalamic astrogliosis allows us to dissect the role of thalamic astrogliosis bypassing cortical injuries, but it has several limitations. First, a single experimental manipulation of astrocytes cannot fully phenocopy the molecular and functional features of reactive astrocytes. Nevertheless, our analyses highlight some features of astrogliosis conserved across experimental conditions—including somatic hypertrophy and reduction in process branching (Sun and Jakobs, 2012), and differential expression of canonical reactivity genes (Liddelow et al., 2017; Zamanian et al., 2012). Second, we did not investigate other elements of the neuroinflammatory cascade—such as the secondary activation of microglia—and therefore do not exclude their possible influence on circuit dysfunction after cortical lesions. Third, we did not

investigate the extent to which astrogliosis-induced changes in cortical sigma and gamma power directly relate to disease-relevant cognitive or behavioral impairments. The absence of major abnormalities in mice with thalamic astrogliosis in standard behavioral assays relying on distributed brain circuits does not preclude other thalamocortical circuit-specific changes such as somatosensation or attention. Fourth, only male mice were included in our study. Given that the link between I_{TONIC} and neuronal excitability is ovarian cycle-dependent (Maguire et al., 2005), further investigations are needed to determine the relevance of our findings in female mice. Another limitation of this study was the limited sample size for post-mortem thalamic human tissue, which excluded reliable statistical analysis of immunofluorescence data. We hope our study will encourage inclusion of the thalamus in standard resection protocols of human post-mortem brain tissue. In addition, because some data included in our study were obtained from patients with a history of epilepsy before and/or after injury, we cannot conclusively demonstrate that the changes in GFAP or GAT-3 were solely due to injury rather than recurrent seizures. Finally, although we present evidence of thalamic GAT-3 perturbation across various model systems and proof-of-concept that thalamic GAT-3 can be targeted to prevent seizure risk in mice, further work in pre-clinical models of cortical injury is needed to understand whether GAT-3 can be safely targeted to ameliorate disease-relevant cellular and circuit pathologies such as spontaneous seizures without compromising the adaptive aspects of neuroinflammation.

Acknowledgments:

We thank Dr. Jamie Maguire, for kindly providing the $Gabrd^{Fl/Fl}$ mice; Drs. John Huguenard and Jordan Sorokin, for providing the custom MATLAB script for thalamic oscillation analysis; Drs. Kevin Kelley and Michael Oldham, for providing assistance in using their published database of

human transcriptomic data; Irene Lew and Hiromi Inoue, for help with animal husbandry; Naznin Jahan, for technical assistance; Drs. Kathryn Claiborn and Francoise Chanut, for providing critical editorial feedback on the manuscript; Dr. Reuben Thomas (Gladstone Bioinformatics Core), for consultation of statistical analyses; Drs. Lennart Mucke and Michael Gill, and Iris Lo and Jeffrey Sims (Gladstone Behavioral Core), for consultation on behavioral experiments; Jim McGuire (Gladstone Genomics Core), for conducting the RNA sequencing library preparation and QCs for sequencing at the Center For Advanced Technology at UCSF; and the Gladstone Histology Core, for technical advice.

Funding:

National Institute of Neurological Disorders and Stroke grant F31 NS111819 (to F.S.C.)

National Institute of Neurological Disorders and Stroke grant R01 NS096369 (to J.T.P.)

National Institute of Neurological Disorders and Stroke grant R01 NS121287 (to J.T.P.)

National Institute of Neurological Disorders and Stroke grant R00 NS078118 (to J.T.P.)

National Institute of Neurological Disorders and Stroke grant R35 NS111583 (to B.S.K.)

National Institute of Mental Health grant DP1 MH104069 (to B.S.K.)

National Institute of Mental Health grant DP2 MH116507 (to A.V.M.)

National Institute of Mental Health grant R01 MH119349 (to A.V.M.)

National Cancer Institute grant P30 CA082103 (to UCSF Laboratory for Cell Analysis)

National Science Foundation grant 1144247 (to F.S.C.)

UCSF Discovery Fellowship (to F.S.C.)

Department of Defense grant EP150038 (to J.T.P.)

Department of Defense grant EP190020 (to J.T.P.)

Gladstone Institutes Animal Facility grant RR18928 (to J.T.P.)

Pew Charitable Trusts (to A.V.M.)

European Union Seventh Framework Programme EPITARGET grant 602102 (to E.A.V., E.A.)

European Union Horizon 2020 Research and Innovation Programme Marie Sklodowska-Curie grant 722053 (to E.A.)

Dutch Epilepsy Foundation project 16-05 (to D.W.M.B., E.A.)

European Union Horizon 2020 WIDESPREAD-05-2020-Twinning, EpiEpiNet grant agreement 952455 (to E.A., E.A.V.)

Author contributions:

F.S.C. and J.T.P. conceived the project. F.S.C. performed stereotaxic viral injections, ECoG implants, *in vivo* recordings and analysis, *ex vivo* electrophysiological studies and analysis, immunohistochemistry, and all related data analysis and visualization. I.D.V. performed, analyzed, and interpreted FACS, bulk transcriptomics, and qPCR studies. I.D.V. and F.S.C. performed, analyzed, and interpreted astrocyte morphology study. D.W.M.B., J.J.A., E.A.V., and E.A. performed, analyzed, and interpreted immunolabeling of post-mortem human tissue. B.S.K. and X.Y. generated the AAV2/5-*GfaABC1D*-GAT3-HA-mCherry construct. B.H., J.T.P., and F.S.C. developed custom MATLAB scripts for analysis of electrophysiology studies. F.A. performed, analyzed, and interpreted kainic acid seizure challenge in mice. F.S.C., A.R.M., and A.C. performed immunohistochemistry of mouse tissue. Y.V., A.C., and F.S.C. performed, analyzed, and interpreted spatial transcriptomic study. J.T.P., A.V.M., E.A., and B.S.K. acquired funding. F.S.C. and J.T.P. discussed and interpreted all data with respective authors. F.S.C. and J.T.P. wrote the original draft of the manuscript, and all authors participated in manuscript revisions.

Materials & Methods

Study Design

The main objective of this study was to investigate whether thalamic astrogliosis acts as a node of vulnerability after brain injuries, and if so, whether it represents a potential disease-modifying target. We developed a mouse model of unilateral thalamic astrogliosis using intra-thalamic delivery of a viral construct previously shown to selectively induce reactive astrocytes in the hippocampus (Ortinski et al., 2010); used established mouse models of cortical injury (photothrombotic stroke and controlled cortical impact); and determined the potential restorative effects of counteracting GAT-3 loss using a viral construct to unilaterally enhance GAT-3 expression (Yu et al., 2018) in thalamic astrocytes. Transduction of reactive astrocytes was validated using established transcriptomic, morphological, and immunohistochemical markers (Escartin et al., 2021), using a combination of transgenic reporter mice, FACS, bulk RNA-Seq, and microscopy. Cellular excitability and synaptic function were assessed *ex vivo* with whole-cell current- and voltage-clamp recordings in thalamic neurons, and exclusion criteria are detailed below. Microcircuit excitability was assessed with extracellular recordings in *ex vivo* thalamic slices. *In vivo* brain excitability and cortical states were assessed with pharmacological seizure assays and electrocorticography recordings. Dysregulation of GAT-3 was assessed using a combination of immunohistochemistry, qPCR, bulk RNASeq, and spatial transcriptomics in mice with thalamic astrogliosis and cortical injury. To assess relevance to human disease, immunohistochemical markers of astrogliosis and GAT-3 were assessed in post-mortem thalamic tissue obtained from human subjects with a history of cortical injuries.

All mouse experiments were performed in adult, male, age-matched mice with similar numbers randomly assigned to different experimental groups. Mice with thalamic astrogliosis were

compared to mice injected unilaterally with sterile saline. Mice with cortical injury were compared to data from mice which received identical surgical procedures but no illumination of the light-sensitive dye (stroke) or impact (TBI). All procedures were approved by the ethics committees at the University of California San Francisco, Gladstone Institutes, and Amsterdam UMC. Sample sizes were based on similar previously published work (Holden et al., 2021; Paz et al., 2010; Ritter-Makinson et al., 2019; Vainchtein et al., 2018) and are provided in figure legends. Data collection and analyses were performed blinded. Raw data provided as data file S1.

Mice

All protocols were approved by the Institutional Animal Care and Use Committee at the University of California, San Francisco and Gladstone Institutes. Precautions were taken to minimize stress and the number of animals used in each set of experiments. Mice were separately housed after surgical implants. Male mice were used for all experiments, and ages ranged between postnatal days 28-300. C57BL6J mice were purchased from the Jackson Laboratory (Jax Strain No. 000664). Aldh1l1-tdTomato mice were bred by A.V.M. Floxed *Gabard* ($Gabrd^{Fl/Fl}$) mice (Jax Strain No. 023836) were a gift from Dr. Jamie Maguire (Tufts University).

Viral injections

Stereotaxic viral injections were carried out as described (Ritter-Makinson et al., 2019; Sorokin et al., 2017). Briefly, mice were anesthetized with 2-5% isoflurane. Adeno-associated viral (AAV) constructs were delivered into the ventrobasal nucleus of the thalamus (VB) using the following coordinates: 1.65 mm posterior to Bregma, 1.5 lateral relative to midline, and 3.3 to 3.5 mm ventral to the cortical surface. For all injections, the MicroSyringe Pump Controller (Micro4, WPI),

NanoFil syringes (10µL, WPI), and 33g beveled NanoFil needles (WPI; NF33BV-2) were used. Viral constructs were infused at a rate of 100-200 nL/min, with a 5–10 minute pause before withdrawing the needle. All viral injections were performed unilaterally. Experiments were performed at least 3 weeks following viral injections. Astrogliosis was induced with a high titer injection of AAV2/5-*Gfa104*-PI.eGFP.WPRE.bGH (AAV2/5-*Gfa104*-eGFP), which transduces astrocytes with enhanced green fluorescent protein (eGFP) expression driven by a *Gfap* promoter (Ortinski et al., 2010) (Addgene #100896-AAV5; previously available through Penn Vector Core, Catalog #AV-5-PV2380). Mice received unilateral injections of 750 nL of AAV2/5-*Gfa104*-eGFP, or saline in control conditions (0.9% sodium chloride; Hospira). The titer of the construct, across various lots and experiments, was validated by Penn Vector Core using qPCR and dd-qPCR, and fell into the range of 0.85-1.7e10 g.c. per injection. For low-titer control experiments, we delivered 1.4e7 g.c. per injection. Previous work demonstrated that this titer does not induce astrogliosis (Ortinski et al., 2010). In describing the results of this study, we use "Control" to refer to mice in which we performed intra-thalamic injection of saline, and we use "Thalamic Astrogliosis" to refer to mice in which we performed intra-thalamic injections of AAV2/5-Gfa104-eGFP, unless specified otherwise. To selectively delete the delta subunit in $Gabrd^{Fl/Fl}$ mice, 600 nL of AAV-CaMKIIα-mCherry-Cre (UNC Vector Core) was used, in combination with 750 nL of either AAV2/5-*Gfa104*-eGFP, or saline. AAV2/5-*GfaABC1D*-GAT3-HA-mCherry (generated by B.S.K. and X.Y.) was used to selectively enhance expression of GAT-3 in astrocytes. 600 nL of AAV-GAT3 was delivered in combination with 750 nL of either AAV2/5-*Gfa104*-eGFP, or saline.

Fluorescence-activated cell sorting (FACS) of reactive astrocytes

Three weeks after unilateral injection of AAV into the VB thalamus, Aldh1l1-tdTomato mice were anesthetized with isoflurane and perfused with ice-cold HBSS-Ca/Mg-free supplemented with Hepes and glucose (Galatro et al., 2017). Ventrobasal (VB) thalami were microdissected into ipsilateral and contralateral samples under a dissecting microscope and dissociated with papain 20 U/ml (Worthington) for 45 minutes at 34 ºC as previously described (Cahoy et al., 2008). A 22% Percoll gradient was run to deplete myelin and subsequently the single cell suspension was incubated with following antibodies in HBSS-Ca/Mg-free supplemented with Hepes, glucose and EDTA (Galatro et al., 2017) on ice for 30 minutes: CD11b APC, CD45 Percp-Cy5.5 and Ly-6C APC/Cy7 (eBioscience/Biolegend). Samples were incubated with DAPI and FACS was performed on a BD Aria3 to collect purified astrocyte populations (**Fig. S4.2**). Ipsilateral reactive astrocytes transduced by AAV-eGFP were gated as $DAPI^{neg}CD11b^{neg}tdTomato^{pos}eGFP^{pos}$, and contralateral "healthy" astrocytes were gated as $DAPI^{neg}CD11b^{neg}tdTomato^{pos}eGFP^{neg}$. DAPI was used for live/dead exclusion and CD11b to exclude microglia. Cells were collected in RLT+ (Qiagen) and stored at -80 ºC.

qPCR and RNA sequencing of FACS-astrocytes

RNA was isolated from FACS-astrocytes with the Rneasy Plus Micro kit (Qiagen) and quality and concentration were assessed with the Agilent RNA 6000 Pico kit on a Bioanalyzer (Agilent). For qPCR analysis, RNA was reverse transcribed using the high capacity cDNA reverse transcription kit (Applied Biosystems) and qPCR was run on a 7900HT Fast Real-Time PCR System (Applied Biosystems) using Fast SYBR Green Master Mix (Applied Biosystems) and the following primers: *Slc6a11* -FW: CGGCTGGGTATATGGAAGCA -RV: ACGACTTTCCAGCACCACTT; *Aldh1l1*

-FW: CTTCATAGGCGGCGAGTTTGTG -RV: CGCCTTGTCAACATCACTCACC; GFP -FW: AAGTTCATCTGCACCACCG -RV: TCCTTGAAGAAGATGGTGCG. CT cycles were analyzed with 7900 SDS v2.4 software (Applied Biosystems) and $2^{-\Delta CT}$ method was used to determine expression. For RNA sequencing, cDNA and libraries were made using the Ovation RNA-Seq System V2 kit (NuGen). Quality was measured by Agilent High Sensitivity DNA kit on a Bioanalyzer (Agilent) and quantified by qPCR. Libraries were pooled and RNA sequencing was performed on an Illumina HiSeq 4000 with single end (SE50) sequencing. Around 60-80 million reads were sequenced per sample.

Transcriptomic analysis of bulk RNA-Seq

Bioinformatic analysis of bulk RNA-Seq of FACS-isolated thalamic astrocytes was performed as previously described (Vainchtein et al., 2018). FastQC was used to assess read quality. Reads were pseudo aligned to the *Mus musculus* transcriptome (cDNA, Ensembl GRCm38) using Kallisto (version 0.44.0) with kmer size 31 and bootstraps set to 100. Kallisto generated transcript per million (TPM) and transcript abundance values that were loaded into R (The R Foundation) using Tximport. TPM values per gene were generated from the per isoform values. DESeq2 package was used to determine differentially expressed genes, where genes with an adjusted p-value < 0.05 were considered significantly differentially expressed. Heatmaps were made using the ComplexHeatmap package.

Immunohistochemistry of mouse brain tissue

Mice were anesthetized with a lethal dose of FatalPlus and perfused with ice-cold 4% paraformaldehyde in phosphate buffered saline (PBS). All brains were visually assessed for signs

of gross damage before sectioning. Serial coronal sections (50 μm) were cut on a sliding microtome (Leica SM2000R), selecting sections near the site of injection (Bregma –1.65 mm). After immunohistochemical protocols, sections were mounted in an antifade medium (Vectashield) and imaged using fluorescence microscopy (Keyence BZ-9000) or confocal microscopy (Zeiss LSM880). Brain sections were visually assessed for signs of gross damage on the side which received a unilateral manipulation (with the contralateral hemibrain used as a control).

To verify the location and extent of thalamic astrogliosis, sections were immunostained with the following antibodies: glial fibrillary acidic protein (GFAP) (1:1000; host species chicken; Abcam ab4674; RRID:AB_304558), GFP (1:1000; host species goat; Abcam ab6673; RRID:AB_305643), GAT-3 (1:200; host species rabbit; Abcam ab431; RRID:AB_304437); mCherry (1:500; host species rabbit; Abcam ab167453; RRID:AB_2571870); and the following secondary antibodies (1:500): donkey anti-chicken AF594 (Jackson ImmunoResearch Labs #703-585-155; RRID:AB_2340377), donkey anti-goat AF488 (Abcam ab150129; RRID:AB_2687506), goat anti-rabbit AF594 (Thermo Fisher #A-11037; RRID:AB_2534095). Sections were blocked in normal donkey or goat serum (Jackson ImmunoResearch Labs #017-000-121 (RRID:AB_2337258) & #005-000-121 (RRID:AB_2336990). Free-floating sections were washed in PBS (3 x 10 min), permeabilized with 0.5% Triton in PBS (PBST-0.5%), washed in PBST-0.05%, and blocked in 10% normal goat or donkey serum (diluted in PBST-0.05%) for 1 hour. Sections were incubated with primary antibodies in 3% normal goat or donkey serum, overnight at 4 °C. Following 3x10 min washes in PBST-0.05%, the sections were incubated with secondary antibodies for 1-2 hr at room temperature. Sections were then washed in PBST and PBS, mounted onto glass slides, and coverslipped with Vectashield antifade reagent (Vector Laboratories, H-1000), and stored at 4 °C.

To verify deletion of the δ-subunit in the Gabrd$^{Fl/Fl}$ mice, we performed DAB-based IHC on free-floating sections (50 μm). Endogenous peroxidase activity was quenched for 30 min in 1% v/v hydrogen peroxide in 30% ethanol. The blocking of nonspecific binding was achieved with 10% normal goat serum (NGS) for 1 hour at room temperature (RT). The antibody against $GABA_AR$ δ-subunit (1:500; host species rabbit, polyclonal, MilliporeSigma AB9752; RRID:AB_672966) was dissolved in 5% NGS and the sections were incubated in RT overnight. For horseradish peroxidase (HRP) staining, sections were incubated with Mach 2 anti-rabbit HRP polymer (Biocare Medical, RHRP520) for 1 hour at RT. The activity of HRP was visualized with a commercially available kit for 3,3′-diaminobenzidine (DAB) peroxide substrate (Vector Laboratories, SK-4100; RRID:AB_2336382). Sections were washed in PBTS-0.1%. between each immunohistochemical step. Finally, immunostained sections were mounted on gelatinized slides, dehydrated in alcohol and xylene and cover-slipped with Cytoseal (ThermoFisher Scientific, 8310-16). Control sections were processed without primary antibodies, and no immunostaining was observed under these conditions.

For morphological characterization of astrocytes, we performed stereotaxic injections of AAV-eGFP into VB thalamus of two-month-old EAAT2-tdTomato mice. After three weeks, mice were anesthetized with isoflurane, and perfused with ice-cold PBS followed by ice-cold 4% PFA. The brains were collected and post-fixed in 4% PFA overnight at 4 ºC. Subsequently, brains were placed in 30% sucrose solution in PBS for two consecutive nights. Brains were frozen and sectioned (60 μm) on a Cryostat (Leica). For immunohistochemistry, sections were treated with 0.01 M citrate buffer pH 6.0 for 2 min at 95 ºC for antigen retrieval, blocked for 1 hour at room temperature with 5% normal goat serum (NGS) in PBS with 0.25% Triton X-100. Primary antibody staining was done overnight at 4 ºC with rat anti-GFAP (1:1000, Invitrogen, 13-0300),

chicken anti-GFP (1:1000, Aves Labs, GFP-1020) and rabbit anti-RFP/DsRed (1:1000, Living Colors DsRed Polyclonal Antibody, Clontech, 632496) in PBS with 2% NGS and 0.25% Triton X-100. For secondary antibody staining, sections were incubated with goat anti-rat AF647, goat anti-chicken AF488, goat anti-rabbit AF555 (all at 1:400, from Thermo Fisher Scientific) in PBS with 2% NGS and 0.25 Triton X-100 for 1.5 hours at RT. Sections were embedded on slides in DAPI Fluoromount-G (SouthernBiotech, 0100-20). Z-stacks with a step size of 1 μm at 40x magnification from the VB thalamus were collected on a Zeiss LSM880. Using Fiji (ImageJ), maximum intensity images were generated and the EAAT2-tdTomato channel images were used to create binary, thresholded images for morphology analysis. Sholl analysis (Ferreira et al., 2014) was performed in Fiji (ImageJ) on astrocytes from the binary images with a step size of 1 μm.

Quantification of mouse immunohistochemical data

Images were obtained with the Keyence fluorescence microscope, using BZ Viewer and BZ Analyzer software. Image quantification was performed in ImageJ (U.S. National Institutes of Health). For image quantification (10x magnification), we chose 2-4 sections for each mouse between -1.3 mm and -1.6 mm posterior from Bregma (Franklin and Paxinos, 2007). Regions of interest (ROI) were selected based on the mouse brain atlas (Franklin and Paxinos, 2007) for both hemispheres (ipsilateral and contralateral to site of injection and/or injury). Fluorescence intensity was obtained from 8-bit images as the sum of the values of the pixels in each ROI (using "Raw Integrated Density" in ImageJ), and normalized by each ROI area. Normalized fluorescence intensity of the ipsilateral side was then divided by the normalized fluorescence intensity of the contralateral side to obtain the fluorescence intensity ratio of one section. For quantification in the thalamus, thalamic nuclei include the ventroposterior medial, ventroposterior lateral, ventrolateral,

posterior medial, dorsal lateral geniculate, and lateral posterior nuclei, unless specified otherwise as in the case of quantification of the reticular thalamic nucleus). Quantification in the hippocampus included CA1, CA3, and dentate gyrus. Quantification in the somatosensory cortex included the S1 barrel field (S1BF) and S1 trunk (S1Tr). Quantification was performed in sections obtained along the AP axis in which all ROIs were visible. No exclusion criteria were applied.

Immunohistochemistry of human post-mortem brain tissue

The cases included in this study were obtained from the archives of the Amsterdam University Medical Centers. Brain samples (peri-lesional cortex and thalamus) were obtained from 4 patients who died after TBI and 3 patients who died after ischemic stroke. Control material was obtained at autopsy from 3 age-matched controls, without a history of seizures or other neurological diseases. All autopsies were performed within 24 h after death. Tissue was obtained and used in accordance with the Declaration of Helsinki and the Amsterdam UMC Research Code provided by the Medical Ethics Committee. All cases were reviewed independently by two neuropathologists. The clinical information of each patient is reported in **Table 4.1**.

Human brain tissue was fixed in 10% buffered formalin and embedded in paraffin. Paraffin embedded tissue was sectioned at 5 μm, mounted on pre-coated glass slides (Star Frost, Waldemar Knittel) and processed for immunohistochemical staining. Sections were deparaffinated in xylene, rinsed in ethanol (100%, 95%, 70%) and incubated for 20 min in 0.3% hydrogen peroxide diluted in methanol. Antigen retrieval was performed using a pressure cooker in 0.01 M sodium citrate buffer (pH 6.0) at 120°C for 10 min. Slides were washed with PBS, pH 7.4) and incubated overnight with primary antibody (GAT-3, 1:450, ab431, Abcam) in PBS at 4°C. Sections were washed in PBS and then stained with a polymer-based peroxidase immunohistochemistry

detection kit (Brightvision plus kit, ImmunoLogic,) according to the manufacturer's instructions. Staining was performed using Bright 3,3'-diaminobenzidine (DAB) substrate solution (ImmunoLogic,). Reaction was stopped by washing in distilled water. Sections were counterstained with Haematoxylin-Mayer solution (Klinipath), dehydrated in alcohol and xylene and coverslipped. For double labeling, slides were incubated overnight with primary antibodies (GAT-3, 1:450 and GFAP (G-3893), 1:2000, Sigma-Aldrich) in PBS at 4°C. Afterwards, sections were incubated for two hours at room temperature with secondary antibodies, Alexa Fluor 568 donkey anti-mouse IgG (H+L) and Alexa Fluor 488 goat anti-rabbit IgG (H+L) (1:200, A10037 and A11008; Invitrogen), washed in PBS and coverslipped. Fluorescent microscopy was performed using a confocal microscope (SP8-X, Leica,) to acquire images of the perilesional cortex and thalamus from all autopsy post-mortem material. Fluorescence images were pseudocolored in ImageJ for visualization.

Quantification of immunoreactivity in human post-mortem tissue

Semi-quantitative analysis was performed by assessing GFAP immunoreactivity in the peri-lesional cortex and thalamus according to the following scale while blinded to condition (table S2): 1=sparse presence of cells with astrocyte-like morphology, of which the majority have a resting morphology; 2= moderate presence of cells with astrocyte-like morphology, with either resting or partially reactive morphology; 3= high presence of cells with astrocyte-like morphology, of which the majority have reactive morphology. Semi-quantitative analysis of GAT-3 immunoreactivity in the peri-lesional cortex and thalamus according to the following scale while blinded to condition (**Table 4.2**): 0=absent, 1=sparse, 2=moderate, 3=dense staining. Quantification of GFAP immunofluorescence was performed by two investigators independently

counting the number of GFAP-positive cells in ImageJ in a blinded manner (**Fig. S4.11**). Inclusion criteria for GFAP-positive cells included distinct immunopositive soma and at least one process protruding from the soma. For each image, the count of the two investigators was averaged. While blinded to condition, images were identified for exclusion if more than half of the image included fibrous white matter. Quantification of GAT-3 immunofluorescence was performed in perilesional cortex and thalamus using ImageJ (**Fig. S4.11**). Immunofluorescence images were converted to 8-bit grayscale then thresholded, such that the range of grayscale pixel values was set consistently across images of the same region, to obtain the mean gray value, as described in (van Vliet et al., 2020). Per group, outliers were identified using ROUT method in GraphPad Prism.

Slice preparation for patch-clamp electrophysiology

Mice were euthanized with 4% isoflurane, then transcardially perfused with ice-cold sucrose cutting solution containing 234 mM sucrose, 2.5 mM KCl, 1.25 mM NaH_2PO_4, 10 mM $MgSO_4$, 0.5 mM $CaCl_2$, 26 mM $NaHCO_3$, and 11 mM glucose, equilibrated with 95% O_2 and 5% CO_2, pH 7.4. The thalamic slice preparation was performed as described (Paz et al., 2011; Ritter-Makinson et al., 2019). Horizontal thalamic slices containing the VB thalamus and nRT were cut at 250-µm (for patch-clamp electrophysiology) or 400-µm (for thalamic microcircuit studies) with a Leica VT1200 microtome (Leica Microsystems). Slices were incubated at 32 °C for 30 min, then at 24-26 °C for 1 hour, in artificial cerebrospinal fluid (aCSF) containing 126 mM NaCl, 2.5 mM KCl, 1.25 mM NaH_2PO_4, 1 mM $MgCl_2$, 2 mM $CaCl_2$, 26 mM $NaHCO_3$, and 10 mM glucose, equilibrated with 95% O_2 and 5% CO_2, pH 7.4. For tonic GABA recordings, slices were incubated and recorded in aCSF containing 126 mM NaCl, 26 mM $NaHCO_3$, 10 mM glucose, 2.5 mM KCl, 2 mM $MgCl_2$—$6H_2O$, 2 mM $CaCl_2$—$2H_2O$, and 1.25 mM NaH_2PO_4 (Pangratz-Fuehrer et al., 2016).

Patch-clamp electrophysiology in thalamic slices

Recordings were performed as described (Paz et al., 2011, 2010; Ritter-Makinson et al., 2019). Thalamocortical neurons in the VB thalamus, and neurons in the reticular thalamic nucleus (nRT), were visually identified by differential contrast optics with an Olympus microscope (60x objective, NA 1.1, WD 1.5 mm; SKU 1-U2M592). Recording electrodes made of borosilicate glass (Sutter Instruments) had a resistance of 2.5–4 MΩ when filled with intracellular solution. Access resistance was monitored in all the recordings, and cells were included for analysis only if the access resistance was <25 MΩ.

To record intrinsic membrane properties and bursting properties in current-clamp mode, and spontaneous excitatory post-synaptic currents in voltage-clamp mode, an internal solution containing 120 mM potassium gluconate, 11 mM KCl, 1 mM $MgCl_2$, 1 mM $CaCl_2$, 10 mM HEPES, and 1 mM EGTA, pH adjusted to 7.4 with KOH (290 mOsm) was used; these recordings were performed in the presence of picrotoxin (50 μM, Sigma-Aldrich, #P1675) in the artificial cerebrospinal fluid (aCSF). The potentials for were corrected offline for -15 mV liquid junction potential.

To record spontaneous inhibitory post-synaptic currents, an internal solution containing 135 mM CsCl, 10 mM HEPES, 10 mM EGTA, 2 mM $MgCl_2$–$6H_2O$, and 5 mM QX-314, pH adjusted to 7.3 with CsOH (290 mOsm) was used. Recordings were performed in the presence of kynurenic acid (2 mM, Sigma-Aldrich #K3375) in aCSF.

To record tonic $GABA_A$ receptor-mediated currents, an internal solution containing 130 mM CsCl, 2 mM $MgCl_2$, 4 mM Mg-ATP, 0.3 mM Na-GTP, 10 mM Na-HEPES, 0.1 mM EGTA, pH adjusted to 7.3 with CsOH (290 mOsm) was used (Cope et al., 2005).

Recordings were performed in the presence of kynurenic acid (2 mM) in aCSF which was kept at 30 $\pm$ 1 °C. To obtain tonic GABA measurements, a bath of 50 μM Gabazine (GBZ; Sigma #SR-95531) prepared in dimethyl sulfoxide (DMSO; Sigma #D8418) was applied. Following GBZ application, slices were recorded for at least 10 minutes. Tonic current was defined as the shift in holding current due to GBZ bath application, and marked by the stopping of phasic IPSCs. Average currents were obtained for at least 2 minutes pre- and post-stabilization of the shift in holding current. Currents were subtracted using Clampfit 10.5 (Molecular Devices, SCR_011323). Currents are presented without normalizing to cell capacitance, as capacitance did not differ between groups (**Table 4.3**).

Analysis of electrophysiological properties of thalamic neurons

Tonic GABA recordings: Following GBZ (50 μM) bath application, neurons were recorded for at least 10 minutes. Tonic GABA current was defined as the shift in holding current due to GBZ application, and marked by the stopping of phasic IPSCs. We obtained an average current at least 2 minutes pre- and post-stabilization of the shift in holding current. Currents were subtracted using Clampfit 10.5 (Molecular Devices, SCR_011323). Currents are presented without normalizing to cell capacitance, as capacitance did not differ between groups (**Table 4.3**). All cellular physiology data were analyzed in a blinded manner.

Action potential properties: To characterize action potentials (APs) elicited by depolarizing intracellular current injections in thalamocortical neurons, we obtained the following parameters for the first AP which occurred at each neuron's rheobase (the amplitude of the first current step which elicited APs): the AP threshold, which was determined as the inflection point of the raw voltage trace immediately preceding the AP; the AP amplitude, defined as the voltage difference

between the AP threshold and the maximal voltage of the AP; the AP duration, defined as the time between the AP threshold and the time at which membrane voltage returned to threshold; and the AP half-duration, defined as the duration between the half-maximal voltage in the depolarizing phase and the half-maximal voltage in the repolarizing phase.

T-Current biophysical properties: To assess steady-state inactivation properties of the T-current, the current-voltage response of each cell was fit with the Boltzmann function to determine the half-maximal voltage (V_{50}) (Paz et al., 2010; Ritter-Makinson et al., 2019) (calculated using Origin Pro 9.0). All parameters (cell capacitance, maximal T-current area, maximal T-current amplitude, T-current density, maximal decay time constant, Boltzmann slope factor) were compared using unpaired t-tests or Mann-Whitney U tests (**Table 4.5**).

Low-threshold spike (LTS) properties: To characterize the LTS-mediated rebound bursting, a custom MATLAB script was used to detect (1) V_H = membrane potential at the end of the hyperpolarizing current injection; (2) the threshold and latency to the LTS, indicated by the first deflection point during the period of depolarization (after the current injection) (Coulter et al., 1989); (3) AP firing rate during these rebound bursts, calculated by the number of APs divided by the duration between the first and last AP. FR was calculated only if there was more than 1 AP during the rebound burst. For each cell, we obtained the LTS parameters from the sweep in which the current injection hyperpolarized the cell the most.

Hyperpolarization-induced depolarizing sag potential properties*:* To characterize the depolarizing "sag" potential induced by hyperpolarization in thalamocortical neurons (McCormick and Pape, 1990), sag potentials were obtained as a function of the maximal hyperpolarized potential in response to a -150 pA intracellular current injection. The amplitude of the sag potential was calculated as the difference between the maximal hyperpolarized membrane potential and the

membrane potential at the offset of the current injection. All recordings were performed at resting membrane potential.

Spontaneous synaptic currents: Frequency and kinetics of spontaneous excitatory and inhibitory synaptic currents were detected and analyzed using WDetecta (Huguenard Lab, Stanford University) as previously described (Paz et al., 2010; Ritter-Makinson et al., 2019). Spontaneous excitatory synaptic currents were obtained from the same samples presented in **Fig. 4.3, B and D**.

Electrophysiological recordings of extracellular thalamic oscillations and data analysis

***Recordings*:** Horizontal slices (400 μm) containing somatosensory thalamus were placed in an interface chamber at 34 °C and superfused at a rate of 2 ml min^{-1} with oxygenated aCSF supplemented with 0.3 mM glutamine for cellular metabolic support (Ritter-Makinson et al., 2019). Extracellular multi-unit activity (MUA) recordings were obtained with a linear 16-channel multi-electrode array (Neuronexus) that spanned the nRT and VB thalamic nuclei (**Fig. 4.2C**). MUA signals were amplified 10,000 times and band-pass filtered between 100 Hz and 6 kHz using the RZ5 from Tucker-Davis Technologies (TDT, SCR_006495). Position of recording array was visually checked for each recording to confirm position of electrodes in nRT and VB thalamic nuclei. Electrical stimuli were delivered to the internal capsule with a bipolar tungsten microelectrodes (50–100 kΩ, FHC). The stimuli were 100 μs in duration, 50 V in amplitude, and delivered once every 30 s for 20 trials.

Comparison of thalamic circuit oscillations in thalamic slices: Extracellular spikes from multi-unit activity (MUA) were detected with custom MATLAB scripts (Huguenard Lab, Stanford University) by taking the first derivative of the signal and thresholding over baseline RMS values. Spikes were excluded if their waveform lasted longer than 2 ms. An experienced user confirmed

parameter settings to optimize for all recordings. For automatic spike detection, the first three seconds of each trial was analyzed (**Fig. 4.2, A, B, and E**). As in previous literature, a burst of thalamic activity was defined as a cluster of ≥ 3 spikes occurring within 1 ms; and an oscillation as ≥ 2 bursts occurring within 1 second following stimulation, with an inter-burst interval of ≤ 1 second (Sorokin et al., 2017). In **Fig. 4.2D**, we characterized the maximal evoked oscillatory activity by manually quantifying the number of evoked bursts and duration of oscillation that occurred in the 30 seconds following electrical stimulation (averaged across 20 trials for each slice), from the most responsive recording site of each slice.

Peri-stimulus time histograms (PSTH): Spikes were aligned to the stimulation onset and were used to calculate PSTH with a bin width of 10 ms (averaged across trials). Color axis represents the firing activity, scaled to the maximal number of spikes obtained in the slice (across all 16 recording sites and across all 20 trials).

Auto-correlation analysis: The spatiotemporal synchrony of oscillatory activity was determined by calculating the auto-correlation of the PSTH summed across the 16 recording sites in the thalamus and across all 20 trials for each slice (**Fig. 4.2, A, B, and E**). Note that only 9 of 16 sites are shown to aid visualization in **Fig. 4.2 A and B**. The PSTH and auto-correlation were calculated for 3 seconds after stimulation (excluding the first 150 ms which included the direct response), but only 1 second is shown in Fig. 4.2 for clarity. The auto-correlation was used to calculate the oscillatory index (O.I.) as previously described (Huntsman et al., 1999; Sorokin et al., 2017).

$$\text{O.I.} = 1 - \left[\frac{t_i}{\frac{p_i + p_{i+1}}{2}}\right]$$

where t_i= the i^{th} local minimum of the auto-correlation (trough) and p_i= the i^{th} local maximum of the auto-correlation (peak).

Surgical implantation of electrocorticography (EcoG) devices in mice

For short (up to 90 min-long recordings) *in vivo* electrophysiological recordings described in **Figs. 4.4, 4.5,** and **Fig. S4.6**, electrocorticogram (EcoG) signal was acquired with a custom-made device containing multiple screws (Ritter-Makinson et al., 2019). Cortical screws were implanted bilaterally in somatosensory cortex S1 (-0.5 mm posterior from Bregma, ± 3.5 mm lateral), in the right primary visual cortex V1 (-2.9 mm posterior from Bregma, ± 3.25 mm lateral), in the prefrontal cortex (+1.0 mm anterior from Bregma, 0 mm lateral), and a reference screw was implanted above the cerebellum (-0.5 mm posterior from Lambda, 0.5 mm lateral). Devices were fixed to the skull using dental cement.

For chronic, continuous 24/7 EcoG recordings (**Fig. 4.6**), mice were implanted with wireless telemetry devices as previously described (Holden et al., 2021) (PhysioTel HD-X02 Implants, Data Sciences International, Inc). Cortical screws were implanted bilaterally in somatosensory cortex S1 (-0.5 mm posterior from Bregma, $\pm$ 3.5 mm lateral) and a reference screw was implanted above the cerebellum (-0.5 mm posterior from Lambda, 0.5 mm lateral). The telemetry transponder was placed in the subcutaneous cavity above the shoulder.

Seizure susceptibility assay in mice implanted with multi-site ECoG electrodes

Following the induction of thalamic astrogliosis (3 weeks, 4 months and 7 months), seizure susceptibility was determined by monitoring video and EcoG activity following i.p. administration of the pro-convulsant pentylenetetrazol (PTZ) (Tocris, #2687). At the beginning of each recording session, mice were briefly anesthetized with ~2% isoflurane prior to connecting the EcoG device to the headstage to minimize potential pain and/or strain to the implant site, and immediately returned to their home cage. For experiments reported in **Fig. 4.4D** and **Fig. S4.6B**, mice were

recorded for a 10-min period during which video and EcoG were monitored to ensure that mice regained mobility. Mice were then injected i.p. with PTZ and recorded with video and ECoG. Each PTZ recording trial lasted 45-90 min. PTZ assays and analysis were performed by investigators blinded to experimental group, and all groups within an experiment were subject to the same conditions.

PTZ is known to act on the thalamocortical circuit, even when administered systemically (Mirski and Ferrendelli, 1986). PTZ dose was optimized based on previously reported concentration ranges and pilot recordings for each cohort (in case there were slight variations depending on strain, age, cohorts). The dose selected was the lowest dose necessary to induce epileptiform discharges in mice with thalamic astrogliosis. Doses used in this study (ranging from 5 to 15 mg/kg) are typically sub-threshold for the same strain of mice in other studies (Bolkvadze and Pitkänen, 2012). Seizure susceptibility was also determined following i.p. administration of the pro-convulsant agent Kainic Acid (KA; 10 mg/kg) (Tocris, #0222). KA induced generalized convulsive seizures. Each mouse was recorded for 60 minutes following KA injection. Recordings and analysis were performed in a blinded manner.

Quantification of *in vivo* electrocorticography

***Detection of epileptiform discharges*:** To quantify the number of epileptiform discharges, induced by PTZ, we used a custom MATLAB script, which enabled detection of synchronous discharges with amplitude three times baseline signal noise and required user input to reject or accept events. Quantification was performed for the somatosensory cortex ipsilateral to thalamic astrogliosis, and compared with a Mann-Whitney U-test. This detection method was validated against manual quantification of epileptiform discharges from the raw ECoG and simultaneously acquired video

recordings of mice. A subset of mice presented in **Fig. 4.4D** underwent the PTZ seizure assay again at 4 and/or 7 months to determine the chronic effects of astrogliosis (presented in **Fig. S4.6**).

Kainic acid seizure detection: Seizures on EEG traces were identified based on high frequency, synchronous discharges with amplitude three times baseline signal noise, using Spike2 software. Detection was cross-validated with behavioral signs of seizures from simultaneously acquired video recordings of mice.

ECoG spectral analysis: For chronic, continuous ECoG recordings, spectral analysis was performed in MATLAB. Absolute power of individual frequency bands was calculated using the bandpower function in MATLAB. Total band power was calculated between 1 to 75 Hz, in order to avoid edge effects of the wireless device bandwidth (0.5 to 80 Hz). For Weeks 1, 5, and 7, we obtained 168 1-hr bins; for Week 3, we obtained 152 1-hr bins. Total band power was calculated between 1 to 75 Hz, in order to avoid edge effects of the wireless device bandwidth (0.5 to 80 Hz). To analyze spectral features at week 7 (the most chronic time-point tested), we calculated the absolute power of individual frequency bands for 12-hour bins corresponding to the light and dark cycle. To investigate spectral features of the somatosensory cortex (S1) functionally connected to the site of thalamic astrogliosis, we performed paired t-tests of frequency bands obtained from ipsilateral and contralateral S1. All statistical comparisons are reported in **Table 4.9**.

Mouse cortical injury models and TBI seizure challenge assay

Stroke model: Cortical photothrombotic stroke was induced in the somatosensory cortex as previously described (Paz et al., 2010). Briefly, the light-sensitive dye Rose Bengal (40 mg/kg; Sigma-Aldrich #330000) dissolved in 0.9% saline was injected i.p. in isoflurane-anesthetized adult C57BL6 male mice. Immediately after RB injection, 2 minutes of 200 W illumination was

delivered to the right somatosensory cortex using a 3-mm diameter fiber optic cable positioned directly on top of the skull (centered at -1 mm posterior from Bregma, 4 mm lateral). The optical system is designed to have an emission spectrum containing the *in vivo* absorption range of RB (maximum absorbance at 562 nm). Sham mice received identical anesthesia and scalp incision and RB but no illumination.

Traumatic brain injury (TBI) model: Controlled cortical impact (CCI) was induced in the somatosensory cortex as previously described (Holden et al., 2021). Briefly, in isoflurane-anesthetized adult C57BL6 adult male mice, a 3-mm diameter craniotomy was performed over the right somatosensory cortex (centered at -1 mm posterior from Bregma, 3 mm lateral). A controlled cortical impact device equipped with a metal piston (Impact One Stereotaxic Impactor for CCI, Leica Microsytems) was used to perform TBI with the following parameters: 3 mm tip diameter, 18° angle, depth 0.8 mm from the dura, velocity 3 m/s, and dwell time 300 ms. Sham mice received identical anesthesia and scalp incision, but received a sham craniotomy of 3-mm diameter (in which the drill bit was used to trace a craniotomy on the skull without penetration), and the injury was not delivered. 3 days after sham or TBI procedures, a subset of mice underwent stereotaxic surgery to receive intra-thalamic injection AAV2/5-*GfaABC1D*-GAT3-HA-mCherry (600 nL), delivered unilaterally to the VB thalamus as described above.

TBI seizure challenge assay: To determine the seizure susceptibility of mice with TBI in a high throughput manner, we assessed behavioral seizures following PTZ challenge (45 mg/kg, i.p.). PTZ dose was selected based on prior studies for C57BL6 mice in our group and others (Bolkvadze and Pitkänen, 2012). Mice were video-recorded for 20 minutes after PTZ, 4 and 11 weeks after TBI induction. A modified Racine scale (Roberson et al., 2007) was used to score behavioral seizures off-line in a blinded manner. Stage 0 = normal behavior; 1 = immobility; 2 = generalized

spasm, tremble, or twitch; 3 = tail extension; 4 = forelimb clonus; 5 = generalized clonic activity; 6 = bouncing or running seizures; 7 = full tonic extension; 8 = death.

Logistic regression model of TBI mouse survival following PTZ challenge

To assess the impact of astrocytic GAT-3 enhancement on mortality/survival following PTZ challenge, we used a logistic regression model consisting of trauma and GAT-3 treatment as independent variables and survival as the dependent variable (GraphPad Prism). Goodness-of-fit assessed with area under the ROC curve and the likelihood ratio test.

$$\ln(odds) = \beta_0 + \beta_1 X_1 + \beta_2 X_2, \text{ where } odds = \frac{P(Y=1)}{P(Y=0)} \text{ and Y = survival}$$

The impact of TBI and of GAT-3 on survival is represented by the β_1 and β_2 parameter estimate, respectively, of our model. The exponentiation of each parameter estimate yields an odds ratio, which represents the "multiplicative effect" that a given parameter has on survival and is reported in **Fig. S4.10**.

Behavioral Assays

Behavioral tasks took place during the light cycle between 7:00 AM and 7:00 PM. Mice were transferred to the behavioral testing room at least 30 min prior to testing to acclimate to the environment and lighting, unless specified otherwise. All tasks were performed and analyzed by experimenters blinded to condition.

Open Field Activity Test: Open field activity is assessed using the Flex-Field/Open Field Photobeam Activity System (San Diego Instruments), which consists of a clear acrylic chamber (41 x 41 x 30 cm) and two sets of photobeam arrays that automatically detect horizontal and vertical movements. Mice are placed in the center of the chamber at the beginning of the test.

Analysis: Ambulatory and fine movements are automatically recorded using Photobeam Activity System software (San Diego Instruments). The open field arena is divided into an outer periphery and center. Proportion of total movements in the periphery relative to the center is used to determine degree of baseline anxiety.

Elevated Plus Maze: The elevated plus maze (EPM) is elevated 30.5" above the ground, and consists of two open arms (15" x 2", length x width) and two closed arms (15" x 2" with 6.5" height walls) (Hamilton-Kinder). During the task, mice are placed at the center of the maze and allowed to explore for 10 minutes. Analysis: Total distance traveled and number of entries into closed arms are calculated based on infrared photobeam breaks, automatically detected using MotorMonitor software (Kinder Scientific). Total distance is used as a measure of general activity. Percent time spent in open arms is used as a measure of baseline anxiety.

Olfactory Habituation: In addition to transferring all mice to the testing room 1 hour prior to testing, each mouse is individually placed into a cage without bedding for 30 min prior to testing. Mice are exposed to three different odors in this order: water, vanilla, and an unfamiliar social odor. The task consists of three trials (2 min each) for each of the three odors. With an inter-odor interval of 1 min. For non-social odors, cotton tip applicators were dipped in each odor solution for 2 sec, immediately before scent presentation to avoid evaporation. Vanilla was diluted 1:100 in water. For the unfamiliar social odor, the cotton tip was used to swipe the bottom of a cage of an unfamiliar mouse of the same strain and sex several times. For each trial, the experimenter secures the cotton tip applicator to the flat wire cage top so that the tip is hanging 2 inches off the cage floor. The experimenter then moves 2 meters away from the cage to score. A new cotton tip was used for each odor. All trials are simultaneously videotaped. Analysis: The experimenter scores the odor exploration in real-time. Bouts of sniffing, as well as cumulative time spent sniffing

the cotton tip, is recorded for each 2-minute trial. Sniffing is scored when the mouse is oriented towards the cotton tip with its snout 2 cm or closer to the tip. Chewing on the cotton tip is counted as sniffing, whereas chewing on the wooden handle of the applicator or climbing the applicator is not counted as sniffing.

Hot Plate Test: During the test, mice are placed into a clear, open-ended cylinder (4" diameter) which is placed on top of a black anodized aluminum hot plate (Hot Plate Analgesia Meter, IITC Life Science). The surface of the hot plate is heated and maintained at 52°C, and cleaned with 70% EtOH between each subject. Once the mouse is placed on the hot plate, the latency to respond with either a hind paw lick, hind paw flick, or jump is measured by an experimenter. To prevent injury, the maximum latency is 30 seconds. Once the mouse responds or reaches the 30 second limit, the mouse is removed from the hot plate and returned to its home cage. Analysis: Once the mouse is placed on the hot plate, the latency to respond with either a hind paw lick, hind paw flick, or jump is measured by an experimenter.

Contextual Fear Conditioning: Mice are brought into the testing room immediately before the trial begins. The contextual fear conditioning task consists of three phases: Training, Context Test, and Generalization Test. All phases take place in a sound-isolated fear conditioning chamber (Med Associates), cleaned with 70% EtOh between trials. During the Training phase (13 min total), mice are placed in the apparatus in which the light setting is 3, fan is on, trays are sprayed with 70% Windex, and metal floor grid is exposed. Following a 5-min baseline period, mice are presented with four 2-second 0.45 mA foot shocks separated by 2-min intervals. 24 hours later, the Context Test (10 min total) takes place. Mice are placed in the same apparatus (same context) for 10 minutes, with no foot shocks delivered. The Generalization Test (10 min total) takes place 24 hours after the Context Test. The context is altered from the Training phase in the following manner:

light setting is 1, fan is off, trays are sprayed with 10% Simple Green, and a solid plastic floor insert is used. Mice are placed in this apparatus for 10 minutes, with no foot shocks delivered. Analysis: Freezing during each trial is monitored by Video Freeze software (Med Associates, Inc). ***Grooming:*** Mice were individually placed in a transparent cage for 10 minutes while being videotaped. Duration of spontaneous whisker grooming was manually quantified off-line using video footage.

10x Visium spatial transcriptomics of mouse brain after traumatic brain injury and stroke

The 10x Visium Spatial Transcriptomics pipeline was performed on three total hemisections obtained from mice 6 weeks after TBI, stroke, or a sham procedure. The brains were harvested in OCT and flash frozen on dry ice. The hemispheres were sectioned coronally to 10 μm on a cryostat and mounted on the Visium Spatial Gene Expression slide. All sections were analyzed for RNA integrity number (>8) measured by a Bioanalyzer. To visualize the section morphology and cell bodies for later spatial alignment of sequencing data, sections were methanol fixed at –20°C for 30 min and stained for hematoxylin and eosin (H&E). The sections were imaged using bright-field microscopy, then enzymatically permeabilized for 12 min, poly-A mRNA captured on each of the spots, and spatial barcodes and unique molecular identifiers (UMIs) were added to the reads. The dual-index Illumina paired-end libraries were sequenced on NovaSeq 6000, and the RNAseq reads were aligned to the mouse reference genome mm10-2020-A and images detected using SpaceRanger pipeline (v.1.3.0).

Data were visualized using 10x Loupe Browser (v.5.1.0). Raw per-spot gene expression UMIs were exported from the SpaceRanger pipeline (v.1.3.0) and aligned using barcodes (**Fig. 4.6, Fig. S4.8, Fig. S4.9,** and **Table 4.10**). To separate out spatial regions that showed unique and

most homogeneous gene expression patterns, we performed unbiased K-means clustering using 10 unique clusters for each section (**Fig. S4.8**). Note that in the thalamus of the TBI section, two regions were separated out as unique clusters 7 and 4, which corresponded to the regions that showed high and low *Gfap* transcripts. After performing the differential expression of genes (DEGs) analysis of cluster 7 (**Fig. S4.8**) compared to all other clusters, we determined that this region is enriched in inflammatory markers such as *Gfap, Serpina3n, C1qa, Tyrobp*, and others (see **Fig. S4.8E** for top 20 DEGs). We used this unbiased separation of thalamic clusters as a rationale for choosing two thalamic regions of interest (*Gfap*-High and *Gfap*-Low) (**Fig. 4.6**). We chose two cortical regions of interest which were proximal and distal to the injury site (**Fig. S4.9**). For investigations of individual genes such as *Gfap* and *Slc6a11*, we performed Kolmogorov-Smirnov tests and adjusted α=0.025 to correct for multiple (two) comparisons made within each sample: *Gfap*-High vs. *Gfap*-Low thalamus, and *Gfap*-High vs. *Gfap*-Low cortex. To assess the relationship between *Gfap* and *Slc6a11*, a simple linear regression was performed separately for cortical and thalamic data. Statistical analyses were performed within-section between *Gfap*-High and *Gfap*-Low regions in the thalamus, and between proximal and distal regions in the cortex.

In vivo electrocorticography (ECoG) data acquisition

To control for circadian rhythms, animals were housed using a regular light/dark cycle, and recordings performed between 7:00 AM and 7:00 PM. Prior to acquisition of multi-site EcoG recordings (**Figs. 4.4, 4.5, S4.6**), mice were allowed to recover for at least one week. EcoG signals were recorded using RZ5 via Synapse software (Tucker Davis Technologies) and sampled at 1221 Hz. Animals were continuously monitored during recordings using a video camera that was synchronized to the signal acquisition via RZ5 (Ritter-Makinson et al., 2019).

Chronic, continuous EcoG recordings (**Fig. 4.6** and **Table 4.9**) were acquired using wireless telemetry devices (PhysioTel HD-X02 implants, Data Sciences International) and sampled at 500 Hz via Ponemah software (DSI). 24/7 recordings were performed for one-week periods (168 hours) at the following timepoints: 1, 3, 5 and 7 weeks after thalamic astrogliosis (**Fig. 4.6C**), and 7 weeks after thalamic astrogliosis with GAT-3 enhancement (**Fig. 4.6D**). Acquisition started immediately following implantation, as the wireless devices allow mice to remain in their home cages.

Statistical Analysis

All numerical values are given as means and error bars are standard error of the mean (SEM) unless stated otherwise. For comparison between two groups, the non-parametric Mann-Whitney U test was performed. For comparisons between multiple groups, a one- or two-way analysis of variance (ANOVA; ordinary or repeated measures) was performed, in addition to post-hoc comparisons with corrections for multiple comparisons (detailed in figure legends). When parametric tests were used, results of the Shapiro-Wilk normality test are provided. The threshold for statistical significance was set to $\alpha=0.05$, unless specified otherwise. Each ***n*** represents an independent biological sample, unless specified otherwise in figure legends. Data analysis was performed with MATLAB, GraphPad Prism 7, OriginPro, SigmaPlot, and SPSS.

Figures

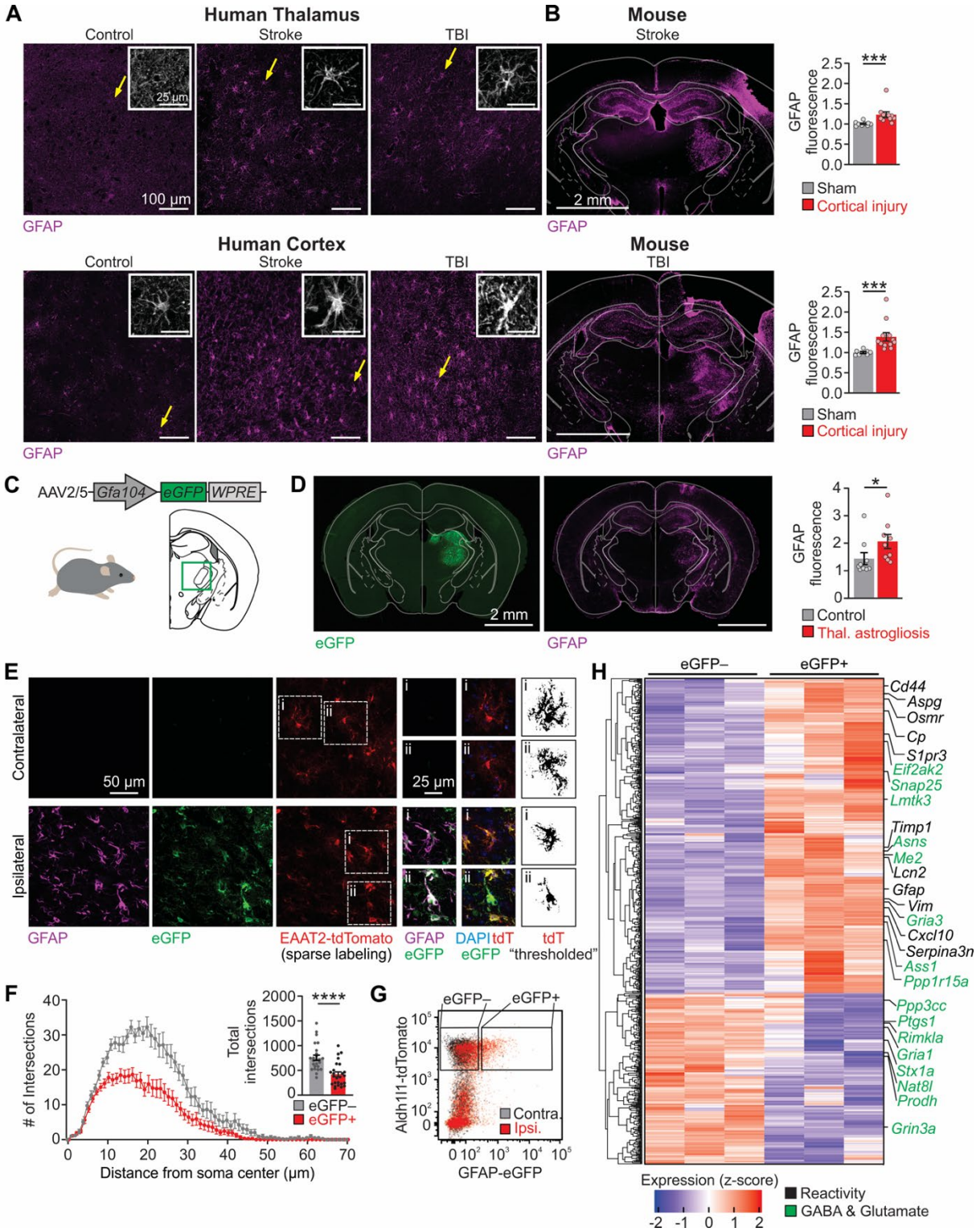
A
Human Thalamus
Control
Stroke
TBI
25 µm
100 µm
GFAP
B
Mouse
Stroke
2 mm
GFAP
GFAP fluorescence
***
Sham
Cortical injury
Human Cortex
Control
Stroke
TBI
GFAP
Mouse
TBI
GFAP
GFAP fluorescence
***
Sham
Cortical injury
C
AAV2/5-Gfa104-eGFP-WPRE
D
2 mm
eGFP
GFAP
GFAP fluorescence
*
Control
Thal. astrogliosis
E
Contralateral
Ipsilateral
50 µm
25 µm
GFAP
eGFP
EAAT2-tdTomato
(sparse labeling)
GFAP
eGFP
DAPI
eGFP
tdT
tdT
"thresholded"
F
# of Intersections
Distance from soma center (µm)
Total intersections
****
eGFP–
eGFP+
G
eGFP–
eGFP+
Aldh1l1-tdTomato
GFAP-eGFP
Contra.
Ipsi.
H
eGFP–
eGFP+
Cd44
Aspg
Osmr
Cp
S1pr3
Eif2ak2
Snap25
Lmtk3
Timp1
Asns
Me2
Lcn2
Gfap
Vim
Gria3
Cxcl10
Serpina3n
Ass1
Ppp1r15a
Ppp3cc
Ptgs1
Rimkla
Gria1
Stx1a
Nat8l
Prodh
Grin3a
Expression (z-score)
Reactivity
GABA & Glutamate

Figure 4.1. Thalamic astrogliosis is a consistent feature of cortical lesions, recapitulated by viral-mediated activation.

(**A**) GFAP immunofluorescence in post-mortem thalamus and peri-lesional cortex from human subjects with history of ischemic stroke or TBI, and age-matched controls, representative of 3 control subjects, 3 subjects with stroke, and 4 subjects with TBI. Insets: magnification of GFAP+ cells with astrocyte-like morphology (putative astrocytes, yellow arrow). (**B**) GFAP immunofluorescence in mouse models of photothrombotic stroke and controlled cortical impact. Right: thalamic GFAP fluorescence ratios between ipsilateral and contralateral regions. **Stroke**: Mann-Whitney U test, ***P=0.0002. Sham: n=9 mice; Stroke: n=10 mice. **TBI**: Mann-Whitney U-test, ***P=0.0002. Sham: n=7 mice; TBI: n=12 mice. (**C**) Viral induction of unilateral thalamic astrogliosis (brain schematic adapted from (Franklin and Paxinos, 2007)). (**D**) Immunofluorescence three weeks after astrogliosis induction. GFAP immunofluorescence quantified as in (B). Mann-Whitney U test, *P=0.019. n=9 mice per group. Quantification in other brain regions shown in Fig. S4.1. (**E**) Representative images of GFAP, eGFP, tdTomato, and DAPI fluorescence in thalamic astrocytes contralateral and ipsilateral to viral transduction of astrocytes in EAAT2-tdTomato reporter mice. (**F**) Sholl analysis of thalamic astrocytes. Inset: Total number of intersections. Mann-Whitney U test, ****P<0.0001. n=25 astrocytes per condition. (**G**) Flow plot of thalamic astrocytes, ipsilateral and contralateral to site of viral transduction in Aldh1l1-tdTomato reporter mice. Gates indicate sorting strategy detailed in Fig. S4.2. (**H**) Differentially expressed genes in ipsilateral eGFP+ versus contralateral eGFP– thalamic astrocytes ($P_{adjusted}$<0.05), highlighting genes related to astrocyte reactivity (Liddelow et al., 2017) and astrocyte modulation of glutamate and GABA (Schousboe et al., 2013; Yu et al., 2018) on the right. Heat map including ipsilateral eGFP– in Fig. S4.3.

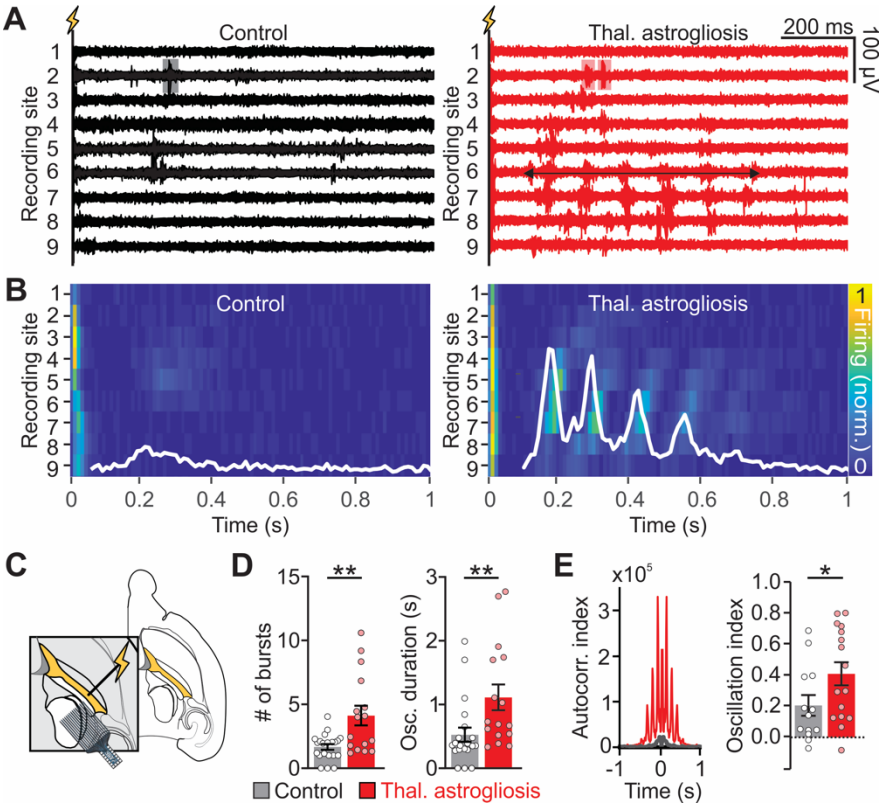

Figure 4.2. Viral-mediated thalamic astrogliosis enhances intra-thalamic circuit rhythmogenesis.

(**A**) Representative intra-thalamic multi-unit activity evoked by stimulation of the internal capsule (lightning bolt) in thalamic slices, as schematized in (C). Only nine out of 16 channels are shown for clarity. Shaded boxes highlight bursts (clusters of ≥3 spikes), horizontal arrow indicates a sustained circuit oscillation (clusters of ≥2 bursts). (**B**) Peri-stimulus time histograms of recordings shown in (A). Color represents multi-unit activity normalized to maximal firing in each slice. White traces represent the spatial summation of firing activity across all recording sites and all trials within each slice during the delayed response (excluding the first 150 ms of direct response). (**C**) Schematic of multi-unit activity recordings in thalamic slices following electrical stimulation of the internal capsule (yellow). Probe schematic adapted from NeuroNexus, brain schematic adapted from (Franklin and Paxinos, 2007). (**D**) Quantification of bursts and circuit oscillations, as shown in (A). Each dot represents the site with maximal multi-unit activity in each slice from n=13 Control and n=16 Thalamic Astrogliosis mice (1 slice/mouse; 20 evoked responses averaged per slice). Mann-Whitney U test; $^{**}P$=0.007 (bursts) and $^{**}P$=0.003 (oscillations). (**E**) Left: auto-correlation analyses of multi-unit activity in the delayed response from (B). Multi-unit activity is summed across all recording sites and all trials within a slice. Right: oscillation index calculated for the first peak of the auto-correlated signal. Mann-Whitney U test, $^{*}P$<0.05. n=13 Control, n=16 Thalamic Astrogliosis mice.

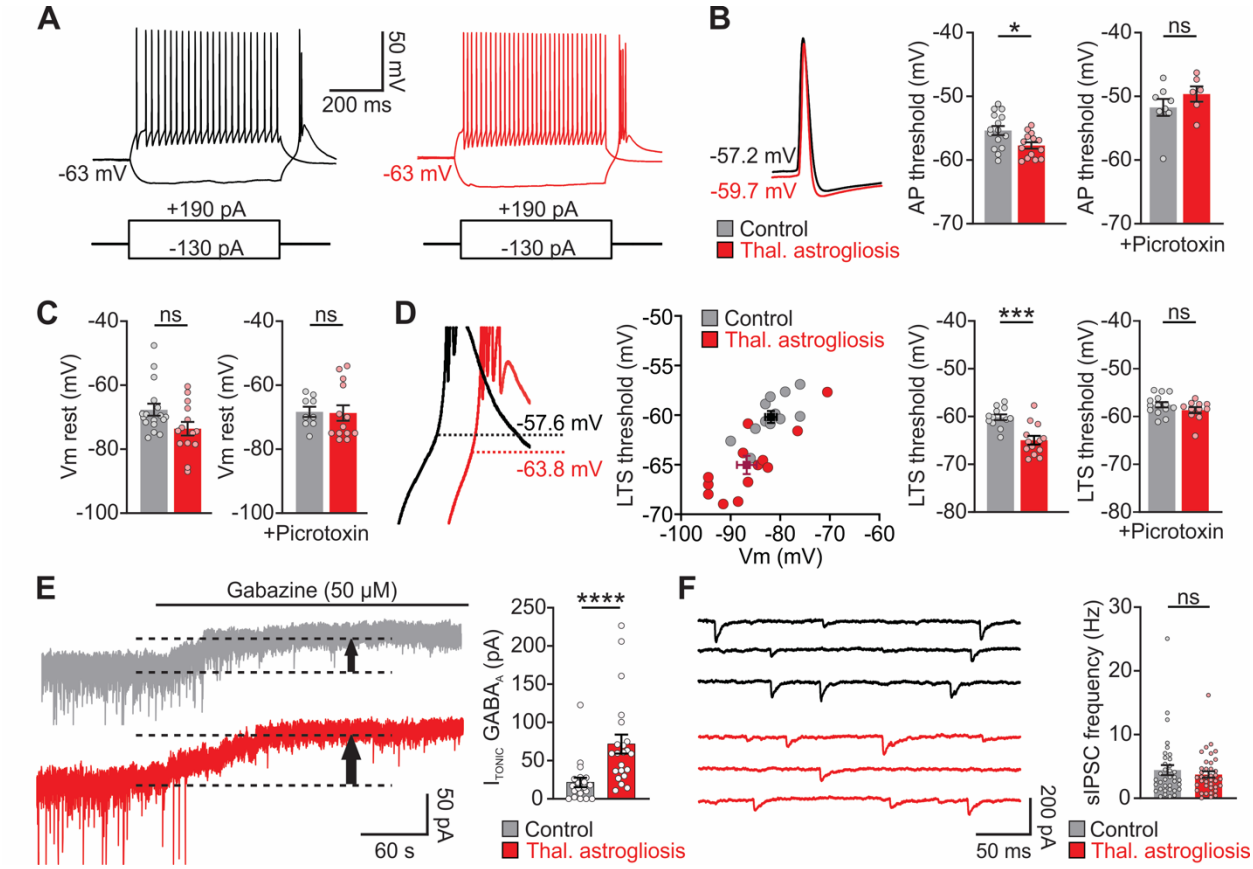

Figure 4.3. Viral-mediated thalamic astrogliosis boosts cellular excitability via extrasynaptic $GABA_AR$-mediated tonic inhibition.

(**A**) Representative whole-cell recordings showing response to hyperpolarizing and depolarizing intracellular current injections. (**B**) Left: Overlay of action potentials (APs) from two representative neurons. Right: AP generation threshold in the presence or absence of Picrotoxin (50 μM). No picrotoxin condition: Mann-Whitney U test, **P*=0.02; Control: n=17 cells (from 8 slices, 4 mice); Thalamic Astrogliosis: n=14 cells (from 7 slices, 5 mice). Picrotoxin condition: *P*=0.28; Control: n=9 cells (from 5 slices, 3 mice). Thalamic Astrogliosis: n=13 cells (from 9 slices, 5 mice). ns: not significant. (**C**) Resting membrane potentials of thalamocortical neurons. No picrotoxin condition: Mann-Whitney U test, *P*=0.053. Picrotoxin condition: Mann-Whitney U-test, *P*=0.52. See (A) for sample size. (**D**) Left: Overlay of the hyperpolarization-induced rebound burst from two representative neurons. Center: Threshold for the T-type Ca^{2+}-mediated low threshold spike (LTS), plotted as a function of the pre-pulse hyperpolarized membrane potential following current injection. Black and burgundy crosses indicate mean±SEM for membrane potential and LTS threshold. Right: LTS threshold. No picrotoxin condition: Mann-Whitney U test, ****P*=0.0005. Control: n=12 cells (from 7 slices, 4 mice). Thalamic Astrogliosis: n=12 cells (from 7 slices, 5 mice). Picrotoxin condition: *P*=0.36. Control: n=13 cells (from 9 slices, 4 mice). Thalamic Astrogliosis: n=11 cells (7 slices, 5 mice). (**E**) Representative whole-cell voltage-clamp recordings. Gabazine (GBZ; 50 μM) was bath-applied to isolate the tonic current, measured by the shift in baseline holding current (black arrow). Mann-Whitney U test,

****P<0.0001. Control: n=20 cells (from 20 slices, 10 mice); Thalamic Astrogliosis: n=22 cells (from 22 slices, 11 mice). (**F**) Representative phasic $GABA_A$ currents. Mann-Whitney U test, P=0.88. Control: n=36 cells (from 36 slices, 14 mice); Thalamic Astrogliosis: n=40 cells (from 40 slices, 16 mice).

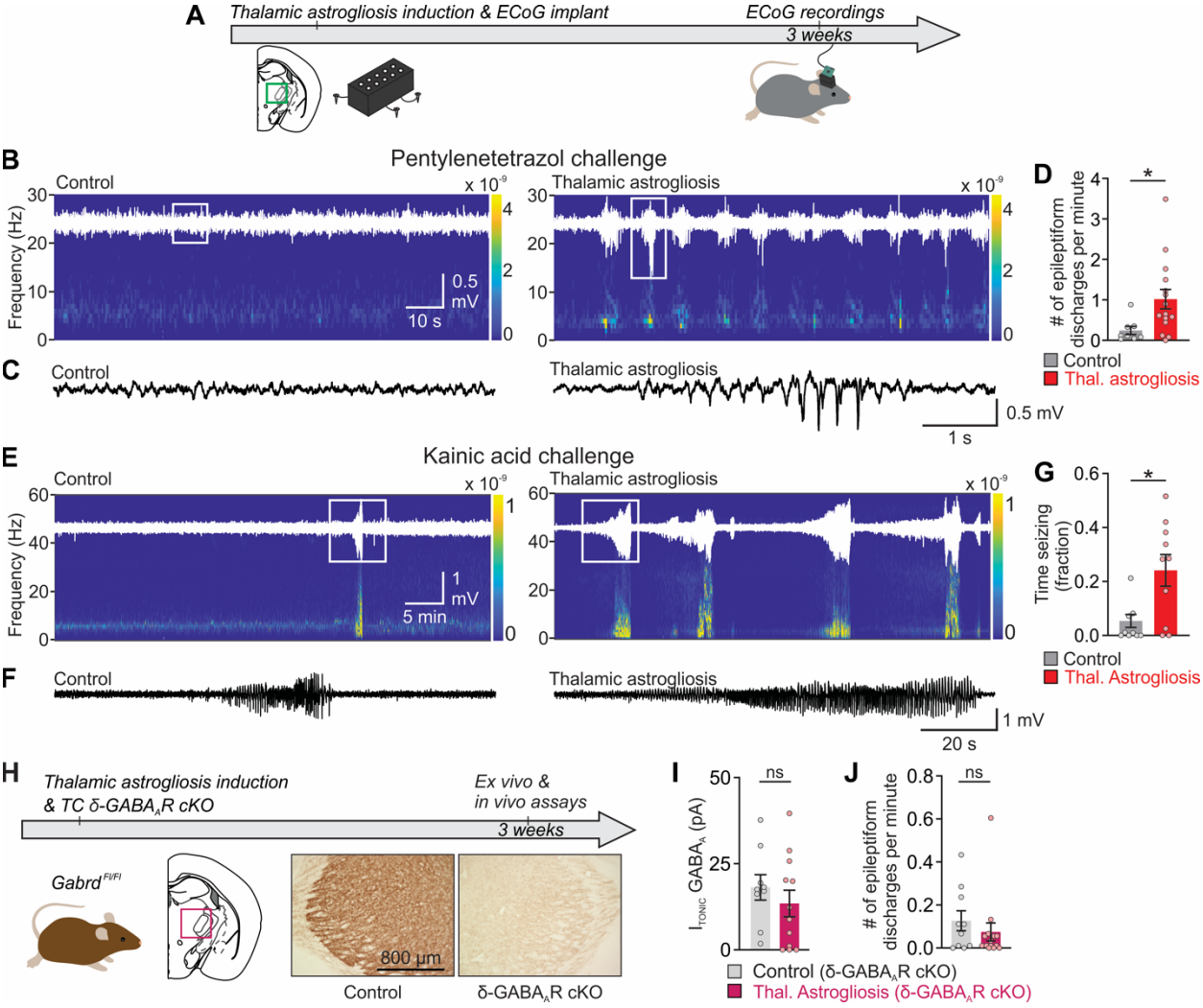

Figure 4.4. Conditional deletion of the extrasynaptic GABA$_A$R δ-subunit (δ-GABA$_A$R-cKO) in thalamocortical neurons prevents thalamic astrogliosis-induced seizure risk.

(**A**) Experimental timeline of ECoG recordings. (**B, E**) Representative ECoG recordings from ipsilateral primary somatosensory cortex (S1), following i.p. injection of pentylenetetrazol (PTZ, 5 mg/kg; B) or of kainic acid (10 mg/kg; E), with raw ECoG traces (white) overlaid onto corresponding spectrograms. (**C, F**) Enlargement of ECoG traces in boxed areas in (B) and (E). (**D**) Frequency of epileptiform discharges in ipsilateral S1 ECoG in the PTZ challenge experiment. Mann Whitney U test: **P*=0.013. Control, n=8 mice; Thalamic Astrogliosis, n=15 mice. (**G**) Time spent seizing in response to Kainic Acid-challenge. Mann-Whitney U test, **P*=0.025. Control: n=10 mice; Thalamic Astrogliosis: n=10 mice. (**H**) Unilateral, conditional deletion of the extrasynaptic GABA$_A$R δ-subunit (δ-GABA$_A$R-cKO) in thalamocortical neurons via viral Cre-mediated (AAV2/5-CaMKIIα-mCherry-Cre) recombination in *Gabrd*$^{Fl/Fl}$ mice. Timeline (top) and DAB labeling in thalamic sections (bottom). (**I**) Quantification of I$_{TONIC}$ in thalamocortical neurons in thalamic *ex vivo* slices from *Gabrd*$^{Fl/Fl}$ mice. Mann-Whitney U test, *P*=0.42. ns: not significant. Control δ-GABA$_A$R-cKO (intra-thalamic transduction of thalamocortical neurons with AAV2/5-CaMKIIα-mCherry-Cre in mice without astrogliosis): n=9 cells (from 9 slices, 5 mice); Thalamic

Astrogliosis δ-GABA$_A$R-cKO (intra-thalamic transduction of thalamocortical neurons with AAV2/5-CaMKIIα-mCherry-Cre in mice with astrogliosis): n=12 cells (from 12 slices, 5 mice). (**J**) Epileptiform discharges from ipsilateral S1 in response to PTZ challenge (5mg/kg) in *Gabrd*$^{Fl/Fl}$ mice with and without thalamic astrogliosis. Mann-Whitney U Test, P=0.37. Control δ-GABA$_A$R-cKO: n=10 mice; Thalamic astrogliosis δ-cKO: n=14 mice.

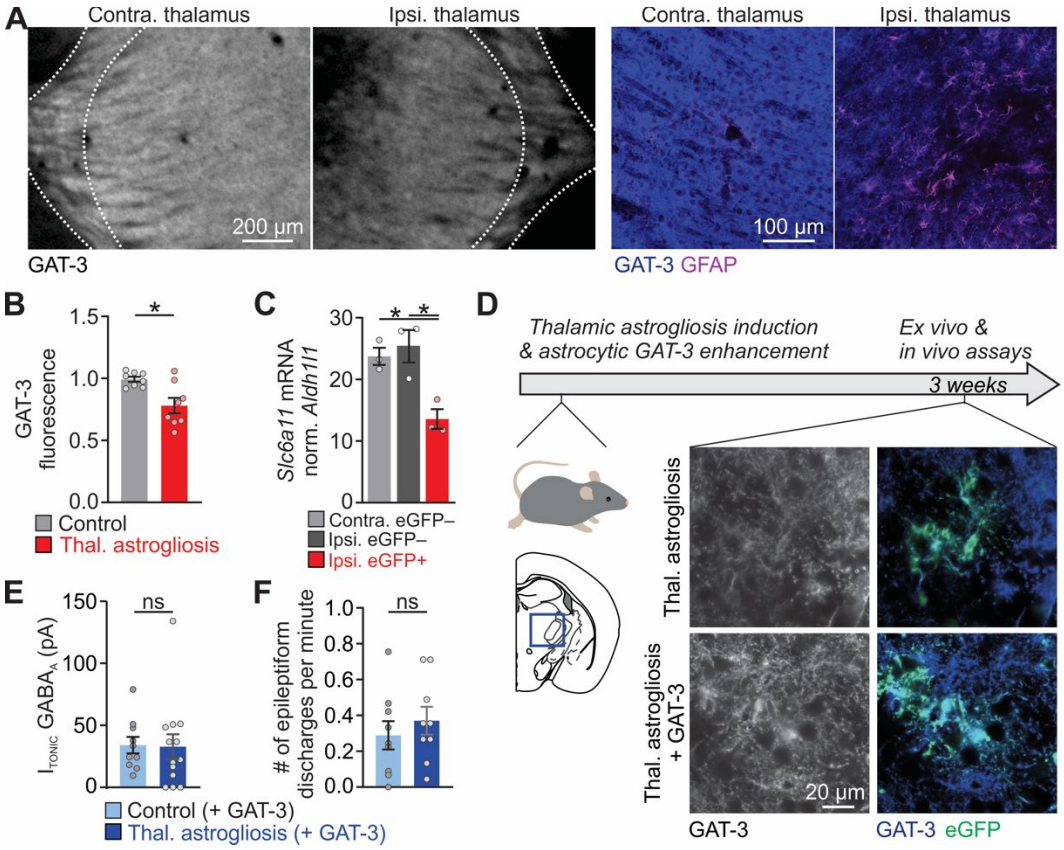

Figure 4.5. Enhancing GAT-3 in thalamic astrocytes prevents astrogliosis-induced tonic inhibition in neurons and seizure risk.

(**A**) GAT-3 immunofluorescence in mouse coronal brain sections (left) and confocal images of GAT-3 and GFAP co-localization in VB thalamus (right), three weeks after unilateral thalamic astrogliosis induction. **(B)** GAT-3 immunofluorescence ratio between regions ipsilateral-and contralateral to thalamic astrogliosis, three weeks following induction. Mann-Whitney U test, **P*=0.028; n=8 mice per group. **(C)** Quantitative PCR analysis of *Slc6a11* expression (encoding GAT-3), normalized to *Aldh1l1* expression in astrocytes FACS-isolated from contralateral and ipsilateral VB thalamus of Aldh1l1-tdTomato mice, three weeks following thalamic astrogliosis induction. Sorting strategy detailed in Fig. S4.2. One-way ANOVA, **P*=0.01; Shapiro-Wilk normality test, P>0.05, Tukey's post-hoc tests, **P*=0.012 and **P*=0.024; n=3 mice. (**D**) Increased GAT-3 expression in thalamic astrocytes was achieved by transducing thalamic astrocytes with AAV2/5-GfaABC1D-GAT3-mCherry (Yu et al., 2018) in adult mice with and without thalamic astrogliosis. Representative confocal images show GAT-3 expression in eGFP+ astrocytes in mice with thalamic astrogliosis, with and without enhanced GAT-3 enhancement. (**E**) Quantification of I_{TONIC} in thalamocortical neurons from thalamic *ex vivo* slices, three weeks following GAT-3 enhancement in mice with and without thalamic astrogliosis. Mann-Whitney U test, *P*=0.60. Control + GAT-3: n=10 cells (from 10 slices, 7 mice); Thalamic Astrogliosis + GAT-3: n=13 cells (from 13 slices, 9 mice). (**F**) Epileptiform discharges in response to PTZ (15 mg/kg). Mann-Whitney U Test, *P*=0.42. n=9 mice per group.

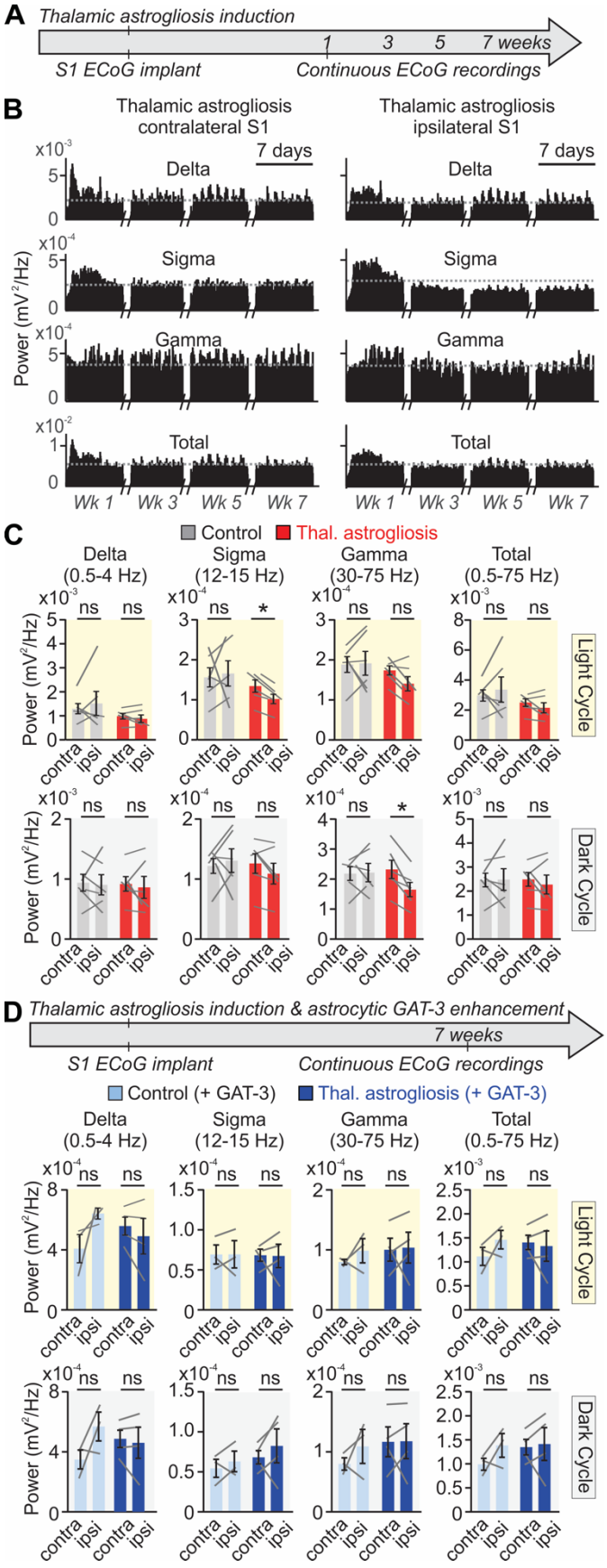
A
Thalamic astrogliosis induction
1
3
5
7 weeks
S1 ECoG implant
Continuous ECoG recordings
B
Thalamic astrogliosis contralateral S1
Thalamic astrogliosis ipsilateral S1
7 days
Delta
Sigma
Gamma
Total
Power (mV²/Hz)
Wk 1
Wk 3
Wk 5
Wk 7
C
Control
Thal. astrogliosis
Delta (0.5-4 Hz)
Sigma (12-15 Hz)
Gamma (30-75 Hz)
Total (0.5-75 Hz)
ns
*
contra
ipsi
Light Cycle
Dark Cycle
D
Thalamic astrogliosis induction & astrocytic GAT-3 enhancement
7 weeks
S1 ECoG implant
Continuous ECoG recordings
Control (+ GAT-3)
Thal. astrogliosis (+ GAT-3)

Figure 4.6. Enhancing GAT-3 in thalamic astrocytes prevents astrogliosis-induced reduction in cortical sigma and gamma frequency power.

(**A**) Schematic of experimental timeline. Chronic wireless ECoG from S1 was obtained bilaterally in freely-behaving mice in their home cage for continuous one-week periods, up to seven weeks following induction of thalamic astrogliosis. (**B**) Representative plots of delta (1-4 Hz), sigma (12-15 Hz), gamma (30-75 Hz), and total band power (1-75 Hz), across weeks 1, 3, 5, and 7, obtained from a mouse with thalamic astrogliosis. Spectral analysis was performed on S1 ECoG in 1-hour bins. Horizontal lines indicate the average power of the frequency band during week one. (**C**) Average ECoG power for each mouse, seven weeks after thalamic astrogliosis induction, during the light (top) and dark cycle (bottom). Control: n=6 mice; Thalamic Astrogliosis: n=6 mice. **(D)** Average ECoG power for each mouse, seven weeks after thalamic astrogliosis induction and astrocytic GAT-3 enhancement. Control + GAT-3: n=3 mice; Thalamic Astrogliosis + GAT-3: n=4 mice. See Table 4.9 for comparison of all frequency bands. Wilcoxon matched-pairs signed rank tests, $*P<0.05$.

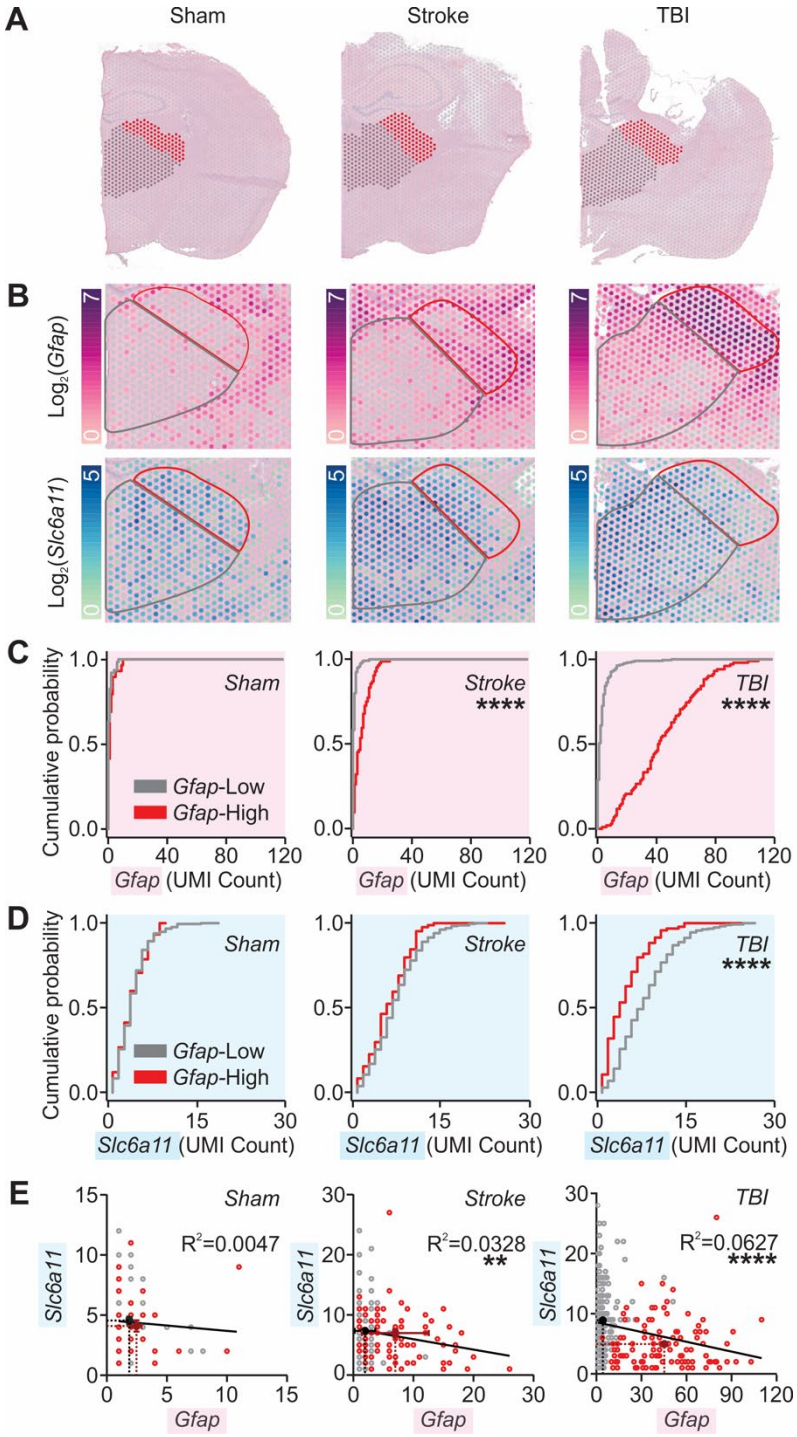

Figure 4.7. Cortical injury-induced thalamic Gfap is negatively correlated with thalamic Slc6a11 expression.

(A) Hemi-brain sections from mice after sham, stroke, and TBI procedures six weeks after surgery overlaid with thalamic regions of interest (grey and red) analyzed with 10x Visium spatial transcriptomics and magnified in (B). **(B)** Thalamic expression of *Gfap* and *Slc6a11* transcripts. Color map indicates log2 of the detected counts of the gene's unique molecular identifier (UMI).

Red and black outlines correspond to regions of interest shown in (A) and to regions with high and low *Gfap* expression in cortical injury, as detailed in (C). **(C, D)** Cumulative probability distribution of *Gfap* (C) or *Slc6a11* (D) expression per spot in regions indicated in (A-B). Kolmogorov-Smirnov test, ****P<0.0001. All spots containing non-zero UMI counts were included. Number of spots from low- and high-*Gfap* regions, respectively, in (C): sham (n=63 & 29); stroke (n=120 & 84); TBI (n=218 & 102); in (D): sham (n=216 & 76); stroke (n=237 & 85); TBI (n=277 & 95). Adjusted $\alpha=0.025$ *for multiple comparisons.* **(E)** Relationship between *Gfap* and *Slc6a11* expression. Circles represent UMI counts per spot in low- (grey) and high-*Gfap* (red) areas; black and burgundy crosses, and corresponding dotted lines, mark mean±SEM for low- and high-*Gfap* areas respectively. Black lines plot the best-fit slopes and intercepts from a simple linear regression. **P=0.0095, ****P<0.0001. Number of spots: sham (n=93); stroke (n=204); TBI (n=322). Similar analysis for cortical regions distal and proximal to injury is described in Fig. S4.9.

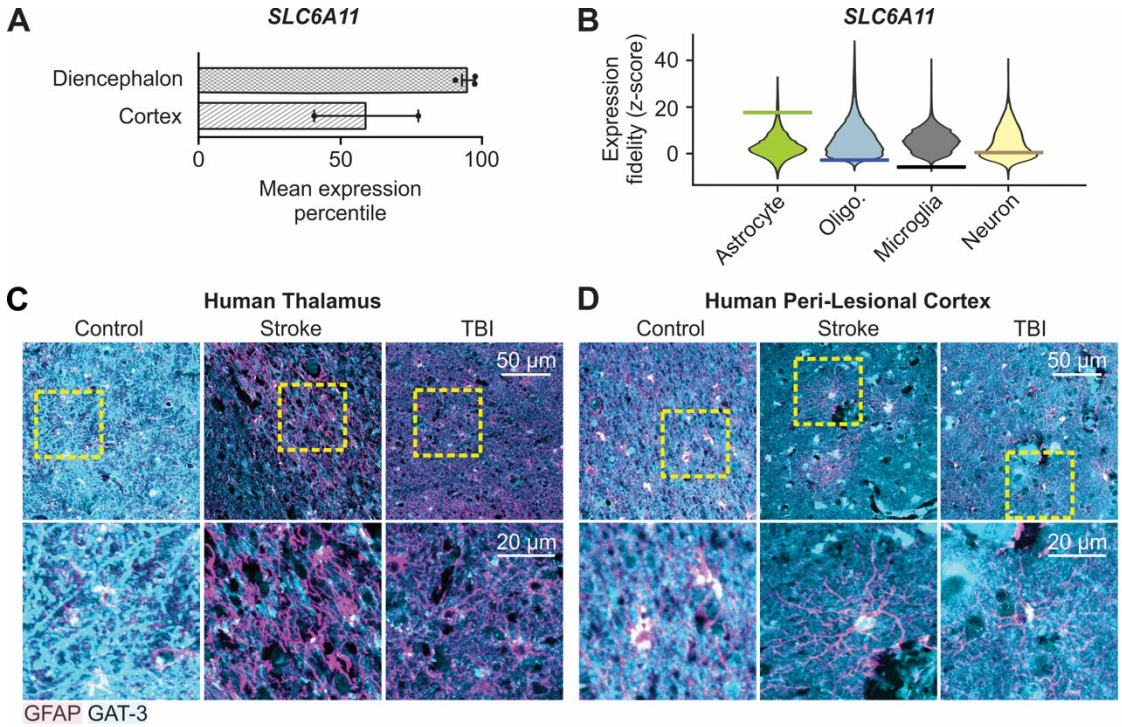

Figure 4.8. Decreased GAT-3 immunoreactivity in human post-mortem thalamic tissue after cortical injuries.

(**A**) Mean expression percentile of *SLC6A11* gene relative to all genes in neurotypical adult human diencephalon and parietal cortex. Data obtained from (Kelley et al., 2018) from 535 human samples. (**B**) Expression fidelity of *SLC6A11* from cell-type specific transcriptomic profiling in the adult human diencephalon compared to transcriptional signatures of major brain cell types, relative to all human genes detected in the database from (Kelley et al., 2018). Higher fidelity indicates higher correlation of *SLC6A11* to cell type. Horizontal bar indicates Z-score for *SLC6A11* relative to that cell type (17.6, -2.8, -5.8, and 0.4 for astrocytes, oliogodendrocytes, microglia, and neurons respectively), violin plot indicates Z-score distribution for all genes detected in that cell type. (**C, D**) GFAP and GAT-3 immunofluorescence in post-mortem thalamic tissue (C) and peri-lesional cortex (D) from human subjects with a history of ischemic stroke or TBI, and age-matched control subjects. Images are representative of 3 control subjects, 3 subjects with stroke, and 4 subjects with TBI. Yellow boxes: regions magnified below. Summary of all data shown in Fig. S4.11 and Table 4.2.

Supplemental Figures

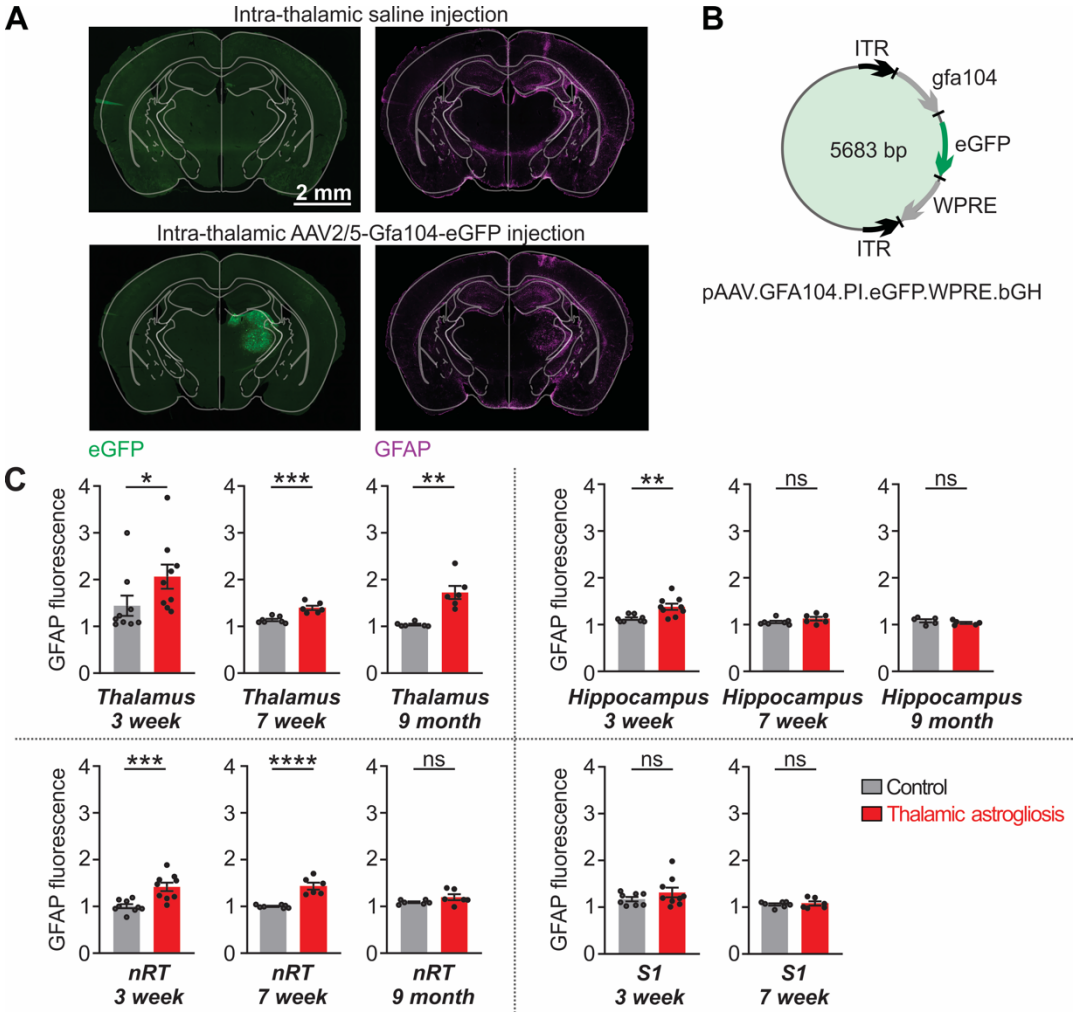

Supplemental Figure 4.1. Persistent increase of GFAP protein in thalamus following viral-mediated astrogliosis.

(A) Immunohistochemical labeling of enhanced green fluorescent protein (eGFP) and glial fibrillary acidic protein (GFAP) following unilateral injection of either saline (top) or AAV2/5-Gfa104-eGFP (bottom) into the ventrobasal (VB) thalamus. Note that the representative images of the AAV2/5-Gfa104-eGFP injection are the same images presented in Fig. 1D, and are included here for visual comparison. **(B)** Schematic of the pAAV.GFA104.PI.eGFP.WPRE.bGH plasmid used to produce the AAV2/5-Gfa104-eGFP construct. Adapted from (Ortinski et al., 2010), Fig. 1H. Four solid black lines indicate multiple cloning sites. Sequence map is available through Addgene (Plasmid #100896). Note that when the *Gfa104* promoter is used with the AAV2/5 pseudotype, the viral construct leads to >99% astrocyte-specific expression (Ortinski et al., 2010). **(C)** GFAP fluorescence in thalamus (including ventroposterior medial, ventroposterior lateral, ventrolateral, posterior medial, dorsal lateral geniculate, and lateral posterior nuclei), reticular thalamic nucleus (nRT), hippocampus, and primary somatosensory cortex (S1). Fluorescence ratio

between regions ipsilateral and contralateral to injection site, obtained three weeks, seven weeks, and nine months after induction of thalamic astrogliosis. Data from thalamus (three week timepoint) are the same data presented in Fig. 1D, and included here for visual comparison. **3 weeks:** n=8-9 mice per group (data averaged from 3 sections/mouse). Mann-Whitney U-test for thalamus (*P=0.018), nRT (**P=0.001), hippocampus (**P=0.0016), and S1 (ns, P=0.54). ns: not significant. **7 weeks:** n=6-7 mice per group. Mann-Whitney U-test for thalamus (**P=0.0012), nRT (**P=0.0012), hippocampus (ns, P=0.295), and S1 (ns, P>0.99). **9 months:** n=5-6 mice per group. Mann-Whitney U-test for thalamus (**P=0.002), nRT (ns, P=0.18), hippocampus (ns, P=0.42). **Related to Figure 4.1.**

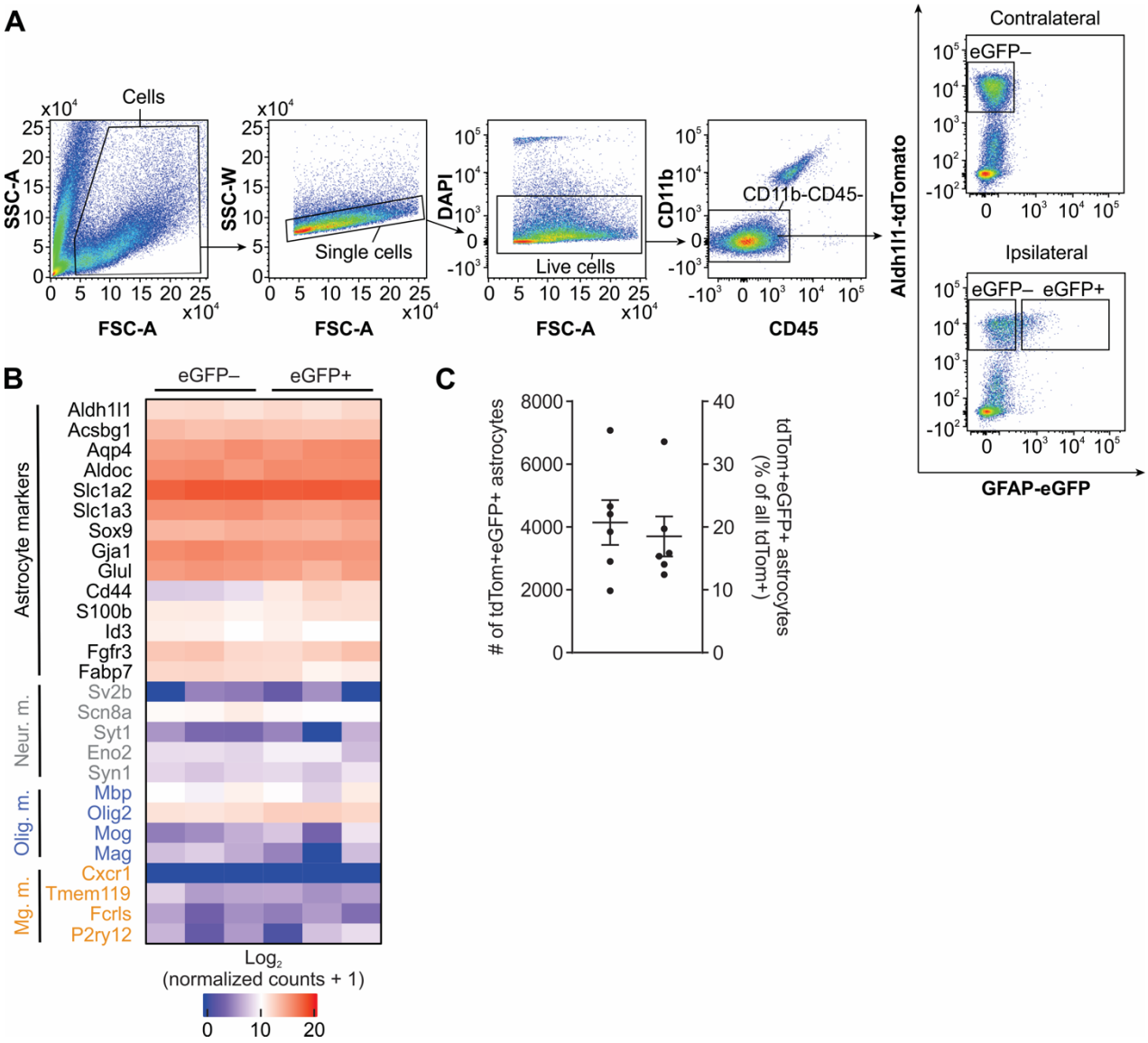

Supplemental Figure 4.2. Molecular characterization of FACS-isolated thalamic reactive astrocytes.

(A) Fluorescence activated cell sorting (FACS) gating strategy for samples collected for RNA sequencing, obtained from the thalamus ipsilateral and contralateral to intra-thalamic transduction of astrocytes in pan-astrocytic reporter Aldh1l1-tdTomato mice. Gates indicate sorting strategy to obtain ipsilateral virally transduced "reactive" astrocytes (tdTomato^{+}eGFP^{+}), and contralateral "healthy" astrocytes (tdTomato^{+}eGFP^{-}). Astrocytes were gated as DAPI^{-}, CD11b^{-} and CD45^{-} followed by Aldh1l1-tdTomato^{+}, GFAP-eGFP^{-} for the contralateral side and Aldh1l1-tdTomato^{+}, GFAP-eGFP^{-} (eGFP–) and Aldh1l1-tdTomato^{+}, GFAP-eGFP^{+} (eGFP+) for the ipsilateral side. FSC-A: forward scatter area; SSC-A: side scatter area; SSC-W: side scatter height. Isolated astrocytes were subsequently used for RNA sequencing (RNA-Seq). **(B)** Heat map of cell-type specific markers, demonstrating the specificity of our FACS approach to isolate astrocytes that showed high expression of astrocytic markers such as *S100b* (indicated in black), and low expression of neuronal markers such as *Syt1* (grey), oligodendrocyte markers such as *Mbp* (blue),

and microglial markers such as *Cxcr1* (orange). Color gradient indicates log2 of the normalized counts (+1) for each gene from the RNA sequencing data of contralateral eGFP– and ipsilateral reactive eGFP+ astrocytes. **(C)** Number (left y-axis) and percentage (right y-axis) of FACS-isolated $tdTom^{pos}eGFP^{pos}$ astrocytes in ipsilateral thalami. 18.5 $\pm$ 0.03% of tdT+ astrocytes were eGFP+. n=6 samples. **Related to Figure 4.1.**

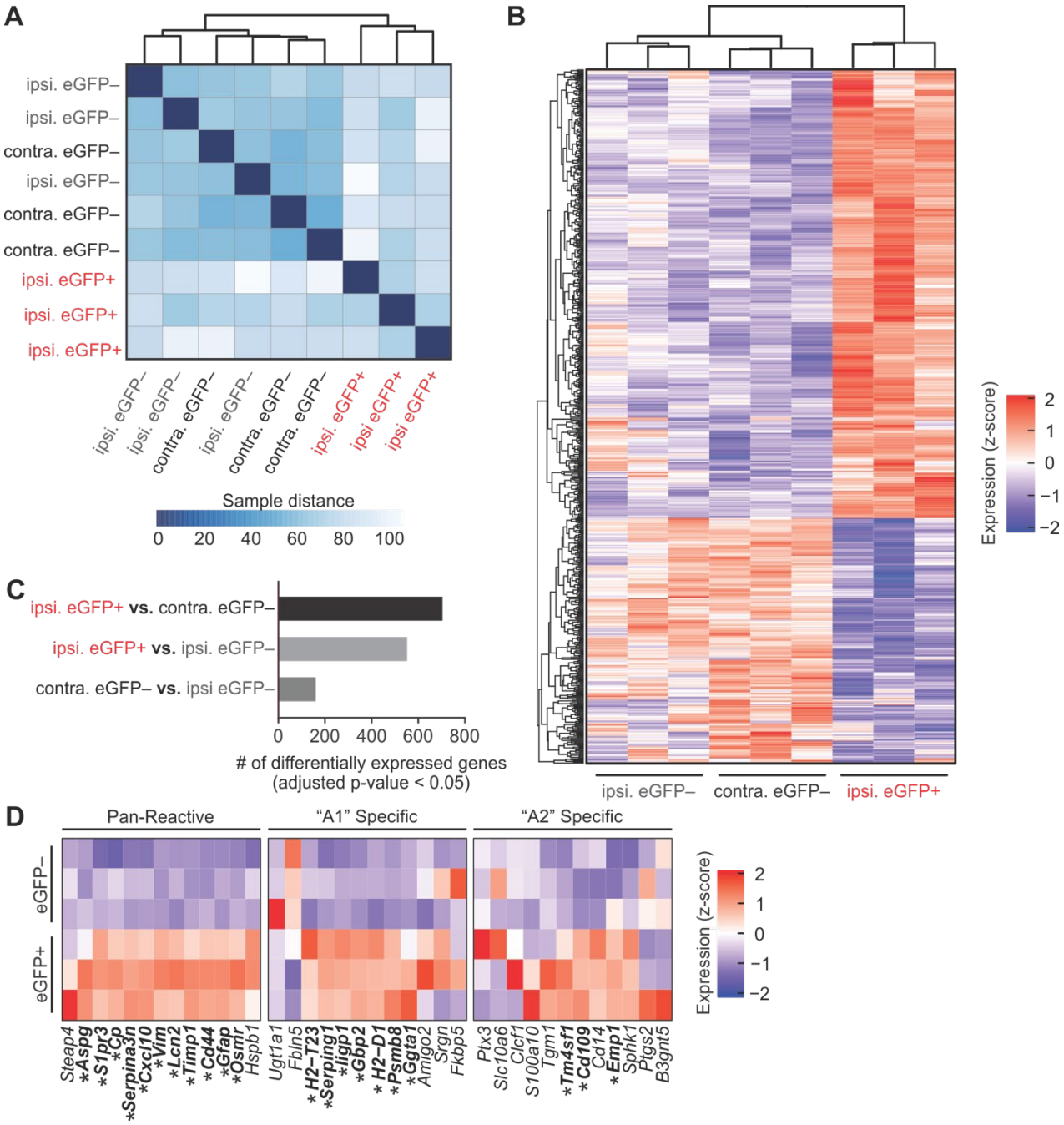

Supplemental Figure 4.3. Transcriptomic comparison of eGFP-positive and eGFP-negative thalamic astrocytes.

(A) Hierarchical clustering of sample distance, a measure of sample-to-sample similarity, reveals clustering of ipsilateral eGFP-positive (eGFP+) astrocyte samples away from ipsilateral eGFP-negative and contralateral eGFP-negative (eGFP–) astrocyte samples. **(B)** Heat map of differentially expressed genes (DEGs) in eGFP+ versus eGFP– thalamic astrocytes (adjusted *P* value < 0.05). Dendograms indicate hierarchical clustering of DEGs. Heat map shows z-scored

expression of DEGs in contralateral eGFP–, ipsilateral eGFP–, and ipsilateral eGFP+ astrocytes. Note that the ipsilateral eGFP+ and contralateral eGFP– astrocyte samples are the same as those shown in Figure 4.1H. **(C)** Number of differentially expressed genes (adjusted P value < 0.05). **(D)** Heat map showing expression of "pan-reactive", lipopolysaccharide-induced ("A1")- and middle cerebral artery occlusion-induced ("A2")- reactive astrocyte genes (as reported in (Liddelow et al., 2017)) in contralateral thalamic eGFP-negative and ipsilateral thalamic reactive eGFP-positive astrocytes. * indicates genes which were significantly upregulated in ipsilateral thalamic reactive eGFP-positive astrocytes. 11 "pan-reactive" genes which were significantly upregulated are highlighted in Figure 4.1H. Adjusted *P<0.05. Color gradient indicates z-scored relative expression. **Related to Figure 4.1.**

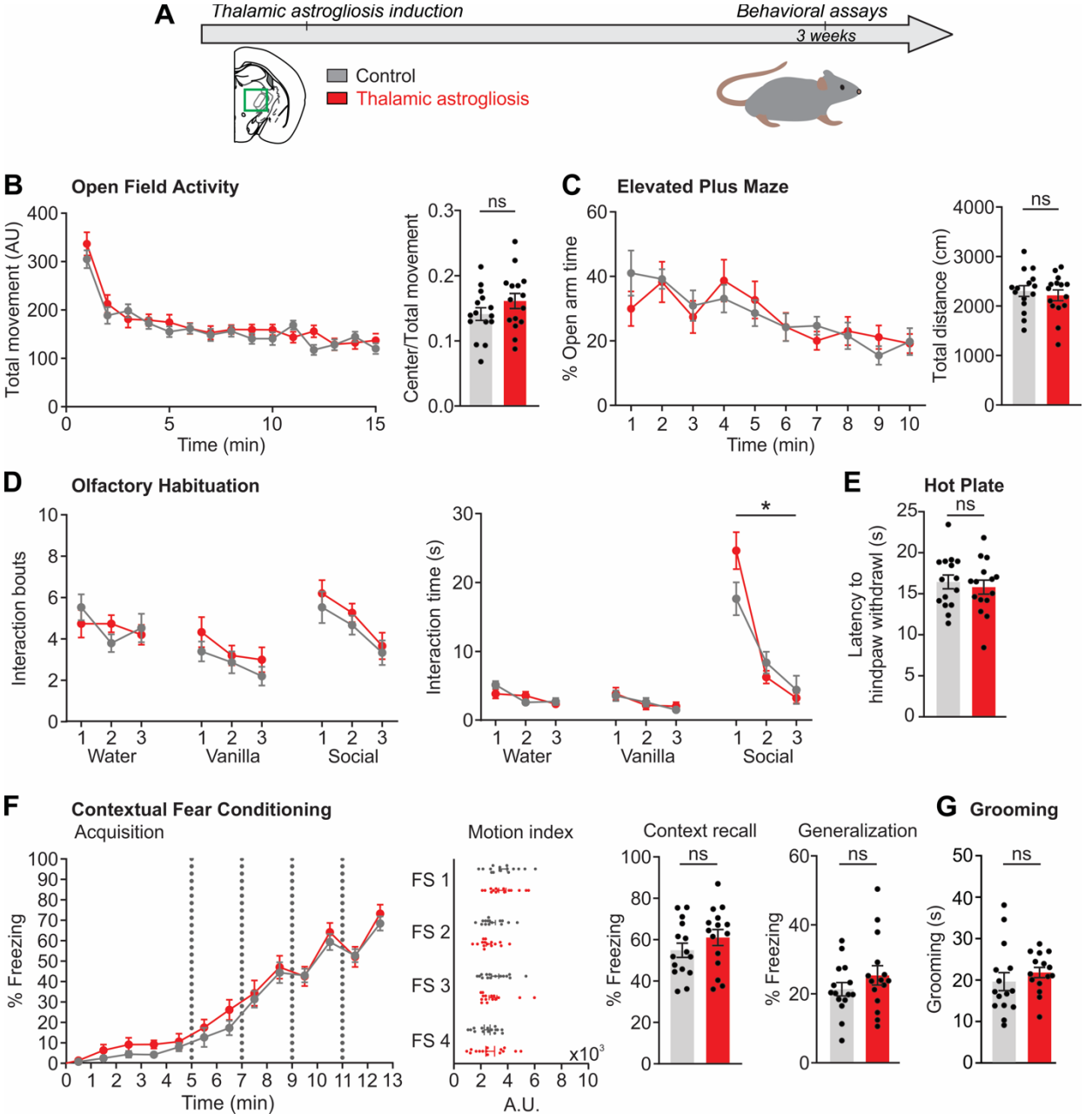

Supplemental Figure 4.4. Behavioral repertoire in mice with thalamic astrogliosis.

(A) Schematic of experimental timeline. Three to four weeks after viral transduction of thalamic astrocytes, mice underwent behavioral testing to assess spontaneous locomotion, anxiety, olfactory habituation, aversion, and contextual learning and memory performance. n=15 mice/group. **(B)** Open field activity. Left: total movement throughout a 15-minute session. Two-way repeated measures ANOVA, $F(14, 392)$, Interaction $P=0.19$. Shapiro-Wilk normality test, $P>0.05$. Right: ratio of movement in the center vs. total arena. Mann-Whitney U test, $P=0.29$. ns: not significant. **(C)** Elevated plus maze. Left: percentage of time exploring open arm throughout a 10-minute session. Two-way repeated measures ANOVA with Geisser-Greenhouse correction, $F(9, 252)$, Interaction $P=0.73$. Shapiro-Wilk normality test, $P>0.05$. Right: total distance traveled. Mann-

Whitney U test, *P*=0.74. **(D)** Olfactory habituation test. Mice were presented with three trials each of three distinct odors: water, vanilla, and an unfamiliar social odor.. Two-way repeated measures ANOVA with Geisser-Greenhouse correction, *F*(2,56). Interaction Bouts: Water (*P*=0.27), Vanilla (*P*=0.82), Social (*P*=0.96). Interaction Time: Water (*P*=0.14), Vanilla (*P*=0.78), Social (**P*=0.03; no significant multiple comparisons, with Sidak's correction for multiple comparisons). Shapiro-Wilk normality test, *P*>0.05. **(E)** Hot plate test. Latency to withdraw left hindpaw (contralateral to thalamic astrogliosis) in response to an aversive stimulus. Mann-Whitney U test, *P*=0.83. **(F)** Contextual fear conditioning. *Acquisition:* percentage of time spent freezing during the acquisition phase. Dashed vertical lines indicate time of foot shocks.Two-way repeated measures ANOVA with Geisser-Greenhouse correction, *F*(12, 336), Interaction *P*=0.96. Shapiro-Wilk normality test, *P*>0.05. *Motion Index*: movement in response to foot shocks (FS). Multiple Mann-Whitney U test design with Holm-Sidak correction. FS 1 (*P*>0.99), FS 2 (*P*=0.82), FS 3 (*P*=0.95), FS 4 (*P*=0.95). *Context Recall*: percentage of time spent freezing during the recall phase. Mann-Whitney U test, *P*=0.27. *Generalization*: percentage of time spent freezing during the generalization phase. Mann-Whitney U test, *P*=0.26. **(G)** Grooming. Total time spent grooming whiskers during a 10-minute session. Mann-Whitney U-test, *P*=0.15. **Related to Figure 4.1.**

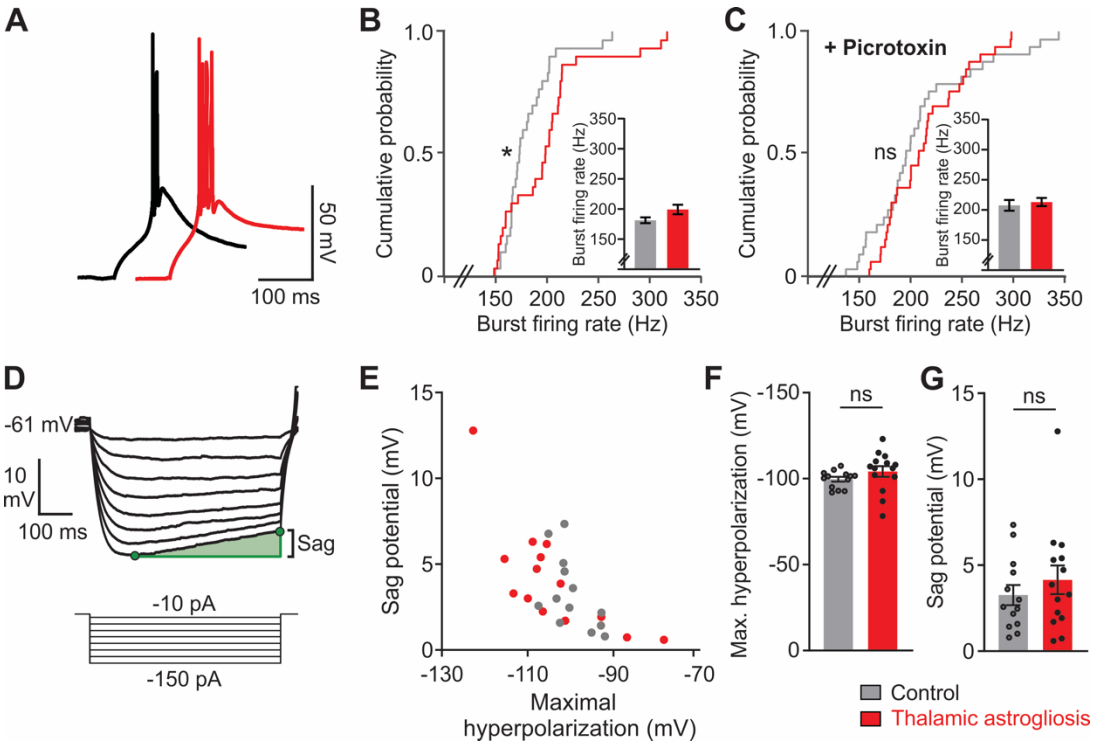

Supplemental Figure 4.5. Properties of hyperpolarization-induced rebound bursting and depolarizing sag potential in thalamocortical neurons.

(A) Overlay of the hyperpolarization-induced rebound burst firing from two representative thalamocortical neurons in response to the same current injection (-130 pA). **(B)** Cumulative probability distribution of the action potential firing rate during the first hyperpolarization-induced rebound burst response. Population data consists of the firing rate obtained from the three most hyperpolarized sweeps for each cell to ensure equal representation. Inset shows bar plot mean ± SEM. Kolmogorov-Smirnov test, **P*=0.026. Control: 3 sweeps/neuron, n=10 neurons; Thalamic astrogliosis: 3 sweeps/neuron, n=10 neurons. **(C)** Same as in (B), but in presence of Picrotoxin. Kolmogorov-Smirnov test, *P*=0.62. ns: not significant. Control: 3 sweeps/neuron, n=11 neurons; Thalamic astrogliosis: 3 sweeps/neuron, n=11 neurons. **(D)** Hyperpolarization-induced 'sag' depolarization was measured in response to hyperpolarizing current steps. The amplitude of the sag depolarization (green shaded region) was calculated as the difference between the maximal hyperpolarized membrane potential and the membrane potential at the end of the current injection. All cells were recorded at resting membrane potential. **(E)** Amplitude of the sag potential as a function of the maximal hyperpolarized potential in response to a -150 pA intracellular current injection. **(F)** Maximal hyperpolarization. Mann-Whitney U test, *P*=0.053. Control: n=13 neurons; Thalamic astrogliosis: n=14 neurons. **(G)** Amplitude of the depolarizing sag potential. Mann-Whitney U test, *P*=0.52. **Related to Figure 4.3.**

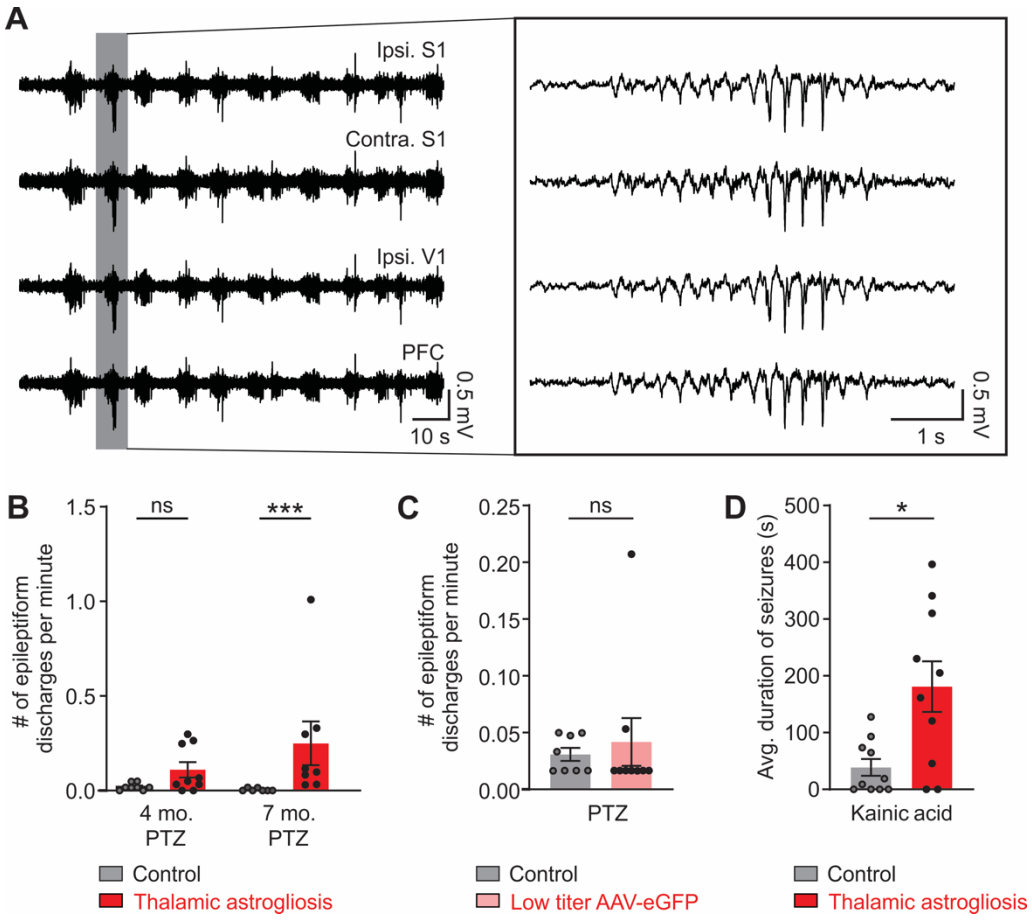

Supplemental Figure 4.6. Characterization of enhanced seizure risk.

(A) Representative ECoG traces in the PTZ challenge experiment from the mouse with thalamic astrogliosis shown in Fig. 3, B and C. Here, we include ECoG traces simultaneously obtained from primary somatosensory cortex S1 ipsilateral and contralateral to site of thalamic astrogliosis, as well as ipsilateral primary visual cortex and prefrontal cortex. **(B)** Quantification of ipsilateral S1 cortical epileptiform discharges induced by PTZ (5 mg/kg), 4 and 7 months after viral-mediated astrogliosis. 4 months: Mann-Whitney U test, P=0.10; Control: n=8 mice; Thalamic astrogliosis: n=9 mice. 7 months: Mann-Whitney U test, ***P=0.0003; Control: n=7 mice; Thalamic astrogliosis: n=8 mice. P-values are not adjusted for multiple comparisons or within-subject comparisons. ns: not significant. **(C)** Quantification of ipsilateral S1 cortical epileptiform discharges induced by a low titer injection of AAV2/5-Gfa104-eGFP (see Methods). Mann-Whitney U test, P=0.98. Control: n=8 mice; Thalamic astrogliosis: n=9 mice. **(D)** Average duration of seizures induced by Kainic Acid (10 mg/kg). Mann-Whitney U test, *P=0.025, n=10 mice/group. **Related to Figure 4.4.**

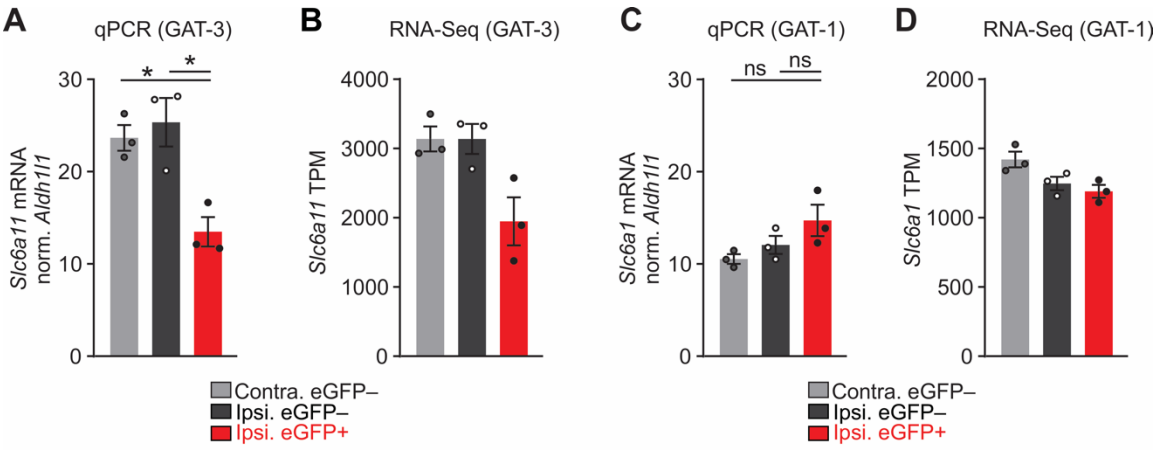

Supplemental Figure 4.7. GAT-3, but not GAT-1, is reduced at the transcript level in eGFP-positive thalamic reactive astrocytes.

(A) *Slc6a11* expression (encoding GAT-3), normalized to *Aldh1l1* expression in FACS-isolated astrocytes. Transcript expression obtained by quantitative PCR (qPCR). FACS was performed to isolate astrocytes from the thalamus, ipsilateral and contralateral to stereotaxic injection of AAV2/5-Gfa104-eGFP in adult Aldh1l1-tdTomato reporter mice. Sorting strategy to obtain astrocytes detailed in Fig. S2. Note that data in (A) is presented in Fig. 5C and included here for visual comparison. One-way ANOVA: $F(2,6)=10.89$, $^*P=0.01$. Shapiro-Wilk normality test, $P>0.05$. Tukey's multiple comparisons: contra. eGFP– vs. ipsi eGFP– (ns, $P=0.816$), contra.eGFP– vs. ipsi eGFP+ ($^*P=0.024$), ipsi eGFP– vs. ipsi eGFP+ ($^*P=0.012$), n=3 mice. **(B)** Normalized gene expression of *Slc6a11*, expressed as Transcripts Per Million (TPM), obtained from our RNA sequencing (RNA-seq) experiment in FACS-isolated astrocytes as described in (A). **(C)** Same as in (A), but for *Slc6a1* (encoding GAT-1). One-way ANOVA, $P=0.11$, Shapiro-Wilk normality test, $P>0.05$. n=3 mice. ns: not significant. **(D)** Same as in (B), but for *Slc6a1*. **Related to Figure 4.5.**

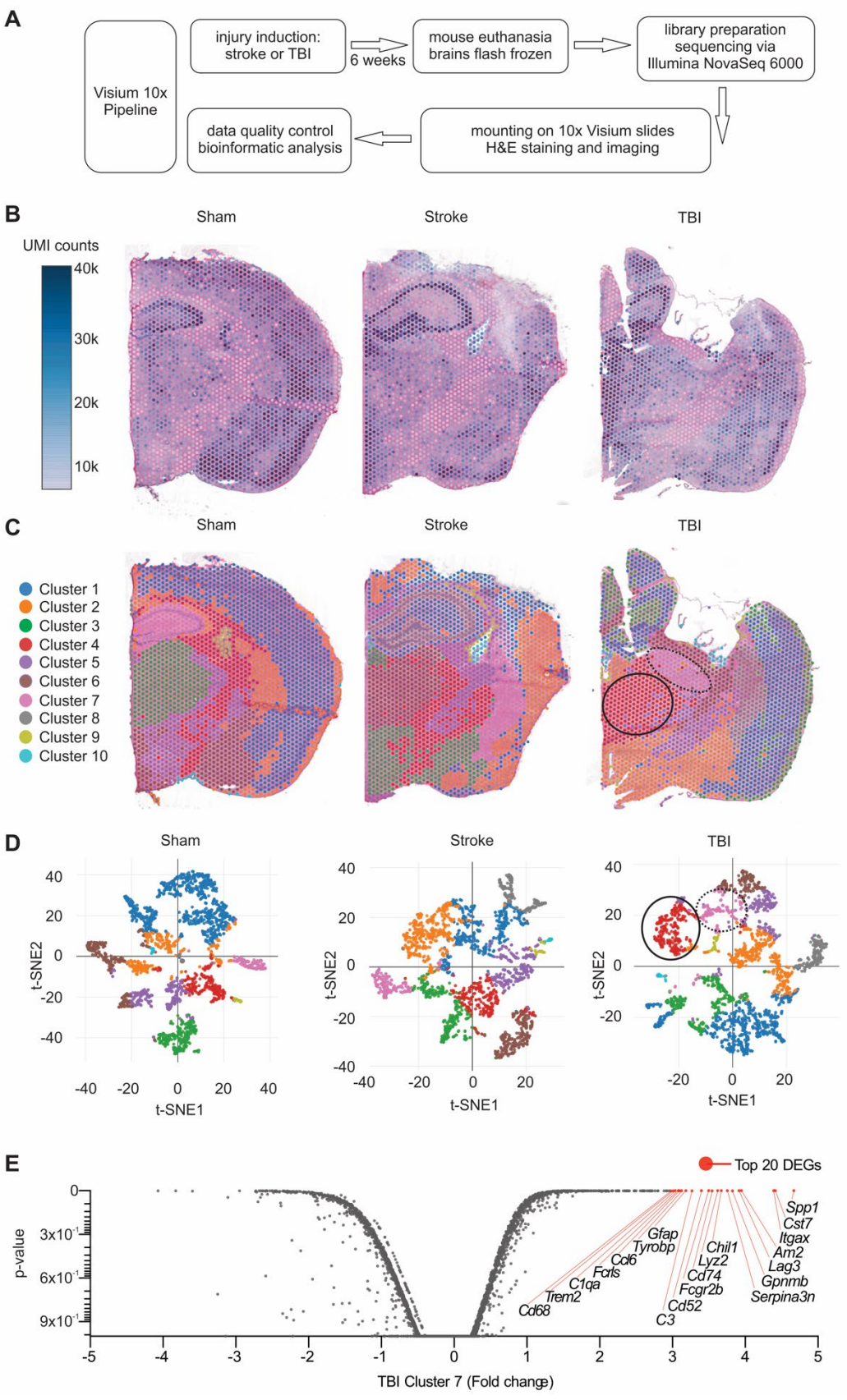
A
Visium 10x Pipeline
injury induction: stroke or TBI
6 weeks
mouse euthanasia brains flash frozen
library preparation sequencing via Illumina NovaSeq 6000
mounting on 10x Visium slides H&E staining and imaging
data quality control bioinformatic analysis
B
Sham
Stroke
TBI
UMI counts
40k
30k
20k
10k
C
Sham
Stroke
TBI
Cluster 1
Cluster 2
Cluster 3
Cluster 4
Cluster 5
Cluster 6
Cluster 7
Cluster 8
Cluster 9
Cluster 10
D
Sham
Stroke
TBI
t-SNE1
t-SNE2
E
Top 20 DEGs
p-value
TBI Cluster 7 (Fold change)
Spp1
Cst7
Itgax
Am2
Lag3
Gpnmb
Serpina3n
Chil1
Lyz2
Cd74
Fcgr2b
Cd52
C3
Gfap
Tyrobp
Cd6
Fcrls
C1qa
Trem2
Cd68

Supplemental Figure 4.8. Spatial transcriptomic analysis of mouse brains after injury.

(A) Schematic of experimental approach for spatial transcriptomics of mice six weeks after stroke or TBI injury. **(B)** Data quality control (QC): tissue plots with spots colored by unique molecular identifier (UMI) count. See Table 4.10 for more data QC measures. **(C)** Separation of spatial regions into 10 clusters using an unbiased k-means clustering algorithm. Each cluster is marked with a unique color. In the TBI section (right), two thalamic regions separated out as unique clusters 7 and 4, corresponding to *Gfap*-High and *Gfap*-Low thalamic regions analyzed in Fig. 7. **(D)** t-SNE projection of spots in each cluster. Cluster 7 from **(C)** is outlined in dotted line, Cluster 4 from **(C)** is outlined in solid line. **(E)** Differentially expressed genes (DEGs) in TBI *Gfap*-High thalamus (Cluster 7). Top 20 significant DEGs (note, all of them are upregulated) are marked in red. **Related to Figure 4.7.**

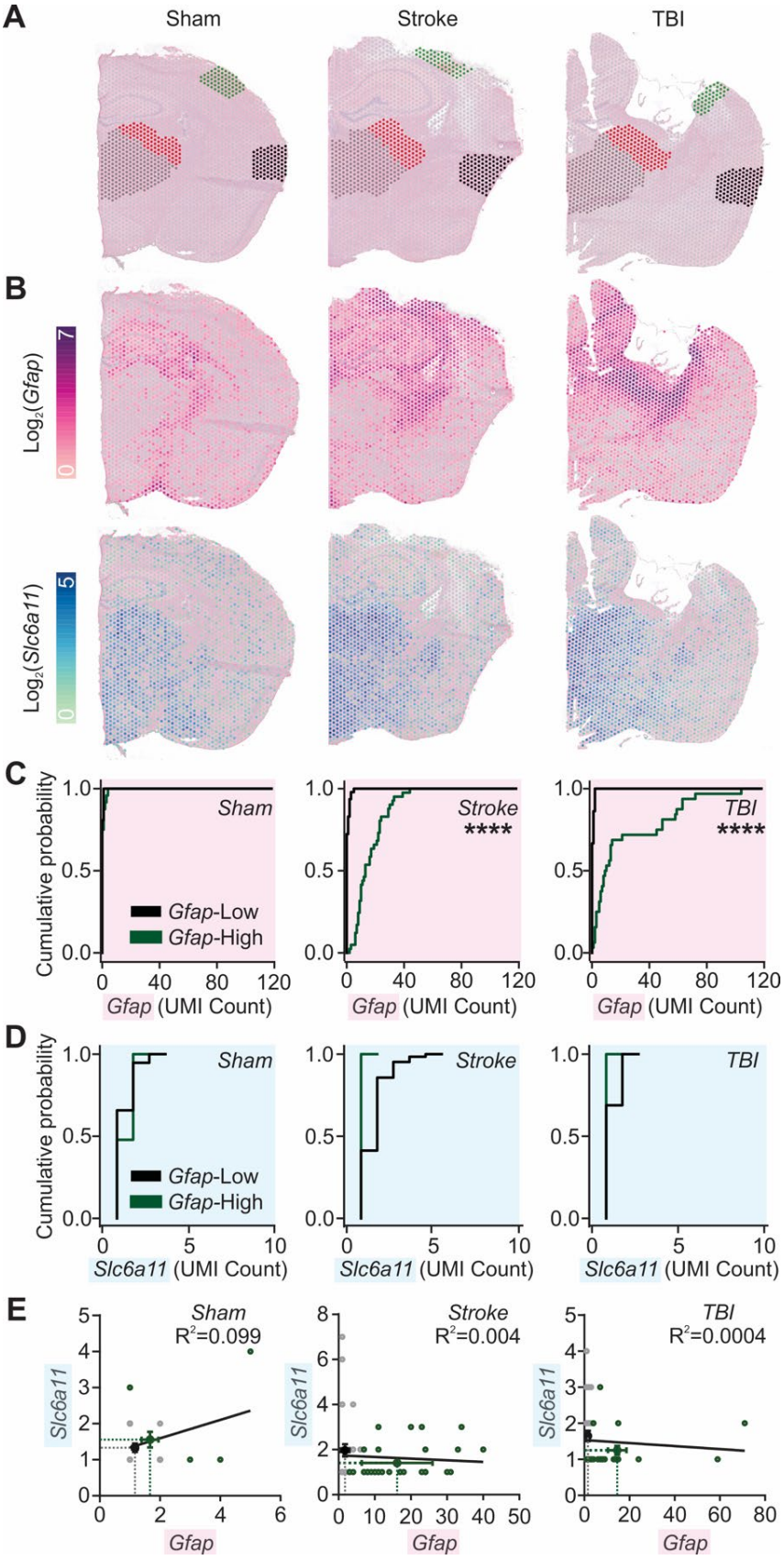
A
Sham
Stroke
TBI
B
Log2(Gfap)
7
0
Log2(Slc6a11)
5
0
C
Cumulative probability
1.0
0.5
0.0
Sham
Gfap-Low
Gfap-High
Stroke
****
TBI
****
0
40
80
120
Gfap (UMI Count)
D
Cumulative probability
Sham
Gfap-Low
Gfap-High
Stroke
TBI
0
5
10
Slc6a11 (UMI Count)
E
Sham
R2=0.099
Stroke
R2=0.004
TBI
R2=0.0004
Slc6a11
Gfap

Supplemental Figure 4.9. Lack of correlation of cortical Gfap and Slc6a11 transcript expression in mouse models of cortical injury.

(A) Hemi-brain sections from mice after sham, stroke, and TBI procedures six weeks after surgery overlaid with regions analyzed with 10x Visium spatial transcriptomics. Black and green spots indicate cortical regions with high and low *Gfap* expression in cortical injury. Red and grey spots indicate thalamic regions with high and low *Gfap* expression in cortical injury, as indicated in Fig. 7. **(B)** Cortical expression of *Gfap* and *Slc6a11* transcripts. Color map indicates log2 of the detected counts of the gene's unique molecular identifier (UMI). **(C, D)** Cumulative probability distribution of *Gfap* (C) or *Slc6a11* (D) expression per spot in regions indicated in (A). Kolmogorov-Smirnov test, ****P<0.0001. All spots containing non-zero UMI counts were included. Number of spots from low- and high-*Gfap* regions (or, distal and proximal cortex), respectively, in (C): sham (n=26 & 24); stroke (n=47 & 41); TBI (n=51 & 32); in (D): sham (n=40 & 51); stroke (n=64 & 26); TBI (n=62 & 13). Adjusted $\alpha=0.025$ *for multiple comparisons.* **(E)** Relationship between *Gfap* and *Slc6a11* expression. Circles represent UMI counts per spot in low- (black) and high-*Gfap* (green) areas; black and green crosses, and corresponding dotted lines, mark mean±SEM for low- and high-*Gfap* areas respectively. Black lines plot the best-fit slopes and intercepts from a simple linear regression. **Related to Figure 4.7.**

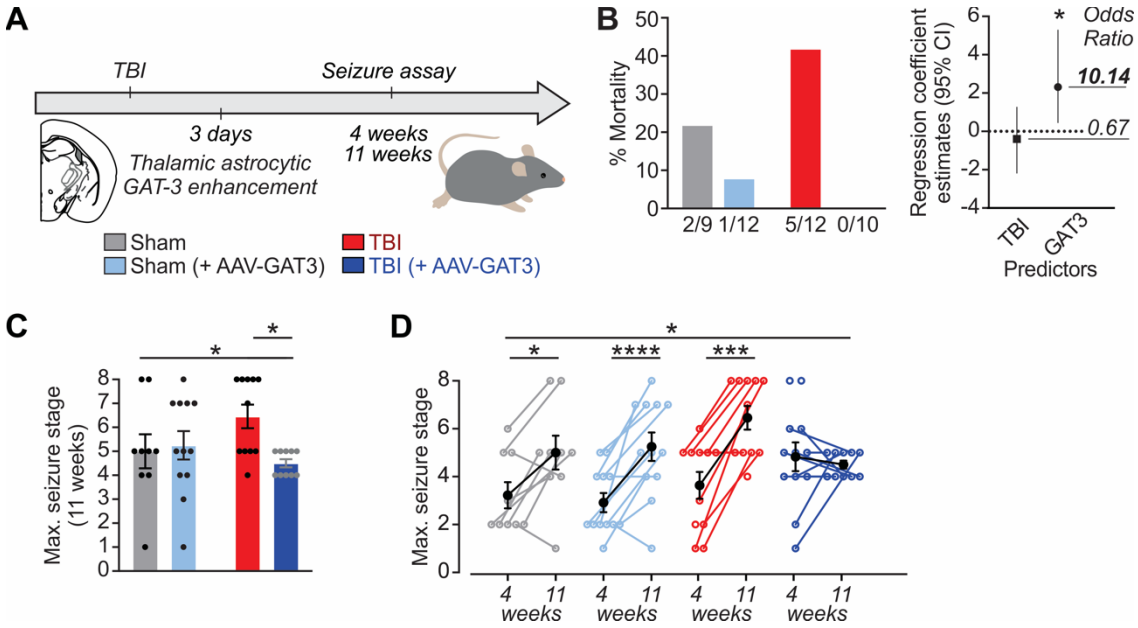

Supplemental Figure 4.10. Enhancing GAT-3 in a mouse model of TBI reduces PTZ-induced seizure severity and mortality.

(A) Schematic of experimental design. In a controlled cortical impact model of traumatic brain injury, a metal piston (3 mm diameter) is used to deliver an impact at a depth of 0.8 mm to the right somatosensory cortex. Three days following injury or sham procedure, increased GAT-3 expression in thalamic astrocytes was achieved by transducing thalamic astrocytes with AAV2/5-GfaABC1D-GAT3-mCherry (Yu et al., 2018) in a subset of mice. We assessed seizure susceptibility at two timepoints (four and eleven weeks post-injury) reported to reflect the "subacute" and "chronic" stages of TBI-induced epileptogenesis and hyperexcitability (Hunt et al., 2009; Manninen et al., 2021). **(B)** *Left:* probability of death following PTZ-induced seizures. Numbers below x-axis indicate the number of deaths as a fraction of the total number of mice in each group. . *Right:* estimates of regression coefficients (representing log odds ratio of survival) obtained from a logistic regression model (81.4% classification performance; area under the ROC = 0.757, **P*=0.025). The impact of each predictor on survival is obtained from the exponentiation of the parameter estimate into an odds ratio (**P*=0.04). Error bars indicate 95% confidence intervals. **(C)** Seizure severity assessed 20 minutes following PTZ (45 mg/kg, i.p.), eleven weeks after injury. Behavioral characterization of seizure stage is scored according to the Racine scale, with stage 8 = death. Sham: n=9 mice; Sham + GAT-3: n=12 mice; TBI: n=11 mice; TBI + GAT-3: n=10 mice. A two-way ANOVA was performed to account for two factors (trauma and treatment): Interaction ($F(1,38)=4.3$, **P*=0.045). Post-hoc Sidak's multiple comparisons: TBI vs. TBI+GAT-3 (adjusted **P*=0.026). Shapiro-Wilk normality test: Sham (*P*>0.05), Sham+GAT-3 (*P*>0.05), TBI (***P*=0.0044), TBI+GAT-3 (****P*=0.0003). α=0.05. An alternative non-parametric analysis (which does not account for both factors, trauma and treatment) was performed as follows: two pairwise comparisons using the non-parametric Mann-Whitney U test, and adjustment of α=0.025 for multiple comparisons. Sham vs. Sham+GAT-3 (*P*=0.88), TBI vs. TBI+GAT-3 (**P*=0.016). Either analysis (two-way ANOVA or multiple Mann-Whitney U tests) supports our conclusion that GAT-3 treatment resulted in reduced seizure severity following TBI. **(D)**

Comparison of seizure severity induced by PTZ at 4 and 11 weeks. Mixed-effects model: Interaction ($F(3,37)=3.85$, $^{*}P=0.017$). Post-hoc comparisons of 4 vs. 11 weeks: Sham ($^{*}P=0.021$), Sham+GAT-3 ($^{****}P<0.0001$), TBI ($^{***}P=0.0003$), TBI+GAT-3 (ns; $P=0.97$). **Related to Figure 4.7.**

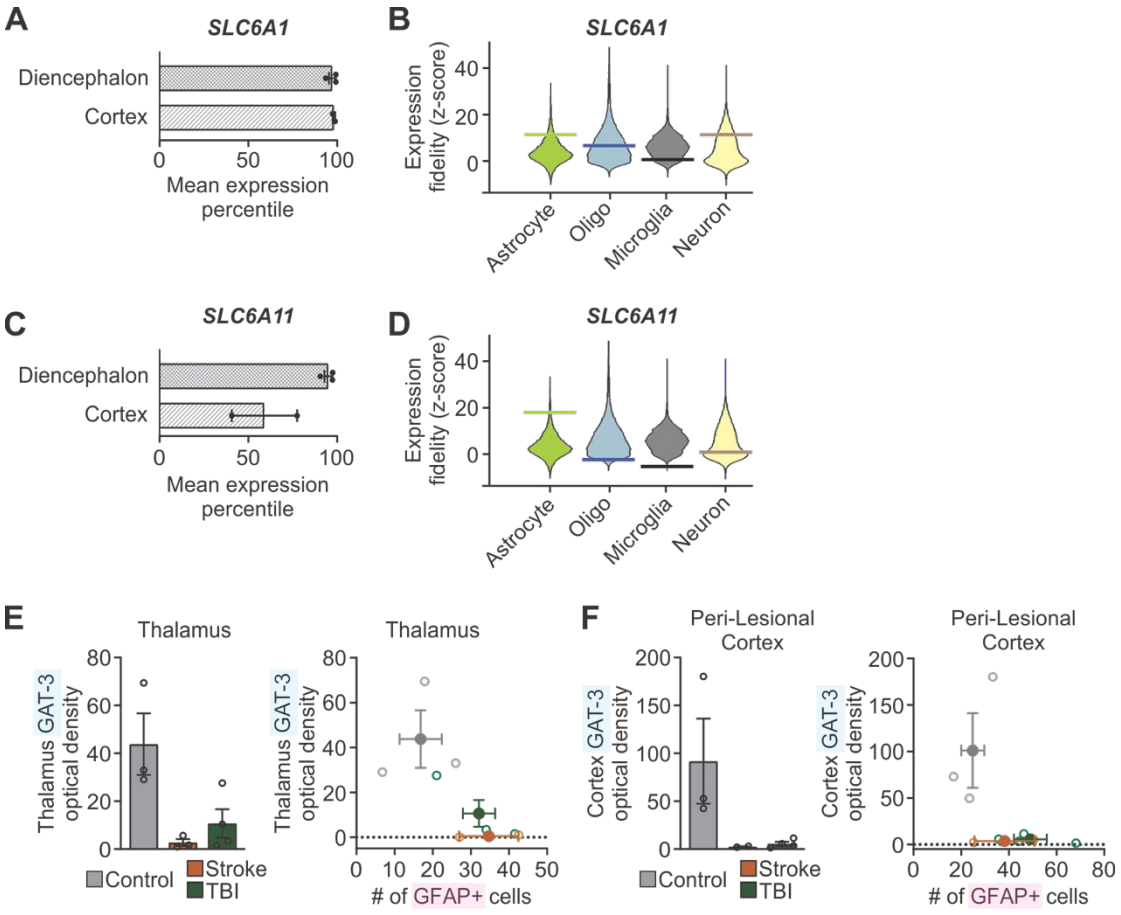

Supplemental Figure 4.11. *SLC6A1* and *SLC6A11* gene expression, and GAT-3 immunofluorescence in adult brain tissue.

(A) Mean expression percentile of *SLC6A1* gene expression relative to all genes in neurotypical adult human diencephalon and parietal cortex. Data obtained from (Kelley et al., 2018). **(B)** Expression fidelity of *SLC6A1*, obtained from cell-type specific transcriptomic profiling in the adult human diencephalon compared to transcriptional signatures of major brain cell types, relative to all human genes detected in the database compiled by (Kelley et al., 2018). Higher fidelity indicates higher correlation of *SLC6A1* to cell type. Horizontal bar indicates Z-score for *SLC6A1* relative to that cell type, violin plot indicates Z-score distribution for all genes detected in that cell type. **(C)** Same as in (A), but for *SLC6A11* (presented in Fig. 8, shown here for clarity). **(D)** Same as in (B), but for *SLC6A11* (presented in Fig. 8, shown here for clarity). **(E, F)** Quantification of GAT-3 and GFAP immunofluorescence obtained from post-mortem tissue from human subjects with a history of ischemic stroke or TBI, and age-matched control subjects (data shown in Fig. 8C, D). *Left*: Optical density of thalamic (E) and cortical (F) GAT-3 immunofluorescence. *Right*: relationship between number of GFAP+ cells and GAT-3 immunofluorescence, averaged across images per subject (open circles). Closed circles indicate mean+SEM. *(E, Left)* Control: n=3 subjects (10 images); Stroke: n=3 subjects (8 images); TBI: n=4 subjects (16 images). *(E, Right)* Control: n=3 subjects (10 images); Stroke: n=2 subjects (4 images); TBI: n=4 subjects (16 images).

(F, left): Control: n=3 subjects (8 images); Stroke: n=2 subjects (6 images); TBI: n=4 subjects (11 images). *(F, Right):* Control: n=3 subjects (6 images); Stroke: n=2 subjects (3 images); TBI: n=4 subjects (11 images). **Related to Figure 4.8.**

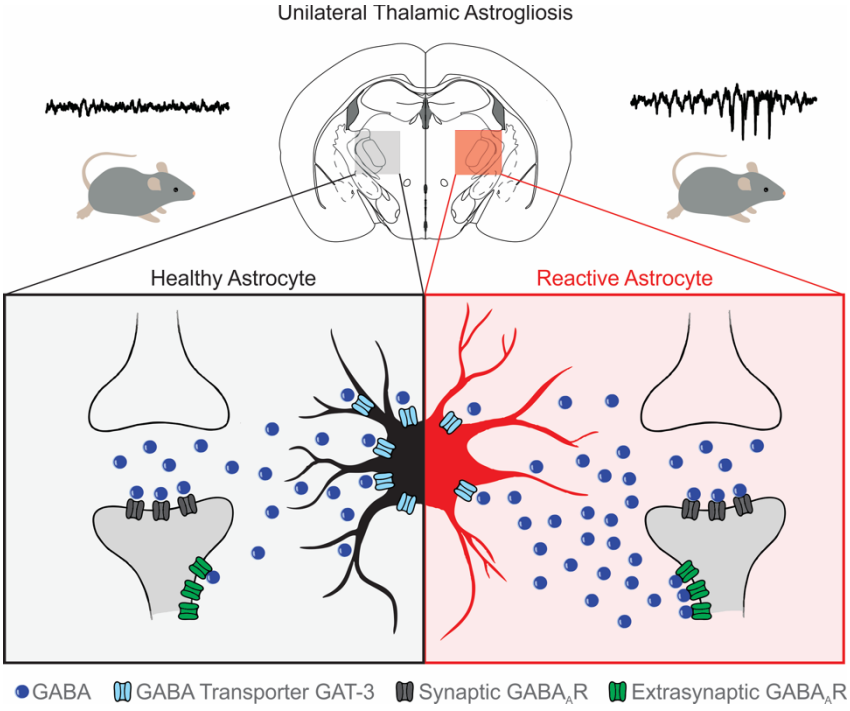

Supplemental Figure 4.12. Graphical summary: Neuroinflammation uses GAT-3 as a substrate to trigger cellular hyperexcitability and seizure risk.

Unilateral induction of thalamic astrogliosis in adult wildtype mice (Fig. 4.1) is sufficient to enhance seizure risk and drive abnormal thalamocortical rhythmogenesis *in vivo* (Fig. 4.2, 4.3, 4.4, 4.6). **Left:** schematic of an unperturbed, "healthy" astrocyte (black) in the thalamus with normal expression of the GABA transporter GAT-3 (light blue), responsible for uptake of GABA (blue). **Right:** schematic of a reactive astrocyte (red) in the thalamus with decreased expression of GAT-3, which is responsible for GABA uptake. The increased availability of GABA in the extrasynaptic regions of the post-synaptic neuron (gray) explains the three-fold increase in the tonic GABA current or I_{TONIC}—mediated by extrasynaptic $GABA_A$ receptors (green)—observed in thalamocortical neurons from *ex vivo* slices affected by astrogliosis (Fig. 4.3E). Note that the frequency and kinetics of inhibitory postsynaptic currents—mediated by synaptic $GABA_A$ receptors (dark gray)—were unaltered (Fig. 4.3F, table 4.7 and 4.8). Blocking increased I_{TONIC} by conditional deletion of the extrasynaptic $GABA_AR$ (Fig. 4.4, H to J) or by enhancing astrocytic GAT-3 (Fig. 4.5, D to F) prevented astrogliosis-induced seizure risk.

Tables

Table 4.1. Clinical characteristics of human post-mortem brain samples.

d= day(s), epi= epilepsy, IS= ischemic stroke, TBI= traumatic brain injury, MCA= middle cerebral artery, FC= frontal cortex, PC= parietal cortex, TC= temporal cortex, d= days, m= months, y= years. FBTCS, focal to bilateral tonic-clonic; FIA, focal impaired awareness; LEV, Levetiracetam; LMT, Lamotrigine; OXC, Oxcarbazepine; PB, phenobarbital; CBZ, carbamazepine.

Case	Pathology	Age	Gender	Cause of Injury	Lesion	Time after Lesion	Cause of Death
1	Control	63	F	-	-	-	Myocardial infarction
2	Control	65	M	-	-	-	Myocardial infarction
3	Control	49	M	-	-	-	Myocardial infarction
4	TBI	79	M	Fall – head injury	TC	8 d	Bronchopneumonia
5	TBI + Epi.	35	M	Horse kick – head injury	FC +TC	6 m	Myocardial infarction
6	TBI + Epi.	52	M	Car accident – head injury	FC + TC	38 y	Bronchopneumonia
7	TBI + Epi.	80	M	Grenade – head injury	FC + TC	54 y	Rupture of an abdominal aneurysm
8	IS	45	M	Infarct arteria cerebri media	FC + PC	1 d	Infarct arteria cerebri media
9	IS + Epi.	67	M	Infarct arteria cerebri media	MCA	19 y	Infarct arteria cerebri media
10	Epi. + IS	69	M	Infarct arteria cerebri media	MCA	3 y	Infarct arteria cerebri media

Case	Pathology	Age Onset Epilepsy	Seizures per Month	Seizure Type	Anti-epileptic Drugs	Post-mortem Delay (hours)
1	Control	-	-	-	-	8
2	Control	-	-	-	-	10
3	Control	-	-	-	-	9
4	TBI	-	-	-	-	11
5	TBI + Epi.	35	5	FIA	CBZ	10
6	TBI + Epi.	15	2-5	FIA	LEV, OXC	9
7	TBI + Epi.	26	2-5	FIA	CBZ, LEV	9
8	IS	45	-	-	-	10
9	IS + Epi.	21	5	FIA	CBZ, LMT	11
10	Epi. + IS	46	3	FIA	LEV, LMT	12

Table 4.2. Semi-quantitative analysis of GFAP immunofluorescence and GAT-3 immunoreactivity in human brain tissue.

Immunoreactivity of glial fibrillary acidic protein (GFAP) and the extent of astrocyte reactivity was scored semi-quantitatively in the lesional cortex, perilesional cortex, and the thalamus, as follows: 1=sparsely present with resting morphology; 2=moderately present with either resting or partially reactive morphology; 3=highly present with reactive morphology. d=days; m=months; y=years. TBI=traumatic brain injury. Immunoreactivity of the GABA transporter GAT-3 was scored semi-quantitatively in the lesional cortex, perilesional cortex, and the thalamus, as follows: 0=absent, 1=sparse, 2=moderate, 3=dense staining.

GFAP Immunoreactivity

	Age	Time after TBI/Stroke	Cortex Lesional	Cortex Perilesional	Thalamus
Control	63	-		1	2
	65	-		1	1
	49	-		2	1
Median (min-max)				**1 (1-2)**	**1 (1-2)**
TBI	79	8 d	3	2	2
	35	6 m	3	3	3
	52	38 y	3	3	2
	80	54 y	2	1	1
Median (min-max)			**3 (2-3)**	**2.5 (1-3)**	**2 (1-3)**
Stroke	45	1 d	3	3	3
	69	3 y	3	3	2
	67	19 y	3	3	3
Median (min-max)			**3**	**3**	**3 (2-3)**

GAT-3 Immunoreactivity

	Age	Time after TBI/Stroke	Cortex Lesional	Cortex Perilesional	Thalamus
Control	63	-		2	3
	65	-		3	3
	49	-		2	3
Median (min-max)				**2 (2-3)**	**3**
TBI	79	8 d	1	2	3
	35	6 m	1	3	3
	52	38 y	1	2	2
	80	54 y	1	2	2
Median (min-max)			**1**	**2 (2-3)**	**2.5 (2-3)**
Stroke	45	1 d	1	3	1
	69	3 y	2	2	2
	67	19 y	1	2	2
Median (min-max)			**1 (1-2)**	**2 (2-3)**	**2 (1-2)**

Table 4.3. Passive electric membrane properties of thalamocortical neurons.

Data represented as mean ± SEM, compared using Mann-Whitney U Test. Last column ("n") indicates the number of cells, slices, and mice (respectively) for each condition.

	V_{REST} (mV)	I_{HOLD} (pA)	Cm (pF)	R_{IN} (MΩ)	Tau (ms)	n
Control	-67.7 ± 1.9	-62.9 ± 26.3	367.41 ± 28.7	192.7 ± 16.5	36.8 ± 2.9	17/8/4
Thalamic Astrogliosis	-73.6 ± 2.1	-1.8 ± 18.1	340.3 ± 32.1	224.8 ± 22.1	32.7 ± 2.4	14/7/5
P-Value	**0.053**	0.1	0.57	0.32	0.31	
50 µM Picrotoxin	V_{REST} (mV)	I_{HOLD} (pA)	Cm (pF)	R_{IN} (MΩ)	Tau (ms)	n
Control	-68.3 ± 1.6	-195.8 ± 38.2	101.1 ± 10.0	290.1 ± 41.1	36.3 ± 7.3	9/5/3
Thalamic Astrogliosis	-68.7 ± 2.4	-196.3 ± 24.2	116.8 ± 7.3	208.3 ± 32.7	37.0 ± 5.3	13/9/5
P-Value	0.59	0.99	0.21	0.39	0.29	

Table 4.4. Active electric membrane properties of thalamocortical neurons.

Data represented as mean ± SEM, compared using Mann-Whitney U Test. Last column ("n") indicates the number of cells, slices, and mice (respectively) for each condition. Action potential (AP). **P*<0.05, ***P*<0.01.

	At -60 mV					
	Rheobase (pA)	**AP Amp. (mV)**	**AP Threshold (mV)**	**AP Duration (ms)**	**AP Half-Duration (ms)**	**n**
Control	86 ± 17.9	67.3 ± 2.6	-55.4 ± 0.7	3.11 ± 0.84	1.35 ± 0.20	15/8/4
Thalamic Astrogliosis	100 ± 17.4	68.3 ± 1.3	-57.7 ± 0.5	2.08 ± 0.08	1.07 ± 0.04	14/7/5
P-Value	0.72	0.81	***0.022**	0.068	0.142	

	At -75 mV					
	Rheobase (pA)	**AP Amp. (mV)**	**AP Threshold (mV)**	**AP Duration (ms)**	**AP Half-Duration (ms)**	
Control	104.1 ± 11.5	69.6 ± 1.7	-57.0 ± 0.7	2.25 ± 0.08	1.15 ± 0.04	17/8/4
Thalamic Astrogliosis	91.4 ± 11.4	69.5 ± 1.1	-58.6 ± 0.6	1.93 ± 0.15	1.04 ± 0.04	14/7/5
P-Value	0.52	0.77	0.11	**0.052**	0.11	

	At -60 mV					
50 µM Picrotoxin	**Rheobase (pA)**	**AP Amp. (mV)**	**AP Threshold (mV)**	**AP Duration (ms)**	**AP Half-Duration (ms)**	**n**
Control	90 ± 35.5	68.2 ± 2.25	-51.7 ± 1.32	1.84 ± 0.09	0.89 ± 0.05	8/4/3
Thalamic Astrogliosis	70 ± 22	66.1 ± 3.86	-49.6 ± 1.21	2.38 ± 0.25	1.10 ± 0.04	5/5/2
P-Value	0.92	0.85	0.28	***0.018**	****0.0083**	

	At -75 mV					
50 µM Picrotoxin	**Rheobase (pA)**	**AP Amp. (mV)**	**AP Threshold (mV)**	**AP Duration (ms)**	**AP Half-Duration (ms)**	
Control	130 ± 33.5	68.5 ± 2.91	-52.6 ± 1.78	1.84 ± 0.09	0.93 ± 0.04	9/5/3
Thalamic Astrogliosis	151.5 ± 22.8	72.1 ± 1.91	-52.7 ± 0.87	2.07 ± 0.16	0.99 ± 0.05	13/9/5
P-Value	0.31	0.32	0.65	0.47	0.37	

Table 4.5. T-Type Ca^{2+} current properties in thalamocortical neurons.

Data represented as mean ± SEM, compared using Mann-Whitney U Test. Last column ("n") indicates the number of cells, slices, and mice (respectively) for each condition.

	Max. Area (pA*ms)	V_{50} (mV)	Max. Tau (ms)	Cm (pF)
Control	-21334 ± 2552	-113.20 ± 0.89	170.8 ± 37.4	96.64 ± 14.43
Thalamic Astrogliosis	-18178 ± 2929	-115.72 ± 0.85	268.3 ± 58.4	92.47 ± 9.57
P-Value	0.23	0.087	0.18	0.95

Table Continued	Max. Amp. (pA)	T-current Density (pA/pF)	Boltzmann Slope Factor	n
Control	-137.21 ± 21.4	-1.44 ± 0.15	-0.024 ± 0.002	6/6/3
Thalamic Astrogliosis	-112.80 ± 22.8	-1.31 ± 0.311	-0.029 ± 0.004	8/5/4
P-Value	0.41	0.35	0.57	

Table 4.6. Spontaneous excitatory and inhibitory post-synaptic currents in thalamocortical neurons.

Data represented as mean ± SEM, compared using Mann-Whitney U test. Last column ("n") indicates the number of cells, slices, and mice (respectively) for each condition. $^{**}P<0.01$.

Spontaneous Excitatory Post-Synaptic Currents (sEPSCs)

	Frequency (Hz)	Amplitude (pA)	Charge (fC)	Decay Tau (ms)	Rise Time (ms)	n
Control	2.23 ± 0.72	17.77 ± 1.33	53.13 ± 4.15	2.18 ± 0.18	0.47 ± 0.05	15/9/4
Thalamic Astrogliosis	1.47 ± 0.33	16.19 ± 0.6	53.19 ± 4.42	2.31 ± 0.15	0.38 ± 0.03	16/8/5
P-Value	0.57	0.65	0.89	0.57	0.32	

Spontaneous Inhibitory Post-Synaptic Currents (sIPSCs)

	Frequency (Hz)	Amplitude (pA)	Charge (fC)	Decay Tau (ms)	Rise Time (ms)	n
Control	4.98 ± 1.23	-27.09 ± 2.01	-292.1 ± 28.85	6.13 ± 0.40	2.35 ± 0.26	12/12/3
Thalamic Astrogliosis	3.17 ± 0.63	-32.86 ± 3.10	-394.1 ± 56.86	7.28 ± 0.64	3.12 ± 0.22	10/10/4
P-Value	0.54	0.2	0.16	0.16	****0.0085**	

Table 4.7. Passive and active electrical membrane properties in reticular thalamic neurons.

Cells were clamped at -75 mV. Data represented as mean ± SEM, compared using Mann-Whitney U Test. Last column ("n") indicates the number of cells, slices, and mice (respectively) for each condition. Action potential (AP). **P<0.01.

	V_{REST} (mV)	Cm (pF)	R_{IN} (MΩ)	Tau (ms)	n
Control	-65.68 ± 5.4	138.97 ± 27.7	495.9 ± 122.6	49.7 ± 9.5	7/5/3
Thalamic Astrogliosis	-64.52 ± 2.3	108.71 ± 10.5	411.2 ± 71.9	32.1 ± 4.9	13/7/4
P-Value	0.66	0.49	0.52	0.068	

50 uM Picro	V_{REST} (mV)	Cm (pF)	R_{IN} (MΩ)	Tau (ms)	n
Control	-56.97 ± 0.67	79.87 ± 7.22	526.5 ± 73.5	57.98 ± 7.65	16/8/3
Thalamic Astrogliosis	-55.98 ± 0.66	69.35 ± 6.13	487.12 ± 65.7	64.20 ± 13.36	22/9/4
P-Value	0.29	0.46	0.63	0.94	

	Rheobase (pA)	AP Amp. (mV)	AP Threshold (mV)	AP Duration (ms)	AP Half-Duration (ms)	n
Control	30.0 ± 10.3	43.64 ± 2.4	49.94 ± 1.53	1.30 ± 0.12	0.66 ± 0.07	7/5/3
Thalamic Astrogliosis	53.3 ± 14.7	47.7 ± 1.9	-52.91 ± 0.71	1.38 ± 0.06	0.67 ± 0.03	13/7/4
P-Value	0.34	0.24	0.097	0.4	0.28	

50 uM Picro	Rheobase (pA)	AP Amp. (mV)	AP Threshold (mV)	AP Duration (ms)	AP Half-Duration (ms)	n
Control	37.5 + 6.6	54.38 ± 1.33	-52.67 ± 0.79	1.15 ± 0.04	0.57 ± 0.02	16/8/3
Thalamic Astrogliosis	50.9 + 6.5	47.89 ± 1.77	-52.12 ± 0.84	1.25 ± 0.05	0.62 ± 0.03	22/9/4
P-Value	0.09	****0.0043**	0.69	0.25	0.29	

Table 4.8. Spontaneous excitatory and inhibitory post-synaptic currents in reticular thalamic neurons.

Data represented as mean ± SEM, compared using Mann-Whitney U Test. Last column ("n") indicates the number of cells, slices, and mice (respectively) for each condition.

Spontaneous Excitatory Post-Synaptic Currents (sEPSCs)

	Frequency (Hz)	Amplitude (pA)	Charge (fC)	Decay Tau (ms)	Rise Time (ms)	Half Width (ms)	n
Control	4.06 ± 0.66	-25.11 ± 0.80	-28.82 ± 1.28	0.70 ± 0.04	0.50 ± 0.009	0.72 ± 0.03	15/8/3
Thalamic Astrogliosis	2.96 ± 0.33	-23.83 ± 0.68	-31.24 ± 1.53	0.80 ± 0.04	0.48 ± 0.01	0.79 ± 0.04	15/6/3
P-Value	0.27	0.25	0.25	0.09	0.062	0.072	

Spontaneous Inhibitory Post-Synaptic Currents (sIPSCs)

	Frequency (Hz)	Amplitude (pA)	Charge (fC)	Decay Tau (ms)	Rise Time (ms)	Half Width (ms)	n
Control	0.78 ± 0.22	-15.37 ± 0.81	-1720 ± 93	64.68 ± 5.86	5.07 ± 0.78	45.66 ± 5.06	10/6/5
Thalamic Astrogliosis	0.69 ± 0.21	-18.34 ± 2.73	-2044 ± 617	75.07 ± 11.35	6.22 ± 1.55	46.68 ± 9.31	8/6/4
P-Value	0.76	0.83	0.32	0.57	0.68	0.63	

Table 4.9. Comparison of S1 ECoG spectral features.

Comparison of S1 ECoG power across different frequency bands, seven weeks following induction of thalamic astrogliosis. P-Values obtained from Wilcoxon matched-pairs signed rank test (non-parametric equivalent of paired t-test) between contralateral S1 and ipsilateral S1 in each group across different frequency bands. *$P<0.05$. Control: n=6 mice; Thalamic Astrogliosis: n=6 mice; Control+GAT-3: n=3 mice; Thalamic Astrogliosis+GAT-3: n=3 mice.

Frequency Band	Light Cycle		Dark Cycle	
	Control	Thalamic Astrogliosis	Control	Thalamic Astrogliosis
	n=6	n=6	n=6	n=6
Delta (1-4 Hz)	0.688	>0.99	0.844	0.844
Theta (4-8 Hz)	0.563	0.563	0.844	>0.99
Alpha (8-12 Hz)	0.844	0.156	>0.99	>0.99
Sigma (12-15 Hz)	0.563	***0.031**	0.844	0.219
Beta (15-30 Hz)	>0.99	0.156	0.688	0.063
Gamma (30-75 Hz)	>0.99	0.094	0.844	***0.031**
Total (1-75 Hz)	0.688	0.563	>0.99	0.563

Frequency Band	Light Cycle		Dark Cycle	
	Control +GAT-3	Thalamic Astrogliosis +GAT-3	Control +GAT-3	Thalamic Astrogliosis +GAT-3
	n=3	n=4	n=3	n=4
Delta (1-4 Hz)	0.25	0.375	0.57	0.875
Theta (4-8 Hz)	0.75	0.875	0.5	0.875
Alpha (8-12 Hz)	0.75	0.875	0.5	0.875
Sigma (12-15 Hz)	0.99	0.875	0.5	0.625
Beta (15-30 Hz)	0.5	0.875	0.5	0.875
Gamma (30-75 Hz)	0.5	0.875	0.5	0.875
Total (1-75 Hz)	0.5	0.875	0.5	0.875

Table 4.10. Data quality control for 10x Visium spatial transcriptomics analysis of mouse brain after cortical injury.

Data QC Measure	Sham	Stroke	TBI
Number of Spots Under Tissue	2,321	2,216	2,214
Mean Reads per Spot	71,181	112,417	161,322
Median Genes per Spot	4,870	5,080	5,326
Sequencing			
Number of Reads	165,211,061	249,115,248	357,166,098
Valid Barcodes	96.8%	96.7%	96.5%
Valid UMIs	100.0%	100.0%	100.0%
Sequencing Saturation	68.1%	76.4%	83.3%
Q30 Bases in Barcode	96.2%	96.3%	96.3%
Q30 Bases in RNA Read	94.7%	94.8%	94.2%
Q30 Bases in UMI	96.0%	96.2%	96.2%
Mapping			
Reads Mapped to Genome	92.9%	92.4%	95.6%
Reads Mapped Confidently to Genome	90.8%	90.1%	93.5%
Reads Mapped Confidently to Intergenic Regions	4.8%	5.4%	4.8%
Reads Mapped Confidently to Intronic Regions	2.7%	3.4%	3.5%
Reads Mapped Confidently to Exonic Regions	83.3%	81.3%	85.3%
Reads Mapped Confidently to Transcriptome	81.6%	79.6%	83.5%
Reads Mapped Antisense to Gene	0.9%	0.8%	0.8%
Spots			
Fraction Reads in Spots Under Tissue	93.0%	92.7%	92.5%
Mean Reads per Spot	71,181	112,417	161,322
Mean Reads Under Tissue per Spot	63,568	99,299	142,732
Median UMI Counts per Spot	15,797	16,812	18,341
Median Genes per Spot	4,870	5,080	5,326
Total Genes Detected	20,489	21,007	21,447

n=1 hemisection for each condition

Other Supplementary Materials for Chapter 4 includes the following:
Data file S1: Data (provided as supplementary Excel file).
Data file S2: Bulk RNASeq data (provided as supplementary Excel file).

References

Abel D, Shen MY, Abid Z, Hennigan C, Boneparth A, Miller EH, Uhlemann AC, McBrian DK, Thakur K, Silver W, Bain JM. 2020. Encephalopathy and bilateral thalamic lesions in a child with MIS-C associated with COVID-19. *Neurology* **95**:745–748. doi:10.1212/WNL.0000000000010652

Agmon A, Yang LT, O'Dowd DK, Jones EG. 1993. Organized growth of thalamocortical axons from the deep tier of terminations into layer IV of developing mouse barrel cortex. *J Neurosci* **13**:5365–5382. doi:10.1523/jneurosci.13-12-05365.1993

Andrade P, Nissinen J, Pitkänen A. 2017. Generalized Seizures after Experimental Traumatic Brain Injury Occur at the Transition from Slow-Wave to Rapid Eye Movement Sleep. *J Neurotrauma* **34**:1482–1487. doi:10.1089/neu.2016.4675

Beattie GC, Glaser CA, Sheriff H, Messenger S, Preas CP, Shahkarami M, Venkatesan A. 2013. Encephalitis with thalamic and basal ganglia abnormalities: Etiologies, neuroimaging, and potential role of respiratory viruses. *Clin Infect Dis* **56**:825–832. doi:10.1093/cid/cis990

Beenhakker MP, Huguenard JR. 2010. Astrocytes as gatekeepers of GABAB receptor function. *J Neurosci* **30**:15262–76. doi:10.1523/JNEUROSCI.3243-10.2010

Burda JE, Sofroniew M V. 2014. Review Reactive Gliosis and the Multicellular Response to CNS Damage and Disease. *Neuron* **81**:229–248. doi:10.1016/j.neuron.2013.12.034

Cao Z, Harvey SS, Bliss TM, Cheng MY, Steinberg GK. 2020. Inflammatory Responses in the Secondary Thalamic Injury After Cortical Ischemic Stroke. *Front Neurol* **11**:1–12. doi:10.3389/fneur.2020.00236

Cho FS, Clemente A, Holden S, Paz JT. 2017. Thalamic Models of Seizures In Vitro. Pitkänen,

Buckmaster, Galanopoulou, Moshé (Editors): Models of Seizures and Epilepsy, Second Edition. Academic Press. pp. 273–284. doi:10.1016/B978-0-12-804066-9.00019-5

Clarkson AN, Huang BS, Macisaac SE, Mody I, Carmichael ST. 2010. Reducing excessive GABA-mediated tonic inhibition promotes functional recovery after stroke. *Nature* **468**:305–309. doi:10.1038/nature09511

Colombo E, Farina C. 2016. Astrocytes: Key Regulators of Neuroinflammation. *Trends Immunol* **37**:608–620. doi:10.1016/j.it.2016.06.006

Cope DW, Di Giovanni G, Fyson SJ, Orbán G, Errington AC, Lőrincz ML, Gould TM, Carter DA, Crunelli V. 2009. Enhanced tonic GABAA inhibition in typical absence epilepsy. *Nat Med* **15**:1392–1398. doi:10.1038/nm.2058.Enhanced

Cope DW, Hughes SW, Crunelli V. 2005. GABAA Receptor-Mediated Tonic Inhibition in Thalamic Neurons. *J Neurosci* **25**:11553–11563. doi:10.1523/JNEUROSCI.3362-05.2005

Coulter DA, Huguenard JR, Prince DA. 1989. Calcium currents in rat thalamocortical relay neurones: kinetic properties of the transient, low-threshold current. *J Physiol* **414**:587–604.

Crunelli V, Hughes SW. 2010. The slow (1 Hz) rhythm of non-REM sleep: A dialogue between three cardinal oscillators. *Nat Neurosci* **13**:9–17. doi:10.1038/nn.2445

Cueni L, Canepari M, Luján R, Emmenegger Y, Watanabe M, Bond CT, Franken P, Adelman JP, Lüthi A. 2008. T-type Ca 2+ channels, SK2 channels and SERCAs gate sleep-related oscillations in thalamic dendrites. *Nat Neurosci* **11**:683–692. doi:10.1038/nn.2124

De Biasi S, Vitellaro-Zuccarello L, Brecha NC. 1998. Immunoreactivity for the GABA transporter-1 and GABA transporter-3 is restricted to astrocytes in the rat thalamus. A light and electron- microscopic immunolocalization. *Neuroscience* **83**:815–828.

doi:10.1016/S0306-4522(97)00414-4

Escartin C, Galea E, Lakatos A, O'Callaghan JP, Petzold GC, Serrano-Pozo A, Steinhäuser C, Volterra A, Carmignoto G, Agarwal A, Allen NJ, Araque A, Barbeito L, Barzilai A, Bergles DE, Bonvento G, Butt AM, Chen W-T, Cohen-Salmon M, Cunningham C, Deneen B, De Strooper B, Díaz-Castro B, Farina C, Freeman M, Gallo V, Goldman JE, Goldman SA, Götz M, Gutiérrez A, Haydon PG, Heiland DH, Hol EM, Holt MG, Iino M, Kastanenka K V, Kettenmann H, Khakh BS, Koizumi S, Lee CJ, Liddelow SA, MacVicar BA, Magistretti P, Messing A, Mishra A, Molofsky A V, Murai KK, Norris CM, Okada S, Oliet SHR, Oliveira JF, Panatier A, Parpura V, Pekna M, Pekny M, Pellerin L, Perea G, Pérez-Nievas BG, Pfrieger FW, Poskanzer KE, Quintana FJ, Ransohoff RM, Riquelme-Perez M, Robel S, Rose CR, Rothstein JD, Rouach N, Rowitch DH, Semyanov A, Sirko S, Sontheimer H, Swanson RA, Vitorica J, Wanner I-B, Wood LB, Wu J, Zheng B, Zimmer ER, Zorec R, Sofroniew M V, Verkhratsky A. 2021. Reactive astrocyte nomenclature, definitions, and future directions. *Nat Neurosci*. doi:10.1038/s41593-020-00783-4

Ferreira TA, Blackman A V., Oyrer J, Jayabal S, Chung AJ, Watt AJ, Sjöström PJ, Van Meyel DJ. 2014. Neuronal morphometry directly from bitmap images. *Nat Methods* **11**:982–984. doi:10.1038/nmeth.3125

Fogerson PM, Huguenard JR. 2016. Tapping the Brakes: Cellular and Synaptic Mechanisms that Regulate Thalamic Oscillations. *Neuron* **92**:687–704. doi:10.1016/j.neuron.2016.10.024

Franklin KBJ, Paxinos G. 2007. The Mouse Brain in Stereotaxic Coordinates, 3rd Editio. ed. Elsevier Academic Press.

Grossman EJ, Ge Y, Jensen JH, Babb JS, Miles L, Reaume J, Silver JM, Grossman RI, Inglese M.

2012. Thalamus and Cognitive Impairment in Mild Traumatic Brain Injury: A Diffusional Kurtosis Imaging Study. *J Neurotrauma* **29**:2318–2327. doi:10.1089/neu.2011.1763

Grossman EJ, Inglese M. 2016. The role of thalamic damage in mild traumatic brain injury. *J Neurotrauma* **33**:163–167. doi:10.1089/neu.2015.3965

Guth JC, Futterer SA, Hijaz TA, Liotta EM, Rosenberg NF, Naidech AM, Maas MB. 2014. Pearls & Oy-sters: Bilateral thalamic involvement in West Nile virus encephalitis. *Neurology* **83**:16–17. doi:10.1212/WNL.0000000000000571

Hazra A, Macolino C, Elliott MB, Chin J. 2014. Delayed thalamic astrocytosis and disrupted sleep-wake patterns in a preclinical model of traumatic brain injury. *J Neurosci Res* **92**:1434–1445. doi:10.1002/jnr.23430

Hiu T, Farzampour Z, Paz JT, Wang EHJ, Badgely C, Olson A, Micheva KD, Wang G, Lemmens R, Tran K V., Nishiyama Y, Liang X, Hamilton SA, O'Rourke N, Smith SJ, Huguenard JR, Bliss TM, Steinberg GK. 2016. Enhanced phasic GABA inhibition during the repair phase of stroke: A novel therapeutic target. *Brain* **139**:468–480. doi:10.1093/brain/awv360

Holden SS, Grandi FC, Aboubakr O, Higashikubo B, Cho FS, Chang AH, Forero AO, Morningstar AR, Mathur V, Kuhn LJ, Suri P, Sankaranarayanan S, Andrews-Zwilling Y, Tenner AJ, Luthi A, Aronica E, Corces MR, Yednock T, Paz JT. 2021. Complement factor C1q mediates sleep spindle loss and epileptic spikes after mild brain injury. *Science* **373**. doi:10.1126/science.abj2685

Huntsman MM, Porcello DM, Homanics GE, DeLorey TM, Huguenard JR. 1999. Reciprocal Inhibitory Connections and Network Synchrony in the Mammalian Thalamus. *Science* **283**:541–543. doi:10.1126/science.283.5401.541

Jeanmonod D, Magnin M, Morel A. 1996. Low-threshold calcium spike bursts in the human thalamus: Common physiopathology for sensory, motor and limbic positive symptoms. *Brain* **119**:363–375. doi:10.1093/brain/119.2.363

Jo S, Yarishkin O, Hwang YJ, Chun YE, Park M, Woo DH, Bae JY, Kim T, Lee J, Chun H, Park HJ, Lee DY, Hong J, Kim HY, Oh SJ, Park SJ, Lee H, Yoon BE, Kim Y, Jeong Y, Shim I, Bae YC, Cho J, Kowall NW, Ryu H, Hwang E, Kim D, Lee CJ. 2014. GABA from reactive astrocytes impairs memory in mouse models of Alzheimer's disease. *Nat Med* **20**:886–896. doi:10.1038/nm.3639

Jones EG. 2001. The thalamic matrix and thalamocortical synchrony. *Trends Neurosci* **24**:595–601. doi:10.1016/S0166-2236(00)01922-6

Kelley KW, Nakao-Inoue H, Molofsky A V., Oldham MC. 2018. Variation among intact tissue samples reveals the core transcriptional features of human CNS cell classes. *Nat Neurosci* **21**:1171–1184. doi:10.1038/s41593-018-0216-z

Klein P, Dingledine R, Aronica E, Bernard C, Blümcke I, Boison D, Brodie MJ, Brooks-Kayal AR, Engel J, Forcelli PA, Hirsch LJ, Kaminski RM, Klitgaard H, Kobow K, Lowenstein DH, Pearl PL, Pitkänen A, Puhakka N, Rogawski MA, Schmidt D, Sillanpää M, Sloviter RS, Steinhäuser C, Vezzani A, Walker MC, Löscher W. 2018. Commonalities in epileptogenic processes from different acute brain insults: Do they translate? *Epilepsia* **59**:37–66. doi:10.1111/epi.13965

Lee TS, Bjørnsen LP, Paz C, Kim JH, Spencer SS, Spencer DD, Eid T, Lanerolle NC. 2006. GAT1 and GAT3 expression are differently localized in the human epileptogenic hippocampus. *Acta Neuropathol* **111**:351–363. doi:10.1007/s00401-005-0017-9

Lee V, Maguire J. 2014. The impact of tonic GABAA receptor-mediated inhibition on neuronal excitability varies across brain region and cell type. *Front Neural Circuits* **8**:1–27. doi:10.3389/fncir.2014.00003

Lee V, Maguire J. 2013. Impact of inhibitory constraint of interneurons on neuronal excitability. *J Neurophysiol* **110**:2520–2535. doi:10.1152/jn.00047.2013

Liddelow SA, Guttenplan KA, Clarke LE, Bennett FC, Bohlen CJ, Schirmer L, Bennett ML, Münch AE, Chung W-S, Peterson TC, Wilton DK, Frouin A, Napier BA, Panicker N, Kumar M, Buckwalter MS, Rowitch DH, Dawson VL, Dawson TM, Stevens B, Barres BA. 2017. Neurotoxic reactive astrocytes are induced by activated microglia. *Nature* **541**:481–487. doi:10.1038/nature21029

Llorente IL, Xie Y, Mazzitelli JA, Hatanaka EA, Cinkornpumin J, Miller DR, Lin Y, Lowry WE, Carmichael ST. 2021. Patient-derived glial enriched progenitors repair functional deficits due to white matter stroke and vascular dementia in rodents. *Sci Transl Med* **13**:1–18. doi:10.1126/scitranslmed.aaz6747

Lu AC, Lee CK, Kleiman-Weiner M, Truong B, Wang M, Huguenard JR, Beenhakker MP. 2020. Nonlinearities between inhibition and t-type calcium channel activity bidirectionally regulate thalamic oscillations. *Elife* **9**:1–36. doi:10.7554/ELIFE.59548

Maguire JL, Stell BM, Rafizadeh M, Mody I. 2005. Ovarian cycle-linked changes in GABAA receptors mediating tonic inhibition alter seizure susceptibility and anxiety. *Nat Neurosci* **8**:797–804. doi:10.1038/nn1469

Maroso M, Balosso S, Ravizza T, Liu J, Aronica E, Iyer AM, Rossetti C, Molteni M, Casalgrandi M, Manfredi AA, Bianchi ME, Vezzani A. 2010. Toll-like receptor 4 and high-mobility group

box-1 are involved in ictogenesis and can be targeted to reduce seizures. *Nat Med* **16**:413–419. doi:10.1038/nm.2127

Maxwell WL, MacKinnon MA, Smith DH, McIntosh TK, Graham DI. 2006. Thalamic nuclei after human blunt head injury. *J Neuropathol Exp Neurol* **65**:478–488. doi:10.1097/01.jnen.0000229241.28619.75

Morel L, Higashimori H, Tolman M, Yang Y. 2014. VGluT1+ Neuronal Glutamatergic signaling regulates postnatal developmental maturation of cortical protoplasmic astroglia. *J Neurosci* **34**:10950–10962. doi:10.1523/JNEUROSCI.1167-14.2014

Necula D, Cho FS, He A, Paz JT. 2021. Secondary thalamic neuroinflammation after focal cortical stroke and traumatic injury mirrors corticothalamic functional connectivity. *J Comp Neurol*. doi:10.1002/cne.25259

Ortinski PI, Dong J, Mungenast A, Yue C, Takano H, Watson DJ, Haydon PG, Coulter DA. 2010. Selective induction of astrocytic gliosis generates deficits in neuronal inhibition. *Nat Neurosci* **13**:584–91. doi:10.1038/nn.2535

Ouellet MC, Beaulieu-Bonneau S, Morin CM. 2015. Sleep-wake disturbances after traumatic brain injury. *Lancet Neurol* **14**:746–757. doi:10.1016/S1474-4422(15)00068-X

Pappata S, Levasseur M, Gunn RN, Myers R, Crouzel C, Syrota A, Jones T, Kreutzberg GW, Banati RB. 2000. Thalamic microglial activation in ischemic stroke detected in vivo by PET and [(11)C]PK11195. *Neurology* **55**:1052–1054. doi:10.1212/WNL.55.7.1052

Patel DC, Tewari BP, Chaunsali L, Sontheimer H. 2019. Neuron–glia interactions in the pathophysiology of epilepsy. *Nat Rev Neurosci* **20**:282–297. doi:10.1038/s41583-019-0126-4

Paz JT, Bryant AS, Peng K, Fenno L, Yizhar O, Frankel WN, Deisseroth K, Huguenard JR. 2011. A new mode of corticothalamic transmission revealed in the Gria4(-/-) model of absence epilepsy. *Nat Neurosci* **14**:1167–73. doi:10.1038/nn.2896

Paz JT, Christian CA, Parada I, Prince DA, Huguenard JR. 2010. Focal Cortical Infarcts Alter Intrinsic Excitability and Synaptic Excitation in the Reticular Thalamic Nucleus. *J Neurosci* **30**:5465–5479. doi:10.1523/JNEUROSCI.5083-09.2010

Paz JT, Davidson TJ, Frechette ES, Delord B, Parada I, Peng K, Deisseroth K, Huguenard JR. 2013. Closed-loop optogenetic control of thalamus as a tool for interrupting seizures after cortical injury. *Nat Neurosci* **16**:64–70. doi:10.1038/nn.3269

Paz JT, Huguenard JR. 2015. Microcircuits and their interactions in epilepsy: is the focus out of focus? *Nat Neurosci* **18**:351–9. doi:10.1038/nn.3950

Pirttimaki T, Parri HR, Crunelli V. 2013. Astrocytic GABA transporter GAT-1 dysfunction in experimental absence seizures. *J Physiol* **591**:823–33. doi:10.1113/jphysiol.2012.242016

Poyiadji N, Shahin G, Noujaim D, Stone M, Patel S, Griffith B. 2020. COVID-19-associated acute hemorrhagic necrotizing encephalopathy: Imaging features. *Radiology* **296**:E119–E120. doi:10.1148/radiol.2020201187

Ramlackhansingh AF, Brooks DJ, Greenwood RJ, Bose SK, Turkheimer FE, Kinnunen KM, Gentleman S, Heckemann RA, Gunanayagam K, Gelosa G, Sharp DJ. 2011. Inflammation after trauma: Microglial activation and traumatic brain injury. *Ann Neurol* **70**:374–383. doi:10.1002/ana.22455

Ritter-Makinson S, Clemente-Perez A, Higashikubo B, Cho FS, Holden SS, Bennett E, Chkaidze A, Rooda OHJE, Cornet MC, Hoebeek FE, Yamakawa K, Cilio MR, Delord B, Paz JT. 2019.

Augmented Reticular Thalamic Bursting and Seizures in Scn1a-Dravet Syndrome. *Cell Rep* **26**:54–64. doi:10.1016/j.celrep.2018.12.018

Robel S, Buckingham SC, Boni JL, Campbell SL, Danbolt NC, Riedemann T, Sutor B, Sontheimer H. 2015. Reactive Astrogliosis Causes the Development of Spontaneous Seizures. *J Neurosci* **35**:3330–3345. doi:10.1523/JNEUROSCI.1574-14.2015

Robel S, Sontheimer H. 2016. Glia as drivers of abnormal neuronal activity. *Nat Neurosci* **19**:28–33. doi:10.1038/nn.4184

Russo M V., McGavern DB. 2016. Inflammatory neuroprotection following traumatic brain injury. *Science* **353**:783–785. doi:10.1126/science.aaf6260

Schijns OEMG, Bisschop J, Rijkers K, Dings J, Vanherle S, Lindsey P, Smeets HJM, Hoogland G. 2020. GAT-1 (rs2697153) and GAT-3 (rs2272400) polymorphisms are associated with febrile seizures and temporal lobe epilepsy. *Epileptic Disord* **22**:176–182. doi:10.1684/epd.2020.1154

Schousboe A, Bak LK, Waagepetersen HS. 2013. Astrocytic control of biosynthesis and turnover of the neurotransmitters glutamate and GABA. *Front Endocrinol (Lausanne)* **4**:1–11. doi:10.3389/fendo.2013.00102

Scott G, Hellyer PJ, Ramlackhansingh AF, Brooks DJ, Matthews PM, Sharp DJ. 2015. Thalamic inflammation after brain trauma is associated with thalamo-cortical white matter damage. *J Neuroinflammation* **12**:1–5. doi:10.1186/s12974-015-0445-y

Senatorov V V., Friedman AR, Milikovsky DZ, Ofer J, Saar-Ashkenazy R, Charbash A, Jahan N, Chin G, Mihaly E, Lin JM, Ramsay HJ, Moghbel A, Preininger MK, Eddings CR, Harrison H V., Patel R, Shen Y, Ghanim H, Sheng H, Veksler R, Sudmant PH, Becker A, Hart B,

Rogawski MA, Dillin A, Friedman A, Kaufer D. 2019. Blood-brain barrier dysfunction in aging induces hyper-activation of TGF-beta signaling and chronic yet reversible neural dysfunction. *Sci Transl Med* **11**. doi:10.1101/537431

Shi SX, Shi K, Liu Q. 2021. Brain injury instructs bone marrow cellular lineage destination to reduce neuroinflammation. *Sci Transl Med* **13**:eabc7029.

Simon DW, McGeachy MJ, Baylr H, Clark RSB, Loane DJ, Kochanek PM. 2017. The far-reaching scope of neuroinflammation after traumatic brain injury. *Nat Rev Neurol* **13**:171–191. doi:10.1038/nrneurol.2017.13

Sorokin JM, Davidson TJ, Frechette E, Abramian AM, Deisseroth K, Huguenard JR, Paz JT. 2017. Bidirectional Control of Generalized Epilepsy Networks via Rapid Real-Time Switching of Firing Mode. *Neuron* **93**:194–210. doi:10.1016/j.neuron.2016.11.026

Steinhäuser C, Seifert G. 2012. Astrocyte dysfunction in epilepsyNoebels, JL, Avoli M, Rogawski MA, et Al., Editors. Jasper's Basic Mechanisms of the Epilepsies. 4th Edition. Bethesda (MD): National Center for Biotechnology Information (US). doi:10.1016/j.brainresrev.2009.10.004

Steriade M, Contreras D, Amzica F, Timofeev I. 1996. Synchronization of fast (30-40 Hz) spontaneous oscillations in intrathalamic and thalamocortical networks. *J Neurosci* **16**:2788–2808. doi:10.1523/jneurosci.16-08-02788.1996

Steriade M, McCormick DA, Sejnowski TJ. 1993. Thalamocortical oscillations in the sleeping and aroused brain. *Science* **262**:679–85. doi:10.1126/science.8235588

Sun D, Jakobs TC. 2012. Structural remodeling of astrocytes in the injured CNS. *Neuroscientist* **18**:567–588. doi:10.1177/1073858411423441

Vainchtein ID, Chin G, Cho FS, Kelley KW, Miller JG, Chien EC, Liddelow SA, Nguyen PT, Nakao-inoue H, Dorman LC, Akil O, Joshita S, Barres BA, Paz JT, Molofsky AB, Molofsky A V. 2018. Astrocyte-derived interleukin-33 promotes microglial synapse engulfment and neural circuit development. *Science* **359**:1269–1273.

Vezzani A, Balosso S, Ravizza T. 2019. Neuroinflammatory pathways as treatment targets and biomarkers in epilepsy. *Nat Rev Neurol* **15**:459–472. doi:10.1038/s41582-019-0217-x

Vitellaro-Zuccarello L, Calvaresi N, De Biasi S. 2003. Expression of GABA transporters, GAT-1 and GAT-3, in the cerebral cortex and thalamus of the rat during postnatal development. *Cell Tissue Res* **313**:245–257. doi:10.1007/s00441-003-0746-9

Wagnon JL, Korn MJ, Parent R, Tarpey TA, Jones JM, Hammer MF, Murphy GG, Parent JM, Meisler MH. 2015. Convulsive seizures and SUDEP in a mouse model of SCN8A epileptic encephalopathy. *Hum Mol Genet* **24**:506–515. doi:10.1093/hmg/ddu470

Wu Z, Guo Z, Gearing M, Chen G. 2014. Tonic inhibition in dentate gyrus impairs long-term potentiation and memory in an Alzhiemer' s disease model. *Nat Commun* **5**:1–13. doi:10.1038/ncomms5159

Yu X, Taylor AMW, Nagai J, Golshani P, Evans CJ, Coppola G, Khakh BS. 2018. Reducing Astrocyte Calcium Signaling In Vivo Alters Striatal Microcircuits and Causes Repetitive Behavior. *Neuron* **99**:1170-1187.e9. doi:10.1016/j.neuron.2018.08.015

Zamanian J, Xu L, Foo L, Nouri N, Zhou L, Giffard R, Barres B. 2012. Genomic Analysis of Reactive Astrogliosis. *J Neurosci* **32**:6391–6410. doi:10.1523/JNEUROSCI.6221-11.2012.Genomic

Zheng J, Wong LYR, Li K, Verma AK, Ortiz M, Wohlford-Lenane C, Leidinger MR, Knudson

CM, Meyerholz DK, McCray PB, Perlman S. 2020. COVID-19 treatments and pathogenesis including anosmia in K18-hACE2 mice. *Nature*. doi:10.1038/s41586-020-2943-z

Chapter 5 : Discussion

5.1. Summary

In this dissertation, we have aimed to integrate astrocytes into the canonical circuit diagram of the thalamus. We now further understand the critical role astrocytes play in shaping the developing thalamus of rodents by providing a key immune signal—IL-33—to control the number of excitatory synapses (**Chapter 3**). Its absence can lead to runaway excitation in the thalamus, paving the path for epileptic activity in mice, as we discuss below. We thus identified a novel astrocytic mechanism capable of triggering pro-epileptic circuit activity in the thalamus. We also identified an aspect of reactive astrocytes—GAT-3 loss of function—sufficient to confer pathological excitability in an otherwise normal thalamic circuit, and one which may underlie thalamic dysfunction observed in cases of brain injuries (**Chapter 4**). By selectively modeling one aspect of secondary damage observed in brain injuries, we found that it could recapitulate several key pathological features, providing strong evidence that reactive astrocytes in the thalamus can be drivers, rather than mere bystanders, of pathological sequelae following injuries such as post-traumatic epilepsy and sleep disruption. Furthermore, we found that enhancing GAT-3 conferred resilience in a mouse model of traumatic brain injury. Altogether, our findings add to the growing evidence supporting the critical role of astrocytes in the modulation of physiological and pathological neural circuits. In **Chapter 5**, we discuss our findings in the context of stable versus flexible modulation of thalamic synapses, as well as common pathways of astrocytic function in brain development and degeneration; we also speculate on the potential role of astrocyte networks in mediating the distinctive computational properties of the reticular thalamic nucleus.

5.2. Stability and flexibility in astrocytic modulation of thalamic synapses

We identified two mechanisms of astrocytic control of thalamic synapses: control of excitatory synapse number (and therefore, excitatory drive) by IL-33 and dysregulation of GABAergic tone by GAT-3. These two mechanisms, identified in different contexts (development and disease), also illustrate distinct forms of astrocytic regulation of thalamic synapses. In the case of astrocytic IL-33, by promoting microglial phagocytic activity, astrocytes enable a permanent way to fine-tune excitatory drive and thereby ensure circuit stability. This is in contrast to other recently identified mechanisms of glial feedback control of neuronal activity (Badimon et al., 2020). GAT-3 loss of function in thalamic reactive astrocytes, although consequential, represents a more flexible method of modulating the thalamic circuit in that it changes the threshold for neuronal excitability. In theory, the loss of GAT-3 and its consequences (i.e. enhanced tonic inhibition in neighboring neurons) may be compensated for, even after its occurrence, with cell- or synapse-specific therapeutic strategies such as exogenously driving enhanced GAT-3 expression in astrocytes via adeno-associated viral vectors (as discussed in Chapter 4). These results warrant further investigations of methods to compensate for GAT-3 function, such as intra-thalamic infusion of pharmacological inhibitors of delta-subunit containing $GABA_A$ receptors, or stimulating the production and/or surface trafficking of GAT-1 in either thalamic astrocytes or neurons.

5.3. Contributions of astrocyte IL-33 and GAT-3 to brain development and degeneration

Given the diverse ways in which astrocytes shape synaptic formation and function during brain development and beyond, it's unsurprising that dysfunction of astrocytes has been suggested to contribute to a variety of neurodevelopmental disorders (reviewed by Sloan and Barres, 2014), psychiatric disorders (reviewed by Verkhratsky and Parpura, 2016), and neurodegenerative

diseases (reviewed by Haim et al., 2015; Rodríguez-Arellano et al., 2016) and neurological disorders such as epilepsy (reviewed by Aronica et al., 2012; Patel et al., 2019; Vezzani et al., 2019). There is mounting evidence implicating common processes underlying neurodevelopmental and neurodegenerative disorders. For example, postnatal reduction of tau—a protein long implicated in Alzheimer's disease—was recently shown to counteract epilepsy and autism-like behaviors in a mouse model of Dravet syndrome, a severe epileptic encephalopathy of early childhood (Shao et al., 2022). In another example, the beneficial role of microglia and the classical complement pathway in synapse development during early postnatal life has also been shown to "reactivate" during the aging process and promote cognitive decline, hyperexcitability in thalamic circuits, neurodegeneration, and obsessive-compulsive disorder-like grooming behavior in mice (Lui et al., 2016; Stevens et al., 2007). Furthermore, aberrant activation of the complement pathway mediates epileptic spikes and sleep spindle loss following brain injury in adult mice (Holden et al., 2021).

Thus, it is plausible that aberrant IL-33 in thalamic astrocytes—although identified for its role in development—shapes vulnerability at both ends of the age spectrum. Indeed, building upon findings presented in Chapter 3, we recently found that conditional deletion of IL-33 in the central nervous system—which leads to excess corticothalamic excitatory synapses and decreased inhibitory synapses onto glutamatergic thalamocortical neurons in the somatosensory thalamus—results in spontaneous spike-and-wave discharges resembling typical absence epileptic seizures associated with corticothalamic circuit dysfunction (Han et al., 2021). Recent studies have found a role for IL-33 in neurodegenerative conditions, although the cellular source of IL-33 is at times unclear (e.g. astrocytes vs. neurons vs. oligodendrocytes). In a mouse model of AD, stimulating IL-33 signaling or exogenous IL-33 administration rescued contextual memory deficits and

reduced the accumulation of beta-amyloid; this rescue was attributed to IL-33 induced activation of phagocytic activity and anti-inflammatory gene expression in microglia (Fu et al., 2016). A recent study of patients with mild cognitive impairment reported that improvements in episodic memory following homotaurine treatment correlated with elevated serum levels of IL-33 (Toppi et al., 2022). Similarly, it is plausible that dysfunction of GABA transporters in thalamic astrocytes shapes brain vulnerability at both ends of the age spectrum (discussed in next section).

5.4. Astrocytic GAT-3 – a critical node of network dysfunction

Our demonstration that reactive astrocytes in the thalamus can dysregulate GABA by downregulating GAT-3, in a way that leads to network hyperexcitability and aberrant cortical rhythms, adds to the growing body of evidence implicating astrocytic GABA transporters in diseases characterized by network dysfunction.

Across an array of disease models and brain regions, the role of altered GABA modulation in reactive astrocytes has gained moderate attention in recent years (reviewed by Escartin et al., 2021; Ishibashi et al., 2019; Patel et al., 2019; Robel and Sontheimer, 2016). Several studies have reported alterations in the metabolism and release of GABA by reactive astrocytes (Chun et al., 2018; Jo et al., 2014; Ortinski et al., 2010; Woo et al., 2017). However, altered GABA modulation can also arise from dysfunctional GABA uptake.

GAT-1 and GAT-3 are the main GABA transporters in the mammalian brain, and there is mounting evidence implicating GABA transporters in disease. Recent studies have identified mutations in *SLC6A1* (encoding GAT-1) as risk factors for autism spectrum disorder (ASD) (Satterstrom et al., 2020), and as a monogenic cause of a spectrum of related neurodevelopmental disorders including epilepsy, autism, motor dysfunction, and developmental delay (reviewed by

Goodspeed et al., 2020), and the exact mechanisms of GAT-1 dysfunction on brain function are currently under investigation.

There is sufficient evidence to suggest regional differences in the relative expression of GAT-1 and GAT-3 in astrocytes and neurons, which will be an important consideration for future investigations. In the rodent external segment of the globus pallidus, GAT-1 is found in both neurons and glial processes while GAT-3 is exclusively located on glial processes (Chazalon et al., 2018). In the stratum radiatum of the rodent hippocampus, GAT-3 but not GAT-1 is colocalized with astrocytic markers, suggesting GAT-3 is astrocytic and GAT-1 is neuronal (Shigetomi et al., 2012). In contrast, in the rodent thalamus, ultrastructural studies suggest that both GAT-1 and GAT-3 are exclusively expressed by astrocytes (De Biasi et al., 1998; Vitellaro-Zuccarello et al., 2003), with distinct subcellular localization (near and far from synapses, respectively) (Beenhakker and Huguenard, 2010). Data obtained from a public transcriptomic profiling of neurotypical adult brain tissue (Kelley et al., 2018) revealed that in the thalamus-containing diencephalon, expression of *SLC6A11* (encoding GAT-3) is highly correlated to an astrocyte transcriptional signature and not to neurons, while expression of *SLC6A1* (encoding GAT-1) is similarly correlated to astrocytic and neuronal transcriptional signatures (Chapter 4). Although there may be regional differences in the specificity and exclusivity of GAT-1 and GAT-3 expression, it is nonetheless clear that they enable astrocytes to play a key role in the reuptake of GABA from the extracellular space (Gadea and López-Colomé, 2001; Kersanté et al., 2013).

In animal models, abnormal astrocytic GAT expression and/or function has been implicated in epilepsy (Cope et al., 2009), stroke (Clarkson et al., 2010; Frahm et al., 2004), Alzheimer's disease (Jo et al., 2014), Parkinson's disease (Chazalon et al., 2018), and Huntington's disease (Wójtowicz et al., 2013; Yu et al., 2018). While most of these studies have focused on

GAT dysfunction in non-reactive astrocytes, there have been separate reports of reactive astrocytes in several of these animal models exhibiting abnormal astrocytic GATs (Chazalon et al., 2018; Huang et al., 2014; Wójtowicz et al., 2013), suggesting an indirect link between dysregulation of GABA uptake and reactive astrocytes. Evidence of *Slc6a11* (encoding GAT-3) downregulation in reactive astrocytes can be found in recent transcriptomic surveys of spinal cord injury in mice (publicly available data published in Anderson et al., 2016), as well as in human post-mortem entorhinal cortex and superior frontal gyrus of individuals with Alzheimer's disease (Leng et al., 2021). Because *Slc6a11* downregulation was merely one of numerous changes observed at a single timepoint in these disease contexts, its functional consequence remained unknown.

Our results are the first to identify GAT-3 loss of function as a mechanistic link which enables reactive astrocytes to mediate maladaptive consequences in neighboring neurons and circuits in the thalamus. We propose that GAT-3 loss of function in thalamic reactive astrocytes—which we observe in multiple preclinical models with secondary thalamic damage as well as in post-mortem thalamic tissue—is a key component of reactive astrocyte dysfunction in the thalamus. Furthermore, our finding that enhancing astrocytic GAT-3 in the thalamus was protective against severe chemoconvulsant-induced seizures and mortality in a mouse model of traumatic brain injury raises the possibility that targeting GAT-3 loss of function may be a broadly useful therapeutic strategy to promote brain resilience.

The occurrence, consequences, and modifiability of GAT-3 loss of function in reactive astrocytes of other brain regions remains to be determined. It also remains unclear the exact upstream mechanisms leading to GAT-3 loss of function in thalamic reactive astrocytes. There is evidence that in the striatum and hippocampus, astrocyte intracellular calcium levels affect GAT-3 functional expression, likely involving posttranslational modifications of GAT-3 trafficking to

the cell membrane (Shigetomi et al., 2012; Yu et al., 2018). Inflammatory mediators alter calcium signaling in astrocytes (Hamby et al., 2012), and changes in calcium dynamics have been reported in reactive astrocytes (Escartin et al., 2021; Shigetomi et al., 2016). Thus, investigating the spatiotemporal dynamics of calcium signaling in reactive astrocytes in the secondarily damaged thalamus may shed light on whether a similar cascade of intracellular signaling leads to GAT-3 dysfunction in pathological contexts.

Ultimately, whether loss of GAT-3 will have a functional consequence on local neurons and circuit may largely depend on the local milieu: the palette of GABA receptor subunit expression and localization, the consequences of GABAergic synaptic and extrasynaptic transmission on neuronal excitability, and whether neighboring neurons and/or astrocytes are capable of compensating for loss of GAT-3. Indeed, I_{TONIC}—which is affected by GAT-3 function—can have different effects on neural circuits depending on properties of the local environment (Lee and Maguire, 2014). For example, enhanced I_{TONIC} renders neurons hypoexcitable in many brain regions such as the cerebellum and hippocampus (Lee and Maguire, 2014). In contrast, in the thalamus, enhanced I_{TONIC} renders neurons hyperexcitable due to their expression of low-threshold T-type Ca^{2+} channels, which are de-inactivated upon hyperpolarization and lead to enhanced burst firing mode (Cope et al., 2005).

5.5. Computational properties of thalamocortical circuits enabled by astrocytes

There is a recent compelling push to integrate astrocytes into systems neuroscience, and conversely, for glial biologists to consider systems neuroscience frameworks (Kastanenka et al., 2020). The burgeoning field of astrocyte biology has generated plenty of evidence supporting the role of astrocytes in modulating local neural circuits and complex behaviors. In their review,

Kastanenka and colleagues propose that astrocytes are well-poised to carry out canonical computations in the brain, such as gain control, coincidence detection, thresholding, and state switching. Such computations are proposed to be enabled by qualities such as the dynamic spatial and temporal properties of astrocytic calcium activity, their close proximity to many synapses, and their ability to respond to and modulate neuronal activity and sensory inputs.

Of particular relevance to the findings described in this dissertation is the ability of astrocytes to mediate switches in network states. Thalamocortical circuits form parallel channels for processing information from distinct modalities (Halassa and Sherman, 2019; Shepherd and Yamakawi, 2021). Coordination across thalamic circuits and thalamocortical circuits is likely required for cohesive perception and attention. Among several sources of thalamic modulation, the reticular thalamic nucleus (nRT)—the GABAergic nucleus strategically positioned between thalamic relay nuclei and cortex—has received considerable support as a "gatekeeper" of thalamic processing (Crick, 1984), capable of switching thalamic output between distinct channels. Intra-nRT connections themselves are proposed to critically control synchrony of thalamic network oscillations (Sohal and Huguenard 2003; Huntsman et al., 1999); cortico-nRT-relay connections, providing feed forward inhibition to thalamic relay neurons, facilitate behavioral attention in the presence of conflicting sensory cues (Ahrens et al., 2015). Kastanenka and colleagues suggest that astrocytes may synchronize brain state through gain control by regulating a network's ratio of excitation versus inhibition, which may be achieved through various mechanisms such as the reduction of glutamate uptake (Poskanzer and Yuste, 2016), calcium-dependent release of ATP/adenosine and glutamate (Fellin et al., 2009; Halassa et al., 2009), or taking up GABA via GAT-3 (Shigetomi et al., 2011). Indeed, the GAT-3 loss of function we identified in thalamic reactive astrocytes led to an imbalance in cortical rhythmic activity (discussed in Chapter 4).

Although it remains unknown whether or not thalamic astrocytes form gap-junctionally coupled networks which adhere to the neural circuit motifs, thalamic astrocyte networks seem well-poised to contribute to the dynamic switching capacity of the nRT and thereby contribute to key neural computations.

While much is known about thalamus with respect to its anatomy, structure, rhythmogenic properties, and relay functions of sensory nuclei, recent questions in the field have turned their focus towards the role of thalamus in mediating higher-order cognitive processes (reviewed by Krol et al., 2018; Perry et al., 2021; Saalmann and Kastner, 2015) in health and disease. Cognitive processes, unlike most sensory processes, tend to operate on a longer timescale and involve a diverse range of inputs and outputs. Astrocytes are well-positioned to facilitate such processes requiring flexibility in space and time. There are many unanswered, outstanding questions which are being tackled with impressive technologies and innovative frameworks, and surely a systematic integration of astrocytes—beyond their effects at the synaptic level—into thalamocortical circuit function will only serve to improve our understanding of the thalamus, in health and disease.

References

Anderson MA, Burda JE, Ren Y, Ao Y, Shea TMO, Kawaguchi R, Coppola G, Khakh BS, Deming TJ, Michael V. 2016. Astrocyte scar formation aids central nervous system axon regeneration. *Nature* **532**:195–200. doi:10.1038/nature17623

Aronica E, Bauer S, Bozzi Y, Caleo M, Dingledine R, Gorter JA, Henshall DC, Kaufer D, Koh S, Löscher W, Louboutin JP, Mishto M, Norwood BA, Palma E, Poulter MO, Terrone G, Vezzani A, Kaminski RM. 2017. Neuroinflammatory targets and treatments for epilepsy validated in experimental models. *Epilepsia* **58**:27–38. doi:10.1111/epi.13783

Aronica E, Ravizza T, Zurolo E, Vezzani A. 2012. Astrocyte immune responses in epilepsy. *Glia* **60**:1258–1268. doi:10.1002/glia.22312

Badimon A, Strasburger HJ, Ayata P, Chen X, Nair A, Ikegami A, Hwang P, Chan AT, Graves SM, Uweru JO, Ledderose C, Kutlu MG, Wheeler MA, Kahan A, Ishikawa M, Wang YC, Loh YHE, Jiang JX, Surmeier DJ, Robson SC, Junger WG, Sebra R, Calipari ES, Kenny PJ, Eyo UB, Colonna M, Quintana FJ, Wake H, Gradinaru V, Schaefer A. 2020. Negative feedback control of neuronal activity by microglia. *Nature* **586**:417–423. doi:10.1038/s41586-020-2777-8

Besag FMC. 2018. Epilepsy in patients with autism: Links, risks and treatment challenges. *Neuropsychiatr Dis Treat* **14**:1–10. doi:10.2147/NDT.S120509

Canetta S, Bolkan S, Padilla-Coreano N, Song LJ, Sahn R, Harrison NL, Gordon JA, Brown A, Kellendonk C. 2016. Maternal immune activation leads to selective functional deficits in offspring parvalbumin interneurons. *Mol Psychiatry* **21**:956–968. doi:10.1038/mp.2015.222

Carvill GL, McMahon JM, Schneider A, Zemel M, Myers CT, Saykally J, Nguyen J, Robbiano A, Zara F, Specchio N, Mecarelli O, Smith RL, Leventer RJ, Møller RS, Nikanorova M, Dimova

P, Jordanova A, Petrou S, Helbig I, Striano P, Weckhuysen S, Berkovic SF, Scheffer IE, Mefford HC. 2015. Mutations in the GABA transporter SLC6A1 cause epilepsy with myoclonic-atonic seizures. *Am J Hum Genet* **96**:808–815. doi:10.1016/j.ajhg.2015.02.016

Chazalon M, Paredes-Rodriguez E, Morin S, Martinez A, Cristóvão-Ferreira S, Vaz S, Sebastiao A, Panatier A, Boué-Grabot E, Miguelez C, Baufreton J. 2018. GAT-3 Dysfunction Generates Tonic Inhibition in External Globus Pallidus Neurons in Parkinsonian Rodents. *Cell Rep* **23**:1678–1690. doi:10.1016/j.celrep.2018.04.014

Chieffo D, Ricci D, Baranello G, Martinelli D, Veredice C, Lettori D, Battaglia D, Dravet C, Mercuri E, Guzzetta F. 2011. Early development in Dravet syndrome; visual function impairment precedes cognitive decline. *Epilepsy Res* **93**:73–79. doi:10.1016/j.eplepsyres.2010.10.015

Cho FS, Clemente A, Holden S, Paz JT. 2017. Thalamic Models of Seizures In VitroPitkänen, Buckmaster, Galanopoulou, Moshé (Editors): Models of Seizures and Epilepsy, Second Edition. Academic Press. pp. 273–284. doi:10.1016/B978-0-12-804066-9.00019-5

Cho KKA, Hoch R, Lee AT, Patel T, Rubenstein JLR, Sohal VS. 2015. Gamma rhythms link prefrontal interneuron dysfunction with cognitive inflexibility in dlx5/6+/- mice. *Neuron* **85**:1332–1343. doi:10.1016/j.neuron.2015.02.019

Chun H, An H, Lim J, Woo J, Lee J, Ryu H, Lee CJ. 2018. Astrocytic proBDNF and tonic GABA distinguish active versus reactive astrocytes in hippocampus. *Exp Neurobiol* **27**:155–170. doi:10.5607/en.2018.27.3.155

Clarkson AN, Huang BS, Macisaac SE, Mody I, Carmichael ST. 2010. Reducing excessive GABA-mediated tonic inhibition promotes functional recovery after stroke. *Nature* **468**:305–309. doi:10.1038/nature09511

Cope DW, Di Giovanni G, Fyson SJ, Orbán G, Errington AC, Lőrincz ML, Gould TM, Carter DA, Crunelli V. 2009. Enhanced tonic GABAA inhibition in typical absence epilepsy. *Nat Med* **15**:1392–1398. doi:10.1038/nm.2058.Enhanced

Cope DW, Hughes SW, Crunelli V. 2005. GABAA Receptor-Mediated Tonic Inhibition in Thalamic Neurons. *J Neurosci* **25**:11553–11563. doi:10.1523/JNEUROSCI.3362-05.2005

Coulter DA, Steinhäuser C. 2015. Role of Astrocytes in Epilepsy. *Cold Spring Harb Perspect Med* **5**. doi:10.1101/cshperspect.a022434

David Y, Cacheaux LP, Ivens S, Lapilover E, Heinemann U, Kaufer D, Friedman A. 2009. Astrocytic dysfunction in epileptogenesis: Consequence of altered potassium and glutamate homeostasis? *J Neurosci* **29**:10588–10599. doi:10.1523/JNEUROSCI.2323-09.2009

De Biasi S, Vitellaro-Zuccarello L, Brecha NC. 1998. Immunoreactivity for the GABA transporter-1 and GABA transporter-3 is restricted to astrocytes in the rat thalamus. A light and electron- microscopic immunolocalization. *Neuroscience* **83**:815–828. doi:10.1016/S0306-4522(97)00414-4

Dibbens LM, Feng HJ, Richards MC, Harkin LA, Hodgson BL, Scott D, Jenkins M, Petrou S, Sutherland GR, Scheffer IE, Berkovic SF, Macdonald RL, Mulley JC. 2004. GABRD encoding a protein for extra- or peri- synaptic GABA A receptors is susceptibility locus for generalized epilepsies. *Hum Mol Genet* **13**:1315–1319. doi:10.1093/hmg/ddh146

Dikow N, Maas B, Karch S, Granzow M, Janssen JWG, Jauch A, Hinderhofer K, Sutter C, Schubert-Bast S, Anderlid BM, Dallapiccola B, Van der Aa N, Moog U. 2014. 3p25.3 microdeletion of GABA transporters SLC6A1 and SLC6A11 results in intellectual disability, epilepsy and stereotypic behavior. *Am J Med Genet* **164**:3061–3068. doi:10.1002/ajmg.a.36761

Escartin C, Galea E, Lakatos A, O'Callaghan JP, Petzold GC, Serrano-Pozo A, Steinhäuser C, Volterra A, Carmignoto G, Agarwal A, Allen NJ, Araque A, Barbeito L, Barzilai A, Bergles DE, Bonvento G, Butt AM, Chen W-T, Cohen-Salmon M, Cunningham C, Deneen B, De Strooper B, Díaz-Castro B, Farina C, Freeman M, Gallo V, Goldman JE, Goldman SA, Götz M, Gutiérrez A, Haydon PG, Heiland DH, Hol EM, Holt MG, Iino M, Kastanenka K V, Kettenmann H, Khakh BS, Koizumi S, Lee CJ, Liddelow SA, MacVicar BA, Magistretti P, Messing A, Mishra A, Molofsky A V, Murai KK, Norris CM, Okada S, Oliet SHR, Oliveira JF, Panatier A, Parpura V, Pekna M, Pekny M, Pellerin L, Perea G, Pérez-Nievas BG, Pfrieger FW, Poskanzer KE, Quintana FJ, Ransohoff RM, Riquelme-Perez M, Robel S, Rose CR, Rothstein JD, Rouach N, Rowitch DH, Semyanov A, Sirko S, Sontheimer H, Swanson RA, Vitorica J, Wanner I-B, Wood LB, Wu J, Zheng B, Zimmer ER, Zorec R, Sofroniew M V, Verkhratsky A. 2021. Reactive astrocyte nomenclature, definitions, and future directions. *Nat Neurosci*. doi:10.1038/s41593-020-00783-4

Estes ML, McAllister AK. 2016. Maternal immune activation: Implications for neuropsychiatric disorders. *Science* **353**:772–777. doi:10.1126/science.aag3194

Frahm C, Haupt C, Weinandy F, Siegel G, Bruehl C, Witte OW. 2004. Regulation of GABA transporter mRNA and protein after photothrombotic infarct in rat brain. *J Comp Neurol* **478**:176–188. doi:10.1002/cne.20282

Fu AKY, Hung KW, Yuen MYF, Zhou X, Mak DSY, Chan ICW, Cheung TH, Zhang B, Fu WY, Liew FY, Ip NY. 2016. IL-33 ameliorates Alzheimer's disease-like pathology and cognitive decline. *Proc Natl Acad Sci U S A* **113**. doi:10.1073/pnas.1604032113

Gadea A, López-Colomé AM. 2001. Glial transporters for glutamate, glycine, and GABA: II. GABA transporters. *J Neurosci Res* **63**:461–468. doi:10.1002/jnr.1040

Goodspeed K, Pérez-Palma E, Iqbal S, Cooper D, Scimemi A, Johannesen KM, Stefanski A, Demarest S, Helbig KL, Kang J, Shaffo FC, Prentice B, Brownstein CA, Lim B, Helbig I, De Los Reyes E, McKnight D, Crunelli V, Campbell AJ, Møller RS, Freed A, Lal D. 2020. Current knowledge of SLC6A1-related neurodevelopmental disorders. *Brain Commun* **2**:1–10. doi:10.1093/braincomms/fcaa170

Griswold AJ, Ma D, Cukier HN, Nations LD, Schmidt MA, Chung RH, Jaworski JM, Salyakina D, Konidari I, Whitehead PL, Wright HH, Abramson RK, Williams SM, Menon R, Martin ER, Haines JL, Gilbert JR, Cuccaro ML, Pericak-Vance MA. 2012. Evaluation of copy number variations reveals novel candidate genes in autism spectrum disorder-associated pathways. *Hum Mol Genet* **21**:3513–3523. doi:10.1093/hmg/dds164

Grossman EJ, Ge Y, Jensen JH, Babb JS, Miles L, Reaume J, Silver JM, Grossman RI, Inglese M. 2012. Thalamus and Cognitive Impairment in Mild Traumatic Brain Injury: A Diffusional Kurtosis Imaging Study. *J Neurotrauma* **29**:2318–2327. doi:10.1089/neu.2011.1763

Grossman EJ, Inglese M. 2016. The role of thalamic damage in mild traumatic brain injury. *J Neurotrauma* **33**:163–167. doi:10.1089/neu.2015.3965

Haim L Ben, Carrillo-de Sauvage MA, Ceyzériat K, Escartin C. 2015. Elusive roles for reactive astrocytes in neurodegenerative diseases. *Front Cell Neurosci* **9**:1–27. doi:10.3389/fncel.2015.00278

Halassa MM, Sherman SM. 2019. Thalamocortical Circuit Motifs: A General Framework. *Neuron* **103**:762–770. doi:10.1016/j.neuron.2019.06.005

Hamby ME, Coppola G, Ao Y, Geschwind DH, Khakh BS, Sofroniew MV. 2012. Inflammatory Mediators Alter the Astrocyte Transcriptome and Calcium Signaling Elicited by Multiple G-Protein-Coupled Receptors. *J Neurosci* **32**:14489–14510.

doi:10.1016/j.immuni.2010.12.017.Two-stage

Han RT, Vainchtein ID, Schlachetzki JCM, Cho FS, Dorman LC, Johung T, Ahn E, Barron JT, Nakao-Inoue H, Joshi A, Molofsky AB, Glass CK, Paz JT, Molofsky A V. 2021. Interleukin-33 coordinates a microglial phagocytic response and limits corticothalamic excitability and seizure susceptibility. *bioRxiv* 1–52.

Hiu T, Farzampour Z, Paz JT, Wang EHJ, Badgely C, Olson A, Micheva KD, Wang G, Lemmens R, Tran K V., Nishiyama Y, Liang X, Hamilton SA, O'Rourke N, Smith SJ, Huguenard JR, Bliss TM, Steinberg GK. 2016. Enhanced phasic GABA inhibition during the repair phase of stroke: A novel therapeutic target. *Brain* **139**:468–480. doi:10.1093/brain/awv360

Holden SS, Grandi FC, Aboubakr O, Higashikubo B, Cho FS, Chang AH, Forero AO, Morningstar AR, Mathur V, Kuhn LJ, Suri P, Sankaranarayanan S, Andrews-Zwilling Y, Tenner AJ, Luthi A, Aronica E, Corces MR, Yednock T, Paz JT. 2021. Complement factor C1q mediates sleep spindle loss and epileptic spikes after mild brain injury. *Science* **373**. doi:10.1126/science.abj2685

Huang L, Wu ZB, ZhuGe Q, Zheng WM, Shao B, Wang B, Sun F, Jin K. 2014. Glial scar formation occurs in the human brain after ischemic stroke. *Int J Med Sci* **11**:344–348. doi:10.7150/ijms.8140

Ishibashi M, Egawa K, Fukuda A. 2019. Diverse actions of astrocytes in GABAergic signaling. *Int J Mol Sci* **20**:1–18. doi:10.3390/ijms20122964

Jo S, Yarishkin O, Hwang YJ, Chun YE, Park M, Woo DH, Bae JY, Kim T, Lee J, Chun H, Park HJ, Lee DY, Hong J, Kim HY, Oh SJ, Park SJ, Lee H, Yoon BE, Kim Y, Jeong Y, Shim I, Bae YC, Cho J, Kowall NW, Ryu H, Hwang E, Kim D, Lee CJ. 2014. GABA from reactive astrocytes impairs memory in mouse models of Alzheimer's disease. *Nat Med* **20**:886–896.

doi:10.1038/nm.3639

Jones EG. 1985. The Thalamus. Plenum Press. doi:10.1007/978-1-4615-1749-8

Kastanenka K V., Moreno-Bote R, De Pittà M, Perea G, Eraso-Pichot A, Masgrau R, Poskanzer KE, Galea E. 2019. A roadmap to integrate astrocytes into Systems Neuroscience. *Glia* 1–22. doi:10.1002/glia.23632

Kelley KW, Nakao-Inoue H, Molofsky A V., Oldham MC. 2018. Variation among intact tissue samples reveals the core transcriptional features of human CNS cell classes. *Nat Neurosci* **21**:1171–1184. doi:10.1038/s41593-018-0216-z

Kersanté F, Rowley SCS, Pavlov I, Gutièrrez-Mecinas M, Semyanov A, Reul JMHM, Walker MC, Linthorst ACE. 2013. A functional role for both γ-aminobutyric acid (GABA) transporter-1 and GABA transporter-3 in the modulation of extracellular GABA and GABAergic tonic conductances in the rat hippocampus. *J Physiol* **591**:2429–2441. doi:10.1113/jphysiol.2012.246298

Kim DU, Kim MK, Cho YW, Kim YS, Kim WJ, Lee MG, Kim SE, Nam TS, Cho KH, Kim YO, Lee MC. 2011. Association of a synonymous GAT3 polymorphism with antiepileptic drug pharmacoresistance. *J Hum Genet* **56**:640–646. doi:10.1038/jhg.2011.73

Klein P, Dingledine R, Aronica E, Bernard C, Blümcke I, Boison D, Brodie MJ, Brooks-Kayal AR, Engel J, Forcelli PA, Hirsch LJ, Kaminski RM, Klitgaard H, Kobow K, Lowenstein DH, Pearl PL, Pitkänen A, Puhakka N, Rogawski MA, Schmidt D, Sillanpää M, Sloviter RS, Steinhäuser C, Vezzani A, Walker MC, Löscher W. 2018. Commonalities in epileptogenic processes from different acute brain insults: Do they translate? *Epilepsia* **59**:37–66. doi:10.1111/epi.13965

Kloth AD, Badura A, Li A, Cherskov A, Connolly SG, Giovannucci A, Bangash MA, Grasselli G,

Agarikano OP, Piochon C, Tsai PT, Geschwind DH, Hansel C, Sahin M, Takumi T, Worley PF, Wang SSH. 2015. Cerebellar associative sensory learning defects in five mouse autism models. *Elife* **4**:1–26. doi:10.7554/eLife.06085

Krol A, Wimmer RD, Halassa MM, Feng G. 2018. Thalamic Reticular Dysfunction as a Circuit Endophenotype in Neurodevelopmental Disorders. *Neuron* **98**:282–295. doi:10.1016/j.neuron.2018.03.021

Kullmann DM, Walker MC. 2012. Tonic GABA A Receptor-Mediated Signaling in EpilepsyJasper's Basic Mechanisms of the Epilepsies. pp. 1–13.

Lacey CJ, Bryant a., Brill J, Huguenard JR. 2012. Enhanced NMDA Receptor-Dependent Thalamic Excitation and Network Oscillations in Stargazer Mice. *J Neurosci* **32**:11067–11081. doi:10.1523/JNEUROSCI.5604-11.2012

Lee TS, Bjørnsen LP, Paz C, Kim JH, Spencer SS, Spencer DD, Eid T, Lanerolle NC. 2006. GAT1 and GAT3 expression are differently localized in the human epileptogenic hippocampus. *Acta Neuropathol* **111**:351–363. doi:10.1007/s00401-005-0017-9

Lee V, Maguire J. 2014. The impact of tonic GABAA receptor-mediated inhibition on neuronal excitability varies across brain region and cell type. *Front Neural Circuits* **8**:1–27. doi:10.3389/fncir.2014.00003

Leekam SR, Nieto C, Libby SJ, Wing L, Gould J. 2007. Describing the sensory abnormalities of children and adults with autism. *J Autism Dev Disord* **37**:894–910. doi:10.1007/s10803-006-0218-7

Leng K, Li E, Eser R, Piergies A, Sit R, Tan M, Neff N, Li SH, Rodriguez RD, Suemoto CK, Leite REP, Ehrenberg AJ, Pasqualucci CA, Seeley WW, Spina S, Heinsen H, Grinberg LT, Kampmann M. 2021. Molecular characterization of selectively vulnerable neurons in

Alzheimer's disease. *Nat Neurosci* **24**:276–287. doi:10.1038/s41593-020-00764-7

Lu AC, Lee CK, Kleiman-Weiner M, Truong B, Wang M, Huguenard JR, Beenhakker MP. 2020. Nonlinearities between inhibition and t-type calcium channel activity bidirectionally regulate thalamic oscillations. *Elife* **9**:1–36. doi:10.7554/ELIFE.59548

Lui H, Zhang J, Makinson SR, Cahill MK, Kelley KW, Huang HY, Shang Y, Oldham MC, Martens LH, Gao F, Coppola G, Sloan SA, Hsieh CL, Kim CC, Bigio EH, Weintraub S, Mesulam MM, Rademakers R, MacKenzie IR, Seeley WW, Karydas A, Miller BL, Borroni B, Ghidoni R, Farese R V., Paz JT, Barres BA, Huang EJ. 2016. Progranulin Deficiency Promotes Circuit-Specific Synaptic Pruning by Microglia via Complement Activation. *Cell* **165**:921–935. doi:10.1016/j.cell.2016.04.001

Malkova N V., Yu CZ, Hsiao EY, Moore MJ, Patterson PH. 2012. Maternal immune activation yields offspring displaying mouse versions of the three core symptoms of autism. *Brain Behav Immun* **26**:607–616. doi:10.1016/j.bbi.2012.01.011

Mann EO, Mody I. 2010. Control of hippocampal gamma oscillation frequency by tonic inhibition and excitation of interneurons. *Nat Neurosci* **13**:205–212. doi:10.1038/nn.2464

Martinez-Losa M, Tracy TE, Ma K, Verret L, Clemente-Perez A, Khan AS, Cobos I, Ho K, Gan L, Mucke L, Alvarez-Dolado M, Palop JJ. 2018. Nav1.1-Overexpressing Interneuron Transplants Restore Brain Rhythms and Cognition in a Mouse Model of Alzheimer's Disease. *Neuron* **98**:75-89.e5. doi:10.1016/j.neuron.2018.02.029

Ortinski PI, Dong J, Mungenast A, Yue C, Takano H, Watson DJ, Haydon PG, Coulter DA. 2010. Selective induction of astrocytic gliosis generates deficits in neuronal inhibition. *Nat Neurosci* **13**:584–91. doi:10.1038/nn.2535

Patel DC, Tewari BP, Chaunsali L, Sontheimer H. 2019. Neuron–glia interactions in the

pathophysiology of epilepsy. *Nat Rev Neurosci* **20**:282–297. doi:10.1038/s41583-019-0126-4

Paz JT, Bryant AS, Peng K, Fenno L, Yizhar O, Frankel WN, Deisseroth K, Huguenard JR. 2011. A new mode of corticothalamic transmission revealed in the Gria4(-/-) model of absence epilepsy. *Nat Neurosci* **14**:1167–73. doi:10.1038/nn.2896

Paz JT, Christian CA, Parada I, Prince DA, Huguenard JR. 2010. Focal Cortical Infarcts Alter Intrinsic Excitability and Synaptic Excitation in the Reticular Thalamic Nucleus. *J Neurosci* **30**:5465–5479. doi:10.1523/JNEUROSCI.5083-09.2010

Paz JT, Davidson TJ, Frechette ES, Delord B, Parada I, Peng K, Deisseroth K, Huguenard JR. 2013. Closed-loop optogenetic control of thalamus as a tool for interrupting seizures after cortical injury. *Nat Neurosci* **16**:64–70. doi:10.1038/nn.3269

Paz JT, Huguenard JR. 2015. Microcircuits and their interactions in epilepsy: is the focus out of focus? *Nat Neurosci* **18**:351–9. doi:10.1038/nn.3950

Perea G, Gómez R, Mederos S, Covelo A, Ballesteros JJ, Schlosser L, Hernández-Vivanco A, Martín-Fernández M, Quintana R, Rayan A, Díez A, Fuenzalida M, Agarwal A, Bergles DE, Bettler B, Manahan-Vaughan D, Martín ED, Kirchhoff F, Araque A. 2016. Activity-dependent switch of GABAergic inhibition into glutamatergic excitation in astrocyte-neuron networks. *Elife* **5**:e20362. doi:10.7554/eLife.20362

Perry BAL, Lomi E, Mitchell AS. 2021. Thalamocortical interactions in cognition and disease: The mediodorsal and anterior thalamic nuclei. *Neurosci Biobehav Rev* **130**:162–177. doi:10.1016/j.neubiorev.2021.05.032

Pirttimaki T, Parri HR, Crunelli V. 2013. Astrocytic GABA transporter GAT-1 dysfunction in experimental absence seizures. *J Physiol* **591**:823–33. doi:10.1113/jphysiol.2012.242016

Poskanzer KE, Yuste R. 2016. Astrocytes regulate cortical state switching in vivo. *Proc Natl Acad Sci U S A* **2016**:1–10. doi:10.1073/pnas.1520759113

Purves-Tyson TD, Weber-Stadlbauer U, Richetto J, Rothmond DA, Labouesse MA, Polesel M, Robinson K, Shannon Weickert C, Meyer U. 2019. Increased levels of midbrain immune-related transcripts in schizophrenia and in murine offspring after maternal immune activation. *Mol Psychiatry*. doi:10.1038/s41380-019-0434-0

Ramlackhansingh AF, Brooks DJ, Greenwood RJ, Bose SK, Turkheimer FE, Kinnunen KM, Gentleman S, Heckemann RA, Gunanayagam K, Gelosa G, Sharp DJ. 2011. Inflammation after trauma: Microglial activation and traumatic brain injury. *Ann Neurol* **70**:374–383. doi:10.1002/ana.22455

Ritter-Makinson S, Clemente-Perez A, Higashikubo B, Cho FS, Holden SS, Bennett E, Chkaidze A, Rooda OHJE, Cornet MC, Hoebeek FE, Yamakawa K, Cilio MR, Delord B, Paz JT. 2019. Augmented Reticular Thalamic Bursting and Seizures in Scn1a-Dravet Syndrome. *Cell Rep* **26**:54–64. doi:10.1016/j.celrep.2018.12.018

Robel S, Sontheimer H. 2016. Glia as drivers of abnormal neuronal activity. *Nat Neurosci* **19**:28–33. doi:10.1038/nn.4184

Rodríguez-Arellano JJ, Parpura V, Zorec R, Verkhratsky A. 2016. Astrocytes in physiological aging and Alzheimer's disease. *Neuroscience* **323**:170–182. doi:10.1016/j.neuroscience.2015.01.007

Saalmann YB, Kastner S. 2015. The cognitive thalamus. *Front Syst Neurosci* **9**. doi:10.1038/nn957

Satterstrom FK, Kosmicki JA, Wang J, Breen MS, De Rubeis S, An JY, Peng M, Collins R, Grove J, Klei L, Stevens C, Reichert J, Mulhern MS, Artomov M, Gerges S, Sheppard B, Xu X, Bhaduri A, Norman U, Brand H, Schwartz G, Nguyen R, Guerrero EE, Dias C, Aleksic B,

Anney R, Barbosa M, Bishop S, Brusco A, Bybjerg-Grauholm J, Carracedo A, Chan MCY, Chiocchetti AG, Chung BHY, Coon H, Cuccaro ML, Curró A, Dalla Bernardina B, Doan R, Domenici E, Dong S, Fallerini C, Fernández-Prieto M, Ferrero GB, Freitag CM, Fromer M, Gargus JJ, Geschwind D, Giorgio E, González-Peñas J, Guter S, Halpern D, Hansen-Kiss E, He X, Herman GE, Hertz-Picciotto I, Hougaard DM, Hultman CM, Ionita-Laza I, Jacob S, Jamison J, Jugessur A, Kaartinen M, Knudsen GP, Kolevzon A, Kushima I, Lee SL, Lehtimäki T, Lim ET, Lintas C, Lipkin WI, Lopergolo D, Lopes F, Ludena Y, Maciel P, Magnus P, Mahjani B, Maltman N, Manoach DS, Meiri G, Menashe I, Miller J, Minshew N, Montenegro EMS, Moreira D, Morrow EM, Mors O, Mortensen PB, Mosconi M, Muglia P, Neale BM, Nordentoft M, Ozaki N, Palotie A, Parellada M, Passos-Bueno MR, Pericak-Vance M, Persico AM, Pessah I, Puura K, Reichenberg A, Renieri A, Riberi E, Robinson EB, Samocha KE, Sandin S, Santangelo SL, Schellenberg G, Scherer SW, Schlitt S, Schmidt R, Schmitt L, Silva IMW, Singh T, Siper PM, Smith M, Soares G, Stoltenberg C, Suren P, Susser E, Sweeney J, Szatmari P, Tang L, Tassone F, Teufel K, Trabetti E, Trelles M del P, Walsh CA, Weiss LA, Werge T, Werling DM, Wigdor EM, Wilkinson E, Willsey AJ, Yu TW, Yu MHC, Yuen R, Zachi E, Agerbo E, Als TD, Appadurai V, Bækvad-Hansen M, Belliveau R, Buil A, Carey CE, Cerrato F, Chambert K, Churchhouse C, Dalsgaard S, Demontis D, Dumont A, Goldstein J, Hansen CS, Hauberg ME, Hollegaard M V., Howrigan DP, Huang H, Maller J, Martin AR, Martin J, Mattheisen M, Moran J, Pallesen J, Palmer DS, Pedersen CB, Pedersen MG, Poterba T, Poulsen JB, Ripke S, Schork AJ, Thompson WK, Turley P, Walters RK, Betancur C, Cook EH, Gallagher L, Gill M, Sutcliffe JS, Thurm A, Zwick ME, Børglum AD, State MW, Cicek AE, Talkowski ME, Cutler DJ, Devlin B, Sanders SJ, Roeder K, Daly MJ, Buxbaum JD. 2020. Large-Scale Exome Sequencing Study Implicates Both

Developmental and Functional Changes in the Neurobiology of Autism. *Cell* **180**:568-584.e23. doi:10.1016/j.cell.2019.12.036

Schijns OEMG, Bisschop J, Rijkers K, Dings J, Vanherle S, Lindsey P, Smeets HJM, Hoogland G. 2020. GAT-1 (rs2697153) and GAT-3 (rs2272400) polymorphisms are associated with febrile seizures and temporal lobe epilepsy. *Epileptic Disord* **22**:176–182. doi:10.1684/epd.2020.1154

Shao AE, Chang C, Li Z, Yu X, Ho K. 2022. Tau ablation in excitatory neurons and postnatal tau knockdown reduce epilepsy, SUDEP, and autism behaviors in a Dravet syndrome model. *Sci Transl Med* **5527**.

Shigetomi E, Patel S, Khakh BS. 2016. Probing the Complexities of Astrocyte Calcium Signaling. *Trends Cell Biol* **26**:300–312. doi:10.1016/j.tcb.2016.01.003

Shigetomi E, Tong X, Kwan KY, Corey DP, Khakh BS. 2012. TRPA1 channels regulate astrocyte resting calcium and inhibitory synapse efficacy through GAT-3. *Nat Neurosci* **15**:70–80. doi:10.1038/nn.3000

Sloan SA, Barres BA. 2014. Mechanisms of astrocyte development and their contributions to neurodevelopmental disorders. *Curr Opin Neurobiol* **27**:75–81. doi:10.1016/j.conb.2014.03.005

Sohal VS. 2016. How close are we to understanding what (If anything) γ oscillations do in cortical circuits? *J Neurosci* **36**:10489–10495. doi:10.1523/JNEUROSCI.0990-16.2016

Sorokin JM, Davidson TJ, Frechette E, Abramian AM, Deisseroth K, Huguenard JR, Paz JT. 2017. Bidirectional Control of Generalized Epilepsy Networks via Rapid Real-Time Switching of Firing Mode. *Neuron* **93**:194–210. doi:10.1016/j.neuron.2016.11.026

Steinhäuser C, Seifert G. 2012. Astrocyte dysfunction in epilepsyNoebels, JL, Avoli M, Rogawski

MA, et Al., Editors. Jasper's Basic Mechanisms of the Epilepsies. 4th Edition. Bethesda (MD): National Center for Biotechnology Information (US). doi:10.1016/j.brainresrev.2009.10.004

Stevens B, Allen NJ, Vazquez LE, Howell GR, Christopherson KS, Nouri N, Micheva KD, Mehalow AK, Huberman AD, Stafford B, Sher A, Litke AMM, Lambris JD, Smith SJ, John SWM, Barres BA. 2007. The Classical Complement Cascade Mediates CNS Synapse Elimination. *Cell* **131**:1164–1178. doi:10.1016/j.cell.2007.10.036

Toppi E, Sireno L, Lembo M, Banaj N, Messina B, Golesorkhtafti S, Spalletta G, Bossù P. 2022. IL-33 and IL-10 Serum Levels Increase in MCI Patients Following Homotaurine Treatment. *Front Immunol* **13**:1–8. doi:10.3389/fimmu.2022.813951

Verkhratsky A, Parpura V. 2016. Astrogliopathology in neurological, neurodevelopmental and psychiatric disorders. *Neurobiol Dis* **85**:254–261. doi:10.1016/j.nbd.2015.03.025

Vezzani A, Balosso S, Ravizza T. 2019. Neuroinflammatory pathways as treatment targets and biomarkers in epilepsy. *Nat Rev Neurol* **15**:459–472. doi:10.1038/s41582-019-0217-x

Vitellaro-Zuccarello L, Calvaresi N, De Biasi S. 2003. Expression of GABA transporters, GAT-1 and GAT-3, in the cerebral cortex and thalamus of the rat during postnatal development. *Cell Tissue Res* **313**:245–257. doi:10.1007/s00441-003-0746-9

Ward LM. 2003. Synchronous neural oscillations and cognitive processes. *Trends Cogn Sci* **7**:553–559. doi:10.1016/j.tics.2003.10.012

Williams S, Boksa P. 2010. Gamma oscillations and schizophrenia. *J Psychiatry Neurosci* **35**:75–77. doi:10.1503/jpn.100021

Wójtowicz AM, Dvorzhak A, Semtner M, Grantyn R. 2013. Reduced tonic inhibition in striatal output neurons from Huntington mice due to loss of astrocytic GABA release through GAT-

3. *Front Neural Circuits* **7**:1–12. doi:10.3389/fncir.2013.00188

Woo J, Im SK, Chun H, Jung SY, Oh SJ, Choi N, Lee CJ, Hur EM. 2017. Functional characterization of resting and adenovirus-induced reactive astrocytes in three-dimensional culture. *Exp Neurobiol* **26**:158–167. doi:10.5607/en.2017.26.3.158

Wu Z, Guo Z, Gearing M, Chen G. 2014. Tonic inhibition in dentate gyrus impairs long-term potentiation and memory in an Alzhiemer' s disease model. *Nat Commun* **5**:1–13. doi:10.1038/ncomms5159

Yin P, Zhang XT, Li J, Yu L, Wang JW, Lei GF, Sun RP, Li BM. 2015. Maternal immune activation increases seizure susceptibility in juvenile rat offspring. *Epilepsy Behav* **47**:93–97. doi:10.1016/j.yebeh.2015.04.018

Yu X, Taylor AMW, Nagai J, Golshani P, Evans CJ, Coppola G, Khakh BS. 2018. Reducing Astrocyte Calcium Signaling In Vivo Alters Striatal Microcircuits and Causes Repetitive Behavior. *Neuron* **99**:1170-1187.e9. doi:10.1016/j.neuron.2018.08.015

Zhang T, Yu F, Xu H, Chen M, Chen X, Guo L, Zhou C, Xu Y, Wang F, Yu J, Wu B. 2021. Dysregulation of REV-ERBα impairs GABAergic function and promotes epileptic seizures in preclinical models. *Nat Commun* **12**. doi:10.1038/s41467-021-21477-w

Publishing Agreement

It is the policy of the University to encourage open access and broad distribution of all theses, dissertations, and manuscripts. The Graduate Division will facilitate the distribution of UCSF theses, dissertations, and manuscripts to the UCSF Library for open access and distribution. UCSF will make such theses, dissertations, and manuscripts accessible to the public and will take reasonable steps to preserve these works in perpetuity.

I hereby grant the non-exclusive, perpetual right to The Regents of the University of California to reproduce, publicly display, distribute, preserve, and publish copies of my thesis, dissertation, or manuscript in any form or media, now existing or later derived, including access online for teaching, research, and public service purposes.

DocuSigned by:
Frances Sungsil Cho
C37E5DBA5FF84D9...
Author Signature

8/28/2022
Date